

Enriching the diversity of polyethylene terephthalate degrading enzymes from metagenomes

Dissertation

with the aim of achieving the degree of Doctor rerum naturalim (Dr. rer. nat.)

at the department of Microbiology and Biotechnology

Faculty of Mathematics, Informatics and Natural Sciences

Universität Hamburg

submitted by

Hongli Zhang

Hamburg, 2024

The following evaluators recommend the admission of this dissertation:

Professor Dr. Wolfgang R. Streit

Professor Dr. Sigrun Reumann

Date of oral defense: **09.01.2025**

Eidesstattliche Erklärung

Hiermit erkläre ich an Eides statt, dass ich die vorliegende Dissertationsschrift selbst verfasst und keine anderen als die angegebenen Quellen und Hilfsmittel benutzt habe.

Declaration on oath

I hereby declare, on oath, that I have written the present dissertation by my own and have not used any other than the acknowledged resources and aids.

Stockdorf, April 27, 2024



.....

Hongli Zhang

Contributions to the quoted articles

Zhang, H., Perez-Garcia, P., Dierkes, R. F., Applegate, V., Schumacher, J., Chibani, C. M., Sternagel, S., Preuss, L., Weigert, S., Schmeisser, C., Danso, D., Pleiss, J., Almeida, A., Höcker, B., Hallam, S. J., Schmitz, R. A., Smits, S., Chow, J. and Streit, W. R. (2022). The Bacteroidetes *Aequorivita* sp. and *Kaistella jeonii* produce promiscuous esterases with PET-hydrolyzing activity. *Frontiers in microbiology*, 12, 3874.

doi: 10.3389/fmicb.2021.803896

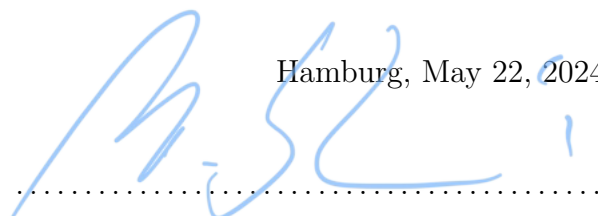
- Planning and co-designing of the study
- Participation in all experimental work, analysis and evaluation of the data
- Co-writing and preparation of the manuscript

***Zhang, H.**, *Dierkes, R., Perez-Garcia, P., Costanzi, E., Dittrich, J., Gurschke, M., Applegate, V., Partus, K., Schmeisser, C., Pflieger, C., Gohlke, H., Smits, S., Chow, J. and Streit, W. R. "The metagenome-derived esterase PET40 is highly promiscuous and hydrolyses polyethylene terephthalate (PET)", *FEBS* (In Review)

**Shared first author has the equal contribution.*

- Planning and co-designing of the study, performance of the biochemical characterization of PET40
- Evaluation of the experimental data and illustration of Phylogenetic and structural analysis
- Co-writing of the manuscript

Hamburg, May 22, 2024



Prof. Dr. Wolfgang R. Streit (Supervisor)

Other publications

Buchholz, P. C., Feuerriegel, G., **Zhang, H.**, Perez-Garcia, P., Nover, L. L., Chow, J., Streit, W. R. and Pleiss, J. (2022). Plastics degradation by hydrolytic enzymes: The plastics-active enzymes database—PAZy. *Proteins: Structure, Function, and Bioinformatics*, 90(7), 1443-1456. doi: 10.1002/prot.26325

- Providing the data regarding PET degrading enzymes and participating in updating the PAZy database
- Proof-reading of parts of the manuscript

Han, Y., Kinfu, B. M., Blombach, F., Cackett, G., **Zhang, H.**, Pérez-García, P., Krohn, I., Salomon, J., Besirlioglu, V., Mirzaeigarakani, T., Schwaneberg, U., Chow, J., Werner, W. and Streit, W. R. (2022). A novel metagenome-derived viral RNA polymerase and its application in a cell-free expression system for metagenome screening. *Scientific Reports*, 12(1), 17882. doi: 10.1038/s41598-022-22383-x

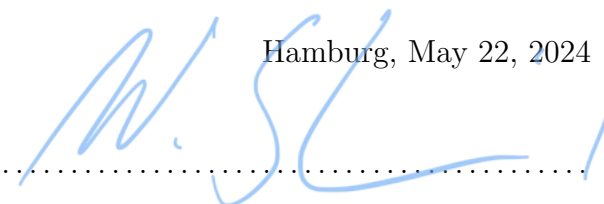
- Participation in purification of nucleotide acid and protein samples. Proof-reading of parts of the manuscript

Book chapters

Perez-Garcia, P., Danso, D., **Zhang, H.**, Chow, J., and Streit, W.S. (2021). Exploring the global metagenome for plastic-degrading enzymes. *Methods in enzymology* (Vol. 648, pp. 137-157). Academic Press. doi: 10.1016/bs.mie.2020.12.022

Zhang, H., Dierkes, R. and Streit, W.S. (2022). *Microbial Degradation of Plastics*. ASM Handbook (Vol. 11B) doi: 10.31399/asm.hb.v11B.a0006866

Hamburg, May 22, 2024



Prof. Dr. Wolfgang R. Streit (Supervisor)

Contents

Abstract	III
Zusammenfassung	V
1 Introduction	1
1.1 Accumulation of plastic waste in the environment	1
1.2 Microbial degradation of plastics	3
1.2.1 Degradation mechanisms of polyethylene terephthalate (PET) . . .	4
1.2.2 Known PET-degrading hydrolases (PETase)	6
1.3 Mining for novel PET-degrading enzymes	8
1.4 Aim of this study	9
2 PET-hydrolyzing esterases from Bacteroidetes	11
3 The metagenome-derived esterase PET40 hydrolyses PET	38
4 Discussion	61
4.1 Bacteroidetes as a rich resource for PET degradation	61
4.2 PET40 - A highly promiscuous esterase hydrolyzing PET	63
4.3 Isolation of a novel polymer-degrader from crude oil-contaminated environmental samples	65
4.4 Identification of PET degradation activity	67
4.4.1 Production of recombinant PET-degrading enzymes	68
4.4.2 Methods for activity verification	69
4.5 Conclusion and Outlook	70
5 Other publication	72
5.1 Plastics degradation by hydrolytic enzymes: The plastics-active enzymes database—PAZy	72
References	109

Abstract

Polyethylene terephthalate (PET) is a durable, chemically and thermally stable polyester. Due to these desirable properties, PET is widely used for various applications in our daily life. However, PET plastics do not degrade to a large degree when released into the environment. Thus, its accumulation in both oceans and on land has become one of the major concerns of plastic pollution. Compared to traditional PET recycling processes requiring lots of energy resources and usually producing harmful contaminants, using microorganism-derived enzymes has provided a novel environment-friendly option to eliminate plastic waste. Few bacterial hydrolases and microorganisms have been identified with the ability to degrade synthetic polymers. However, their degradation activities are relatively low for an industrial use. In addition, despite bioinformatic analysis revealing that the Bacteroidetes phylum has the potential for PET degradation, none of enzymes affiliated with this phylum has been functionally verified. Therefore, the main goal of the present study was to achieve a better understanding of the molecular mechanisms involved in the microbial degradation of PET and to extend the biodiversity of enzymes that are capable of degrading this complex polymer.

In order to identify novel PET-active enzymes, thirty candidate genes encoding putative PETases found by a Hidden-Markov-Model based search (HMM search) were synthesized. Combined with functional screening methods, three enzymes, PET27, PET30 and PET40, have been identified with ability to break down PET. PET27 and PET30, affiliated with Bacteroidetes, showed the hydrolytic activity on PET, providing the first evidences of the involvement of this phylum in PET degradation. Additional assessments indicate that PET30 has significant activities on PET and *para*-nitrophenyl hexanoate (*p*NP-C6) at even 4°C. Furthermore, all three enzymes were characterized in detail. The obtained results show that they were able to hydrolyze a variety of substrates including the polymer polycaprolactone (PCL), the PET-monomer bis-(2-hydroxyethyl) terephthalate (BHET), and the polyester polyurethane Impranil@DLN. Although the observed degradation rates on PET were relatively low, it can be assumed that PET hydrolysis may be a side reaction because of their activities on various substrates, which

indicates the promiscuity of these enzymes. In addition, the crystallization and binding studies of PET30 and PET40 were carried out, providing structural insights into the substrates binding pocket involved in the degradation processes. The analysis of the global distribution of PET27, PET30 and their homologs revealed that promising enzyme candidates affiliated with Bacteroidetes are occurring through diverse climate zones. The majority of these enzymes are associated with the aquatic metagenomes. This may suggest a promising impact on the plastics hydrolysis in the marine environment.

In summary, this work provides detailed biochemical characteristics of the novel PET-active enzymes and extends the knowledge of the mechanisms on the structural level. The presented results enable a better understanding of microbial degradation in general and enrich the biodiversity of PET-hydrolyzing enzymes.

Zusammenfassung

Polyethylenterephthalat (PET) ist ein langlebiger, chemisch und thermisch stabiler Polyester. Aufgrund dieser wünschenswerten Eigenschaften wird PET in zahlreichen Anwendungen unseres Alltags eingesetzt. Allerdings zersetzen sich PET-Kunststoffe, wenn sie in die Umwelt freigesetzt werden, nur in geringem Maße. Daher ist seine Anreicherung sowohl in den Ozeanen als auch an Land zu einem der Hauptprobleme der Plastikverschmutzung geworden. Im Vergleich zu herkömmlichen PET-Recyclingprozessen, die viele Energiequellen erfordern und in der Regel schädliche Schadstoffe produzieren, bietet die Verwendung von mikroorganismengenerierten Enzymen eine neuartige, umweltfreundliche Option zur Beseitigung von Plastikabfällen.

Bisher wurden nur wenige bakterielle Hydrolasen und Mikroorganismen mit der Fähigkeit identifiziert, synthetische Polymere abzubauen, wobei ihre Abbauaktivitäten für einen industriellen Einsatz relativ gering sind. Darüber hinaus hat die bioinformatische Analyse gezeigt, dass das Phylum der Bacteroidetes das Potenzial zum PET-Abbau besitzt, wenngleich bislang kein Enzym, das diesem Phylum zugeordnet ist, funktionell verifiziert werden konnte. Das Hauptziel der vorliegenden Studie bestand daher darin, ein besseres Verständnis der molekularen Mechanismen zu erlangen, die am mikrobiellen Abbau von PET beteiligt sind, und die Biodiversität der Enzyme, die in der Lage sind, dieses komplexe Polymer abzubauen, zu erweitern.

Um neuartige PET-aktive Enzyme zu identifizieren, wurden dreißig Kandidatengene, die putative PETasen kodieren und mittels einer auf Hidden-Markov-Modellen basierenden Suche (HMM-Suche) identifiziert wurden, synthetisiert. In Kombination mit funktionellen Screening-Methoden wurden drei Enzyme – PET27, PET30 und PET40 – identifiziert, die in der Lage sind, PET abzubauen. PET27 und PET30, die dem Phylum Bacteroidetes zugeordnet sind, zeigten eine hydrolytische Aktivität gegenüber PET und lieferten somit den ersten funktionellen Nachweis für die Beteiligung dieses Phylums am PET-Abbau. Weitere Untersuchungen zeigen, dass PET30 selbst bei 4°C signifikante Aktivitäten gegenüber PET und *p*-Nitrophenylhexanoat (*p*NP-C6) aufweist. Zudem wurden alle drei Enzyme detailliert charakterisiert.

Die gewonnenen Ergebnisse belegen, dass die Enzyme in der Lage sind, eine Vielzahl von Substraten zu hydrolysieren, darunter das Polymer Polycaprolacton (PCL), das PET-Monomer Bis-(2-hydroxyethyl)terephthalat (BHET) und das Polyesterpolyurethan Impranil®DLN. Obwohl die beobachteten Abbauraten von PET relativ gering waren, kann angenommen werden, dass die PET-Hydrolyse eine Nebenreaktion infolge ihrer Aktivität auf verschiedene Substrate darstellt, was auf die Promiskuität dieser Enzyme hinweist. Darüber hinaus wurden Kristallisations- und Bindungsstudien an PET30 und PET40 durchgeführt, welche strukturelle Einblicke in die an den Abbauprozessen beteiligte Substratbindungsstelle lieferten.

Die Analyse der globalen Verbreitung von PET27, PET30 und ihren Homologen ergab, dass vielversprechende Enzymkandidaten, die dem Phylum Bacteroidetes zugeordnet sind, in unterschiedlichen Klimazonen vorkommen. Der Großteil dieser Enzyme ist mit aquatischen Metagenomen assoziiert, was auf einen potenziell positiven Einfluss auf die Kunststoffhydrolyse in marinen Umgebungen hindeuten könnte.

Zusammenfassend liefert diese Arbeit detaillierte biochemische Charakterisierungen der neuartigen PET-aktiven Enzyme und erweitert das Wissen über die zugrunde liegenden Mechanismen auf struktureller Ebene. Die präsentierten Ergebnisse ermöglichen ein besseres Verständnis des mikrobiellen Abbaus im Allgemeinen und bereichern die Biodiversität der PET-hydrolysierenden Enzyme.

1 Introduction

The use of fossil-based plastics has become ubiquitous in the industry and our day-to-day lives. In 2021, the annual production of plastics increased up to 390 million tons (Plasticseurope, 2022), with polyethylene terephthalate (PET) being one of the most produced synthetic polymers. However, the unique traits of these synthetic polymers, including extreme stability and durability, have resulted in the accumulation of plastic pollutants in our environment. It is estimated that the degradation of a single plastic bottle will take 100 - 500 years in nature (Barnes et al., 2009; Danso et al., 2019). Application of microorganisms and enzymes that hydrolyze plastics can be a promising and sustainable approach to reduce the accumulation of plastic pollution. Therefore, one of the future challenges for microbiologists is to identify novel biocatalysts involved in the plastics degradation (Wei und Zimmermann, 2017; Chow et al., 2022; Tamoor et al., 2021).

1.1 Accumulation of plastic waste in the environment

With the discovery of petroleum-based polymer, polystyrene (PS), in 1839 by Eduard Simon, the use of plastics began to be exploited (Simon, 1839). Plastic products can be found in various fields such as packaging, clothing, construction, medical devices etc. The majority of their applications is to produce disposable products such as PET-bottles for drinks and plastic cups, which led to a large consumption of plastics (Geyer et al., 2017). In the last few decades, the production of plastic materials has increased tremendously. In 1990, 100 million tons of plastics were produced globally. This number has amounted almost four times to 390 million tons by 2021 (Plasticseurope, 2022). The main synthetic plastics that are commonly used are polyethylene (PE), polypropylene (PP), polyvinylchloride (PVC), polyethylene terephthalate (PET), polyurethane (PU), polystyrene (PS) and polyamide (PA) (statista.com, 2022; Chow et al., 2022). PET is one of the most commonly synthesized plastics, with 24 million tons produced annually (Plasticseurope, 2022).

Even though the recycling rates of the plastics have increased over the past few

years, only a minor portion of these post-consumer plastics is currently recycled. Even in the EU, an advanced economy with leading regulations, only 10% of post-consumer plastics are recycled and made into new products (Plasticseurope, 2022). The rest of these waste plastics ends up their journey in ecological niches, especially in oceans, which causes environmental issues due to their low-degradation rate in nature (Webb et al., 2013; Barnes et al., 2009). According to recent studies, plastics can be found as the main component of 60 - 80% of marine waste and even up to 95% in some areas (Derraik, 2002; Gregory, 2009; Eriksen et al., 2014; Wang et al., 2018). Scientists estimated that about 398.000 tons of plastic debris have been accumulated and floating in the ocean by 2020 and will remain there for decades (Hohn et al., 2020; Howard, 2002). Researchers showed that hundreds of marine species, including fishes, sea birds, turtles and mammals, are affected by plastic waste. Marine animals get trapped in floating plastics such as discarded fishing nets and plastic bags, which leads them to drowning (Moore, 2008). However, plastic waste of large size is not the only concern of the environmental pollution. A vast amount of microplastics (diameter < 5 mm) also ends up in the biosphere and leads to further pollution of our environment (Gigault et al., 2018; Mitrano et al., 2021; Danso et al., 2019). They are derived from primary sources, including additives used for the friction of products (e.g. toothpaste and cosmetic products) or secondary sources, which are converted from large plastics by mechanical impacts (Andrady, 2011; Browne et al., 2011; Carr et al., 2016). It is estimated that from 0.8 to 2.5 million tons of microplastics are released into the oceans yearly (Miranda et al., 2020). Microplastics can be consumed by sea animals along with their food. Plastic debris accumulated in the gastrointestinal system damage the stomach, block the digest track and result in death of animals (Laist, 1987; Derraik, 2002). Because of their presence in seafood species, human-made plastics can now also be found in our food chain. Recently, studies have demonstrated the presence of microplastics in the human blood, lung tissue and placenta (Ragusa et al., 2021; Jenner et al., 2022; Leslie et al., 2022). The impact of these particles on the human organism is still not clear. However, the toxicity of breakdown products and additives is considered a potential contributor to causes of health problems (Prata et al., 2020; Rahman et al.,

2021). According to reports, phthalates, which are frequently linked to PET, can operate as endocrine disruptors and are considered harmful (Sax, 2010).

1.2 Microbial degradation of plastics

As mentioned above, petroleum-based plastics only degrade very slowly in nature due to their high stability and durability (Chamas et al., 2020; Webb et al., 2013). The initial degradation is often driven by abiotic processes, including weathering through UV radiation, winds and other mechanical disruptions. In addition, temperature and pH changes are also considered as abiotic factors (Day und Wiles, 1972; Shaw und Day, 1994; Fagerburg und Clauberg, 2004). In aquatic environments, it is assumed that the mechanical actions led by sea waves and winds, as well as by abrasion from rocks and sand contribute primarily to the breakdown of plastics (Shaw und Day, 1994). Plastics released into the environment are eventually fragmented into smaller pieces (micro- and nano-plastics) by the mechanical processes, providing a larger total surface for the biodegradation caused by microorganisms (Cooper und Corcoran, 2010). The so-called weathering also contributes to fragment plastics and multiplies their surface, which make them more accessible to microbial attachment Zhang et al. (2022b); Gewert et al. (2015); Duan et al. (2021); Flemming et al. (2016). Earlier research demonstrated that exposure to UV light alters the physical characteristics of PET, causing the color change from clear to slightly yellow (Mohammadian et al., 1991; Shaw und Day, 1994). Notably, aromatic ring structures present in PET and other polymers increase their susceptibility to UV radiation (Gotoh et al., 2011; Falkenstein et al., 2020).

Furthermore, several studies have observed that certain invertebrates such as the wax moth *Galleria mellonella*, the mealworm *Tenebrio molitor* and their associated microbiomes can break down man-made polymers into smaller particles. Unfortunately, none of the specific enzymes related to these degradation processes has been verified (Bombelli et al., 2017; Brandon et al., 2018; Yang et al., 2014; Cassone et al., 2020). Various bacterial and fungal species are known for their capability to colonize plastic surfaces. However it is still not clear how and to what extent they affect the structures

and the breakdown of plastics (Kirstein et al., 2016, 2019; Amaral-Zettler et al., 2020). Notably, bacterial colonization does not necessarily imply the occurrence of degradation (Zhang et al., 2022b; Chow et al., 2022). It appears that bacteria consume additives as an energy source, as these additives can be found in most polymers and are often preferred carbon or nitrogen sources over polymer (Chow et al., 2022).

Since synthetic plastics are often composed of various building blocks such as aromatic rings, ester and ether bonds, it is assumed that they require a different set of enzymes for their degradation (Zhang et al., 2022b). Thus, it is unlikely that a single organism is able to break down the polymer alone in nature, but rather a group of microbes (Chow et al., 2022). Moreover, the degree of the crystallinity of the synthetic polymers has a significant impact on enzymatic degradation. The majority of fossil-based polymers is semi-crystalline and contains both amorphous as well as highly crystalline regions. As the crystalline regions are resistant to enzymatic attachment, the degradation appears to occur mainly in the amorphous regions (Webb et al., 2013). In recent years, the microbial degradation of plastics has been extensively discussed. To date, only a limited number of enzymes and microorganisms that act on plastics are known, and they are mainly involved in the degradation of PET, PUR and PA (Danso et al., 2019; Wei und Zimmermann, 2017). These enzymes are mainly hydrolases, including esterases, lipases, cutinases, proteases and amidases. The Plastic-Active-Enzyme database (PAZy) has summarized and listed a total of 141 verified enzymes that act in fossil-based plastics (as of December 2023) (Buchholz et al., 2022). Recently, a report has been published, demonstrating the first evidences of two enzymes derived from wax worm saliva being able to randomly oxidize PET, however, with very low efficiency (Sanluis-Verdes et al., 2022).

1.2.1 Degradation mechanisms of polyethylene terephthalate (PET)

Polyethylene terephthalate (PET) was discovered in 1941 (Rex und Tennant, 1949) and is synthesized by the polycondensation of its monomers terephthalic acid (TPA) and ethylene glycol (EG). PET is a solid thermoplastic with a melting point of 250 - 260 °C and is almost insoluble in water (Lim, 2017). In 1973, PET bottles were patented

by engineer Nathaniel Wyeth, and since then they quickly found their application in the marketplace and become a dominant option as beverage containers. In our daily lives, the most consumed PET in packaging is semi-crystalline. As mentioned before, the highly crystalline areas are nearly completely resistant to enzymatic hydrolysis. The degradation occurs most likely in amorphous and low crystalline areas that are accessible to enzymatic attachment (Webb et al., 2013).

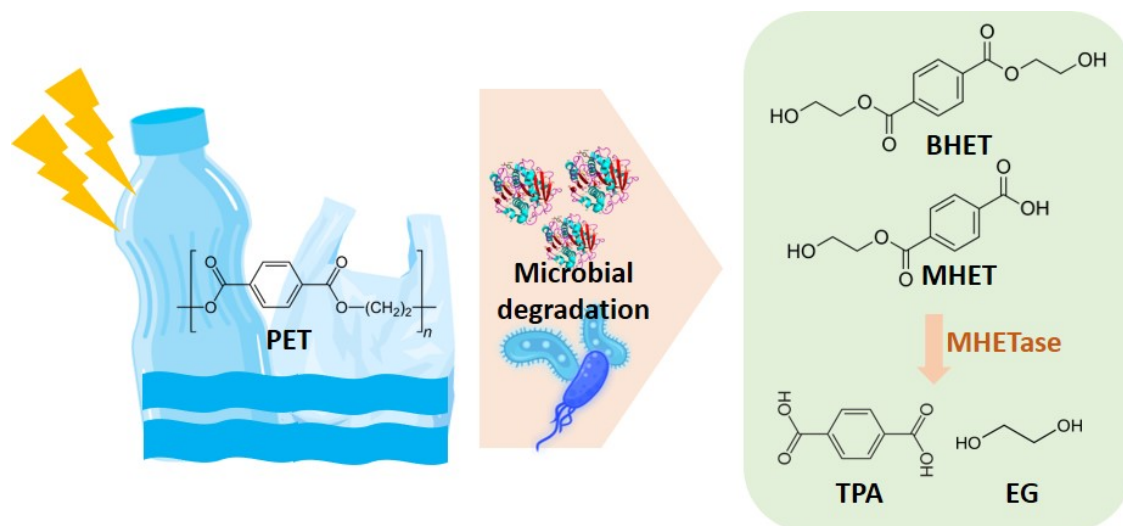


Figure 1: Graphical overview of microbial degradation of PET. Bacteria or enzymes act on the surface of PET polymer and transform it to its intermediates BHET or MHET. MHET can be further metabolized by microorganisms. PET, polyethylene terephthalate; BHET, bis(2-hydroxyethyl) terephthalic acid; MHET, mono(2-hydroxyethyl) terephthalic acid; MHETase, MHET hydrolase; TPA, terephthalic acid; EG, ethylene glycol.

Currently, the mechanism of PET degradation is still being investigated further. Due to its physical properties and large molecular mass ($30 - 80 \text{ kg mol}^{-1}$), it is believed that the enzymes have to be secreted into the environment to act on PET that is too large to be transported into the cell (Awaja und Pavel, 2005; Zhang et al., 2022b). These so-called extracellular enzymes hydrolyze the surface of PET and release smaller intermediates such as mono-(2-hydroxyethyl) terephthalate (MHET) and TPA, which can be imported into the cell for further metabolism (Mueller, 2006; Zhang et al., 2022b) (Figure 1).

In 2016, the first complete *in vivo* hydrolysis pathway of PET was described by Yoshida et al. (Yoshida et al., 2016). Through a two-step process, two enzymes, a PETase and a MHETase from the bacterium *Ideonella sakaiensis* were able to degrade

PET completely. The bacteria uses PETase to partially hydrolyze the PET into MHET, which is a major intermediate of PET hydrolysis. Then, a MHETase break down MHET further into TPA and EG that are transported into the cell for metabolism (Yoshida et al., 2016).

1.2.2 Known PET-degrading hydrolases (PETase)

PET-degrading hydrolase (PETase; EC 3.1.1.101) represents an enzyme class that hydrolyzes the ester bond of PET polymer and releases its oligomers (BHET and MHET) and / or monomers (TPA and EG). The first PETase was reported by Yoshida et al. and only a handful of the representative enzymes have been classified to this class in the BRENDA database (<https://www.brenda-enzymes.org/enzyme.php?ecno=3.1.1.101>). Before the discovery of the IsPETase (PETase from *Ideonella sakaiensis*), other types of PET-active enzymes have been studied, and these include for example cutinases (EC 3.1.1.74), esterases (EC 3.1.1.1), and lipases (EC 3.1.1.3) (Müller et al., 2005; Kleeberg et al., 2005; Ribitsch et al., 2015; Zheng et al., 2005; Araújo et al., 2007).

In the last two decades, a few phyla of bacteria and fungi have been demonstrated to harbor enzymes capable of breaking down PET. Although researchers envisioned that enzymes from Archaea might be able to contribute to the PET degradation, these enzymes have yet to be experimentally identified (Danso et al., 2018). The best-characterized enzymes are the previously mentioned IsPETase that is affiliated with Proteobacteria (Yoshida et al., 2016), LCC derived from a leaf branch compost metagenome (Schmidt et al., 2017; Taniguchi et al., 2019) and the cutinases from *Thermobifida* species (Roth et al., 2014; Hegde und Veeranki, 2013; Ribitsch et al., 2017) which are all affiliated with Actinobacteria. In addition, results published in recent studies showed that *Candida antarctica* CalB (Carniel et al., 2017) and *Fusarium oxysporum* FsC are also able to degrade PET. While some enzymes have rather low degradation rates, Ronkvist et al. reported a highly active and thermostable enzyme designated HiC isolated from *Humicola insolens*. HiC could fully break down amorphous PET within 96 hours at 70°C (Ronkvist et al., 2009). Thermostable enzymes perform

mostly a better hydrolytic activity towards PET, as their optimal temperatures are close to the glass transition temperature (T_g) of PET, at which the amorphous regions become more accessible to enzymatic attack (Alves et al., 2002). The effect of the enzyme thermostability benefiting hydrolysis efficiency was observed among the other PET-active enzymes, such as the above-mentioned metagenome-derived LCC and PET2 (Danso et al., 2018; Schmidt et al., 2017). Therefore, protein engineering intends to enhance the thermostability of PETases to achieve better enzymatic performance. A recently published study showed that an engineered LCC was able to decompose PET into monomers within 10 hours, outperforming all PET-active enzymes identified to date (Tournier et al., 2020).

While it is true that we have a better understanding of the enzymes involved in the degradation of PET in comparison with other fossil-based polymers, it appears that PET degradation is only limited to a few bacterial phyla. Despite the BsEstB from Bacillota (Ribitsch et al., 2011) and the metagenome-derived PET2 (Danso et al., 2018), all the functionally identified bacterial enzymes are phylogenetically affiliated with Actinobacteria and Proteobacteria (as of January 2022). Remarkably, Danso et al. identified that the Bacteroidetes phylum is the most potential host providing PET-degrading enzyme candidates. These enzymes hits are dominant in the marine metagenome sequences (Danso et al., 2018, 2019). Unfortunately, none of these enzymes has been functionally verified and identified about their affiliation with the PET degradation. It is noteworthy that the Bacteroidetes phylum can be found in nearly all ecological niches (Wexler, 2007; Krieg et al., 2015; Hahnke et al., 2016; Munoz et al., 2016) and has been reported as highly effective degraders of a variety of polymers (Foley et al., 2016; Thomas et al., 2011; Church, 2008).

In the present work, we were able to identify two novel PET-active enzymes, PET27 and PET30, that are affiliated with two genera of Bacteroidetes, *Aequorivita* and *Kaistella* respectively. Furthermore, the global distribution search showed that their homologs can be found in the marine environment through a wide range of climate zones (Zhang et al., 2022a).

1.3 Mining for novel PET-degrading enzymes

The search for enzymes that are able to break down synthetic polymers is a very demanding task that requires a combination of different strategies. In general, there are no pre-described strict standards for the screening methods. Most past studies that aimed to identify plastic-active microorganisms used enrichment techniques, where the defined medium, cultivation conditions and present carbon sources are given. Thereby, weight losses or surface changes of plastic materials are often implanted as an indicator of the degradation activity. However, the taxonomic diversity of PET-active enzymes and microorganisms is very limited (Barth et al., 2015; Kale et al., 2015; Kawai et al., 2014; Pérez-García et al., 2021; Danso et al., 2018) considering that over 99% of the microbes are not cultivable under laboratory conditions (Mora et al., 2011).

Studies revealed that the marine environment serves as a potential habitat for bacteria that are able to produce unique metabolites, such as enzymes, antibiotics as well as antiviral and anticancer chemicals (Laurila-Pant et al., 2015; Cragg und Newman, 2013; Li et al., 2012). The main obstacle to the optimal use of this potential is the difficulty in cultivating the majority of microbial species in an artificial culture medium due to their extremely specific growth requirements (Zengler et al., 2002). Therefore, function-based metagenomic approaches provide a possibility to overcome this obstacle and to utilize the various environmental sources for enzyme discovery without cultivating individual microbes (Streit und Schmitz, 2004). Different screening methods were developed depending on the desired properties and functions of an enzyme (Steele et al., 2009; Ferrer et al., 2016; Pérez-García et al., 2021). Danso et al. applied a well-designed HMM profile based on known PET-active enzymes and successfully identified multiple promising PET-active enzyme candidates, some of which have been verified experimentally (Danso et al., 2018, 2019). Still, the heterogeneous expression in appropriate hosts is the foundation of practically all of the functional screening techniques. *E. coli* combined with specifically designed plasmids is the most used expression system (Charles et al., 2017), which sometimes can only achieve a low production rate of the enzymes. To facilitate the metagenomic strategies, advanced approaches based on *in vitro* expression

system have been developed for the high-throughput screening (Markel et al., 2020). Given a huge amount of accessible sequencing resources such as IMG, UniProt or NCBI, the metagenomic screening method should be able to deliver new biodiversity of this rare PET-degrading enzyme.

For assessment of the PET degradation, PET substrates from different origins in the form of powder or thin foils are often used and combined with the high-pressure liquid chromatography technique (HPLC) for determining released breakdown products as a result of enzymatic activity (Danso et al., 2018; Bollinger et al., 2020; Ronkvist et al., 2009; Herrero Acero et al., 2011; Zhang et al., 2022b). In addition, reporter strains based on fluorescent that act as bioindicators were developed. These approaches can sense degrading products released by enzymatic reactions and thus detect the degradation activity of enzymes of interest (Masaki et al., 2005; Wei et al., 2012; Chaves et al., 2018; Bayer et al., 2022; Dierkes et al., 2023). While these methods are rather sophisticated, several other assays using indicator plates enable a primary assessment of the degradation ability of microorganisms or enzymes. In this case, model substrates or plastic nanoparticles are supplemented in agar plates and used as indicators. Alterations in the clearance of the plates imply that the hydrolytic activity is occurring (Welzel et al., 2002; Wei et al., 2014).

1.4 Aim of this study

The main goal of this work was to achieve a better understanding of the microbial degradation of PET in general and to expand the biodiversity of the PET-active enzymes. Therefore, about thirty gene candidates encoding putative PET-active enzymes were identified using a specific HMM-based search and were synthesized or cloned into suitable expression vectors. Their activity on various substrates and biochemical characteristics were experimentally investigated. In addition, enrichment techniques were implanted to isolate microorganisms capable of acting on PET plastics.

In order to obtain a detailed insight into the enzymatic mechanisms of the identified PET-degrading enzymes, the crystal structures were elucidated and analyzed.

Additionally, the global distribution of homologs of the bacteroidetal enzymes was investigated to attain an initial understanding of their possible role in reducing plastic pollution in our environment.

By combining various approaches such as enrichment cultures, bioinformatic analysis, biochemical characterization and functional screening methods, novel PET-degrading enzymes have been identified and studied in detail. With this, the present work will contribute to understanding of the PET degradation in general and advance our knowledge of this rare but crucial enzyme.

2 The Bacteroidetes *Aequorivita sp.* and *Kaistella jeonii* produce promiscuous esterases with PET-hydrolyzing activity

Hongli Zhang¹, Pablo Perez-Garcia^{1,2}, Robert F. Dierkes¹, Violetta Applegate³, Julia Schumacher³, Cynthia Maria Chibani², Stefanie Sternagel⁴, Lena Preuss¹, Sebastian Weigert⁵, Christel Schmeisser¹, Dominik Danso¹, Juergen Pleiss⁶, Alexandre Almeida^{7,8}, Birte Höcker⁵, Steven J. Hallam^{4,9,10,11,12}, Ruth A. Schmitz², Sander H. J. Smits^{3,13}, Jennifer Chow¹ and Wolfgang R. Streit^{1*}

¹Department of Microbiology and Biotechnology, University of Hamburg, Hamburg, Germany, ² Molecular Microbiology, Institute for General Microbiology, Kiel University, Kiel, Germany, ³ Center for Structural Studies, Heinrich-Heine-University, Düsseldorf, Germany, ⁴ Department of Microbiology and Immunology, University of British Columbia, Vancouver, BC, Canada, ⁵ Department of Biochemistry, University of Bayreuth, Bayreuth, Germany, ⁶ Institute of Biochemistry and Technical Biochemistry, University of Stuttgart, Stuttgart, Germany, ⁷ European Bioinformatics Institute (EMBL-EBI), Hinxton, United Kingdom, ⁸ Wellcome Sanger Institute, Hinxton, United Kingdom, ⁹ Graduate Program in Bioinformatics, University of British Columbia, Vancouver, BC, Canada, ¹⁰ Genome Science and Technology Program, University of British Columbia, Vancouver, BC, Canada, ¹¹ Life Sciences Institute, University of British Columbia, Vancouver, BC, Canada, ¹² ECOSCOPE Training Program, University of British Columbia, Vancouver, BC, Canada, ¹³ Institute of Biochemistry, Heinrich-Heine-University, Düsseldorf, Germany

Published in:

Proteins: Structure, Function, and Bioinformatics doi: 10.3389/fmichb.2021.803896



The Bacteroidetes *Aequorivita* sp. and *Kaistella jeonii* Produce Promiscuous Esterases With PET-Hydrolyzing Activity

Hongli Zhang¹, Pablo Perez-Garcia^{1,2}, Robert F. Dierkes¹, Violetta Applegate³, Julia Schumacher³, Cynthia Maria Chibani², Stefanie Sternagel⁴, Lena Preuss¹, Sebastian Weigert⁵, Christel Schmeisser¹, Dominik Danso¹, Juergen Pleiss⁶, Alexandre Almeida^{7,8}, Birte Höcker⁵, Steven J. Hallam^{4,9,10,11,12}, Ruth A. Schmitz², Sander H. J. Smits^{3,13}, Jennifer Chow¹ and Wolfgang R. Streit^{1*}

OPEN ACCESS

Edited by:

Kian Mau Goh,
University of Technology Malaysia,
Malaysia

Reviewed by:

Fusako Kawai,
Okayama University Japan, Japan
Lukasz Jaroszewski,
University of California, Riverside,
United States
Alessandro Pellis,
University of Genoa, Italy

*Correspondence:

Wolfgang R. Streit
wolfgang.streit@uni-hamburg.de

Specialty section:

This article was submitted to
Microbiotechnology,
a section of the journal
Frontiers in Microbiology

Received: 28 October 2021

Accepted: 22 November 2021

Published: 05 January 2022

Citation:

Zhang H, Perez-Garcia P,
Dierkes RF, Applegate V,
Schumacher J, Chibani CM,
Sternagel S, Preuss L, Weigert S,
Schmeisser C, Danso D, Pleiss J,
Almeida A, Höcker B, Hallam SJ,
Schmitz RA, Smits SHJ, Chow J and
Streit WR (2022) The Bacteroidetes
Aequorivita sp. and *Kaistella jeonii*
Produce Promiscuous Esterases With
PET-Hydrolyzing Activity.
Front. Microbiol. 12:803896.
doi: 10.3389/fmicb.2021.803896

¹ Department of Microbiology and Biotechnology, University of Hamburg, Hamburg, Germany, ² Molecular Microbiology, Institute for General Microbiology, Kiel University, Kiel, Germany, ³ Center for Structural Studies, Heinrich-Heine-University, Düsseldorf, Germany, ⁴ Department of Microbiology and Immunology, University of British Columbia, Vancouver, BC, Canada, ⁵ Department of Biochemistry, University of Bayreuth, Bayreuth, Germany, ⁶ Institute of Biochemistry and Technical Biochemistry, University of Stuttgart, Stuttgart, Germany, ⁷ European Bioinformatics Institute (EMBL-EBI), Hinxton, United Kingdom, ⁸ Wellcome Sanger Institute, Hinxton, United Kingdom, ⁹ Graduate Program in Bioinformatics, University of British Columbia, Vancouver, BC, Canada, ¹⁰ Genome Science and Technology Program, University of British Columbia, Vancouver, BC, Canada, ¹¹ Life Sciences Institute, University of British Columbia, Vancouver, BC, Canada, ¹² ECOSCOPE Training Program, University of British Columbia, Vancouver, BC, Canada, ¹³ Institute of Biochemistry, Heinrich-Heine-University, Düsseldorf, Germany

Certain members of the Actinobacteria and Proteobacteria are known to degrade polyethylene terephthalate (PET). Here, we describe the first functional PET-active enzymes from the Bacteroidetes phylum. Using a PETase-specific Hidden-Markov-Model- (HMM-) based search algorithm, we identified several PETase candidates from Flavobacteriaceae and Porphyromonadaceae. Among them, two promiscuous and cold-active esterases derived from *Aequorivita* sp. (PET27) and *Kaistella jeonii* (PET30) showed depolymerizing activity on polycaprolactone (PCL), amorphous PET foil and on the polyester polyurethane Impranil®DLN. PET27 is a 37.8 kDa enzyme that released an average of 174.4 nmol terephthalic acid (TPA) after 120 h at 30°C from a 7 mg PET foil platelet in a 200 µl reaction volume, 38-times more than PET30 (37.4 kDa) released under the same conditions. The crystal structure of PET30 without its C-terminal Por-domain (PET30ΔPorC) was solved at 2.1 Å and displays high structural similarity to the *Is*PETase. PET30 shows a Phe-Met-Tyr substrate binding motif, which seems to be a unique feature, as *Is*PETase, LCC and PET2 all contain Tyr-Met-Trp binding residues, while PET27 possesses a Phe-Met-Trp motif that is identical to Cut190. Microscopic analyses showed that *K. jeonii* cells are indeed able to bind on and colonize PET surfaces after a few days of incubation. Homologs of PET27 and PET30 were detected in metagenomes, predominantly aquatic habitats, encompassing a wide range of different global climate zones and suggesting a hitherto unknown influence of this bacterial phylum on man-made polymer degradation.

Keywords: metagenomics, metagenomic screening, PET degradation, polyethylene terephthalate (PET), PETase, Bacteroidetes, Flavobacteriaceae

INTRODUCTION

PET is one of the major plastic pollutants found in landfills, oceans and other environments (Jambeck et al., 2015; Geyer et al., 2017). Our knowledge of microbial degradation of most plastics is rather limited, but recent research has demonstrated that some bacteria are able to degrade PET (Yoshida et al., 2016). Although it is unclear if larger crystalline fibers are degraded by bacteria, it is well known that some cutinases (EC 3.1.1.74), lipases (EC 3.1.1.3) and carboxylesterases (EC 3.1.1.1) can act on amorphous and low crystalline PET. These enzymes, often referred to as “PETases,” cleave the ester bond of the polymer to either produce bis-(2-hydroxyethyl) terephthalate (BHET), mono-hydroxyethyl terephthalate (MHET) or they complete degradation to terephthalic acid (TPA) and ethylene glycol (EG). TPA monomers can be further degraded via cleavage of the aromatic ring structure using known aryl pathways and can then enter the β -ketoacid pathway (Wei and Zimmermann, 2017; Danso et al., 2019; Wright et al., 2021).

To date, only a limited number of bacterial and fungal species have been identified that are capable of breaking down PET to either its oligomers or monomers, TPA and EG. Most bacterial isolates with verified enzymatic PET-degrading activity are affiliated with the Gram-positive phylum Actinobacteria (Acero et al., 2011). The best characterized examples belong to the genera *Thermobifida* or *Thermomonospora* (Kleeberg et al., 1998; Chen et al., 2008; Hu et al., 2010; Acero et al., 2011; Ribitsch et al., 2012; Wei et al., 2014). Further, the leaf compost-derived cutinase LCC is closely related to Actinobacterial enzymes and is currently one of the best described and most active PETases (Sulaiman et al., 2012, 2014). Regarding Proteobacteria, the Gram-negative Betaproteobacterium *Ideonella sakaiensis* 201-F6 is capable of using amorphous PET as a major energy and carbon source (Yoshida et al., 2016). *I. sakaiensis*' genome also encodes a tannase which is designated MHETase as it is capable of degrading MHET. Besides, a number of other PETases affiliated with the Proteobacteria have been identified originating from e.g., *Pseudomonas aestusnigri* and *Vibrio gazogenes* (Ronkvist et al., 2009; Haernvall et al., 2017; Danso et al., 2018; Bollinger et al., 2020).

In a previous study, we identified potential PET esterases affiliated with the Bacteroidetes phylum using HMM profile database searches (Danso et al., 2018, 2019). These enzyme hits mainly occurred in metagenomes and genomes from marine environments and were annotated solely on the basis of homology. However, their enzymatic function and environmental distributions have not been studied within that framework, and we target these questions in the present study. Bacteroidetes representatives can be found in nearly all ecological niches including soils, oceans and fresh water and are part of the microbiome of many animals, especially as inhabitants of the intestinal tract (Wexler, 2007; Krieg et al., 2015; Hahnke et al., 2016; Munoz et al., 2016). The Bacteroidetes phylum, however, is highly heterogeneous and contains at least four classes of bacteria (e.g., Bacteroidia, Flavobacteria, Sphingobacteria, and Cytophagia), with each class having several thousand described species. The phylum contains non-spore forming and rod shaped

microorganisms, some aerobic, but often anaerobic, with an enormous metabolic diversity (Krieg et al., 2015). The global distribution of Bacteroidetes representatives is likely due to their ability to decompose a very wide variety of bio-based polymers such as cellulose, chitin or algal cell walls. In particular, the decomposition of polysaccharides (cellulose and hemicellulose) by Bacteroidetes inhabiting the intestinal tract of humans and animals has been well-studied in gut microbiome research (Thomas et al., 2011).

Here, we provide the first experimental evidence that different Bacteroidetes representatives have evolved promiscuous esterases that degrade the PET polymer. We show that at least two Bacteroidetes genera, *Aequorivita* and *Kaistella* (formerly *Chryseobacterium*), harbor PET-active enzymes and elucidated the crystal structure of PET30. These enzymes have relatively low turnover rates, indicating that PET hydrolysis may be a side reaction. Still, given their abundance and diversity, we speculate that the described bacteroidetal PET-active enzymes could have considerable impact on long-term degradation of PET in the marine environment.

MATERIALS AND METHODS

Bacterial Strains, Plasmids, and Primers

Bacterial strains, plasmids and primers used in this study are listed in **Supplementary Tables 1, 2**. If not mentioned otherwise, *Escherichia coli* clones were grown in LB medium (1% tryptone/peptone, 0.5% yeast extract, 1% NaCl) supplemented with appropriate antibiotics (25 μ g/ml kanamycin, or 100 μ g/ml ampicillin) at 37°C for 18 h.

Databases Used in This Study and Bioinformatic Analyses

Nucleotide and amino acid sequences of putative and confirmed PETases were acquired from databases integrated into the NCBI¹, UniProt² and IMG (JGI)³ servers (Markowitz et al., 2012; NCBI Resource Coordinators, 2017; The UniProt Consortium, 2017). Human gut sequences were retrieved from the Unified Human Gastrointestinal Protein (UHGP) catalog (PMID: 32690973). Sequences were compared to others deposited in the NCBI databases using BLAST alignment tools (Agarwala et al., 2016). Amino acid sequence HMM search was carried out using the HMMER⁴ webpage or a local version of the software (v3.1b2) (Mistry et al., 2013) with downloaded datasets. Structural information on the enzymes was retrieved from the RCSB-PDB (Berman et al., 2000) database.

Sequence data were processed and analyzed using ChromasPro 2.1.8 (Technelysium, Brisbane Australia) or SnapGene (GSL Biotech LLC, San Diego CA, United States). Amino acid alignment was constructed using structural alignments with T-Coffee (Notredame et al., 2000) and was

¹<https://www.ncbi.nlm.nih.gov/>

²<http://www.uniprot.org/>

³<http://jgi.doe.gov/>

⁴<http://hmmer.org>

TABLE 1 | Key traits of predicted bacteroidetal PET esterases.

Predicted PETase	GenBank entry/MGY identifier	Phylogenetic Affiliation	aa/MW (kDa)	Derived from	Expression level/solubility	Active on						
						pNP-C6/-C10	TBT	Impranil® DLN	PCL	BHET	PET-foil	PET particles
PET27	WP_111881932	<i>Aequorivita</i> sp. CIP111184	364/37.8	Antarctic source (Li et al., 2017)	High/majority in inclusion bodies	+	+	+	+	+	+	+
PET28	WP_073216622	<i>Aequorivita viscosa</i>	365/38.3	Seaweed (Li et al., 2017)	High/majority in inclusion bodies	+	+	+	+	+	-	-
PET29	WP_052671284	<i>Aequorivita vladivostokensis</i>	365/39.3	Troitsa bay, Sea of Japan (Li et al., 2017)	High/majority in inclusion bodies	+	+	+	+	+	-	-
PET30	WP_039353427	<i>Kaistella jeonii</i>	366/37.4	Antarctic moss (Li et al., 2017)	High/majority soluble	+	+	+	+	+	+	+
PET38	WP_083900582.1/GCA_000194605.1	<i>Fluviicola taffensis</i>	447/40.4	River, United Kingdom (Woyke et al., 2011)	Low	-	-	N.D.	-	-	-	-
PET53	k99_709705_13	<i>Aequorivita</i> sp.	294/37.8	Marine aquaculture fish tank metagenome/unpublished data University of Hamburg	Low	-	-	N.D.	-	N.D.	N.D.	N.D.
PET57	GUT_GENOME137663_00143	<i>Porphyromonas</i> sp.	323/36.3	Human gut (Mitchell et al., 2019; Almeida et al., 2021)	High/majority soluble	-	-	+	+	N.D.	N.D.	N.D.
PET58	GUT_GENOME065712_01381	<i>Porphyromonas bennonis</i>	338/37.6	Human gut (Mitchell et al., 2019; Almeida et al., 2021)	High/majority in inclusion bodies	-	-	-	+	N.D.	N.D.	N.D.
PET59	GUT_GENOME243617_00165	<i>Porphyromonas</i> sp.	345/38.4	Human gut (Mitchell et al., 2019; Almeida et al., 2021)	High/majority soluble	-	-	-	+	N.D.	N.D.	N.D.

TBT, tributyrin; BHET, bis-(2-hydroxyethyl) terephthalate; PCL, polycaprolactonate; pNP-C6/C10, para-nitrophenyl esters with chain length C6 or C10; aa, amino acids; MW, molecular weight. N.D. not determined. +, active; -, not active.
 PET57-59 were extracted from the gut genomes available at: <https://www.ebi.ac.uk/metagenomics/genomes/MGYG-HGUT-01059> (PET57); <https://www.ebi.ac.uk/metagenomics/genomes/MGYG-HGUT-01060> (PET58) and <https://www.ebi.ac.uk/metagenomics/genomes/MGYG-HGUT-00764> (PET59).

further visualized with Bioedit (Hall, 1999). The model structures of bacteroidetal PETase-candidates were modeled with the Robetta server (Kim et al., 2004) using the IsPETase crystal structure (6EQE) as a backbone. A phylogenetic tree was constructed using the RAxML-NG autoMRE algorithm (Kozlov et al., 2019) with the treesapp create command implemented in TreeSAPP (Morgan-Lang et al., 2020) with maximum bootstraps set at 1,000. RAxML-MG has recently been shown to return the best scoring tree for highest number of datasets when compared against other fast maximum likelihood (ML) methods (Kozlov et al., 2019), allowing a large number of maximum bootstraps to be used to produce as conservative a tree as possible. Sequences were assigned NCBI lineages according to source organisms listed in **Table 1** and **Supplementary Table 3**, and colors were assigned to the tree at the phylum level using the treesapp color command. The tree was visualized in iTOL (Letunic and Bork, 2019).

Scanning IMG/M was completed on 19/November/2020 for PET30 and on 14/January/2021 for PET27. Geo locations were used as provided whenever available. In case no Geo location was available, whenever possible, information about isolation source/location/city/country were used to look up Geo coordinates on GeoHack.⁵ The map representing the frequency and geographical distribution of PET hydrolases in metagenomes (**Figure 1**) was constructed using QGIS Desktop 2.18.5⁶.

Heterologous Expression of Putative Polyethylene Terephthalate Esterase Genes in *Escherichia coli* BL21 (DE3)

The putative PETases were extracted from metagenomic datasets (**Table 1**), therefore the gene sequences were optimized for expression in *E. coli* and synthesized into pET21a(+) vector at Biomatik (Wilmington, United States). The obtained constructs were sequenced at Microsynth Seqlab GmbH (Goettingen, Germany) and checked for correctness by comparing to the original sequences. *E. coli* T7-Shuffle or *E. coli* BL21 (DE3) cells were used for heterologous expression of possible PETases. The IsPETase gene in pMAL-p4x was expressed in *E. coli* BL21 and purified by its maltose-binding tag. The cultures were grown aerobically in auto-induction medium (ZYM-5052) (Studier, 2005) containing 100 µg/ml ampicillin at 37°C until they reached an OD₆₀₀ of 1.0. The proteins were expressed afterward at 22°C for 16–20 h. The cells were harvested and lysed with pressure using a French press. Afterward, the proteins harboring a sixfold C-terminal histidine tag were purified with nickel-ion affinity chromatography using Ni-NTA agarose (Qiagen, Hilden, Germany) and analyzed by SDS-PAGE. The elution buffer was exchanged against 0.1 mM potassium phosphate buffer pH 8.0 in a 10 kDa Amicon Tube (GE Health Care, Solingen, Germany).

Biochemical Characterization of PET27 and PET30

For activity tests, both enzymes were assayed using purified recombinant protein. bis-(2-hydroxyethyl) terephthalate (BHET)

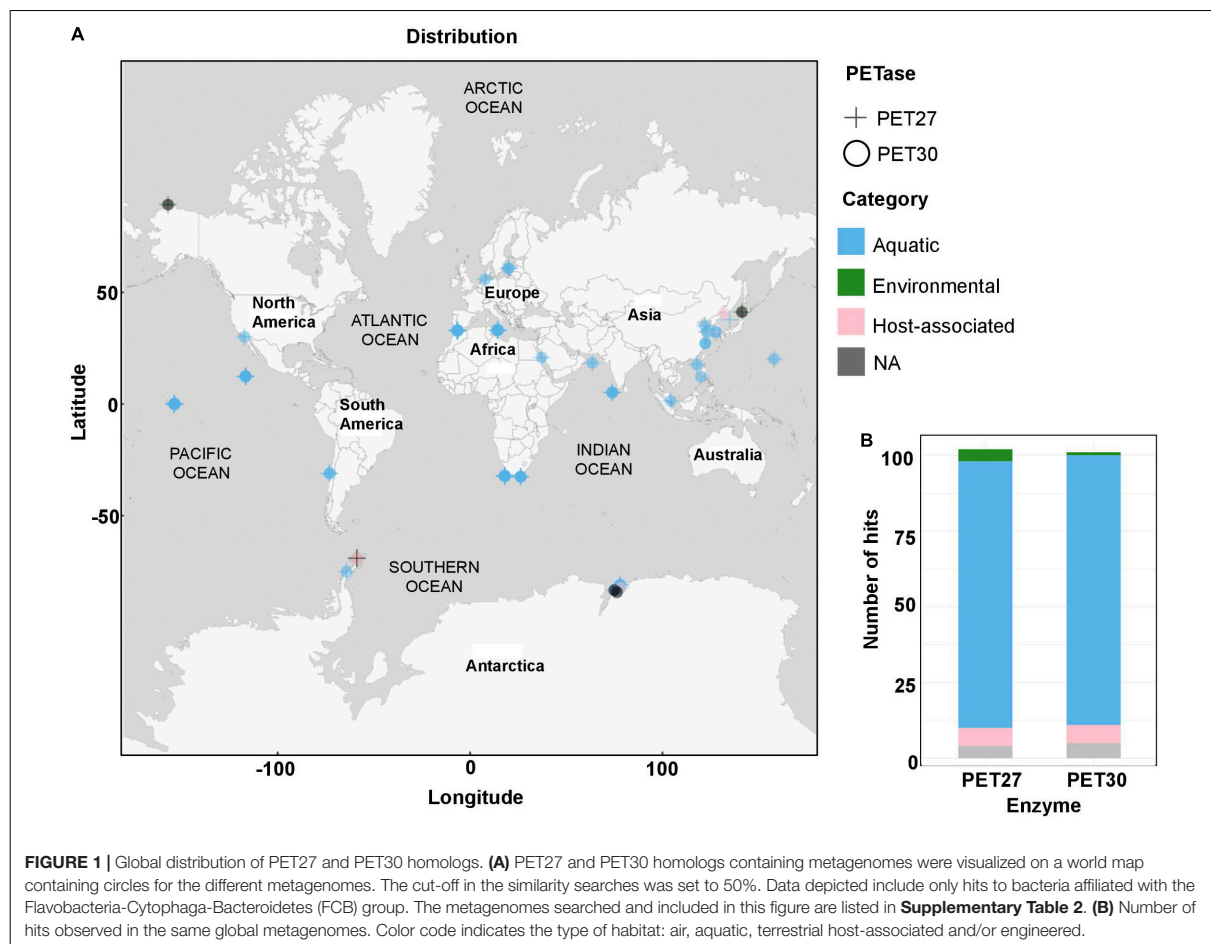
and polycaprolactone (PCL) agar plates were prepared as described elsewhere (Pérez-García et al., 2021). The polyester polyurethane Impranil DLN containing LB agar plates were prepared according to Molitor et al. (2020) with LB medium. For the pNP-assay, unless otherwise indicated, a total amount of 0.1–1 µg of the enzymes were added to a substrate solution containing 190 µl of either 0.2 M sodium phosphate buffer or 0.1 M potassium phosphate with a defined pH between 7 and 8 and 10 µl of 0.1 mM pNP-substrate dissolved in isopropanol. After incubating the samples for 10 min, the assay was stopped by adding 200 mM of Na₂CO₃. Afterward, the samples were centrifuged at 4°C, 13,000 rpm for 3 min. As substrates, pNP-esters with chain lengths of C4, C6, C8, C10, C12, C14, C16 and C18 were tested. After incubation at defined temperatures, the color change from colorless to yellow was measured at 405 nm in a plate reader (Biotek, Winooski, United States). All samples were measured in triplicate. To determine the optimal temperature, samples were incubated between 10 and 90°C for 10 min. The influence of pH conditions on the activity of each enzyme was measured in citrate phosphate (pH 3.0, 4.0, and 5.0), potassium phosphate (pH 6.0, 7.0, and 8.0) and carbonate bicarbonate buffer (pH 9.2 and 10.2). The impact of cofactors, solvents, detergents, and inhibitors was assayed at different concentration levels. The possible cofactors Ca²⁺, Co²⁺, Cu²⁺, Fe³⁺, Mg²⁺, Mn²⁺, Rb²⁺, and Zn²⁺ with a final concentration of 1 and 10 mM were used. Detergent stability was assayed with sodium dodecyl sulfate (SDS), Triton X-100 and Tween 80 at 1 and 5% (w/v, v/v) concentration. The inhibitory effect of ethylenediaminetetraacetic acid (EDTA), dithiothreitol (DTT) and phenylmethanesulfonyl fluoride (PMSF) was tested at 1 and 10 mM concentration. After 1 h incubation in the presence of these substances, the residual activity was determined after 10 min incubation at the optimal temperature with *para*-nitrophenol- (pNP-) C6 and at the optimal pH.

For the verification of enzymatic PET hydrolysis, a 7 mg platelet (Ø 5 mm) of low-crystallinity PET film (Goodfellow GmbH, Bad Nauheim, Germany), which corresponds to 36.4 µmol of the terephthalic acid-ethylene glycol (TPA-EG) unit, was folded in half and used as substrate together with 200 µg of enzyme in 200 µl of 100 mM potassium phosphate buffer at pH 8.0. Incubation was carried out under continuous shaking at 400 rpm in 1.5 ml microcentrifuge tubes at 30°C, if not stated otherwise.

Analysis of breakdown products was performed with an UltiMate™ 3000 UHPLC system from Thermo Fisher Scientific (Waltham, MA, United States) using a Triart C18 column (YMC Europe GmbH, Dinslaken, Germany) with a dimension of 100 × 2.0 mm containing particles with 1.9 µm diameter. Isocratic elution was performed using a mobile phase consisting of 20:80 (v/v) acetonitrile and water (acidified with 0.1% vol trifluoroacetic acid) at a flowrate of 0.4 ml min⁻¹. UHPLC samples were prepared by mixing 50 µl of incubation supernatant with 200 µl acetonitrile (acidified with 1% vol trifluoroacetic acid), followed by centrifugation at 10,000 × g for 3 min and transferring 200 µl of the supernatant into 600 µl water. Fifteen microliter of sample were injected per measurement and detection was performed at 254 nm with a VWD-3400

⁵<https://geohack.toolforge.org>

⁶<http://www.qgis.org>



detector from Thermo Scientific (Waltham, MA, United States). The UHPLC profiles were plotted and edited using the software MATLAB version R2020b [The MathWorks, Inc., Natick, MA, United States (Matlab, 2012)]. Quantification of peak areas was performed using data analysis software supplied with the Compass HyStar software package from Bruker (Billerica, MA, United States).

Crystallization and Data Collection

Crystallization of PET30 Δ PorC was achieved by sitting-drop vapor-diffusion at 12°C. 0.2 μ l of 10.2 mg/ml PET30 Δ PorC in 100 mM phosphate buffer pH 8.0 and 0.1 μ l reservoir solution consisting of 0.1 M sodium acetate pH 4.6 and 25% (w/v) PEG 4000 were mixed. This drop was equilibrated against reservoir solution and crystals formed after several weeks. Crystallization drops were overlaid with mineral oil and the crystals were dragged through it for cryoprotection, flash frozen and diffraction data were collected at beamline P13 (DESY, Hamburg, Germany). The PET30 Δ PorC crystals had the space group P 4₃ 2₁ 2 and diffracted to 2.1 Å resolution.

Structure Determination

A complete data set of the PET30 Δ PorC was collected at beamline P13 (DESY, EMBL, Hamburg, Germany) at 100 K and wavelength 0.9795 Å up to 2.1 Å resolution. All data were processed using the automated pipeline at the EMBL HAMBURG and reprocessed afterward using XDS (Kabsch, 2014). The above obtained model for PET30 Δ PorC by TOPMODEL was successfully used to phase the 2.1 Å data set of PET30 Δ PorC using the PHASER program from the PHENIX program suite (Afonine et al., 2012; Mulnaes et al., 2020). The structure was then refined in iterative cycles of manual building and refinement in cool followed by software-based refinements using the program suite Phenix (Emsley and Cowtan, 2004; Liebschner et al., 2019). All residues were in the preferred and additionally allowed regions of the Ramachandran plot. The data collection and refinement statistics are listed in **Supplementary Table 4**. The images of the models were prepared using PyMOL (DeLano, 2002) and UCSF Chimera X.⁷ The structure was deposited at the worldwide protein data bank under the accession code 7PZJ.

⁷www.cgl.ucsf.edu/chimera

Confocal Laser Scanning Microscopy of Polyethylene Terephthalate Foil Platelets

The starter culture of *K. jeonii* was grown in R2A medium at 22°C and 130 rpm to a cell density of 0.2. 1% of the starter culture was inoculated into 30 ml fresh R2A medium and PET foil platelets were put into the cultures. PET platelets were removed after 5–7 days, washed three times with PBS and subsequently given into μ -Slide 8 wells plates from ibidi GmbH (Martinsried, Germany). Cells were stained using 100 μ l of LIVE/DEAD stain BacLight Viability Kit (Thermo Fisher Scientific). The stain is composed of propidium iodide (PI) dyeing dead cells with a damaged membrane and causing red fluorescence and green fluorescence SYTO 9™ dyeing all bacterial membranes of living cells. Therefore, 10 μ l PI and 10 μ l SYTO 9™ were mixed. 15 μ l of the nucleic acid-binding stains were pipetted into 5 ml PBS. The PET platelets were incubated for 1 h in the dark at room temperature. Afterward, the samples were investigated under the microscope Axio Observer Z1/7, LSM 800 using objective C-Apochromat 63x/1.20 W Korr UV VisIR (both Carl Zeiss Microscopy GmbH, Jena, Germany) using the Channels Syto 09 (528/20 nm emission wavelength) and PI (645/20 nm emission wavelength).

RESULTS

Profile Hidden Markov Model Searches Identify Potential Bacteroidetal PETases

Protein sequences from both genomes and metagenomes were screened using the previously described Hidden Markov Model (HMM) (Danso et al., 2018) to enrich the diversity of PET-active enzymes from Bacteroidetes. The global searches were performed in publicly available datasets of NCBI GenBank and additionally in several private datasets harboring human-associated and environmental Bacteroidetes sequences (Table 1). Searches were conducted from January until March 2019. This global search initially resulted in the identification of 37 potential PETase sequences from Bacteroidetes with a bit score above 298.7. After sequence comparison, nine distinct hits were chosen. These candidates belonged to bacteroidetal genomes originating from either Seaweed (Li et al., 2017), Antarctic moss (Li et al., 2017), river sediment (Woyke et al., 2011), an aquaculture (own unpublished dataset) or human gut microbiomes (Mitchell et al., 2019; Almeida et al., 2021; Table 1). Most of these candidates were affiliated with the Flavobacteriaceae genus *Aequorivita* sp. (PET27–29, PET31 and PET53). PET29 and PET31 were highly similar on amino acid level (< 98% identity) but differed in the length of their sequence by 10 amino acids (aa). PET30, annotated as a potential lipase, was derived from the published genome sequence of *Kaistella jeonii* NCTC 13459. The predicted PETases PET57–59 were derived from bacteria affiliated with the genus *Porphyromonas* sp. (Porphyromonadaceae), while the predicted enzyme PET38 was derived from the species *Fluviicola taffensis* (Cryomorphaceae).

Recombinant PET27 and PET30 Hydrolyze Polycaprolactone, Impranil®-DLN and Polyethylene Terephthalate Foil

The nine candidate genes of the predicted PETases were synthesized, cloned into the expression vector pET21a(+) (Biomatik, Wilmington, DA, United States) and transformed in *E. coli* BL21 and T7-Shuffle cells (Supplementary Table 1). Initial tests using recombinant purified proteins and tributyrin (TBT)-containing agar plates indicated that the genes PET27–30 coded for active esterases. The remaining enzymes PET38, PET53, PET57, and PET58 were inactive and were either produced as insoluble proteins and/or only at very low amounts (Table 1). Because of these obvious difficulties facing their expression, these four predicted enzymes were not further characterized. Additional tests with PET27–PET30 indicated that these enzymes hydrolyzed the esters *p*NP-hexanoate (C6), and *p*NP-decanoate (C10, Table 1). All four recombinant enzymes were able to hydrolyze the polymeric polycaprolactone (PCL), the PET-constituent BHET, and the polyester polyurethane Impranil®DLN (Covestro AG, Leverkusen, Germany) (Table 1 and Figure 2A). The enzymes produced clear halos on agar plates containing these substrates after overnight incubation at 30°C (Figure 2A and Table 1). PET-hydrolyzing activities were confirmed for the enzymes PET27 and PET30 on amorphous PET foil as substrate in a 200 μ l reaction volume by UHPLC analyses. In these tests, 1 mg ml⁻¹ PET27 released 871.8 \pm 200.4 μ M (corresponds to 174.4 \pm 40.0 nmol in 200 μ l reaction volume) of TPA in 120 h at 30°C from a 7 mg PET platelet. PET foil (7 mg) corresponds to 36.4 μ mol of a TPA-EG monomer unit (Figure 2B and Table 2). Surprisingly, under the same conditions, PET30 released only 15.9 \pm 9.5 μ M TPA (corresponds to 3.2 \pm 1.9 nmol; Figure 2C and Table 2). These results were directly benchmarked with recombinant *Is*PETase, of which 1 mg ml⁻¹ released under the same conditions 4,055.7 \pm 516.9 μ M of TPA (corresponds to 811.1 \pm 103.4 nmol). Thus, *Is*PETase is 4.7-fold more active compared to PET27 and approximately 253-fold more active compared to PET30. Because of the relatively low turnover rates observed for PET27 and PET30 on PET foil, it can be assumed that PET is not the preferred substrate of both enzymes.

Biochemical Characterization and Activity of PET27 and PET30 on Esterase Substrates

Both recombinant enzymes were characterized in more detail with *p*NP-esters. A substrate spectrum was recorded with *p*NP-esters, which had acyl chain lengths of 4–18 C-atoms. PET27 and PET30 revealed a relatively narrow spectrum of substrates they could hydrolyze. The highest activities were observed with *p*NP-hexanoate (-C6) for PET30 and *p*NP-octanoate (-C8) for PET27 (Figure 3A). The optimal temperature of PET30 is 30°C, but 80% activity was observed at 20°C and between 40 and 50°C (Figure 3B). In contrast to that, PET27 shows a better activity at higher temperatures with an optimum at 40°C and even 45% activity at 90°C. Surprisingly, at 10°C, both enzymes still showed

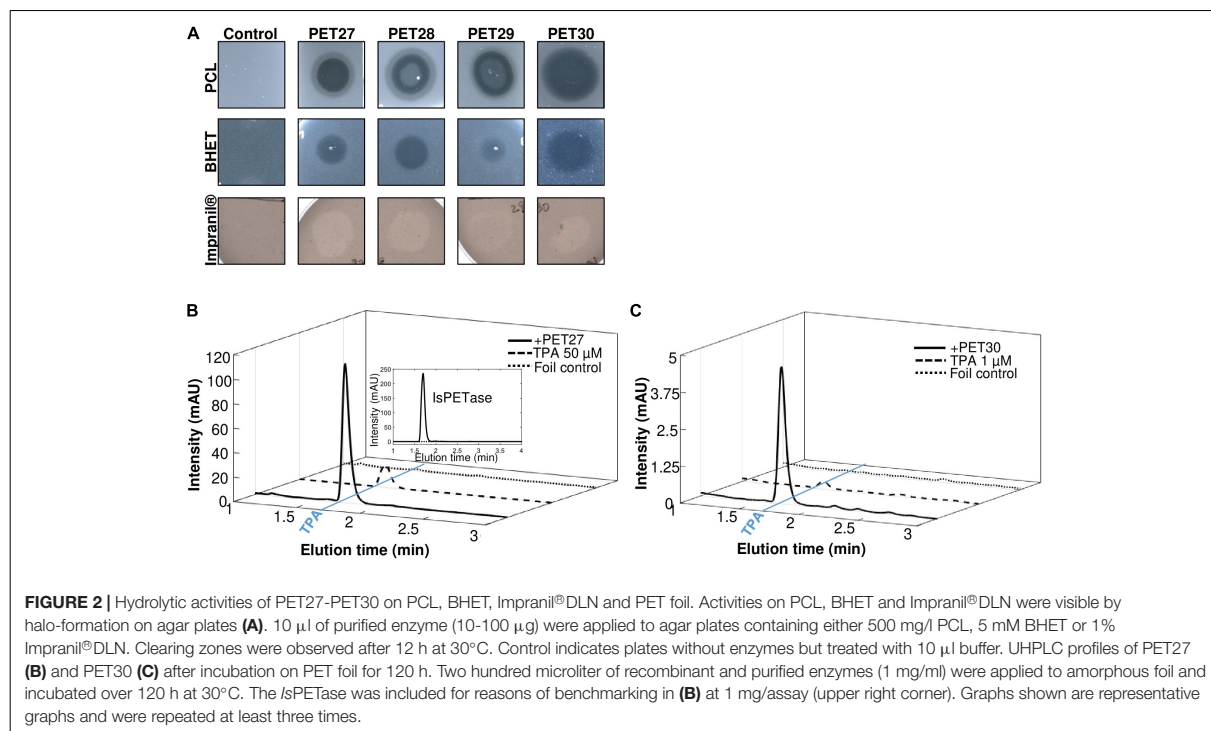


TABLE 2 | Amount of TPA released by different PET active enzymes.

Enzyme	Released TPA-EG unit			Av. weight loss of PET foil [%]
	[μ M]	[nmol]	[μ g]	
PET27	871.8 \pm 200.4	174.4 \pm 40.0	33.5 \pm 7.7	0.45
PET30	15.9 \pm 9.5	3.2 \pm 1.9	0.6 \pm 0.3	0.01
PET30 Δ PorC	23.3 \pm 9.2	4.7 \pm 1.8	0.9 \pm 0.3	0.01
<i>IsPETase</i>	4,055.7 \pm 516.9	811.1 \pm 103.4	155.8 \pm 19.9	2.23

The different recombinant and purified enzymes were incubated at a concentration of 1 mg ml⁻¹ for a time period of 120 h at 30°C. For the tests a circular piece of 7 mg PET foil which corresponds to 36.4 μ mol of the TPA-EG unit (\varnothing 5 mm, and as specified in section "Materials and Methods") was employed and folded once in the middle. Incubations were carried out in a reaction volume of 200 μ l. Data are mean values with standard deviations of a minimum of 3 and up to 6 measurements per sample.

a relative activity of 65% (PET30) and 73% (PET27). PET30 remained active at 4°C showing a relative activity of 42% on pNP-C6. Concerning the optimal pH, PET27 was most active between pH 7–8 and PET30 between pH 6–8 when tested in 0.1 M potassium phosphate (Figure 3C).

To further characterize the effects of metal ions, different ions (Ca²⁺, Co²⁺, Cu²⁺, Fe³⁺, Mg²⁺, Mn²⁺, Ni²⁺, and Zn²⁺) were added to the assays at 1 and 10 mM final concentrations. Metal ions have a minor influence on PET27. Addition of Ca²⁺ resulted in a 1.4-fold increase of the activity (Supplementary Figure 1A). In case of PET30, addition of Zn²⁺, Ni²⁺, and Co²⁺ resulted in an up to threefold increase of activity.

The kinetic parameters for PET27 and PET30 were determined with pNP-C6 at 30°C and pH 8 according to Michaelis-Menten. Thereby, PET27 revealed a v_{max} of 4.9 nmol min⁻¹, a k_{cat} of 19.08 s⁻¹, a K_m of 1.37 mM and a k_{cat}/K_m value

of 13,859.27 M⁻¹ s⁻¹. For PET30, we calculated a v_{max} of 2.3 nmol min⁻¹, a k_{cat} of 8.9 s⁻¹, a K_m of 0.3 mM and a k_{cat}/K_m value of 26,136.11 M⁻¹ s⁻¹.

Further, PET30 was investigated in more detail. To assess thermostability, the enzyme was incubated at 50 and 60°C for 3 h, after which the enzyme retained only 23 and 5% of its original activity, respectively (Supplementary Figure 1B). As inhibiting substances, EDTA, DTT and PMSF were applied in final concentrations of 1 and 10 mM (Supplementary Figure 1C). The presence of DTT and PMSF (1 and 10 mM) inactivated PET30 almost completely, whereas EDTA at 1 and 10 mM had no large impact on the enzyme's activity. A concentration of 1 and 5% of the detergents Triton X-100, Tween 80 and SDS decreased PET30's activities (Supplementary Figure 1D).

As both enzymes were active at lower temperatures, PET foil degradation was assayed at 4°C. Over a time of 30 days in

a 200 μ l reaction volume, TPA release was measured. Under these conditions, 1 mg ml⁻¹ of PET30 released an average of 6.1 μ M of TPA (corresponds to 1.2 nmol). Interestingly, *IsPETase* released under the same conditions a similar amount (5.9 μ M TPA corresponds to 1.2 nmol). Notably, under these conditions, no detectable amounts of TPA were released with PET27 after 30 days.

Amino Acid Sequence and Structural Analyses Identify Unique Traits of Bacteroidetal Polyethylene Terephthalate-Hydrolyzing Enzymes

While all four enzymes PET27-PET30 were able to hydrolyze PCL, BHET and Impranil®DLN, only PET27 and PET30 were able to depolymerize PET. To identify the key differences that confer this activity on PET, all predicted PETases were studied on sequence and structural level. With an average of 330 aa, the predicted molecular weights of the enzymes ranged from 36 to 48 kDa. Each candidate contained a C-terminal signal domain for protein transport to the periplasm as predicted with SignalP 5.0 (Almagro Armenteros et al., 2019), supporting the notion that these are secreted proteins (Table 3). Remarkably, the predicted PETases PET27-PET30 and PET38 showed a type IX secretion system (T9SS)/PorC-type sorting domain-containing part at the C-terminus. It has been described earlier by a profile HMM from the TIGRFAM database (TIGR04183). T9SS sorting domains are involved in protein transport across the bacterial outer membrane and have so far been described as a Bacteroidetes-specific secretion system (Sato et al., 2010; Shoji et al., 2011; de Diego et al., 2016). The predicted domain encompassed 62–64 aa in the cases of PET27-PET30 and PET38. PET57 and 58 carried truncated sorting domains of 42 and 55 aa in length. This observation also implies that these enzymes are most likely exoenzymes (Table 3 and Supplementary Figures 3, 4). To ensure that this C-terminus does not affect catalytic activity, a deletion mutant designated PET30 Δ PorC was created that lacked the sorting sequence between the amino acids 300–366. Activity tests confirmed that it was not affected in its activities using *p*NP-C6 or PET foil (Supplementary Figure 1E and Table 2). The enzyme released similar amounts of TPA as it was observed for the native PET30 (Table 2).

Further analyses of the amino acid sequences identified a G-x-S-x-G motif which is typical for α/β serine hydrolases (Ollis et al., 1992) and a catalytic triad that consists of the residues Asp-His-Ser (Figure 4 and Supplementary Figure 4). Potential substrate binding sites in all bacteroidetal enzymes were identified containing the aa Phe-Met-(Trp/Tyr/Ala). The latter differed from the known *IsPETase*, the LCC and PET2 binding sites, in which a Tyr-Met-Trp motif is present (Table 3). PET57 is the only exception with a Trp-Met-Tyr binding site. PET27, however, has the Tyr replaced with a Phe that is identical to Cut190, while PET30 has in addition the Trp in position 3 replaced with a Tyr (Table 3). This single amino acid substitution in the predicted substrate binding pocket of PET30, however, is not solely responsible for PET-degrading activity. The mutants PET30_F80Y and PET30_Y178W as well as a version containing

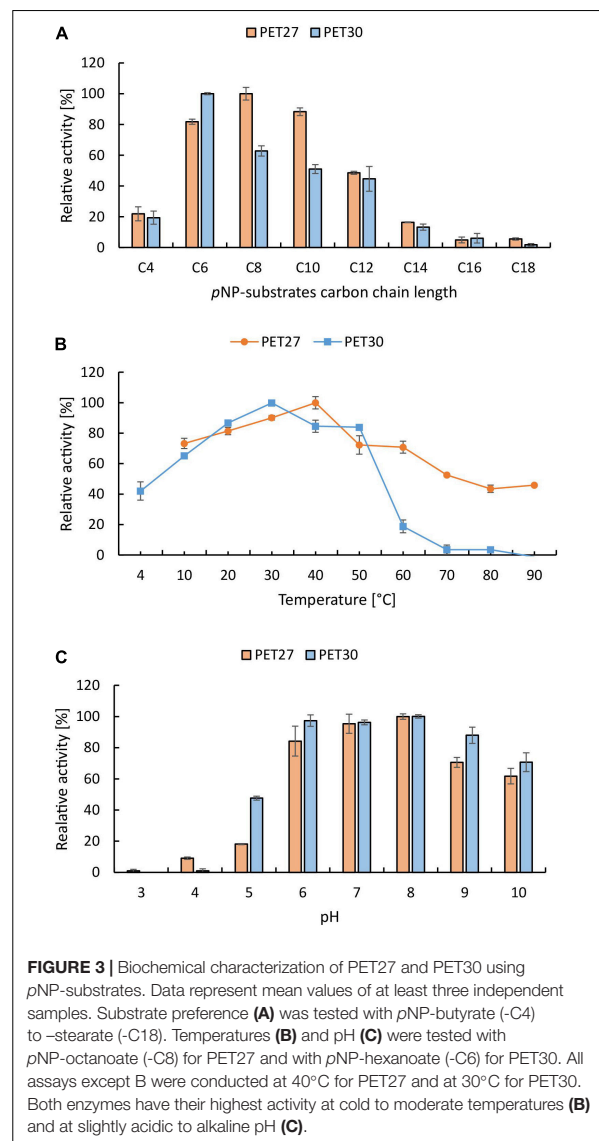


FIGURE 3 | Biochemical characterization of PET27 and PET30 using *p*NP-substrates. Data represent mean values of at least three independent samples. Substrate preference (A) was tested with *p*NP-butyrate (-C4) to -stearate (-C18). Temperatures (B) and pH (C) were tested with *p*NP-octanoate (-C8) for PET27 and with *p*NP-hexanoate (-C6) for PET30. All assays except B were conducted at 40°C for PET27 and at 30°C for PET30. Both enzymes have their highest activity at cold to moderate temperatures (B) and at slightly acidic to alkaline pH (C).

both of these point mutations even lost BHET- and PET-degrading activity (data can be shown upon request).

Structure Determination of PET30 and Structural Modeling of the Other Putative PETases

For structural insights into the mechanism of polymer degradation, the structures of all predicted PETases, except PET30, were modeled using the *IsPETase* (PDB code 6EQE) as template. Crystallization was conducted with purified PET30 Δ PorC and X-ray structure determination using a model of PET30 for molecular replacement. The structure was solved at 2.1 Å resolution, containing one monomer in the asymmetric

unit, with 16.2% for R_{work} and 21.9% for R_{free} . Data collection and structure refinement statistics are given in **Supplementary Table 4**. Coordinates of PET30 Δ PorC were deposited under the PDB accession code 7PZJ. The PET30 Δ PorC protein shows a canonical α/β -fold consisting of a central twisted β -sheet composed of 9 β -strands flanked by 7 α -helices on both sides (**Figure 4A**), as already reported for homologous structures, i.e., PETases and cutinases (Han et al., 2017; Numoto et al., 2018). The structure of PET30 Δ PorC revealed an extra β -sheet (β_{10}) which is located at the C-terminus and connects the PorC domain which has been deleted in this construct. PET30 Δ PorC represents the overall fold of several PETases as revealed by a similarity search performed by PDBFold.⁸ Here, especially the known structures of the PETase from *Ideonella sakaiensis* (for example PDB code 5XH3; Han et al., 2017), show high consistency indicated by the rmsd of 1.3–1.5 Å. Also, high structural similarity can be seen with the structure of PE-H from *Pseudomonas aestusnigri* (PDB code 6SCD rmsd 1.3) and the cutinase from a member of the Burkholderiales bacteria family (PDB code 7CWQ, rmsd of 1.32 (Bollinger et al., 2020; Chen et al., 2021)). One disulfide bond is present in PET30 Δ PorC (C262–C285), a common feature for Type II PET-degrading enzymes (Joo et al., 2018). In the PETase from *I. sakaiensis* (PDB code 5YNS), a second disulfide bond is present which is located closely to the active site. Mutational analysis revealed that this disulfide bond plays a crucial role in activity since mutation of the involved cysteine to serine completely abolished activity, likely due to a destabilizing effect on the active site. The sequence in PET30 Δ PorC at this position deviates, and here, G195 and V232 are present. In the PE-H structure, also no disulfide bridge can be found, although one cysteine residue remained (G195 and C251). From the many structures of the PETase from *I. sakaiensis*, one was solved in complex with 2-hydroxyethyl methyl terephthalate (HEMT; PDB code 5XH3). Here, HEMT is bound via interactions with W156, I179, H208, A131, W130, Y58, and M132. We looked into the active site and overlaid the HEMT molecule with our PET30 Δ PorC structure (**Supplementary Figure 2**). Here similar interactions of the HEMT molecule by the PET30 Δ PorC protein can be deduced mediated by Y178, T200, H230, W152, F80, and M154 (**Figure 4B**).

The largest differences can be seen in the C-terminal part affiliated with the T9SS-domain. It differed largely from the *IsPETase* and consisted of up to seven predicted β -sheets and, occasionally, a few α -helices (**Supplementary Figure 3A** and **Table 3**). Another difference between PET27, PET30, *IsPETase* and LCC is the surface hydrophobicity of the region channeling the substrates to the active site (**Figure 4C**). PET30 shows a less hydrophobic surrounding of the catalytic pocket when compared to the structures of Type I and Type II PET-degrading enzymes (Joo et al., 2018). PET27 contains a bulkier hydrophobic domain on one of the sides of the channel. This feature might influence accommodation of the substrate and activity on the polymers. A similar catalytic pocket was predicted for PET28 and PET29 (**Supplementary Figure 3**). Although active on BHET and PCL, these enzymes showed no measurable activity on PET.

⁸www.ebi.ac.uk/msd-srv/ssm/

The enzymes derived from the human gut present a larger hydrophobic surface around the catalytic site, especially PET58 and PET59 (**Supplementary Figure 3B**).

Bacteroidetal Polyethylene Terephthalate-Degrading Esterases Forming Two Phylogenetic Subclusters Are Globally Occurring Enzymes

Using the amino acid sequences of published and functionally verified PETases and employing the RAXML-NG autoMRE algorithm via TreeSAPP (Morgan-Lang et al., 2020), a phylogenetic analysis was performed. Multiple phylogenetic clusters formed that roughly corresponded to Actinobacteria, Proteobacteria, Firmicutes and Ascomycota (**Figure 5A**). While the putative and now confirmed Bacteroidetal PET-degrading hydrolases appear to be polyphyletic when added into the tree, distinct subclusters were formed. Notably, the two enzymes PET27 and PET30, shown to be active on PET foil, were grouped as part of subcluster that consisted of predicted and functional enzymes affiliated with genera *Aequorivita* and *Kaistella*. Furthermore, the predicted but functionally not verified enzymes from the genus *Porphyromonas* (PET57–PET59) formed a separate subcluster. Interestingly, these two subclusters harbored only sequences of aquatic and environmental origin or gut-affiliated sequences, respectively. Overall, sequences derived from Bacteroidetes seem to group by both taxonomy and environment, though low bootstrap values do not show a high degree of confidence. However, the interleaving of Bacteroidetal sequences from both a Firmicute, *B. subtilis*, and the eukaryotic Ascomycota sequences may suggest that PET-active enzymes are widely distributed phylogenetically, and further characterization studies resulting in additions to the tree are likely to provide better phylogenetic resolution. Additionally, the pairwise distance on the level computed in MEGAX with the p-distance model (**Figure 5B**) confirmed these groupings, with the highest similarity, as indicated by low pairwise distanced, occurring within the subclusters described. This analysis also indicated rather low similarity between the putative bacteroidetal PETases and the known PETases (*IsPETase*, LCC, PE-H, and PET2), mounting further evidence for the wide phylogenetic distribution of these enzymes.

The diversity of bacteroidetal enzymes acting on PET raised the question to what extent these enzymes could impact plastic degradation in the environment. To address this question in part, we analyzed the global distribution of PET27 and PET30 and their homologs. The protein sequences of PET27 and PET30 were analyzed for their occurrence and frequency in global databases available in IMG/M ER (Woyke et al., 2011; Mukherjee et al., 2020). Using both enzymes for a BLASTp-based search (cutoffs 50% identity; 80% coverage), we were initially able to identify very few (<10) possible homologs in the global databases analyzed and affiliated with the genera *Aequorivita* and *Kaistella* (**Figure 1A**). Interestingly, when we extended our search to the Flavobacterium-Cytophaga-Bacteroidetes (FCB), we were able to identify 98 possible homologs in our global searches including single-cell amplified genomes (SAGs) from the Baltic Sea

TABLE 3 | Conserved motifs and structural features identified in the predicted bacteroidetal PET-hydrolyzing esterases.

Enzyme	N-terminus			Catalytic triad	Substrate binding site	Disulf. bridge*	C-terminus			
	Aln 1st aa	Length [N]	SP cleavage site				Aln last aa	Length [N]	Secondary structure	CD
IsPETase	A47	47	27–28	D-H-S	Y-M-W	2x	C273	18	N/A	N/A
LCC	D53	53	21–22	D-H-S	Y-M-W	1x	L274	19	N/A	N/A
Cut190	R64	64	N/A	D-H-S	F-M-W	2x	L278	29	N/A	N/A
PET27	P36	36	23–24	D-H-S	F-M-W	1x	L265	99	7x β	PorC
PET28	P36	36	23–24	D-H-S	F-M-W	1x	L265	100	6x β	PorC
PET29	P36	36	23–24	D-H-S	F-M-W	1x	L265	100	α , 4x β , α , 2x β	PorC
PET30	P36	36	23–24	D-H-S	F-M-Y	1x	A266	100	7x β	PorC
PET38	S7	7	19–20	D-H-S	F-M-A	1x	I279	168	5x β , α , 2x β	PorC
PET53	T36	36	22–23	D-H-S	F-M-W	1x	V268	86	4x β	N/A
PET57	N35	35	25–26	D-H-S	W-M-Y	N/A	F289	34	α + loops	N/A
PET58	I34	34	24–25	D-H-S	F-M-Y	N/A	F293	45	loops + α	N/A
PET59	Y48	48	24–25	D-H-S	F-M-Y	N/A	Y294	51	α + semi- α	N/A

The *Ileoneella sakaiensis* PETase (IsPETase, PDB: 6EQE; Yoshida et al., 2016; Austin et al., 2018), the LCC (4EB0; Sulaiman et al., 2014) and the Cut190 (4WFI; Miyakawa et al., 2015) were included for benchmarking purposes.

Aln: Alignment; SP: Signal Peptide; α , α -helix; β , β -sheet; N/A, not identified; *, verified and predicted disulfide bonds; CD: Conserved Domain; PorC, Por secretion system C-terminal sorting domain.

(Supplementary Table 5). 47 hits were affiliated with the genus of the *Marinimicrobia* (candidate phylum of the FCB group), indicating a potential role for these ubiquitous and abundant marine microorganisms in PET-degradation. Others were more closely associated with Bacteroidetes (Austin et al., 2018). As expected, the majority of these homologs were associated with marine and aquatic samples (Figure 1B).

Kaistella jeonii Is Able to Colonize Polyethylene Terephthalate Surfaces

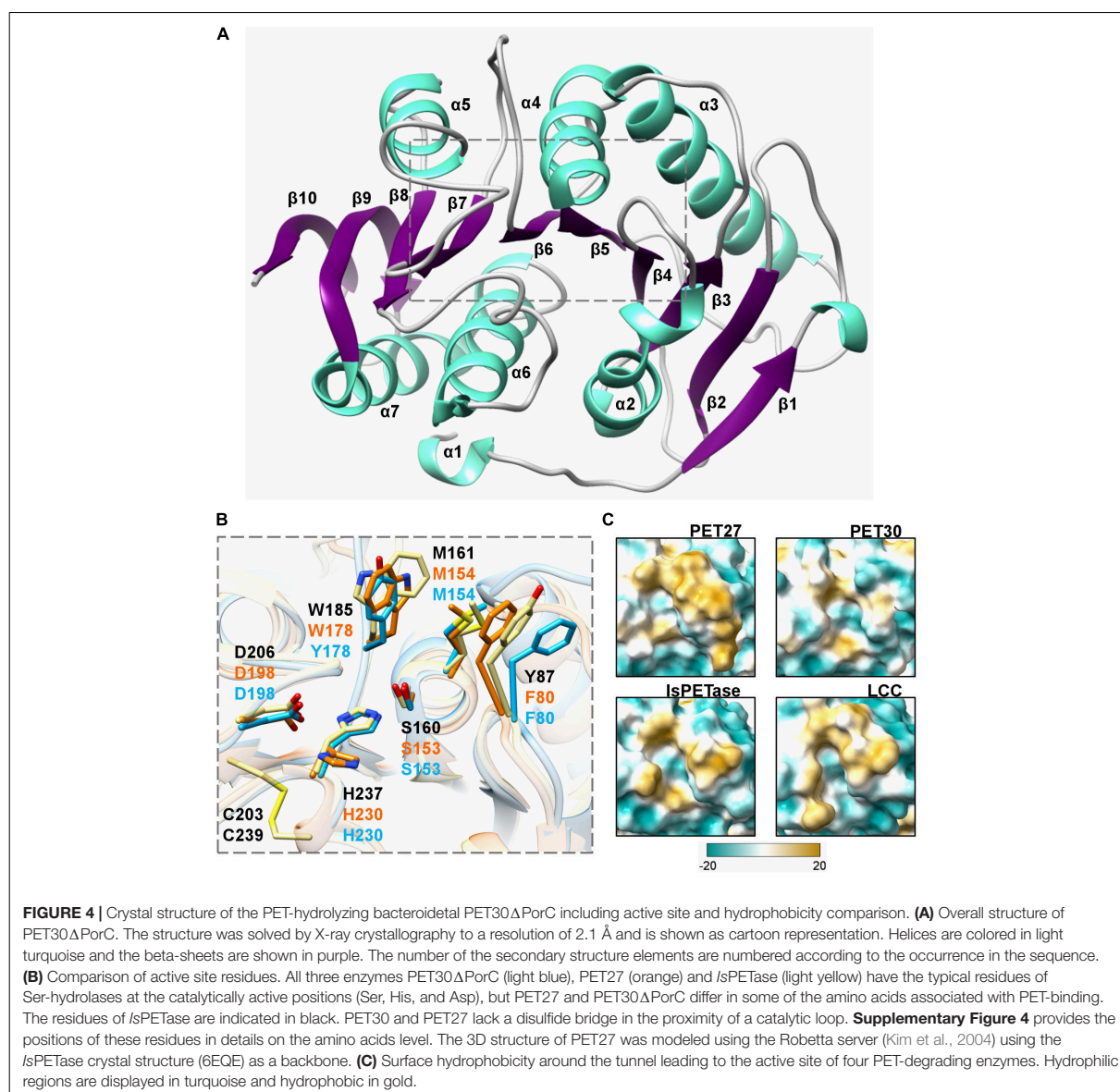
These metagenomic analyses showed that *K. jeonii*, the organism from which PET30 originates, exists primarily in aquatic habitats. To illustrate that it not only exists there, but is also able to actively colonize PET surfaces, a culture of this organism was incubated with PET foil platelets. The foil sections were incubated for up to 1 week in R2A medium with *K. jeonii*, removed from the culture, and washed three times with buffer before staining with LIVE/DEAD staining solution. Samples were investigated under the confocal laser scanning microscope Axio Observer Z1/7, LSM 800 by Carl Zeiss Microscopy GmbH (Jena, Germany). Cells visible in Supplementary Figure 5 resisted repeated washing, indicating that they adhere under these laboratory conditions to the surface and an increasing number of cells was visible on the amorphous PET-foil after 5–7 days. The exact mechanism of attachment is not known. Nonetheless, it can be speculated that SusD binding modules, which are crucial for sugar polymer binding, could be involved. They can be found in both genomes of *K. jeonii* (GenBank acc. no. WP_039349586.1; RagB/SusD family nutrient uptake outer membrane protein) and *Aequorivita* sp. CIP111184 (GenBank acc. no. WP_111879847.1; SusD/RagB family nutrient-binding outer membrane lipoprotein).

DISCUSSION

Currently, only a handful of known bacterial phyla are known to produce active PET-esterases (Figure 5 and Supplementary Table 3). Here, we have identified and partially characterized two novel functional PET-hydrolyzing enzymes affiliated with the *Kaistella* and *Aequorivita* genera within the Bacteroidetes phylum. Bacteria belonging to the genus *Kaistella* are globally occurring aerobic organisms colonizing a wide range of different habitats including plants, soil, fish, the human gut, and sea water. Within the genus *Kaistella*, over one hundred species have been described of which few are pathogens, but many are beneficial and host-associated (Bernardet et al., 2005; Loch and Faisal, 2015). Only a few species have been identified within the genus *Aequorivita*, mainly belonging to marine or fresh-water organisms that are mostly psychrotolerant and aerobic (Bowman and Nichols, 2002). Notably, Bacteroidetes have been described as very potent degraders of polymers, and they harbor a multitude of hydrolases and binding modules (Dodd et al., 2011; Thomas et al., 2011; Foley et al., 2016).

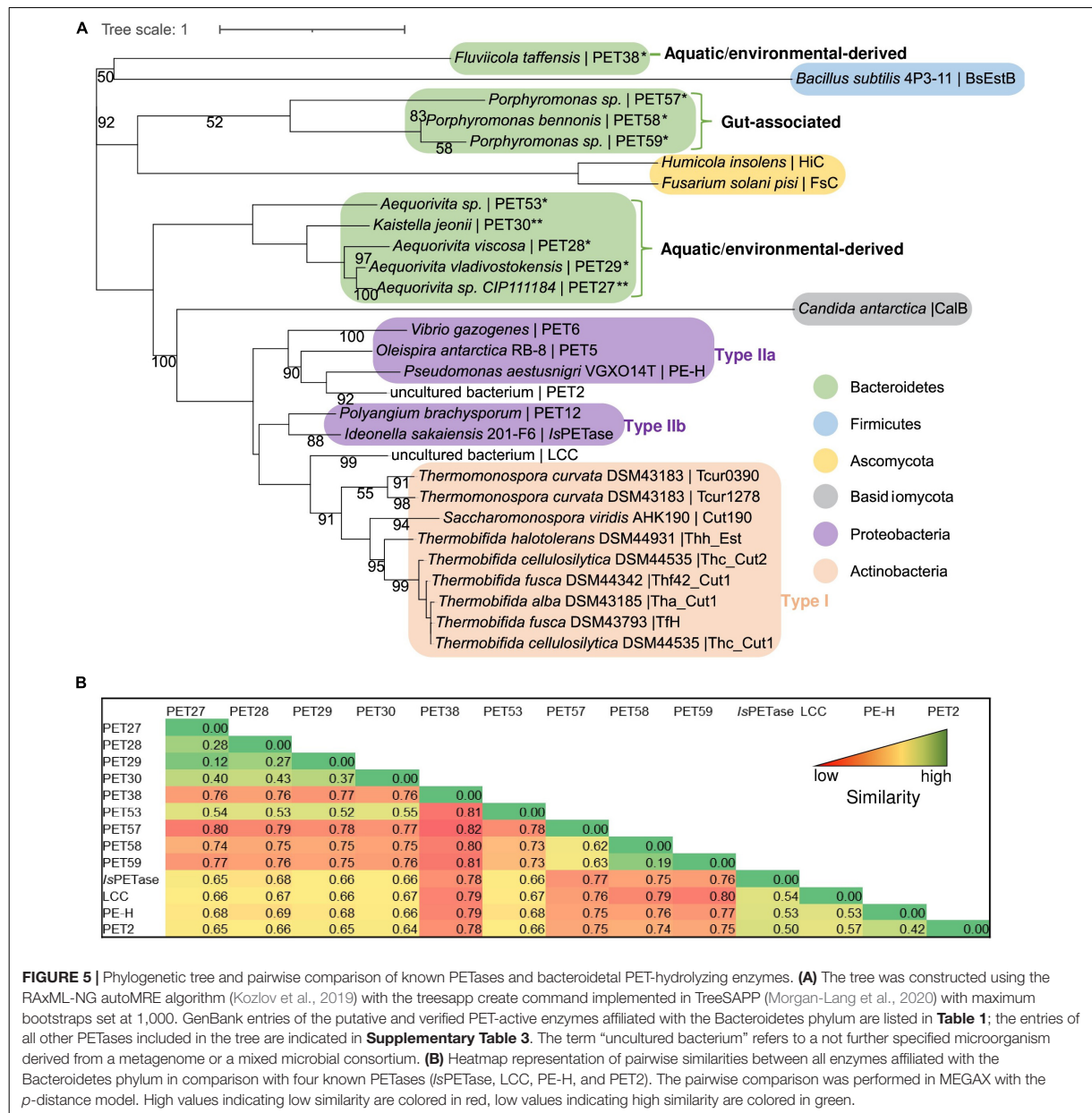
The enzymes PET27 and PET30 characterized here are both typical esterases (i.e., serine hydrolases) belonging to the EC 3.1. Both appear to be secreted enzymes as they carry an C-terminal secretion signal linked to the transport into the periplasm (Desvaux et al., 2009) and one secretion PorC-like motif which is related to the type IX secretion system (T9SS) (Sato et al., 2010; de Diego et al., 2016). The T9SS is composed of several outer membrane, periplasmic and inner membrane proteins, whereby it is responsible for the secretion of pathogenicity factors, hydrolases and also for gliding motility in the Bacteroidetes phylum (Sato et al., 2010; de Diego et al., 2016).

PET27 and PET30 were active on PET foil, but differed strongly in their overall activities. PET27 contains a Phe-Met-Trp



motif and PET30 a Phe-Met-Tyr. The most active enzymes such as LCC and IsPETase both carry a Tyr-Met-Trp consensus binding motif while the non-active enzymes PET38, PET53, PET57, PET58 and PET59 revealed either a Phe-Met-Ala, a Phe-Met-Trp or a Trp-Met-Tyr substrate binding motif. PET30 mutants, in which the amino acids were adjusted according to the active PETases, did not show the expected increase in activity. Therefore, we assume that not only individual amino acids are decisive, but rather that an interplay of hydrophobicity, location and accessibility of the catalytic triad is crucial for whether polymers can be degraded (Figure 4).

Benchmarking activities of polymer active enzymes with literature values is not trivial since most studies use different types of foils with different degrees of crystallinity and distinct assay conditions. To partially overcome this challenge, we produced our own recombinant wildtype enzymes of the IsPETase and compared its activities with PET27 and PET30. As expected, IsPETase was 4.7-fold more active at 30°C than PET27 and up to 253-fold more active than PET30. With respect to the overall activity of the IsPETase, however, our data are in line with published data for this enzyme (Son et al., 2019). The observation here that the activities of the PET27 and PET30 enzymes are relatively low compared to the IsPETase and certainly with



respect to the published values of the even more active LCC imply that PET27 and PET30 are not PET esterases *in sensu strictu*. However, our data imply that both are short-chain fatty acid acting esterases revealing promiscuity in their substrate profile (**Table 3** and **Figure 3**).

Intriguingly, the observation that both enzymes were catalytically active on PET foil could imply a wider role in the degradation of PET and especially PET nanoparticles. Because of the significant activities even at 4°C, these enzymes may in fact play a yet unknown role in long-term degradation of

PET microparticles in cold environments. This hypothesis is supported by our observations that homologs of both enzymes can be found on a global level covering a wide range of climate zones (**Figure 1**) and that at least the cultivable *K. jeonii* is able to attach to PET surfaces.

In summary, our biochemical results significantly extend the knowledge of PET-degrading enzymes and provide promising candidates for biotechnological applications at low temperatures. Furthermore, the data presented here will help to advance our knowledge on the ecological role of the

Bacteroidetes in the decomposition of marine PET litter and enable the development of an expanded phylogenetic framework for identifying the diversity of putative PETases in diverse marine microbial groups throughout the global ocean.

DATA AVAILABILITY STATEMENT

The original contributions presented in the study are included in the article/**Supplementary Material**, further inquiries can be directed to the corresponding author/s.

AUTHOR CONTRIBUTIONS

WS, JC, and PP-G designed the study, contributed to manuscript writing and designing bioassays. HZ and RD conducted experiments and contributed to planning and writing. PP-G, JC, and HZ were involved in enzyme structural work, bioinformatics, and initial phylogenetic analyses. VA, JS, and SSm conducted crystallization and structure determination. CS and JP contributed to planning and corrections. RS and CC were involved in global data base searches. DD performed HMM searches. SW and BH delivered clone producing the *IsPETase*. LP did microscopic analyses. AA was involved in gut microbiome data mining. SSt and SH were involved in phylogenetic analysis. All authors contributed to manuscript writing and editing.

FUNDING

This work was in part supported by the BMBF within the programs MarBiotech (031B0562A) MetagenLig (031B0571B), MethanoPEP (031B0851B), LipoBiocat (031B0837B), PlastiSea (031B867B), and MetagenLig (031B0571A) at the Universities of Hamburg, Kiel, Düsseldorf and Stuttgart. The support for the University of Bayreuth was given by the Deutsche Forschungsgemeinschaft (DFG, German Research Foundation)—Project Number 391977956—SFB 1357. Further funding came from the US Department of Energy (DOE) Joint Genome Institute, an Office of Science User Facility, supported by the Office of Science of the U.S. Department of Energy under Contract DE-AC02-05CH11231, the Natural Sciences and Engineering Research Council (NSERC) of Canada, the G. Unger Vetlesen and Ambrose Monell Foundations, the Canada Foundation for Innovation (CFI) and Compute Canada through grants awarded to SH. AA was funded by EMBL core funds. The Center for Structural Studies was funded by the Deutsche Forschungsgemeinschaft (DFG Grant number 417919780; INST 208/740-1 FUGG; INST 208/761-1 FUGG).

REFERENCES

Acero, E. H., Ribitsch, D., Steinkellner, G., Gruber, K., Greimel, K., Eiteljoerg, I., et al. (2011). Enzymatic surface hydrolysis of PET: effect of structural diversity on kinetic properties of cutinases from

ACKNOWLEDGMENTS

The synchrotron MX data were collected at beamline P13 operated by EMBL Hamburg at the PETRA III storage ring (DESY, Hamburg, Germany). We thank Dr. Michael Agthe for the assistance in using the beamline. We also thank the staff of the ID23-eh1 at the ESRF, Grenoble for help with initial screening of the crystal quality.

SUPPLEMENTARY MATERIAL

The Supplementary Material for this article can be found online at: <https://www.frontiersin.org/articles/10.3389/fmicb.2021.803896/full#supplementary-material>

Supplementary Figure 1 | Further biochemical characterization of PET27 and PET30 using *p*NP-substrates. Cofactor requirements were tested for PET27 with *p*NP-C8 at 40°C and for PET30 with *p*NP-C6 at 30°C (A). For PET30, all other tests were carried out with *p*NP-C6 and all assays except (B) were conducted at 30°C. Thermostability of PET30 was assessed at 50 and 60°C over 3 h with *p*NP-C6 (B). Inhibitors (C) and detergents (D) generally decrease the activity of PET30, particularly with higher concentrations. Activity of PET30 and PET30ΔPorC were compared under the same conditions using *p*NP-C6 (E). Data represent mean values of at least three independent measurements.

Supplementary Figure 2 | Zoom into the active site of PET30ΔPorC. Overlaid are the structures of PET30ΔPorC (blue) with the PETase from *I. sakaiensis* (light yellow, black labeling) in complex with HEMT (purple; PDB code 5XH3). The residues involved in binding are highlighted and numbered according to their structure. *The structure 5XH3 is a mutant where the catalytic Serine was mutated to an Alanine.

Supplementary Figure 3 | Structure prediction models of verified and predicted PETases affiliated with the phylum of the Bacteroidetes. (A) 3D structures were modeled using the Robetta server using the *IsPETase* crystal structure (light yellow, 6EQE) as a backbone. For PET30, the crystal structure was shown. (B) Surface hydrophobicity around the tunnel leading to the active site of putative bacteroidetal PETases and functionally verified PET-degrading enzymes. Hydrophilic regions are displayed in turquoise and hydrophobic in gold.

Supplementary Figure 4 | Amino acid alignment of 9 potential PETases affiliated with the Bacteroidetes phylum. The original sequences were used for the structural alignment and the alignment was constructed with T-Coffee. Alignment was visualized with Bioedit version 7.0.5. The *IsPETase* was included for reasons of benchmarking. Blue arrows indicate the start and the end of the active PET27 and PET30 clones. We introduced a methionine as the first aa of the protein sequences. The signal peptide deleted version of the enzymes was functionally verified. The red arrow labeled with CS indicates the predicted cleavage site of C-terminal PorC domain (Lasica et al., 2017). The gray arrow indicates the C-terminus of the truncated version of PET30 (PET30Δ300-366), number indicates the position of amino acid). PET30Δ300-366 was active on PCL and BHET.

Supplementary Figure 5 | Confocal microscopic pictures of *K. jeonii* colonizing PET foil. The pictures were taken after 5–7 days of incubation of *K. jeonii* in R2A medium. Cells are dyed with LIVE/DEAD™ stain. Green fluorescence shows living cells, red fluorescence indicates dead cells. 2D front pictures were taken with Axio Observer Z1/7, LSM 800 (Carl Zeiss, Jena, Germany) of a 3D Z-stack image.

Thermobifida. *Macromolecules* 44, 4632–4640. doi: 10.1021/ma200949p

Afonine, P. V., Grosse-Kunstleve, R. W., Echols, N., Headd, J. J., Moriarty, N. W., Mustyakimov, M., et al. (2012). Towards automated crystallographic structure refinement with phenix. *Acta*

- Crystallogr. D Biol. Crystallogr.* 68, 352–367. doi: 10.1107/S0907444912001308
- Agarwala, R., Barrett, T., Beck, J., Benson, D. A., Bollin, C., Bolton, E., et al. (2016). Database resources of the national center for biotechnology information. *Nucleic Acids Res.* 44, D7–D19.
- Almagro Armenteros, J. J., Tsirigos, K. D., Sønderby, C. K., Petersen, T. N., Winther, O., Brunak, S., et al. (2019). SignalP 5.0 improves signal peptide predictions using deep neural networks. *Nat. Biotechnol.* 37, 420–423. doi: 10.1038/s41587-019-0036-z
- Almeida, A., Nayfach, S., Boland, M., Strozzi, F., Beracochea, M., Shi, Z. J., et al. (2021). A unified catalog of 204,938 reference genomes from the human gut microbiome. *Nat. Biotechnol.* 39, 105–114. doi: 10.1038/s41587-020-0603-3
- Austin, H. P., Allen, M. D., Donohoe, B. S., Rorrer, N. A., Kearns, F. L., Silveira, R. L., et al. (2018). Characterization and engineering of a plastic-degrading aromatic polyesterase. *Proc. Natl. Acad. Sci. U.S.A.* 115, E4350–E4357. doi: 10.1073/pnas.1718804115
- Berman, H. M., Westbrook, J., Feng, Z., Gilliland, G., Bhat, T. N., Weissig, H. I., et al. (2000). The protein data bank. *Nucleic Acids Res.* 28, 235–242.
- Bernardet, J. F., Vancanney, M., Matte-Tailliez, O., Grisez, L., Tailliez, P., Bizet, C., et al. (2005). Polyphasic study of *Chryseobacterium* strains isolated from diseased aquatic animals. *Syst. Appl. Microbiol.* 28, 640–660. doi: 10.1016/j.syapm.2005.03.016
- Bollinger, A., Thies, S., Knieps-Grünhagen, E., Gertzen, C., Kobus, S., Hoppner, A., et al. (2020). A novel polyester hydrolase from the marine bacterium *Pseudomonas aestuans*—structural and functional insights. *Front. Microbiol.* 11:114. doi: 10.3389/fmicb.2020.00114
- Bowman, J. P., and Nichols, D. S. (2002). *Aequorivita* gen. nov., a member of the family Flavobacteriaceae isolated from terrestrial and marine Antarctic habitats. *Int. J. Syst. Evol. Microbiol.* 52, 1533–1541. doi: 10.1099/00207713-52-5-1533
- Chen, C.-C., Han, X., Li, X., Jiang, P., Niu, D., Ma, L., et al. (2021). General features to enhance enzymatic activity of poly (ethylene terephthalate) hydrolysis. *Nat. Catal.* 4, 425–430. doi: 10.1038/s41929-021-00616-y
- Chen, S., Tong, X., Woodard, R. W., Du, G., Wu, J., and Chen, J. (2008). Identification and characterization of bacterial cutinase. *J. Biol. Chem.* 283, 25854–25862. doi: 10.1074/jbc.m800848200
- NCBI Resource Coordinators (2017). Database resources of the national center for biotechnology information. *Nucleic Acids Res.* 45, D12–D17.
- Danso, D., Chow, J., and Streit, W. R. (2019). Plastics: microbial degradation, environmental and biotechnological perspectives. *Appl. Environ. Microbiol.* 85, 1–14. doi: 10.1007/978-3-030-48973-1_1
- Danso, D., Schmeisser, C., Chow, J., Zimmermann, W., Wei, R., Leggewie, C., et al. (2018). New insights into the function and global distribution of polyethylene terephthalate (PET)-degrading bacteria and enzymes in marine and terrestrial metagenomes. *Appl. Environ. Microbiol.* 84:e02773-17. doi: 10.1128/AEM.02773-17
- de Diego, I., Ksiazek, M., Mizgalska, D., Koneru, L., Golik, P., Szmigielski, B., et al. (2016). The outer-membrane export signal of *Porphyrromonas gingivalis* type IX secretion system (T9SS) is a conserved C-terminal β -sandwich domain. *Sci. Rep.* 6:23123. doi: 10.1038/srep23123
- DeLano, W. L. (2002). Pymol: an open-source molecular graphics tool. *CCP4 Newsl. Protein Crystallogr.* 40, 82–92.
- Desvaux, M., Hébraud, M., Talon, R., and Henderson, I. R. (2009). Outer membrane translocation: numerical protein secretion nomenclature in question in mycobacteria. *Trends Microbiol.* 17, 338–340. doi: 10.1016/j.tim.2009.05.008
- Dodd, D., Mackie, R. I., and Cann, I. K. O. (2011). Xylan degradation, a metabolic property shared by rumen and human colonic Bacteroidetes. *Mol. Microbiol.* 79, 292–304. doi: 10.1111/j.1365-2958.2010.07473.x
- Emsley, P., and Cowtan, K. (2004). Coot: model-building tools for molecular graphics. *Acta Crystallogr. D Biol. Crystallogr.* 60, 2126–2132. doi: 10.1107/s0907444904019158
- Foley, M. H., Cockburn, D. W., and Koropatkin, N. M. (2016). The Sus operon: a model system for starch uptake by the human gut Bacteroidetes. *Cell. Mol. Life Sci.* 73, 2603–2617. doi: 10.1007/s00018-016-2242-x
- Geyer, R., Jambek, J. R., and Law, K. L. (2017). Production, use, and fate of all plastics ever made. *Sci. Adv.* 3:e1700782. doi: 10.1126/sciadv.1700782
- Haervall, K., Zitzenbacher, S., Amer, H., Zumstein, M. T., Sander, M., McNeill, K., et al. (2017). Polyol structure influences enzymatic hydrolysis of bio-based 2,5-furandicarboxylic acid (FDCA) polyesters. *Biotechnol. J.* 12:1600741. doi: 10.1002/biot.201600741
- Hahnke, R. L., Meier-Kolthoff, J. P., García-López, M., Mukherjee, S., Huntemann, M., Ivanova, N. N., et al. (2016). Genome-based taxonomic classification of bacteroidetes. *Front. Microbiol.* 7:2003. doi: 10.3389/fmicb.2016.02003
- Hall, T. A. (1999). *BioEdit: A User-Friendly Biological Sequence Alignment Editor and Analysis Program for Windows 95/98/NT*. *Nucleic Acids Symposium Series*. London: Information Retrieval Ltd., c1979–c2000.
- Han, X., Liu, W., Huang, J. W., Ma, J., Zheng, Y., Ko, T. P., et al. (2017). Structural insight into catalytic mechanism of PET hydrolase. *Nat. Commun.* 8:2106.
- Hu, X., Thumarat, U., Zhang, X., Tang, M., and Kawai, F. (2010). Diversity of polyester-degrading bacteria in compost and molecular analysis of a thermoactive esterase from *Thermobifida alba* AHK119. *Appl. Microbiol. Biotechnol.* 87, 771–779. doi: 10.1007/s00253-010-2555-x
- Jambek, J. R., Geyer, R., Wilcox, C., Siegler, T. R., Perryman, M., Andrady, A., et al. (2015). Plastic waste inputs from land into the ocean. *Science* 347, 768–771. doi: 10.1126/science.1260352
- Joo, S., Cho, I. J., Seo, H., Son, H. F., Sagong, H. Y., Shin, T. J., et al. (2018). Structural insight into molecular mechanism of poly(ethylene terephthalate) degradation. *Nat. Commun.* 9:382.
- Kabsch, W. (2014). Processing of X-ray snapshots from crystals in random orientations. *Acta Crystallogr. D Biol. Crystallogr.* 70, 2204–2216. doi: 10.1107/S1399004714013534
- Kim, D. E., Chivian, D., and Baker, D. (2004). Protein structure prediction and analysis using the Robetta server. *Nucleic Acids Res.* 32, W526–W531.
- Kleeberg, I., Hetz, C., Kroppenstedt, R. M., Müller, R. J., and Deckwer, W. D. (1998). Biodegradation of aliphatic-aromatic copolyesters by *Thermomonospora fusca* and other thermophilic compost isolates. *Appl. Environ. Microbiol.* 64, 1731–1735. doi: 10.1128/AEM.64.5.1731-1735.1998
- Kozlov, A. M., Darriba, D., Flouri, T., Morel, B., and Stamatakis, A. (2019). RAxML-NG: a fast, scalable and user-friendly tool for maximum likelihood phylogenetic inference. *Bioinformatics* 35, 4453–4455. doi: 10.1093/bioinformatics/btz305
- Krieg, N., Ludwig, W., Euzéby, J., and Whitman, W. (2015). “Bacteroidetes phyl. nov.” in *Bergey’s Manual of Systematics of Archaea and Bacteria*, eds M. E. Trujillo, S. Dedysh, P. DeVos, et al. (Hoboken, NJ: John Wiley & Sons, Inc.), 1–2. doi: 10.1002/9781118960608.pbm00004
- Lasica, A. M., Ksiazek, M., Madej, M., and Potempa, J. (2017). The type IX secretion system (T9SS): highlights and recent insights into its structure and function. *Front. Cell. Infect. Microbiol.* 7:215. doi: 10.3389/fcimb.2017.00215
- Letunic, I., and Bork, P. (2019). Interactive tree of life (iTOL) v4: recent updates and new developments. *Nucleic Acids Res.* 47, W256–W259. doi: 10.1093/nar/gkz239
- Li, N., Zhu, Y., LaFrentz, B. R., Evenhuis, J. P., Hunnicutt, D. W., Conrad, R. A., et al. (2017). The type IX secretion system is required for virulence of the fish pathogen *Flavobacterium columnare*. *Appl. Environ. Microbiol.* 83:e01769-17.
- Liebschner, D., Afonine, P. V., Baker, M. L., Bunkóczi, G., Chen, V. B., Croll, T. I., et al. (2019). Macromolecular structure determination using X-rays, neutrons and electrons: recent developments in Phenix. *Acta Crystallogr. D Struct. Biol.* 75, 861–877. doi: 10.1107/S2059798319011471
- Loch, T. P., and Faisal, M. (2015). Emerging flavobacterial infections in fish: a review. *J. Adv. Res.* 6, 283–300. doi: 10.1016/j.jare.2014.10.009
- Markowitz, V. M., Chen, I. M., Palaniappan, K., Chu, K., Szeto, E., Grechkin, Y., et al. (2012). IMG: the integrated microbial genomes database and comparative analysis system. *Nucleic Acids Res.* 40, D115–D122.
- Matlab, S. (2012). *Matlab*. Natick, MA: The MathWorks.
- Mistry, J., Finn, R. D., Eddy, S. R., Bateman, A., and Punta, M. (2013). Challenges in homology search: HMMER3 and convergent evolution of coiled-coil regions. *Nucleic Acids Res.* 41:e121. doi: 10.1093/nar/gkt263
- Mitchell, A. L., Almeida, A., Beracochea, M., Boland, M., Burgin, J., Cochrane, G., et al. (2019). MGnify: the microbiome analysis resource in 2020. *Nucleic Acids Res.* 48, D570–D578. doi: 10.1093/nar/gkz1035
- Miyakawa, T., Mizushima, H., Ohtsuka, J., Oda, M., Kawai, F., and Tanokura, M. (2015). Structural basis for the Ca²⁺-enhanced thermostability and activity of PET-degrading cutinase-like enzyme from *Saccharomonospora viridis* AHK190. *Appl. Microbiol. Biotechnol.* 99, 4297–4307. doi: 10.1007/s00253-014-6272-8

- Molitor, R., Bollinger, A., Kubicki, S., Loeschke, A., Jaeger, K. E., and Thies, S. (2020). Agar plate-based screening methods for the identification of polyester hydrolysis by *Pseudomonas* species. *Microb. Biotechnol.* 13, 274–284. doi: 10.1111/1751-7915.13418
- Morgan-Lang, C., McLaughlin, R., Armstrong, Z., Zhang, G., Chan, K., and Hallam, S. J. (2020). TreeSAPP: the tree-based sensitive and accurate phylogenetic profiler. *Bioinformatics* 36, 4706–4713. doi: 10.1093/bioinformatics/btaa588
- Mukherjee, S., Stamatis, D., Bertsch, J., Ovchinnikova, G., Sundaramurthi, J. C., Lee, J., et al. (2020). Genomes OnLine Database (GOLD) v.8: overview and updates. *Nucleic Acids Res.* 49, D723–D733. doi: 10.1093/nar/gkaa983
- Mulnaes, D., Porta, N., Clemens, R., Apanasenko, I., Reiners, J., Gremer, L., et al. (2020). TopModel: template-based protein structure prediction at low sequence identity using top-down consensus and deep neural networks. *J. Chem. Theory Comput.* 16, 1953–1967. doi: 10.1021/acs.jctc.9b00825
- Munoz, R., Rosselló-Móra, R., and Amann, R. (2016). Revised phylogeny of Bacteroidetes and proposal of sixteen new taxa and two new combinations including Rhodothermaota phyl. nov. *Syst. Appl. Microbiol.* 39, 281–296. doi: 10.1016/j.syapm.2016.04.004
- Notredame, C., Higgins, D. G., and Heringa, J. (2000). T-Coffee: a novel method for fast and accurate multiple sequence alignment. *J. Mol. Biol.* 302, 205–217.
- Numoto, N., Kamiya, N., Bekker, G.-J., Yamagami, Y., Inaba, S., Ishii, K., et al. (2018). Structural dynamics of the PET-degrading cutinase-like enzyme from *Saccharomonospora viridis* AHK190 in substrate-bound states elucidates the Ca²⁺-driven catalytic cycle. *Biochemistry* 57, 5289–5300. doi: 10.1021/acs.biochem.8b00624
- Ollis, D. L., Cheah, E., Cygler, M., Dijkstra, B., Frolow, F., Franken, S. M., et al. (1992). The alpha/beta hydrolase fold. *Protein Eng.* 5, 197–211.
- Pérez-García, P., Danso, D., Zhang, H., Chow, J., and Streit, W. R. (2021). Exploring the global metagenome for plastic-degrading enzymes. *Methods Enzymol.* 648, 137–157. doi: 10.1016/bs.mie.2020.12.022
- Ribitsch, D., Herrero Acero, E., Greimel, K., Dellacher, A., Zitzenbacher, S., Marold, A., et al. (2012). A new esterase from *Thermobifida halotolerans* hydrolyses polyethylene terephthalate (PET) and polylactic acid (PLA). *Polymers* 4, 617–629. doi: 10.3390/polym4010617
- Ronkvist, Å.M., Xie, W., Lu, W., and Gross, R. A. (2009). Cutinase-catalyzed hydrolysis of poly(ethylene terephthalate). *Macromolecules* 42, 5128–5138.
- Sato, K., Naito, M., Yukitake, H., Hirakawa, H., Shoji, M., McBride, M. J., et al. (2010). A protein secretion system linked to bacteroidete gliding motility and pathogenesis. *Proc. Natl. Acad. Sci. U.S.A.* 107, 276–281. doi: 10.1073/pnas.0912010107
- Shoji, M., Sato, K., Yukitake, H., Kondo, Y., Narita, Y., Kadowaki, T., et al. (2011). Por secretion system-dependent secretion and glycosylation of *Porphyromonas gingivalis* hemin-binding protein 35. *PLoS One* 6:e21372. doi: 10.1371/journal.pone.0021372
- Son, H. F., Cho, I. J., Joo, S., Seo, H., Sagong, H.-Y., Choi, S. Y., et al. (2019). Rational protein engineering of thermo-stable PETase from *Ideonella sakaiensis* for highly efficient PET degradation. *ACS Catal.* 9, 3519–3526.
- Studier, F. W. (2005). Protein production by auto-induction in high-density shaking cultures. *Protein Exp. Purif.* 41, 207–234.
- Sulaiman, S., Yamato, S., Kanaya, E., Kim, J. J., Koga, Y., Takano, K., et al. (2012). Isolation of a novel cutinase homolog with polyethylene terephthalate-degrading activity from leaf-branch compost by using a metagenomic approach. *Appl. Environ. Microbiol.* 78, 1556–1562. doi: 10.1128/AEM.06725-11
- Sulaiman, S., You, D. J., Kanaya, E., Koga, Y., and Kanaya, S. (2014). Crystal structure and thermodynamic and kinetic stability of metagenome-derived LC-cutinase. *Biochemistry* 53, 1858–1869. doi: 10.1021/bi401561p
- The UniProt Consortium (2017). UniProt: the universal protein knowledgebase. *Nucleic Acids Res.* 45, D158–D169.
- Thomas, F., Hehemann, J. H., Rebuffet, E., Czjzek, M., and Michel, G. (2011). Environmental and gut Bacteroidetes: the food connection. *Front. Microbiol.* 2:16. doi: 10.3389/fmicb.2011.00093
- Wei, R., Oeser, T., and Zimmermann, W. (2014). Synthetic polyester-hydrolyzing enzymes from thermophilic actinomycetes. *Adv. Appl. Microbiol.* 89, 267–305. doi: 10.1016/B978-0-12-800259-9.00007-X
- Wei, R., and Zimmermann, W. (2017). Microbial enzymes for the recycling of recalcitrant petroleum-based plastics: how far are we? *Microb. Biotechnol.* 10, 1308–1322. doi: 10.1111/1751-7915.12710
- Wexler, H. M. (2007). *Bacteroides*: the good, the bad, and the nitty-gritty. *Clin. Microbiol. Rev.* 20, 593–621. doi: 10.1128/CMR.00008-07
- Woyke, T., Chertkov, O., Lapidus, A., Nolan, M., Lucas, S., Del Rio, T. G., et al. (2011). Complete genome sequence of the gliding freshwater bacterium *Fluviicola taffensis* type strain (RW262). *Stand. Genomic Sci.* 5, 21–29. doi: 10.4056/sigs.2124912
- Wright, R. J., Bosch, R., Langille, M. G., Gibson, M. I., and Christie-Oleza, J. A. (2021). A multi-OMIC characterisation of biodegradation and microbial community succession within the PET plastisphere. *Microbiome* 9, 1–22. doi: 10.1155/2021/6620574
- Yoshida, S., Hiraga, K., Takehana, T., Taniguchi, I., Yamaji, H., Maeda, Y., et al. (2016). A bacterium that degrades and assimilates poly(ethylene terephthalate). *Science* 351, 1196–1199. doi: 10.1126/science.aad6359

Conflict of Interest: SH is a co-founder of Koonkie Inc., a bioinformatics consulting company that designs and provides scalable algorithmic and data analytics solutions in the cloud.

The remaining authors declare that the research was conducted in the absence of any commercial or financial relationships that could be construed as a potential conflict of interest.

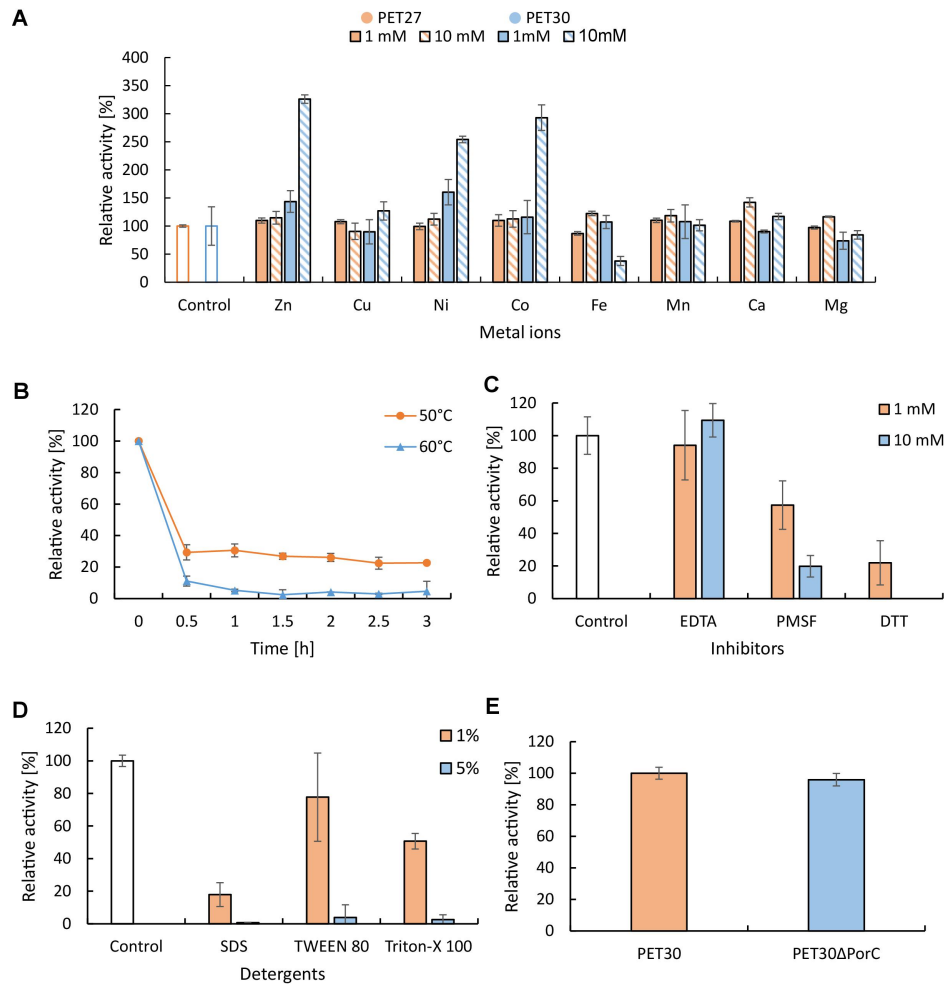
Publisher's Note: All claims expressed in this article are solely those of the authors and do not necessarily represent those of their affiliated organizations, or those of the publisher, the editors and the reviewers. Any product that may be evaluated in this article, or claim that may be made by its manufacturer, is not guaranteed or endorsed by the publisher.

Copyright © 2022 Zhang, Perez-Garcia, Dierkes, Applegate, Schumacher, Chibani, Sternagel, Preuss, Weigert, Schmeisser, Danso, Pleiss, Almeida, Höcker, Hallam, Schmitz, Smits, Chow and Streit. This is an open-access article distributed under the terms of the Creative Commons Attribution License (CC BY). The use, distribution or reproduction in other forums is permitted, provided the original author(s) and the copyright owner(s) are credited and that the original publication in this journal is cited, in accordance with accepted academic practice. No use, distribution or reproduction is permitted which does not comply with these terms.

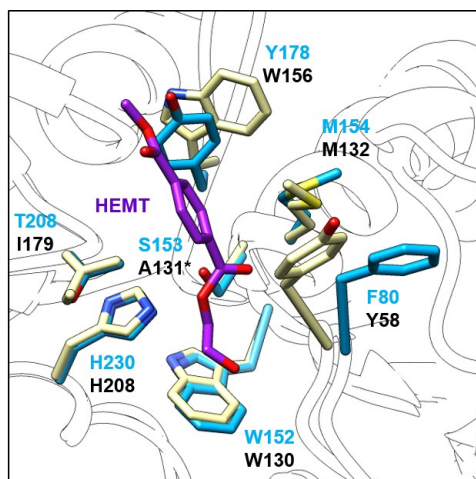
Supplementary Material

All Supplementary Material for this article can be found online at:

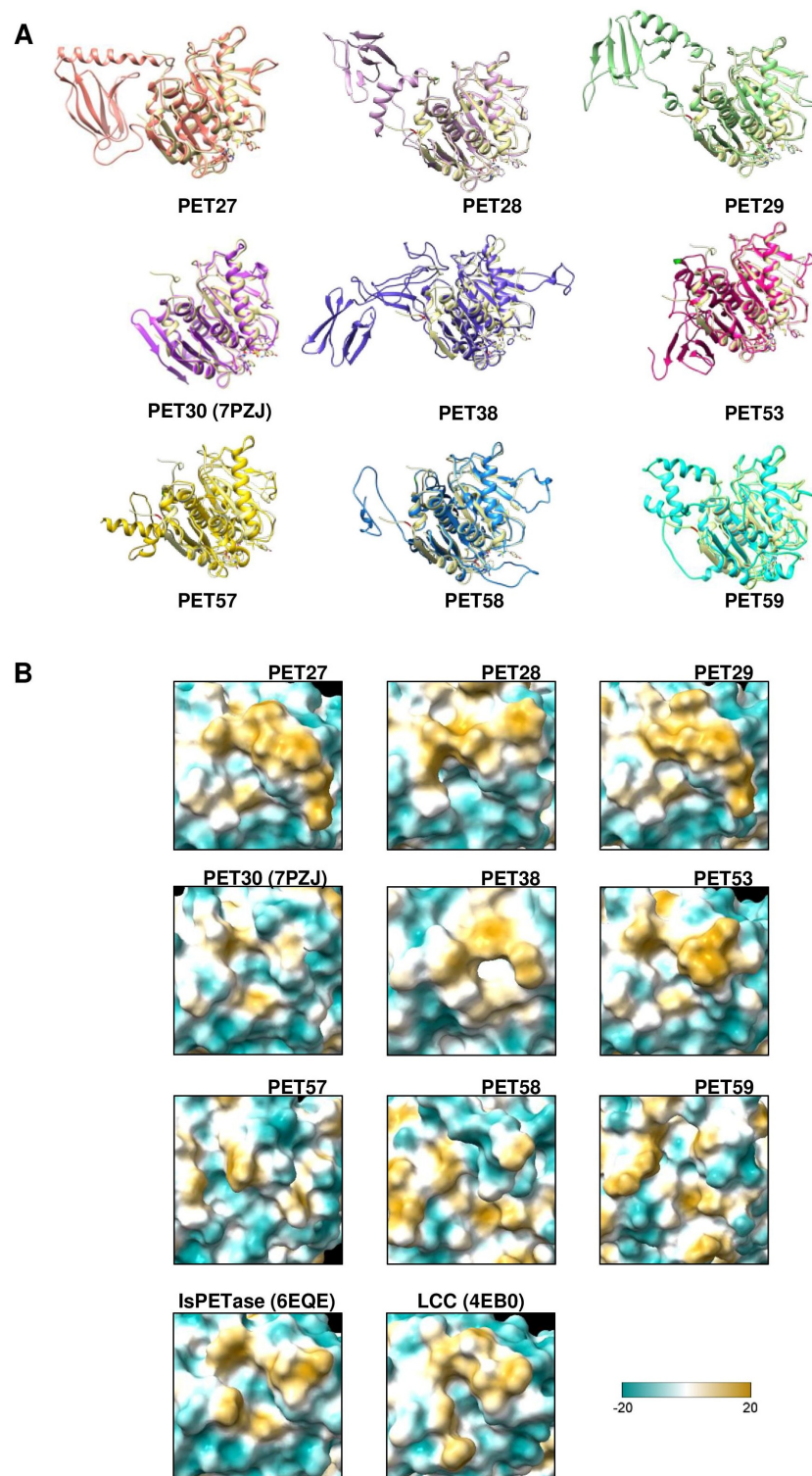
<https://www.frontiersin.org/articles/10.3389/fmicb.2021.803896/full#supplementary-material>



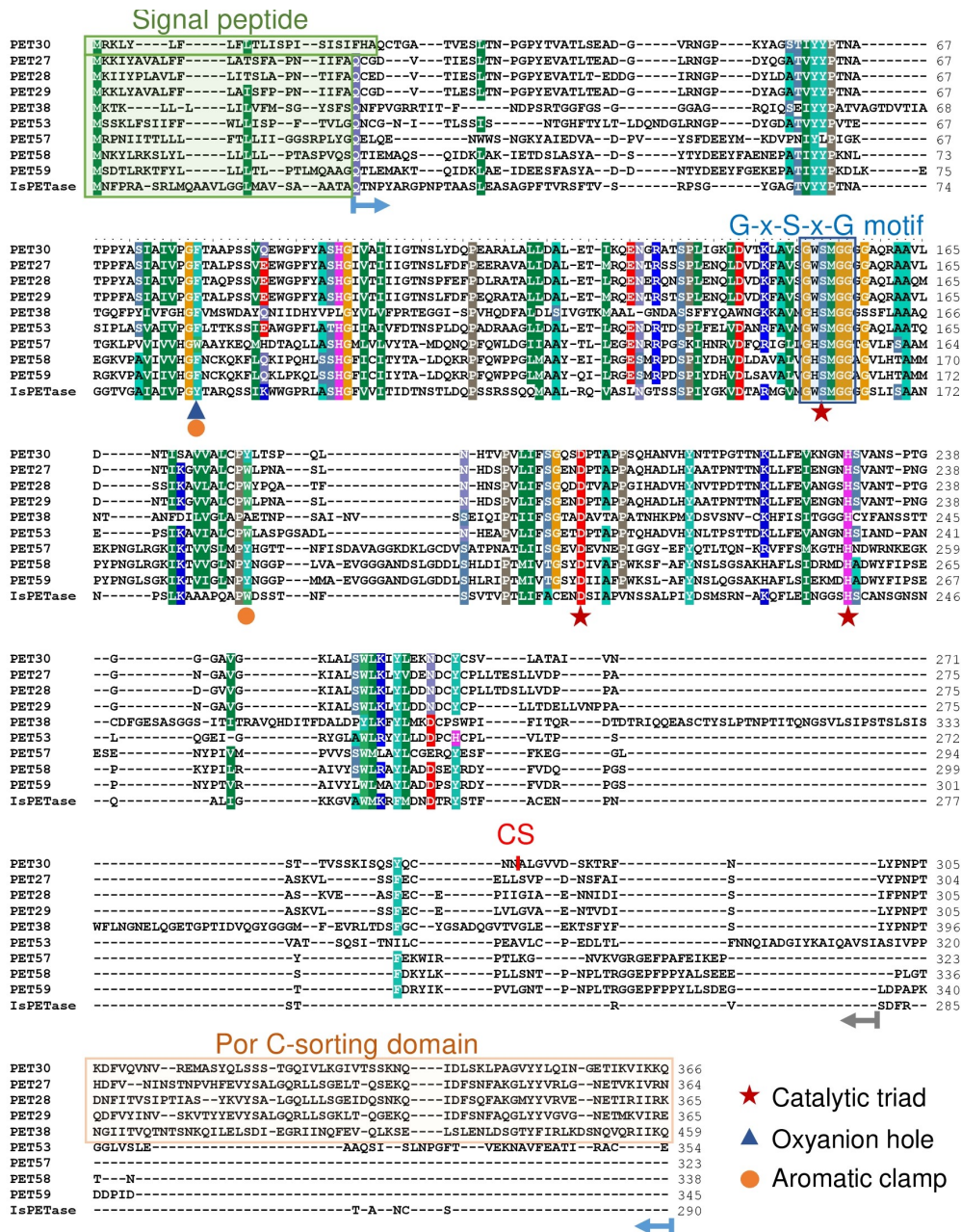
Supplementary Figure 1: Further biochemical characterization of PET27 and PET30 using *p*NP-substrates. Cofactor requirements were tested for PET27 with *p*NP-C8 at 40°C and for PET30 with *p*NP-C6 at 30°C (A). For PET30, all other tests were carried out with *p*NP-C6 and all assays except (B) were conducted at 30°C. Thermostability of PET30 was assessed at 50 and 60°C over 3 h with *p*NP-C6 (B). Inhibitors (C) and detergents (D) generally decrease the activity of PET30, particularly with higher concentrations. Activity of PET30 and PET30 Δ PorC were compared under the same conditions using *p*NP-C6 (E). Data represent mean values of at least three independent measurements.



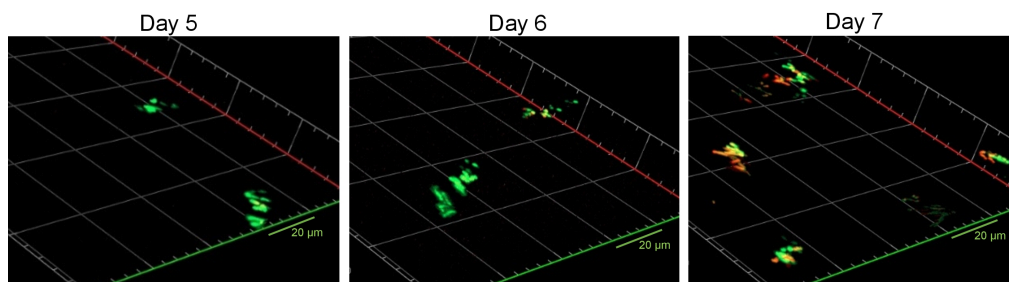
Supplementary Figure 2: Zoom into the active site of PET30ΔPorC. Overlaid are the structures of PET30ΔPorC (blue) with the PETase from *I. sakaiensis* (light yellow, black labeling) in complex with HEMT (purple; PDB code 5XH3). The residues involved in binding are highlighted and numbered according to their structure. *The structure 5XH3 is a mutant where the catalytic Serine was mutated to an Alanine.



Supplementary Figure 3: Structure prediction models of verified and predicted PETases affiliated with the phylum of the Bacteroidetes. (A) 3D structures were modeled using the Robetta server using the IsPETase crystal structure (light yellow, 6EQE) as a backbone. For PET30, the crystal structure was shown. (B) Surface hydrophobicity around the tunnel leading to the active site of putative bacteroidetal PETases and functionally verified PET-degrading enzymes. Hydrophilic regions are displayed in turquoise and hydrophobic in gold.



Supplementary Figure 4: Amino acid alignment of 9 potential PETases affiliated with the Bacteroidetes phylum. The original sequences were used for the structural alignment and the alignment was constructed with T-Coffee. Alignment was visualized with Bioedit version 7.0.5. The IsPETase was included for reasons of benchmarking. Blue arrows indicate the start and the end of the active PET27 and PET30 clones. We introduced a methionine as the first aa of the protein sequences. The signal peptide deleted version of the enzymes was functionally verified. The red arrow labeled with CS indicates the predicted cleavage site of C-terminal PorC domain. The gray arrow indicates the C-terminus of the truncated version of PET30 (PET30 Δ 300-366), number indicates the position of amino acid). PET30 Δ 300-366 was active on PCL and BHET.



Supplementary Figure 5: Confocal microscopic pictures of *K. jeonii* colonizing PET foil. The pictures were taken after 5–7 days of incubation of *K. jeonii* in R2A medium. Cells are dyed with LIVE/DEAD™ stain. Green fluorescence shows living cells, red fluorescence indicates dead cells. 2D front pictures were taken with Axio Observer Z1/7, LSM 800 (Carl Zeiss, Jena, Germany) of a 3D Z-stack image.

TABLE S1: Bacterial strains and plasmids used in this work.

Strain	Properties	Reference/source
<i>E. coli</i> DH5 α	<i>supE44</i> Δ <i>lacU169</i> (Φ 80 <i>lacZ</i> Δ M15) <i>hsdR17 recA1 endA1 gyrA96 thi-1 relA1</i>	Invitrogen (Karlsruhe, Germany)
<i>E. coli</i> BL21 (DE3)	F ⁻ , <i>ompT</i> , <i>hsdS B</i> (<i>r_B</i> ⁻ <i>m_B</i> ⁻) <i>gal</i> , <i>dcm</i> , λ DE3	Novagen/Merck (Darmstadt, Germany)
<i>E. coli</i> SHuffle® T7	<i>huA2 lacZ::T7 gene1</i> [<i>lon</i>] <i>ompT ahpC gal</i> λ att::pNEB3-r1-cDsbC (SpecR, <i>lacIq</i>) Δ <i>trxB sulA11</i> R(<i>mcr-73::miniTn10--TetS</i>)2 [<i>dcm</i>] R(<i>zgb-210::Tn10 -TetS</i>) <i>endA1</i> Δ <i>gor</i> Δ (<i>mcrC-mrr</i>)114::IS10	NEB (Frankfurt am Main, Germany)
Vector	Properties	Reference/source
pET21a(+)	Expression vector, <i>lacI</i> , Amp ^R , T7- <i>lac</i> - promoter, C-terminal His ₆ -tag coding sequence	Novagen/Merck (Darmstadt, Germany)
pET21a(+):PET27	1026 bp insert in pET21a(+) coding for PET27	This work
pET21a(+):PET28	1029 bp insert in pET21a(+) coding for PET28	This work
pET21a(+):PET29	1029 bp insert in pET21a(+) coding for PET29	This work
pET21a(+):PET30	1032 bp insert in pET21a(+) coding for PET30	This work
pET21a(+):PET30_ Δ 300-366	831 bp insert in pET21a(+) coding for PET30, truncated protein lacking PorC	This work
pET21a(+):PET38	1341 bp insert in pET21a(+) coding for PET38	This work
pET21a(+):PET53	1072 bp insert in pET21a(+) coding for PET53	This work
pET21a(+):PET57	969 bp insert in pET21a(+) coding for PET57	This work
pET21a(+):PET58	1014 bp insert in pET21a(+) coding for PET58	This work
pET21a(+):PET59	1035 bp insert in pET21a(+) coding for PET59	This work
pMAL-p4x::IsPETase	795 bp insert in pMAL-p4x coding for the wildtype IsPETase from <i>Ideonella sakaiensis</i>	This work

TABLE S2: Primers used in this work.

Primer	Sequence (5' \rightarrow 3')	Length (bp)	T _m (°C)	Source
T7_prom	TAATACGACTCACTATAGGG	20	53	Eurofins MWG (Elsberg, Germany)
T7_term	CTAGTTATTGCTCAGCGGT	19	54	Eurofins MWG (Elsberg, Germany)
PET_for	ATATAGGCGCCAGCAACC	18	59	Novagen/Merck (Darmstadt, Germany)
PET_rev	TCCGGATATAGTTCCTC	17	52	Novagen/Merck (Darmstadt, Germany)

TABLE S3: Identifiers and GenBank entries employed in the phylogenetic clustering of PET active enzymes in FIGURE 4.

Name	GenBank or PDB entry	Phylogenetic Affiliation	Reference
BsEstB	ADH43200.1	<i>Bacillus subtilis</i> 4P3-11	Herrero Acero <i>et al.</i> 2011
CalB	4K6G_A	<i>Candida antarctica</i>	Andersen <i>et al.</i> 1999; Xie <i>et al.</i> 2014
Cut190	BAO42836.1	<i>Saccharomonospora viridis</i> AHK190	Kawai <i>et al.</i> 2014
FsC	1CEX	<i>Fusarium solani</i> pisi	Silva <i>et al.</i> 2005
HiC	4OYY	<i>Humicola insolens</i>	Ronkvist <i>et al.</i> 2009
IsPETase	GAP38373.1	<i>Ideonella sakaiensis</i> 201-F6	Yoshida <i>et al.</i> 2016
LCC	AEV21261.1	uncultured bacterial species (leaf-branch compost)	Sulaiman <i>et al.</i> 2012
PE-H	A0A1H6AD45	<i>Pseudomonas aestusnigri</i> VGXO14T	Bollinger <i>et al.</i> 2020
PET2	C3RYL0	uncultured bacterium	
PET5	R4YKL9	<i>Oleispira antarctica</i> RB-8	Danso <i>et al.</i> 2018
PET6	A0A1Z2SIQ1	<i>Vibrio gazogenes</i>	
PET12	A0A0G3BI90	<i>Polyangium brachysporum</i>	
Tcur0390	WP_012850775.1	<i>Thermomonospora curvata</i> DSM43183	Wei <i>et al.</i> 2014
Tcur1278	WP_012851645.1	<i>Thermomonospora curvata</i> DSM43183	Chertkov <i>et al.</i> 2011
TfH	WP_011291330.1	<i>Thermobifida fusca</i> DSM43793	Müller <i>et al.</i> 2005
Thc_Cut1	ADV92526.1	<i>Thermobifida cellulosilytica</i> DSM44535	
Thc_Cut2	ADV92527.1	<i>Thermobifida cellulosilytica</i> DSM44535	Herrero Acero <i>et al.</i> 2011
Thf42_Cut1	ADV92528.1	<i>Thermobifida fusca</i> DSM44342	
Tha_Cut1	ADV92525.1	<i>Thermobifida alba</i> DSM43185	Ribitsch <i>et al.</i> 2012
Thh_Est	AFA45122.1	<i>Thermobifida halotolerans</i> DSM44931	

TABLE S4: Data collection and refinement statistics for PET30

	PET30
Wavelength	0.9795
Resolution range	38.8 - 2.1 (2.175 - 2.1)
Space group	P 43 21 2
Unit cell	109.755 109.755 41.803 90 90 90
Total reflections	267429 (24691)
Unique reflections	15447 (1505)
Multiplicity	17.3 (16.4)
Completeness (%)	99.95 (100.00)
Mean I/sigma(I)	13.95 (5.38)
Wilson B-factor	24.09
R-merge	0.1746 (0.7031)
R-meas	0.1799 (0.7255)
R-pim	0.04277 (0.1772)
CC1/2	0.997 (0.945)
CC*	0.999 (0.986)
Reflections used in refinement	15443 (1507)
Reflections used for R-free	716 (78)
R-work	0.1619 (0.1655)
R-free	0.2187 (0.2460)
CC(work)	0.962 (0.901)
CC(free)	0.932 (0.840)
Number of non-hydrogen atoms	2208
macromolecules	2006
solvent	202
Protein residues	273
RMS(bonds)	0.011
RMS(angles)	1.21
Ramachandran favored (%)	95.57
Ramachandran allowed (%)	3.69
Ramachandran outliers (%)	0.74
Rotamer outliers (%)	0.00
Clashscore	5.01
Average B-factor	27.12
macromolecules	26.45
solvent	33.82

Statistics for the highest-resolution shell are shown in parentheses.

TABLE S5: Homologs of bacteroidetal PET27 and PET30 hydrolases in metagenomes.

Locus Tag	Gene ID	Genome Name (GREEN=Bacteroidetes; YELLOW=FCB)	NCBI Biosample Accession	Pubmed ID /GenBank entry
Ga0266410_112824	2790477168	<i>Aequorivita</i> sp. CPC67	SAMEA2621812	25999513
Ga0267287_12740	2786516536	<i>Marinimicrobia</i> bacterium SP4388	SAMEA2621812	25999513
Ga0214074_111348	2758370761	<i>Psychroflexus torquis</i> ATCC 700755	SAMN02603919	24391155 , 32431677
Ga0441744_095_43538_44635	2893010289	<i>Psychroflexus gondwanensis</i> ACAM 365	SAMN10790446	24391155, 32431677
Ga0452869_05_68007_69104	2890419200	<i>Brumimicrobium glaciale</i> IC156	SAMN10779751	24391155, 32431677
Ga0125537_104199	2776033716	<i>Altibacter lentus</i> JL2010	SAMN02988278	25342673
Ga0101260_1142	2663974789	<i>Bacteroidetes</i> bacterium SCGC AD-308-D03 - v2	SAMN06314724	373136
Ga0266415_110121	2790487960	<i>Aequorivita</i> sp. SAT106	SAMEA2620929	25999513
Ga0266677_12858	2778555477	<i>Flavobacteriaceae</i> bacterium SAT1509	SAMEA2620929	25999513
Ga0267170_100812	2814895288	<i>Gemmatimonadetes</i> bacterium RS373	SAMEA2620929	25999513
Ga0267250_100918	2786410539	<i>Marinimicrobia</i> bacterium RS418	SAMEA2620929	25999513
Ga0267252_10536	2786413511	<i>Marinimicrobia</i> bacterium RS816	SAMEA2620929	25999513
Ga0267252_10542	2786413517	<i>Marinimicrobia</i> bacterium RS816	SAMEA2620929	25999513
Ga0266410_112825	2769034576	<i>Aequorivita</i> sp. CPC68	SAMEA2621812	25999513
Ga0267287_12741	2767134878	<i>Marinimicrobia</i> bacterium SP4389	SAMEA2621812	25999513
Ga0214074_111349	2765235181	<i>Psychroflexus torquis</i> ATCC 700756	SAMN02603919	24391155 , 32431678
Ga0441744_095_43538_44636	2763335483	<i>Psychroflexus gondwanensis</i> ACAM 366	SAMN10790446	24391155, 32431677
Ga0452869_05_68007_69105	2761435786	<i>Brumimicrobium glaciale</i> IC157	SAMN10779751	24391155, 32431677
Ga0267200_1431	2786528832	<i>Marinimicrobia</i> bacterium EAC25	SAMEA2620855	25999513, 29337314
Ga0267200_1544	2786528992	<i>Marinimicrobia</i> bacterium EAC25	SAMEA2620855	25999513, 29337314
Ga0416765_13_4825_5925	2860314059	<i>Chryseobacterium</i> sp. 16F	SAMN14915977	25824943
PI23P_05397	639004873	<i>Polaribacter irgensii</i> 23-P	SAMN02436114	9542092 /NZ_CH724148.1
Aeqsu_2514	2509583556	<i>Aequorivita subliithicola</i> QSSC9-3, DSM 14238	SAMN02232006	28604660
Ga0266584_11073	2788314349	<i>Cryomorphaceae</i> bacterium CPC63	SAMEA2622923	25999513
Ga0266589_10312	2787698016	<i>Cytophagia</i> bacterium NAT375	SAMEA2622923	25999513
Ga0267262_14611	2786499724	<i>Marinimicrobia</i> bacterium SAT24	SAMEA2622923	25999513
Ga0267263_11113	2786500508	<i>Marinimicrobia</i> bacterium SAT2619	SAMEA2622923	25999513
Ga0267267_12326	2786498443	<i>Marinimicrobia</i> bacterium SP108	SAMEA2622923	25999513
Ga0267268_10328	2786441642	<i>Marinimicrobia</i> bacterium SP173	SAMEA2622923	25999513
Ga0267268_1112	2786442127	<i>Marinimicrobia</i> bacterium SP173	SAMEA2622923	25999513
Ga0267270_13120	2786484524	<i>Marinimicrobia</i> bacterium SP276	SAMEA2622923	25999513
Ga0267272_1173	2786478779	<i>Marinimicrobia</i> bacterium SP3060	SAMEA2622923	25999513
Ga0267273_13417	2786477564	<i>Marinimicrobia</i> bacterium SP3097	SAMEA2622923	25999513
Ga0267276_13625	2786480397	<i>Marinimicrobia</i> bacterium SP3117	SAMEA2622923	25999513
Ga0267279_10440	2786489803	<i>Marinimicrobia</i> bacterium SP328	SAMEA2622923	25999513
Ga0267280_12433	2786520859	<i>Marinimicrobia</i> bacterium SP359	SAMEA2622923	25999513
Ga0267282_10178	2786519018	<i>Marinimicrobia</i> bacterium SP4039	SAMEA2622923	25999513
Ga0063505_10623	2606052547	<i>Roseivirga seohaensis aquiponti</i> D-25	SAMN03145748	27107724/ JSVA01000000

2 PET-hydrolyzing esterases from Bacteroidetes

Ga0267161_105313	2814952585	<i>Gemmatimonadetes bacterium</i> EAC635	SAMEA2623295	25999513
Ga0267164_1577	2814955360	<i>Gemmatimonadetes bacterium</i> NAT196	SAMEA2623295	25999513
Ga0267234_12226	2786460090	<i>Marinimicrobia bacterium</i> NAT495	SAMEA2623295	25999513
Ga0267237_1518	2786446587	<i>Marinimicrobia bacterium</i> NAT62	SAMEA2623295	25999513
Ga0267238_1416	2786464404	<i>Marinimicrobia bacterium</i> NAT74	SAMEA2623295	25999513
Ga0267239_13724	2786462435	<i>Marinimicrobia bacterium</i> NP104	SAMEA2623295	25999513
Ga0215720_101116	2756777030	<i>Marinirhabdus gelatinilytica</i> DSM 101478	SAMN08776299	QRAO00000000
Ga0266586_11614	2788308996	<i>Cryomorpaceae bacterium</i> SP53	SAMEA2619927	25999513
Ga0267165_10476	2814943193	<i>Gemmatimonadetes bacterium</i> NP105	SAMEA2619818	25999513
SCB49_04680	641143976	<i>Ulvibacter</i> sp. SCB49	SAMN02981237	ABCO00000000
G440DRAFT_00359	2524126300	<i>Aequorivita capsosiphonis</i> DSM 23843	SAMN02440880	AUBG00000000
Ga0266370_16423	2789796087	<i>Altibacter</i> sp. EAC109	SAMEA2619376	25999513
Ga0266560_154	2825980380	<i>Crocinitomicaceae bacterium</i> NAT165	SAMEA2619376	25999513
Ga0267217_1484	2786425266	<i>Marinimicrobia bacterium</i> MED806	SAMEA2619376	25999513
Ga0267217_16831	2786425767	<i>Marinimicrobia bacterium</i> MED806	SAMEA2619376	25999513
Ga0267218_1219	2786426885	<i>Marinimicrobia bacterium</i> MED808	SAMEA2619376	25999513
Ga0267219_10943	2786427199	<i>Marinimicrobia bacterium</i> MED812	SAMEA2619376	25999513
Ga0267220_10096	2786428744	<i>Marinimicrobia bacterium</i> MED829	SAMEA2619376	25999513
Ga0267220_10106	2786428754	<i>Marinimicrobia bacterium</i> MED829	SAMEA2619376	25999513
Ga0267224_14310	2786401069	<i>Marinimicrobia bacterium</i> NAT217	SAMEA2619376	25999513
Ga0267226_12918	2786404156	<i>Marinimicrobia bacterium</i> NAT220	SAMEA2619376	25999513
Ga0267227_13041	2786403315	<i>Marinimicrobia bacterium</i> NAT224	SAMEA2619376	25999513
Ga0267228_1422	2786399119	<i>Marinimicrobia bacterium</i> NAT230	SAMEA2619376	25999513
Ga0267208_10372	2786507568	<i>Marinimicrobia bacterium</i> MED586	SAMEA2619667	25999513
Ga0267208_10412	2786507636	<i>Marinimicrobia bacterium</i> MED586	SAMEA2619667	25999513
Ga0267209_1018	2786508441	<i>Marinimicrobia bacterium</i> MED589	SAMEA2619667	25999513
Ga0267212_106014	2786417419	<i>Marinimicrobia bacterium</i> MED648	SAMEA2619667	25999513
Ga0267212_10712	2786417608	<i>Marinimicrobia bacterium</i> MED648	SAMEA2619667	25999513
Ga0267212_110812	2786418228	<i>Marinimicrobia bacterium</i> MED648	SAMEA2619667	25999513
Ga0267213_15817	2786422578	<i>Marinimicrobia bacterium</i> MED757	SAMEA2619667	25999513
Ga0267214_1214	2786420423	<i>Marinimicrobia bacterium</i> MED764	SAMEA2619667	25999513
Ga0267214_12210	2786420472	<i>Marinimicrobia bacterium</i> MED764	SAMEA2619667	25999513
Ga0267214_1225	2786420467	<i>Marinimicrobia bacterium</i> MED764	SAMEA2619667	25999513
Ga0267214_14025	2786421083	<i>Marinimicrobia bacterium</i> MED764	SAMEA2619667	25999513
Ga0344934_2405	2839770976	<i>Dokdonia sinensis</i> SH27	SAMN10250232	32228747
Ga0441973_01_775875_776969	2890600833	<i>Ulvibacter</i> sp. KK4	SAMD00166796	32539909
LY87DRAFT_1302	2597312806	<i>Dokdonia</i> sp. Hel_I_5	SAMN05661066	32539909
Ga0267202_1226	2786524372	<i>Marinimicrobia bacterium</i> EAC649	SAMEA2620230	25999513
Ga0267202_13210	2786524561	<i>Marinimicrobia bacterium</i> EAC649	SAMEA2620230	25999513
Ga0267202_13216	2786524567	<i>Marinimicrobia bacterium</i> EAC649	SAMEA2620230	25999513
Ga0350409_3222	2848310855	<i>Psychroflexus</i> sp. MES1-P1E	SAMN08125772	PJBS00000000, CM009131
Ga0066802_10753	2623289129	<i>Aequorivita viscosa</i> DSM 26349	SAMN04487908	FQYV00000000
Ga0077144_1092	2641186029	<i>Chryseobacterium jeonii</i> DSM 17048	SAMN03145167	JSYL00000000
Ga0079842_10854	2668214597	<i>Aequorivita viscosa</i> CGMCC 1.11023	SAMN05216556	FNNS00000000

Ga0104531_1111	2676887423	<i>Chryseobacterium jeonii</i> DSM 17048	SAMN05421876	FOLA00000000
Ga0114183_10545	2656209723	<i>Roseivirga seohaensis</i> SW-152	SAMN04423148	28077207
Ga0170448_3258	2729662814	<i>Ulvibacter antarcticus</i> DSM 23424	SAMN06264851	REFC00000000
Ga0310487_0626	2799156613	<i>Roseivirga ehrenbergii</i> DSM 102268	SAMN10864729	SMGS00000000
Ga0336340_1074	2835308220	<i>Winogradskyella</i> sp. KYW1333	SAMN09667312	QPHL00000000
Ga0336670_2825	2837407865	<i>Aequorivita lipolytica</i> CIP 107455	SAMEA4644770	30225207
Ga0336672_3534	2835103747	<i>Aequorivita antarctica</i> CIP 107457	SAMEA4644771	PMC6139392
Ga0443045_01_3096381_3097484	2884436497	<i>Nonlabens</i> sp. Ci31	SAMN12697551	CP043633
pgond44_05165	2533771942	<i>Psychroflexus gondwanensis</i> ACAM 44	SAMN02471957	24391155
Ga0077372_102327	2628626758	<i>Aequorivita vladivostokensis</i> KMM 3516	SAMN03084320	JSVU00000000
Ga0114184_10616	2654412999	<i>Roseivirga echinicomitans</i> KMM 6058	SAMN04382068	LRDB00000000.1
Ga0248413_145580	2812952679	<i>Roseivirga ehrenbergii</i> KMM 6017	SAMN03084331	LQZQ00000000
Ga0373279_1152	2830035069	<i>Lewinella antarctica</i> DSM 105096	SAMN13172327	PMC6139392
Ga0336671_791	2835108492	<i>Aequorivita</i> sp. CIP 111184	SAMEA4704834	UEFQ00000000
Ga0399719_270	2836794304	<i>Aequorivita</i> sp. H23M31	SAMN10518960	CP034951
Ga0441974_01_521424_522518	2890652824	<i>Ulvibacter marinus</i> KCTC 32322T	SAMD00166797	BKCG00000000.1

3 The metagenome-derived esterase PET40 is highly promiscuous and hydrolyses polyethylene terephthalate (PET)

Hongli Zhang¹⁺, Robert Dierkes¹⁺, Pablo Perez-Garcia^{1,2}, Elisa Costanzi³, Jonas Dittrich⁴, Marno Gurschke¹, Violetta Applegate³, Kristina Partus¹, Christel Schmeisser¹, Christopher Pflieger⁴, Holger Gohlke^{4,5}, Sander H.J. Smits^{3,6}, Jennifer Chow¹ and Wolfgang R. Streit^{1*}

¹Department of Microbiology and Biotechnology, University of Hamburg, 22609 Hamburg, Germany ²Molecular Microbiology, Institute for General Microbiology, Kiel University, Kiel, Germany ³Center for Structural Studies, Heinrich Heine University, Düsseldorf, Germany ⁴Institute for Pharmaceutical and Medicinal Chemistry, Heinrich Heine University, Düsseldorf, Germany ⁵Institute of Bio- and Geosciences (IBG-4: Bioinformatics), John von Neumann Institute for Computing and Jülich Supercomputing Centre, Forschungszentrum Jülich GmbH, Jülich, Germany ⁶Institute of Biochemistry, Heinrich Heine University, Düsseldorf, Germany

+shared first authors, equal contributions

Published in:

The FEBS Journal doi:10.1111/febs.16924



The metagenome-derived esterase PET40 is highly promiscuous and hydrolyses polyethylene terephthalate (PET)

Hongli Zhang¹, Robert F. Dierkes¹ , Pablo Perez-Garcia^{1,2} , Elisa Costanzi³, Jonas Dittrich⁴ , Pablo A. Cea⁴ , Marno Gurschke¹, Violetta Applegate³ , Kristina Partus¹, Christel Schmeisser¹, Christopher Pflieger⁴ , Holger Gohlke^{4,5} , Sander H. J. Smits^{3,6} , Jennifer Chow¹ and Wolfgang R. Streit¹

1 Department of Microbiology and Biotechnology, University of Hamburg, Germany

2 Molecular Microbiology, Institute for General Microbiology, Kiel University, Germany

3 Center for Structural Studies, Heinrich Heine University, Düsseldorf, Germany

4 Institute for Pharmaceutical and Medicinal Chemistry, Heinrich Heine University, Düsseldorf, Germany

5 Institute of Bio- and Geosciences (IBG-4: Bioinformatics), John von Neumann Institute for Computing and Jülich Supercomputing Centre, Forschungszentrum Jülich GmbH, Germany

6 Institute of Biochemistry, Heinrich Heine University, Düsseldorf, Germany

Keywords

HMM; hydrolases; metagenome; PET degradation; promiscuity

Correspondence

W. R. Streit, Department of Microbiology and Biotechnology, University of Hamburg, Ohnhorststr. 18, D-22609 Hamburg, Germany

Tel: +49 40 42816 463

E-mail: wolfgang.streit@uni-hamburg.de

Hongli Zhang and Robert F. Dierkes shared first authorship

Dedicated to Karl-Erich Jaeger for his pioneering contributions in the field of molecular enzyme technology

(Received 31 January 2023, revised 24 July 2023, accepted 7 August 2023)

doi:10.1111/febs.16924

Polyethylene terephthalate (PET) is a widely used synthetic polymer and known to contaminate marine and terrestrial ecosystems. Only few PET-active microorganisms and enzymes (PETases) are currently known, and it is debated whether degradation activity for PET originates from promiscuous enzymes with broad substrate spectra that primarily act on natural polymers or other bulky substrates, or whether microorganisms evolved their genetic makeup to accepting PET as a carbon source. Here, we present a predicted diene lactone hydrolase designated PET40, which acts on a broad spectrum of substrates, including PET. It is the first esterase with activity on PET from a GC-rich Gram-positive *Amycolatopsis* species belonging to the Pseudonocardiaaceae (Actinobacteria). It is highly conserved within the genera *Amycolatopsis* and *Streptomyces*. PET40 was identified by sequence-based metagenome search using a PETase-specific hidden Markov model. Besides acting on PET, PET40 has a versatile substrate spectrum, hydrolyzing δ -lactones, β -lactam antibiotics, the polyester-polyurethane Impranil® DLN, and various *para*-nitrophenyl ester substrates. Molecular docking suggests that the PET degradative activity is likely a result of the promiscuity of PET40, as potential binding modes were found for substrates encompassing mono(2-hydroxyethyl) terephthalate, bis(2-hydroxyethyl) terephthalate, and a PET trimer. We also solved the crystal structure of the inactive PET40 variant S178A to 1.60 Å resolution. PET40 is active throughout a wide pH (pH 4–10) and temperature range (4–65 °C) and remarkably stable in the

Abbreviations

aa, amino acids; BHET, bis(2-hydroxyethyl) terephthalate; CalB, *Candida antarctica* lipase B; CEC, cefaclor; CFT, cefotiam; DTT, dithiothreitol; EDTA, ethylenediaminetetraacetic acid; EG, ethylene glycol; EPPS, *N*-(2-hydroxyethyl)piperazine-*N*-(3-propanesulfonic acid); HEPES, hydroxyethylpiperazine-1-ethanesulfonic acid; HMM, hidden Markov model; IPM, imipenem; isPETase, *Ideonella sakaiensis* PETase; LB, lysogeny broth; LCC, leaf compost cutinase; MA, cefamandole; MEZ, mezlocillin; MH, methyl hexanoate; MHET, mono(2-hydroxyethyl) terephthalate; PCL, polycaprolactone; PCL₃, polycaprolactone trimer; PEG, polyethylene glycol; PET, polyethylene terephthalate; PET₃, polyethylene terephthalate trimer; PMSF, phenylmethylsulfonyl fluoride; *p*NP, *para*-nitrophenyl; *p*NP-C10, 4-nitrophenyl decanoate; *p*NP-C12, 4-nitrophenyl dodecanoate; RMSD, root-mean-square deviation; TBT, tributyrin; TPA, terephthalic acid; UHPLC, ultra-high performance liquid chromatography; ZOI, zone of inhibition.

presence of 5% SDS, making it a promising enzyme as a starting point for further investigations and optimization approaches.

Introduction

Petroleum-based plastics are, in general, extremely stable and durable. The global use at a multimillion tons scale over 70 years and the lack of recycling and circular use concepts have resulted in unprecedented pollution in nearly all environments [1,2]. Microbial- and enzyme-driven plastics degradation have made enormous progress in the last years, and several reviews have summarized the current knowledge [3–7].

Currently, around 80 enzymes originating from four different bacterial phyla are biochemically characterized PET-active hydrolases (www.pazy.eu database search, accessed on 02.05.23; [8]) (Fig. 1). These enzymes comprise cutinases (EC3.1.1.74), lipases (EC3.1.1.3), and carboxylesterases (EC3.1.1.1) that can act on amorphous and low-crystalline PET. They hydrolyze ester bonds in the polymer yielding bis-(2-hydroxyethyl) terephthalate (BHET), mono-(2-hydroxyethyl) terephthalate (MHET), terephthalic acid (TPA), and ethylene glycol (EG). Some bacteria can hydrolyze MHET using an MHETase [9,10]. TPA can be degraded via cleavage of the aromatic ring structure using known aryl pathways [11,12]. While EG is often oxidized to glycolate before entering glyoxylate degradative pathways.

The best-studied enzymes are derived from the Gram-negative proteobacterium *Ideonella sakaiensis* 201-F6 [9] and from a leaf branch compost metagenome [15]. The latter is a designated leaf and branch compost cutinase (LCC) and is phylogenetically affiliated with the Gram-positive genus *Thermobifida* [15]. This genus together with the closely related genera *Thermomonospora* and *Saccharomonospora* are phylogenetically grouped within Actinobacteria and have been a rich source for PET hydrolases [16–22] (Fig. 1). Also, it has been shown that the Gram-negative genus *Pseudomonas* (Proteobacteria) harbors a diverse set of PET-active enzymes, listed in the PAZy database (www.pazy.eu). Among them are PpCutA from *P. pseudoalcaligenes*, PpelaLip derived from *P. pelagia* and PE-H from *P. aestusnigri* [23–25]. Additionally, we recently reported on PET-degrading enzymes found in the Bacteroidetes phylum [26]. Altogether, these studies have significantly advanced our knowledge of the structural and biochemical processes affiliated with PET hydrolysis [10,27,28]. Furthermore, *Candida antarctica* lipase B (CalB), *Fusarium solani* FsC, and *Humicola insolens* HiC were affiliated with PET degradation as part of promiscuous enzyme activities [29]. Since it is well-known that some esterases are highly

Fig. 1. PET40 shares sequence similarities with other actinobacterial PETases and LCC. The unrooted phylogenetic tree is based on amino acid sequence homologies. Overall, a selection of 23 enzymes was included in this alignment. The structural alignment was calculated with T-COFFEE EXPRESSO [13]. The tree was constructed by a Maximum Likelihood method using MEGAX [14] with 1000 bootstraps. The bootstrap values are indicated as percentages at the branches. GenBank entries of the sequences used are listed in Table 1 and on www.pazy.eu. The phylogenetic groups are highlighted with distinct colors, as shown in the legend.

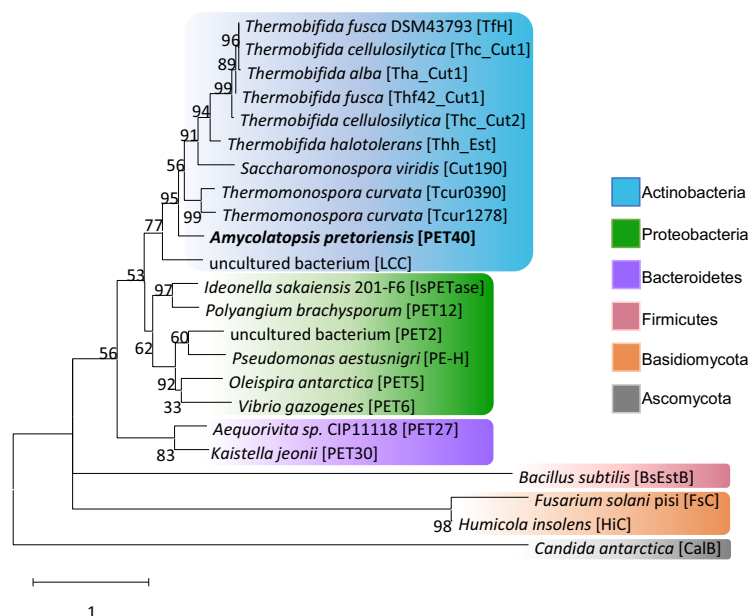


Table 1. Functionally verified and known PET-active enzymes in the phylum of the Actinobacteria.

Name	GenBank accession	Phylogenetic affiliation	Reference	aa sequence identity with PET40 (%)
PET40	WAU86704.1	<i>Amycolatopsis</i> sp.	This work	100.00
Cut190	BAO42836.1	<i>Saccharomonospora viridis</i> AHK190	[19]	65.40
LCC	AEV21261.1	Uncultured bacterium	[15]	58.94
Tcur0390	WP_012850775.1	<i>Thermomonospora curvata</i> DSM43183	[38]	68.34
Tcur1278	WP_012851645.1	<i>Thermomonospora curvata</i> DSM43183	[20]	69.14
TfH	WP_011291330.1	<i>Thermobifida fusca</i> DSM43793	[21]	63.70
Thc_Cut1	ADV92526.1	<i>Thermobifida cellulosilytica</i> DSM44535	[22]	63.60
Thc_Cut2	ADV92527.1	<i>Thermobifida cellulosilytica</i> DSM44535		62.84
Thf42_Cut1	ADV92528.1	<i>Thermobifida fusca</i> DSM44342		62.45
Tha_Cut1	ADV92525.1	<i>Thermobifida alba</i> DSM43185	[16]	62.45
Thh_Est	AFA45122.1	<i>Thermobifida halotolerans</i> DSM44931		68.97

promiscuous [30,31] and the turnover rates of wild-type enzymes on PET are low to moderate, we assume that PETases are in general rather promiscuous enzymes and PET is not the native substrate. Our understanding of the origin, evolution, and role of PET-active enzymes in the environment is still very poor. These challenges can only be met by mining biodiversity for novel enzymes and analyzing and comparing their structural, phylogenetic, and kinetic characteristics.

Within this framework, and to further enrich the biodiversity of known PET-active enzymes, we have searched for new PET-active enzymes. Therefore, we used a previously published hidden Markov model (HMM) search algorithm to mine global genomes and metagenomes [32,33]. We identified a single novel esterase, designated PET40, that is distinct from previously identified enzymes in the Actinobacteria. Intriguingly, PET40 is highly conserved within the genera of *Amycolatopsis* and *Streptomyces*. The enzyme is highly active on a wide range of different substrates, including PET, and has remarkably good activity on *para*-nitrophenyl (*p*NP)-esters even at temperatures as low as 4 °C. While it is already known that some predicted diene lactone hydrolases can degrade PET [34], this study is one of the first that highlights substrate promiscuity aspects of a PET-active esterase by delivering experimental and structural evidence.

Results

Profile hidden Markov model search identifies the novel actinobacterial PET-active esterase PET40

Previous research has shown that bacterial PET esterases occur in four bacterial phyla (Fig. 1). Most of the verified PET-active enzymes have been identified in

the phylum of the *Actinomycetes* with 33 biochemically characterized enzymes (www.pazy.eu, accessed on 02.05.23). Since hitherto only in the three closely related genera *Thermobifida*, *Thermomonospora*, and *Saccharomonospora* active PETases had been identified, we wondered whether other GC-rich Gram-positive Actinobacterial genera code for PET-active enzymes. To address this question, we performed global database searches on publicly available bacterial genomes and metagenomes from the NCBI GenBank [35], and IMG database [36], combined with a previously published HMM-based search approach [32,33]. Among others, this search identified a potential diene lactone hydrolase in a soil metagenome affiliated with the Gram-positive genus *Amycolatopsis* from a biochar metagenome (Table 1) [37]. We designated this putative PETase PET40. A phylogenetic analysis of the deduced amino acid sequence implied that the predicted enzyme was phylogenetically related to known actinobacterial sequences, but not affiliated with any of the three genera *Thermobifida*, *Thermomonospora*, and *Saccharomonospora*. The amino acid alignment shows that the amino acid sequence similarity of PET40 ranged from 58.9% to 69.1% compared with the known high-GC bacterial PETases listed in Table 1. Based on this observation, we performed additional BLASTP searches using the PET40-deduced amino acid sequence. Interestingly, the enzyme is relatively conserved within the genus of *Amycolatopsis*. It is present in 21 of the 68 *Amycolatopsis* genomes deposited in GenBank with *E*-values ranging from $7e^{-172}$ to $1e^{-149}$ and the lowest identity of 93% (94% coverage). Using an arbitrary identity cutoff of 80%, we found the protein sequence in 73 of the 564 *Streptomyces* genomes from the NCBI genome database with the highest *E*-value of $7e^{-144}$ (81% identity at 95% query coverage). These data imply that the protein is widely distributed within these two genera and may have been

acquired via horizontal gene transfer within these GC-rich Gram-positive microorganisms.

Recombinant PET40 hydrolyzes TBT, PCL, BHET, the ester-based polyurethane Impranil DLN, and PET

To verify our bioinformatic analysis, we expressed PET40 in *Escherichia coli* for functional characterization. For this, the candidate gene was synthesized, cloned into the expression vector pET21a(+) (Biomatik, Wilmington, DA, USA), and transformed in *E. coli* BL21 (DE3). Initial tests using recombinant purified proteins and agar plates containing tributyrin (TBT) indicated the PET40-gene codes for an active esterase (Fig. 2A). PET40 was able to hydrolyze BHET (Fig. 2A), which is a monomeric constituent of PET used as a screening substrate to indicate possible activity on PET. Activity on polycaprolactone (PCL), a polyester model-substrate, could also be shown

(Fig. 2A). The hydrolysis of these model substrates also indicates possible activity on the polymeric and more complex PET. Additionally, we observed that PET40 was able to cleave Impranil® DLN, which is an aliphatic polyester polyurethane. After an incubation for 20 min at 40 °C with 5 µg PET40 (250 µL reaction volume), a release of $790 \pm 21 \mu\text{M}$ of H^+ was detectable using phenol red as the indicator (Fig. 2B). Ultra-high-performance liquid chromatography (UHPLC) analyses confirmed the release of hydrolysis products such as TPA from semicrystalline (> 40% crystallinity) PET powder after incubation with PET40 (Fig. 2C).

PET40 ($0.1 \text{ mg}\cdot\text{mL}^{-1}$ enzyme in 200 µL corresponding to $3.54 \mu\text{M}$) was incubated together with 5 mg PET powder for 72 h at 40 °C. After the incubation, a concentration of aromatic degradation products TPA, MHET, and BHET of $50.41 \pm 10.21 \mu\text{M}$ was measured in the reaction supernatant corresponding to a relative amount of $0.17 \pm 0.03 \mu\text{mol}$ TPA-EG unit

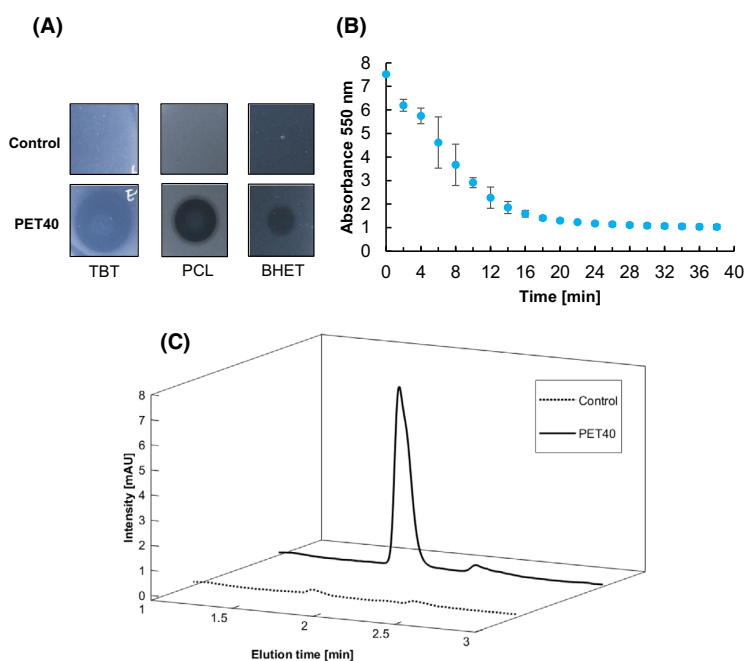


Fig. 2. PET40 hydrolyses various esters, including PET. (A) Activities of PET40 on TBT, PCL, and BHET using agar plates. 10 µL containing 10–100 µg of purified enzyme were applied to agar plates containing either 33.08 mm TBT, 4.38 mm PCL, or 5 mm BHET. Halos were observed after 12 h. Control indicates plates with 10 µL enzyme-free buffer. (B) Activity on Impranil® DLN was assessed using phenol red as pH indicator. Decreasing values of absorbance at 550 nm revealed the breakdown of Impranil® DLN by PET40. Error bars represent standard deviation (SD) values of $n = 3$ measurements. (C) UHPLC profile of PET40 reaction supernatant after incubation on PET powder for 72 h showing the release of TPA (elution time: 1.7 min). $0.1 \text{ mg}\cdot\text{mL}^{-1}$ of recombinant and purified enzyme were applied to 5 mg of PET powder in a reaction volume of 200 µL and incubated over 72 h at 40 °C. The chromatograms are representative measurements, which were repeated in separate experiments at least three times. A control of an equal amount of PET powder was incubated at the same conditions without added enzyme to rule out non-enzymatic TPA release.

released from the polymer per mg of enzyme per day (Table 2). For comparison, we assessed the activity of PET40 to self-produced recombinant IsPETase and LCC under equal conditions at suitable temperatures. Here, IsPETase released at 30 °C $4.33 \pm 0.56 \mu\text{mol}_{\text{TPA-EG}} \cdot \text{mg}_{\text{enzyme}}^{-1} \cdot \text{day}^{-1}$ and LCC at 50 °C released $12.78 \pm 1.44 \mu\text{mol}_{\text{TPA-EG}} \cdot \text{mg}_{\text{enzyme}}^{-1} \cdot \text{day}^{-1}$.

Even though activity on PET can be detected for PET40 through HPLC measurements, the overall PET degradation takes place at a low rate with a substrate conversions below 0.1% in the incubations specified above. The low activity compared with IsPETase or LCC may be related to a single amino acid substitution in the predicted substrate binding pocket of PET40 (Table 3). Notably, IsPETase and LCC carry a Tyr-Met-Trp motif in their binding sites. PET40, however, carries a Phe-Met-Trp motif (Fig. 3, Table 3).

Promiscuity assays using esterase, lactonase, and β -lactamase substrates

Due to the rather recent occurrence of PET in the environment, it is unlikely that the primary substrate of a natural esterase is PET and degradation of the polymer is often only a side activity, as esterases are known to be promiscuous enzymes [30,31]. This also justifies the low turnover rates of PET40 on PET. Therefore, we further characterized PET40 on *p*NP esters, lactones, and β -lactams. Furthermore, we tested the effect of metal ions on PET40 activity.

Para-nitrophenyl-esters are commonly used substrates for the biochemical characterization of carboxylesterases. Using *p*NP esters with a C-chain length ranging from 4 to 18 (*p*NP C4-C18), PET40 showed activities on all substrates, with higher activities observed on *p*NP-esters with acyl chain lengths between C6 and C14 (Fig. 4A). Significantly lower activities were measured with shorter (C4) and longer

Table 2. TPA-EG units (μM) released from PET by PET40 in comparison with IsPETase and LCC. The recombinant and purified enzymes were incubated at a concentration of $0.1 \text{ mg} \cdot \text{mL}^{-1}$ for a time period of 72 h at 40 °C (PET40), 50 °C (LCC) and 30 °C (IsPETase), respectively. For the tests, 5 mg of PET powder (as specified in Materials and methods) were employed. Incubations were carried out in a reaction volume of 200 μL . Data are mean values with standard deviations derived from three measurements per sample.

Enzyme	Phylum	Released $\mu\text{mol}_{\text{TPA-EG}} \cdot \text{mg}_{\text{enzyme}}^{-1} \cdot \text{day}^{-1}$
PET40	Actinobacteria	0.17 ± 0.03
LCC		12.78 ± 1.44
IsPETase	Proteobacteria	4.33 ± 0.57

(C16–18) C-chain lengths. The kinetic parameters of PET40, determined according to Michaelis–Menten for *p*NP-C12 at 30 °C and pH 8, are $v_{\text{max}} = 0.86 \text{ nmol} \cdot \text{min}^{-1}$, $k_{\text{cat}} = 8.26 \text{ s}^{-1}$, $K_{\text{m}} = 0.73 \text{ mM}$, and $k_{\text{cat}}/K_{\text{m}}$ value of $1.14 \times 10^4 \text{ M}^{-1} \cdot \text{s}^{-1}$.

Using 1 mM *p*NP-C12 as substrate, PET40 revealed a remarkably broad temperature range. PET40 was most active at pH 8.0 when tested in 0.1 M potassium phosphate buffer with 1 mM of substrate at the temperature optimum of 40 °C. Surprisingly, at 4 °C, the enzyme still showed a relative activity of 59% compared with the activity at optimal conditions (Fig. 4A). At 40 °C, PET40 is also active over a broad pH range (pH 5–10), for which more than 75% residual activity was observed. To assess the enzyme's thermostability, it was incubated at 50 °C and 60 °C for 2 h, after which the enzyme only showed 11% and 5% residual activity, respectively, compared with the control without incubation (data not shown). At 50 °C, PET40 has a half-life time of 30 min (Fig. 4B). Nano differential scanning fluorimetry (NanoDSF) measurements indicated a T_{m} of $54.56 \pm 0.24 \text{ }^{\circ}\text{C}$ of the protein. To further characterize the effects of metal ions, possibly conveying activity through increased stability to the enzyme, Ca^{2+} , Co^{2+} , Cu^{2+} , Fe^{3+} , Mg^{2+} , Mn^{2+} , Ni^{2+} , or Zn^{2+} , were added to the assays at 1 and 10 mM. The activity was measured with *p*NP-C12 and compared with a metal-free control. The activity of PET40 slightly decreased at a 10 mM concentration for most of these ions and was mostly unaffected at the 1 mM concentration (Fig. 4A). Therefore, we conclude that the enzyme does not need metal ions for its activity. To probe PET40's tolerance against chelating agents and inhibitors, we tested the influences of ethylenediaminetetraacetic acid (EDTA), dithiothreitol (DTT), or phenylmethylsulfonyl fluoride (PMSF) in concentrations of 1 and 10 mM. The presence of EDTA, DTT, and PMSF resulted in < 20% reduction in activity which, regarding EDTA, is also in line with the findings about the unaffected activity through metal ions. Finally, we tested the sensitivity of PET40 toward detergents. A concentration of 5% (v/v) of the detergents Tween 80 and Triton X-100 lead to a decrease of 80% and 32%, respectively. SDS at the same concentrations had no negative impact on the enzyme's activity (Fig. 4A). Thus, PET40 has a relatively high stability against denaturing agents.

Lactonase activity of PET40 was further investigated in a phenol red assay, where the hydrolysis on δ -dodecalactone, γ -dodecalactone, δ -octalactone, and γ -caprolactone was detected due to the release of protons. These lactones differ in their chain length and ring structure. PET 40 showed the highest activity on δ -octalactone ($0.43 \text{ U} \cdot \text{mg}^{-1}$). While δ -dodecalactone

Table 3. Conserved motifs and structural features identified in PET40 and other PETases. The *Ideonella sakaiensis* PETase (IsPETase, PDB: 6EQE; [9,39]), LCC (4EB0; [40]), PET2 [32], the Bacteroidetal enzyme PET27 and PET30 were included for benchmarking purposes. PorC, Por secretion system C-terminal sorting domain; SP, signal peptide; β , β -sheet; –, none.

Predicted PETase	SP cleavage site	Catalytic triad	Substrate binding site	Disulfide bonds ^a	N-terminal SP	C-terminus	
						Secondary structure	Conserved domain
IsPETase	27–28	Asp-His-Ser	Tyr-Met-Trp	2×	Sec/SPI	–	–
LCC	21–22	Asp-His-Ser	Tyr-Met-Trp	1×	Sec/SPI	–	–
PET2	27–28	Asp-His-Ser	Tyr-Met-Trp	2×	Sec/SPI	–	–
PET27	23–24	Asp-His-Ser	Phe-Met-Trp	1×	Sec/SPI	7x β	PorC
PET30	23–24	Asp-His-Ser	Phe-Met-Tyr	1×	Sec/SPI	7x β	PorC
PET40	47–48	Asp-His-Ser	Phe-Met-Trp	2×	Sec/SPI	–	–

^aVerified and predicted disulfide bonds.

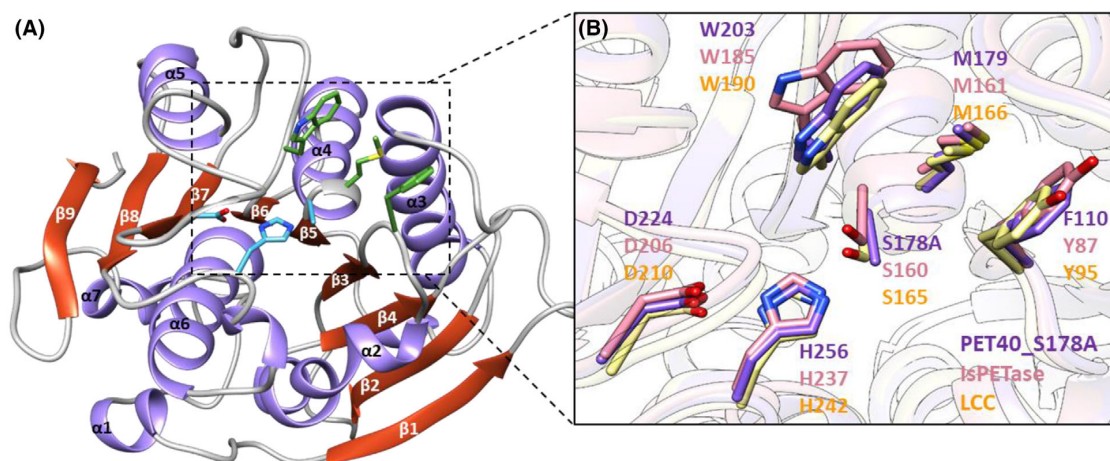


Fig. 3. Crystal structure of PET40_S178A and alignment with known IsPETase and LCC. (A) The structure of PET40_S178A was solved by X-ray crystallography. Cartoon representation showing the secondary structure elements and the active site (box). The catalytically active amino acids are colored in blue, and the substrate binding site is colored green. In the solved crystal structure the catalytic serine was mutated to alanine. (B) The residues of the active site of PET40_S178A (purple), IsPETase (pink; PDB code 6EQE), and LCC (yellow; PDB code 4EB0) were overlaid by CHIMERA 1.13.1. The amino acids related to the catalytic activity are labeled. The catalytic triad is conserved within all three structures (Ser; Asp; His), but PET40 has Phe instead of Tyr at the first position of the substrate binding site. Structures were generated using USC CHIMERA version 1.13.1 [41].

was cleaved rather quickly ($0.22 \text{ U}\cdot\text{mg}^{-1}$), γ -dodecalactone was not ($0.06 \text{ U}\cdot\text{mg}^{-1}$). The hydrolysis rate of γ -caprolactone ($0.02 \text{ U}\cdot\text{mg}^{-1}$) was similar to that of γ -dodecalactone.

The activity of PET40 on different β -lactams (Fig. 5A) was tested in a standard disk diffusion assay on agar plates. The commercially available disks used in this assay contained indicated amounts of antibiotic compounds (Fig. 5B). The zone of inhibition (ZOI) of bacterial growth around these disks was evaluated after incubation of the disks with PET40. Susceptible *E. coli* DH5 α cells were cultivated together with the pre-incubated disks on lysogeny

broth (LB)-agar plates. The inhibition zones are smaller or even not present when the antibiotics have been inactivated. The results were compared with control disks incubated without enzyme. PET40 was able to reduce the inhibitory effect of mezlocillin 30 μg (MEZ 30, ureidopenicillin group), cefamandole 30 μg (MA 30), and cefaclor 30 μg (CEC 30, cephalosporin 2nd generation) completely, and cefotiam 30 μg (CFT 30, cephalosporin 3rd generation) to 95.9%. Interestingly, PET40 did not reduce the inhibitory effect of imipenem 10 μg (IPM 10), which belongs to the carbapenem group (Fig. 5B) and is an antibiotic of last resort.

PET-degradation by PET40

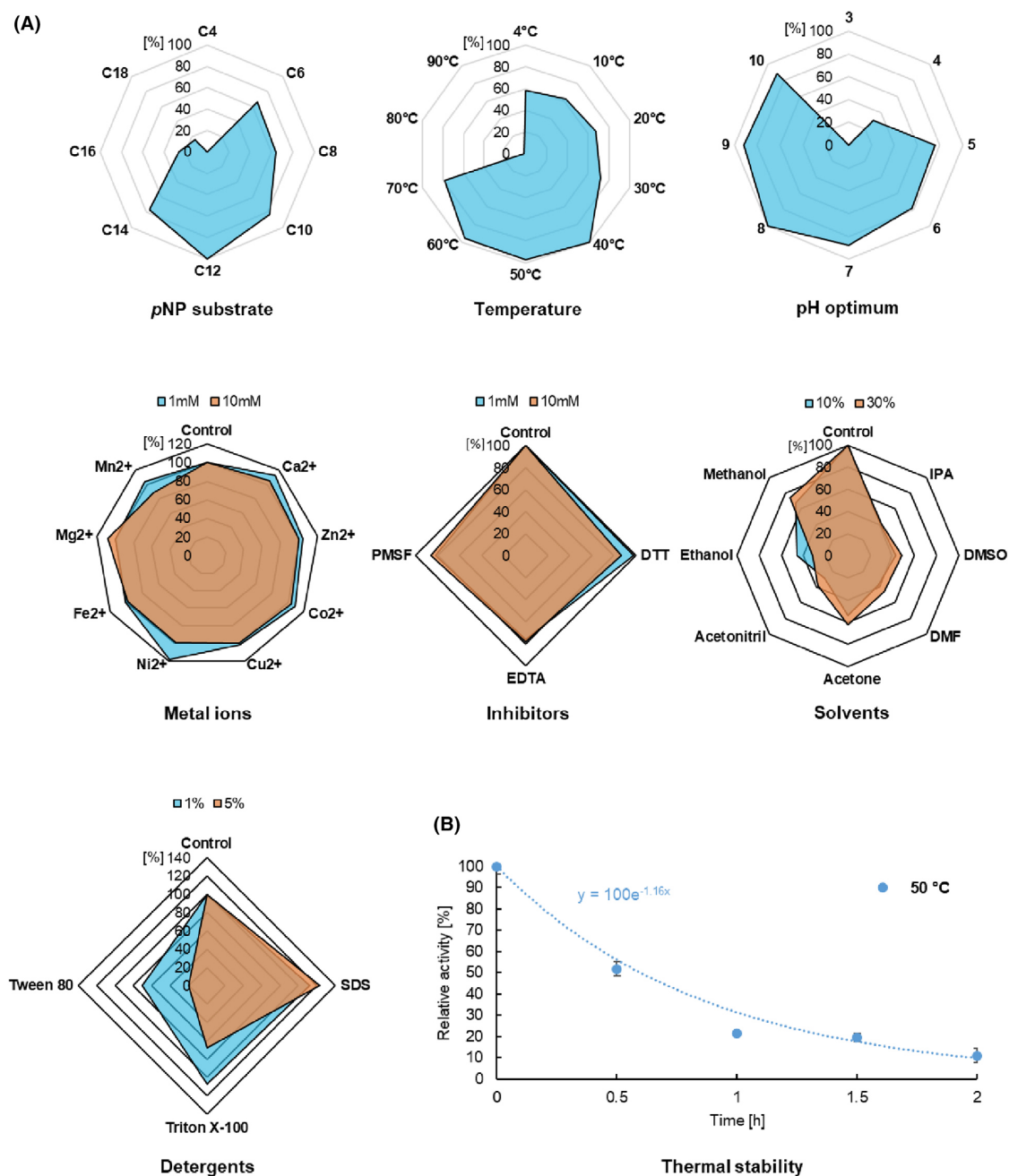
H. Zhang *et al.*

Fig. 4. Biochemical characterization of PET40 using C4-C18 pNP esters. (A) Net diagrams depicting the substrate preference, temperature optimum, pH optimum as well as the influence of different metal ions, inhibitory agents, solvents and detergents on the activity of PET40. In all cases, standard deviations were lower than 7%. (B) Graph showing the thermal stability of PET40 at 50 °C over 2 h with an exponential fit ($R^2 = 0.94$). Data represent mean values of three replicates ($n = 3$). Error bars represent standard deviations (SD). During all incubations, 0.25 μg enzyme were incubated for 10 min in 200 μL reaction volume under the different tested conditions. All tests besides substrate preferences were carried out with pNP-C12.

H. Zhang *et al.*

PET-degradation by PET40

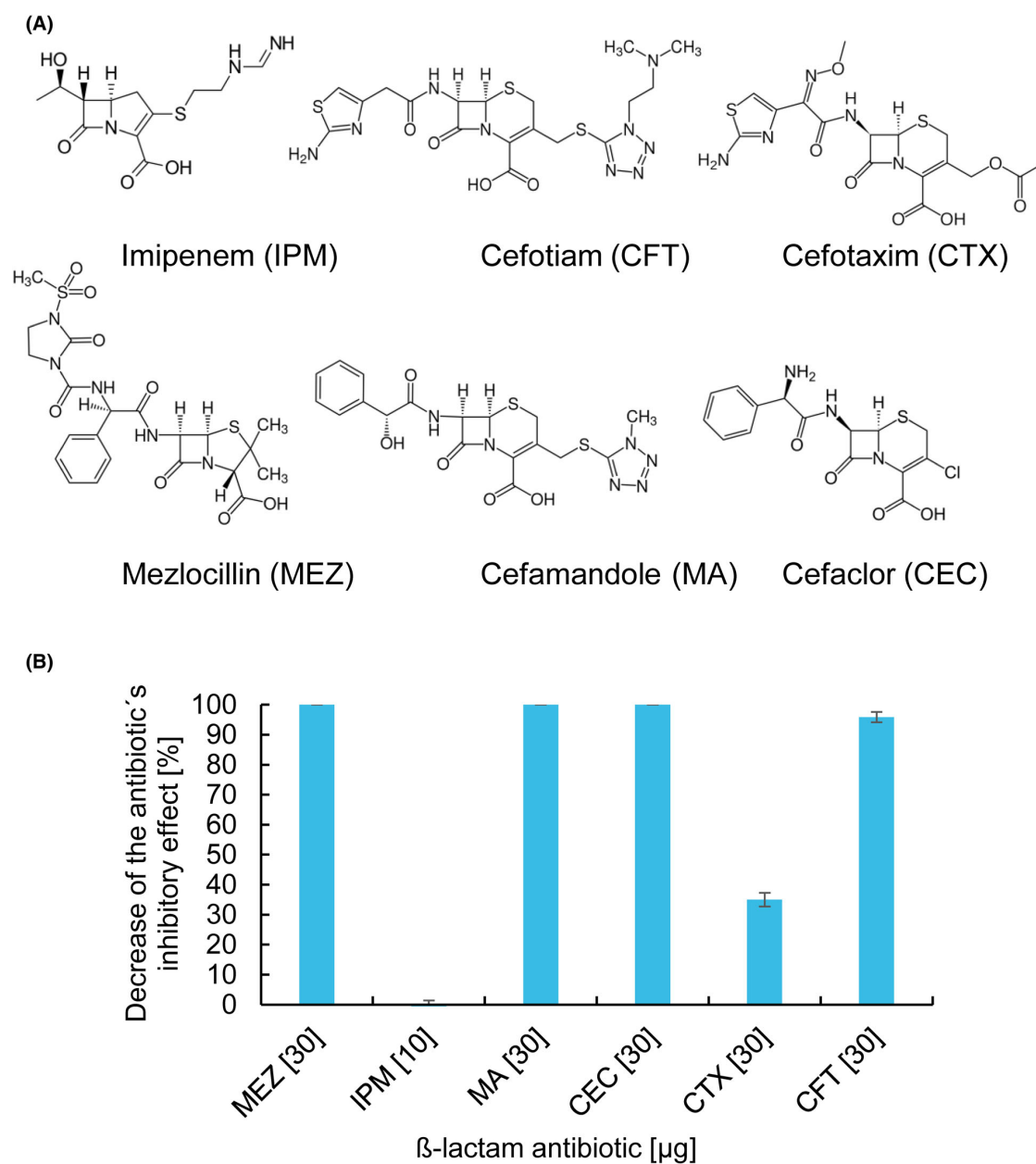


Fig. 5. The promiscuous PET40 degrades β -lactam antibiotics. (A) Overview and structures of β -lactam antibiotics used in degradation tests. (B) Inhibitory effect of PET40 on different β -lactam-antibiotics. Antibiotic assay disks (total amounts as stated in square brackets) were incubated over 17 h in 20 μL potassium phosphate buffer (0.1 M, pH 8) containing 1 $\text{mg}\cdot\text{mL}^{-1}$ purified PET40. After incubation the plates were laid on agar plates on which susceptible *Escherichia coli* DH5 α cells had been plated out. Disks that were incubated only with buffer served as controls. The ZOI was determined by measuring the halo around the disks. The inhibitory effect of MEZ 30, MA 30, and CEC 30 was diminished completely by PET40 and in the case of CFT 30 to more than 95%. Abbreviations for the used antibiotics are as follows: Mezlocillin 30 μg (MEZ 30), imipenem 10 μg (IPM 10), cefamandole 30 μg (MA 30), cefaclor 30 μg (CEC 30), cefotaxim 30 μg (CTX 30) and cefotiam 30 μg (CFT 30). Error bars represent standard deviations (SD) of nine replicates ($n = 9$).

In summary, the data show that PET40 is a promiscuous, cofactor-independent, mesophilic enzyme that is able to act on the polymers PET, Impranil and PCL, as well as *p*NP-esters, lactones and β -lactams. Its temperature optimum lies at 40 °C. PET40 retained more than 50% relative activity at temperatures as low as 4 °C (Fig. 4). The enzyme was rapidly deactivated when incubated at temperatures above 50 °C.

Amino acid sequence and structural analyses identify unique traits of PET40

Amino acid sequence analysis revealed that PET40 contained N-terminal signal domains for protein transport as predicted with SignalP 6.0 [42]. The predicted cleavage site was located between amino acid (aa) positions 47 and 48 with the signal peptide using the standard secretory signal peptides (likelihood of 0.73) (Table 3). Further sequence analysis identified a G-x-S-x-G motif typical for α/β serine hydrolases between aa positions 176 and 180 [43]. To investigate the structural traits of this promiscuous enzyme, PET40_S178A, an inactive variant of PET40, was generated by restriction-free cloning. We obtained well-diffracting crystals of PET40_S178A reaching a resolution of 1.60 Å. The crystal was packed in space group P2₁, with two molecules in the asymmetric unit. As confirmed by PISA [44], the biological unit is a monomer, and the overall root-mean-square deviation (RMSD) between the two chains present in the asymmetric unit is 0.161 Å, making them virtually identical. We were able to unambiguously model the protein chains in the electron density from residues 48 and 49 for chains A and B, respectively, to residue 309. A portion of the His-tag was also visible in the electronic density for both chains, mediating crystal contacts with symmetric molecules. The final model was refined to $R_{\text{work}}/R_{\text{free}}$ values of 14.59/17.90. All data collection and refinement statistics are reported in [Materials and methods](#) section.

The crystal structure shows that PET40 shares the typical fold of α/β serine hydrolases, composed by a central twisted β -sheet surrounded by α -helices. For PET40, the β -sheet consists of nine β -strands and is surrounded by seven α -helices (Fig. 3). The RMSD between PET40 and IsPETase (PDB ID: 6EQE) is 0.570 Å, while it is 0.561 Å with LCC, which confirms the high structural similarity with known PETases. As previously shown for other Type II PET-degrading enzymes, a disulfide bond is present in PET40 between C289 and C305 [26,27]. PET40 possesses a catalytic triad consisting of the residues Asp-His-Ser, in a spatial arrangement highly similar to IsPETase and LCC

(Fig. 3). The substrate binding site contains the aa residues Phe-Met-Trp. The latter differs from the known IsPETase and LCC binding sites in which a Tyr was reported in the first position (Fig. 3, Table 3). It is, however, in consonance with the bacteroidetal PETase PET27 [26] and Cut190 [45].

Binding mode prediction via molecular docking

To obtain insights into the potential binding modes of the diverse substrates in the active site of PET40, we performed molecular docking using a combination of AutoDock3 [46] as a docking engine and DrugScore²⁰¹⁸ [47,48] as an objective function as done previously [24,49,50]. We focused on the ester substrates investigated experimentally in this study for the docking, that is mono(2-hydroxyethyl) terephthalate (MHET), bis(2-hydroxyethyl) terephthalate (BHET), PET trimer (PET₃), methyl hexanoate (MH), polycaprolactone trimer (PCL₃), propane-1,2,3-triyl tributanoate (tributylin, TBT), 4-nitrophenyl decanoate (*p*NP-C10), and 4-nitrophenyl dodecanoate (*p*NP-C12). We performed 100 independent docking runs for each substrate, which were subsequently clustered into distinct docking poses based on structural similarity (RMSD cut-off < 2 Å).

For all substrates, except *p*NP-C10/12, the binding pose identified as best based on the binding score (Table 4), shows a conformation in which the reactive carbonyl carbon of the ester moiety is close to the Ser of the catalytic triad (Fig. 6). For *p*NP-C10/12, the best-scored binding pose involves interactions of the nitro moiety with the catalytic triad. The docking pose from the largest cluster only scored marginally worse (< 2% compared with the best-scored solution)

Table 4. Docking scores of the representatives of up to the three best-scored clusters for all docking substrates.

Substrate	Lowest docked energy ^a		
	Cluster 1	Cluster 2	Cluster 3
MHET	-8.52	-8.44	-8.37
BHET	-9.84	-9.62	-9.53
PET ₃	-16.58	-15.61	-15.58
MH	-6.33	-5.51	n.a. ^b
<i>p</i> NP-C10	-11.94	-11.50	-11.32
<i>p</i> NP-C12	-12.75	-12.28	-12.11
PCL ₃	-12.72	-12.28	-12.04
TBT	-11.20	-10.66	-10.60

^aSum of the estimated intermolecular energy and internal energy of the ligand in kcal·mol⁻¹. The energy of the pose depicted in Fig. 6 is marked in bold.; ^bNot available as only two clusters were obtained.

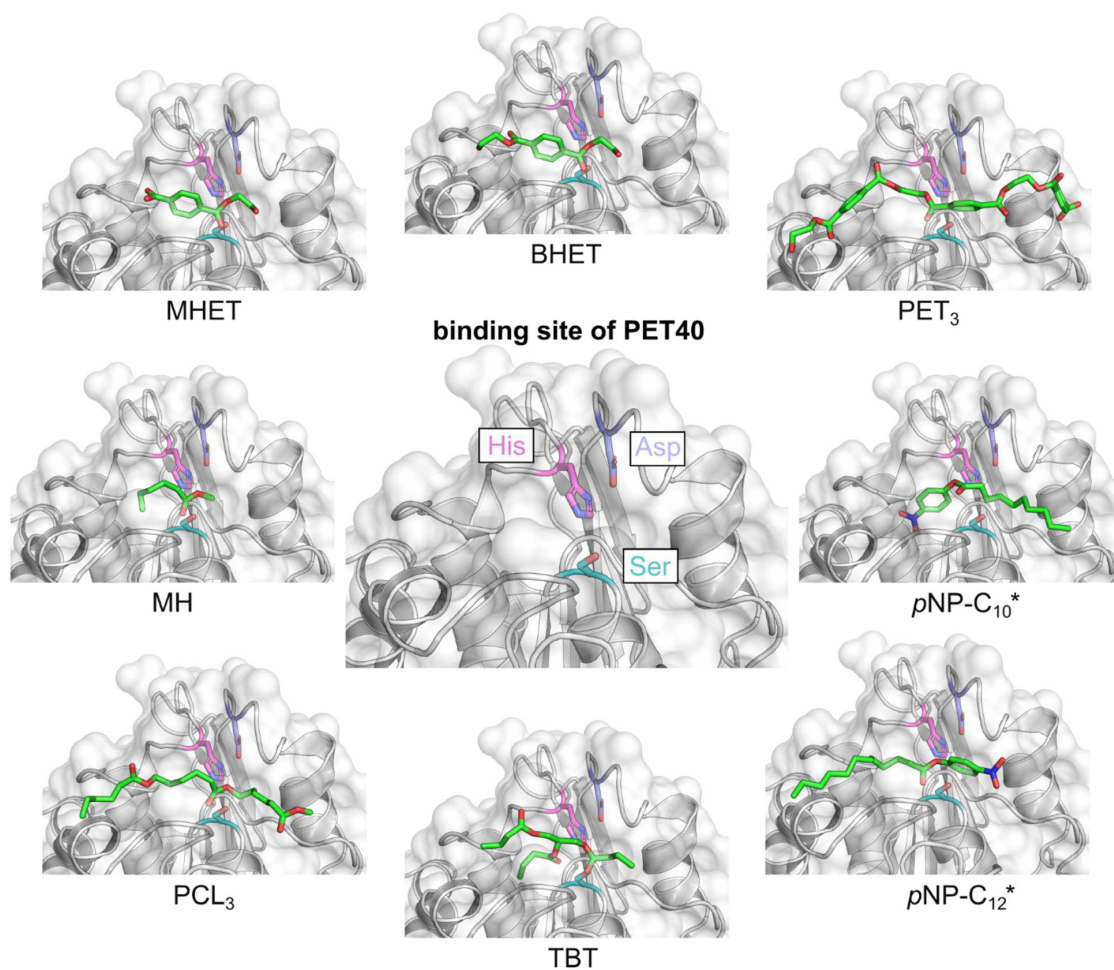


Fig. 6. PET40 has an active site cavity that can accommodate a large variety of substrates. Docking poses identified as best for mono(2-hydroxyethyl) terephthalate (MHET), bis(2-hydroxyethyl) terephthalate (BHET), PET trimer (PET₃), methyl hexanoate (MH), polycaprolactone trimer (PCL₃), propane-1,2,3-triyl tributanoate (tributyrin, TBT) in the binding site of PET40 (depicted without substrate in the center). *For 4-nitrophenyl decanoate (pNP-C10) and 4-nitrophenyl dodecanoate (pNP-C12), binding modes from the largest cluster were chosen rather than those with the lowest energy. Structures were generated using PYMOL [54].

and captures the key interactions of the ester carbonyl carbon with the serine. Thus, we consider this docking pose more relevant for the reaction of pNP-esters in PET40. The aliphatic chains of pNP-C10 or 12 point in opposite directions. However, it is not uncommon that a ligand or ligands with minor structural changes can bind to a protein in different poses [51,52], and the determined binding pose can even be impacted by the method used for structure elucidation [53].

For small ligands with a limited number of degrees of freedom, such as MH and MHET, our docking converges to two and three binding poses, respectively.

However, for more complex ligands with a high number of degrees of freedom, such as PET₃ and PCL₃, we obtain a high number of clusters that mainly differ in the conformation at the end of the oligomer chain. However, the orientation of the reactive carbonyl carbon atom to the hydroxyl group oxygen of the serine is similar in most cases. Therefore, we calculated the minimum distance between the serine hydroxyl group oxygen and the reactive carbonyl carbon of each substrate for all docking runs (Fig. 7) to evaluate whether the substrate is close enough to the catalytic triad for a reaction to take place. This distance is < 5 Å for all substrates for the majority (> 55% for all cases, up to

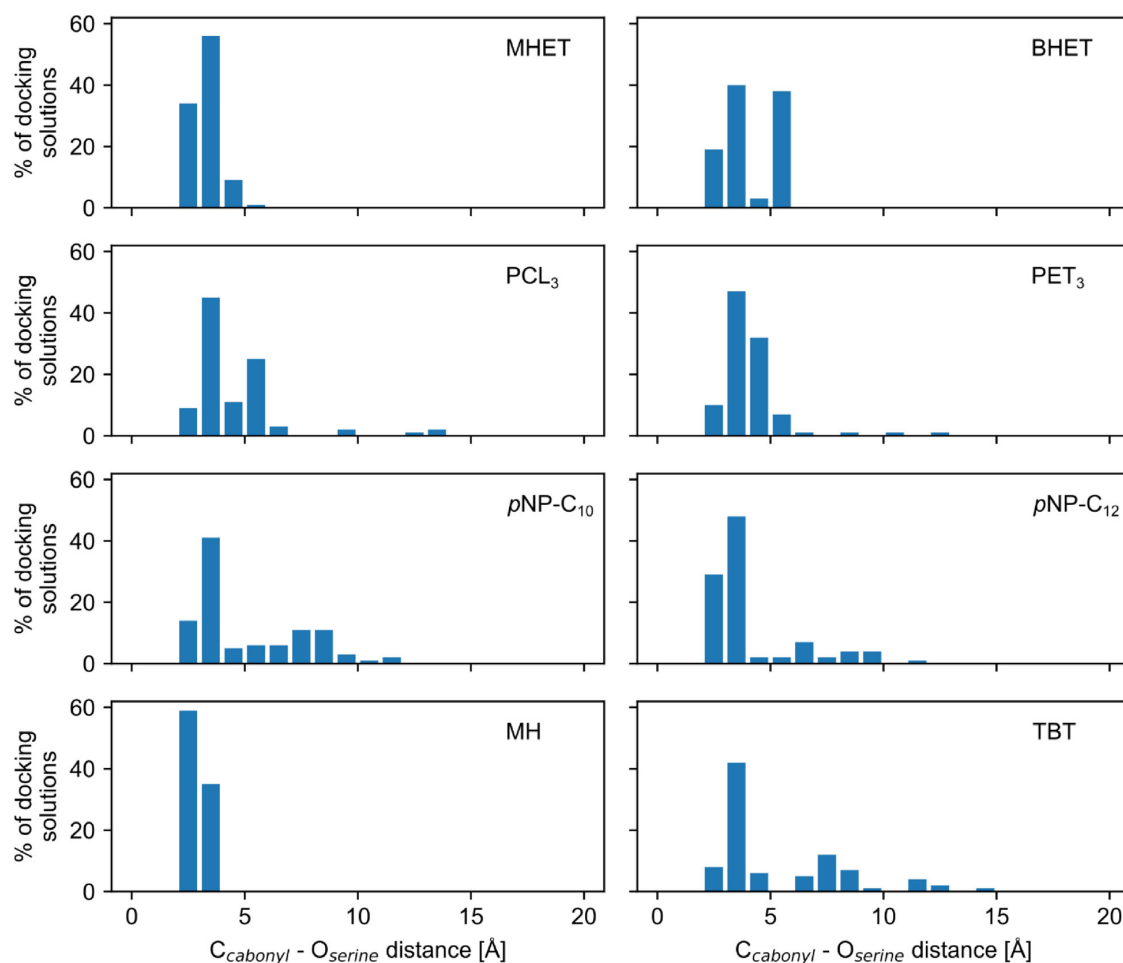


Fig. 7. Histograms of the minimum distance between the serine hydroxy group oxygen of PET40 and the electrophilic carbonyl carbon of the substrate for all obtained docking solutions. The following substrates were docked: mono(2-hydroxyethyl) terephthalate (MHET), bis(2-hydroxyethyl) terephthalate (BHET), a polycaprolactone trimer (PCL_3), a PET trimer (PET_3), 4-nitrophenyl decanoate (pNP-C10), 4-nitrophenyl dodecanoate (pNP-C12), methyl hexanoate (MH), and propane-1,2,3-triyl tributanoate (tributyryn, TBT).

95% for MH) of the docking solutions (Fig. 7). Thus, our docking approach yields binding poses in line with the geometry required for a reaction for all substrates, despite the high number of degrees of freedom of some of the investigated substrates.

Overall, we find that relatively small substrates such as the polymeric building blocks MHET, BHET, and MH, but also bulky ligands such as TBT and the pNP-esters are well-accommodated by the active site of PET40 and can come close to the Ser of the catalytic triad with their electrophilic carbon. The binding site is located at the protein surface, facilitating the access of small and bulky substrates. Even for such

binding sites, using an appropriate docking engine and objective function as done here can yield good binding modes with only a moderate drop-off compared with docking to “classical” binding sites [55]. Moreover, more complex substrates such as PET_3 and PCL_3 are also well-docked into the catalytic site, again pointing the reactive ester moiety toward the catalytic Ser. These results mirror the activity analyses on these substrates, which all were cleaved by PET40.

In the case of the β -lactam antibiotics, the binding poses generated by AutoDock3-DrugScore²⁰¹⁸ did not yield catalytically viable complexes. For this reason, we employed GLIDE as an alternative to generate putative

binding poses. We docked the six experimentally tested antibiotics and assessed the distance between the serine hydroxyl group of PET40 and the carbonyl carbon of the lactam group, as well as the angle described by the serine hydroxyl group, the carbonyl carbon, and the carbon opposite to it in the lactam ring, and compared the obtained values with the values of a crystallized Michaelis–Menten complex of a serine β -lactamase (Fig. 8A). The results show that for the five degraded antibiotics, we identified at least one docking solution with pairs of distance/angle values close to the values observed in the crystal structure (Fig. 8B). However, for imipenem, the only nondegraded antibiotic, no catalytically viable docking solution was identified. In the predicted binding poses of the five degraded antibiotics, the β -lactam ring is positioned in a consistent orientation within the active site (Fig. 9). Overall, the docking results can provide a structure-based explanation for the observations in the disk diffusion assays.

Discussion

Today's major global plastic pollution in all environments makes the study of plastic-degrading microorganisms and enzymes compulsory. Still, the number of functionally verified microbial enzymes is limited, and, today, there are only a handful of known bacterial phyla encoding active PET esterases (Fig. 1). PET-degrading enzymes belong to the classes of cutinases (EC3.1.1.74), lipases (EC3.1.1.3), or carboxylesterases (EC3.1.1.1). Diene lactone hydrolases (often grouped into EC3.1.1.45 of carboxymethylenebutenolidases) are not commonly known to degrade PET. Therefore, PET40 is one of the few enzymes known that belongs to this enzyme class and can act on PET.

Here, we identified and partially characterized the novel promiscuous esterase PET40, derived from a biochar metagenome. A more detailed phylogenetic analysis indicated that PET40 was affiliated with the genus *Amycolatopsis* within the Actinobacteria phylum. This genus is well-known to involve species that degrade a wide range of aromatic substances and plant-based polymers. It contains microorganisms that are ubiquitous and frequently isolated from soil and sediment samples. Furthermore, bacteria from this genus are well-known for their secondary metabolite production [56]. The genus currently contains more than 70 species. Most genomes appear to have sizes of 10 Mbp and larger. The genus is relatively closely related to the *Streptomyces* [57–60]. PET40 homology can be found in a significant fraction (21 out of 68) of the *Amycolatopsis* and also *Streptomyces* (104 out of 564) genomes. This implies that enzymes with

activity on PET are probably occurring more frequently than previously assumed.

PET40 appears to be a secreted enzyme, as it carries an N-terminal secretion signal, implying that the enzyme is probably released into the surrounding environment and can act on its substrates. Since it is well-known that some esterases are highly promiscuous enzymes being able to convert a large number of diverse substrates, it can be assumed that PET is not the primary substrate of PET40, as the polymer is present only relatively recent in nature next to much more favorable carbon sources and, especially, as turnover rates of PET40 are low compared with enzymes, whose primary substrate is PET, such as IsPETase. Promiscuous enzymes such as PET40 can turn over a broad range of substrates probably because of an exposed active site, a certain cavity volume-to-surface ratio [30] and certain structural rigidity characteristics [31]. Substrates that do not fit well into the active or binding site are turned over with lower rates than those substrates that fit best [30,31,61,62].

The activity of PET40 on PET was shown through the release of the degradation product TPA. In 200 μ L reaction volume, it released $50.41 \pm 10.21 \mu$ M of monomeric PET degradation products in a 72-h time period at 40 °C. Comparing activities of PET-active enzymes is generally difficult, as in most studies, different types of PET substrates with different degrees of crystallinity and distinct assay conditions have been used. To partly overcome this problem, we cloned and expressed the recombinant IsPETase and LCC and compared their activities with PET40 at suitable temperatures under otherwise identical assay conditions. Here, even though PET40 is less active than IsPETase and LCC, it still exhibited a distinct degradation activity on PET (Table 2). The observation that PET40 is catalytically active on PET implies a wider role of homologous enzymes in the degradation of this plastic, especially micro- and nanoparticles in nature. Particles reduced in size have an increased surface-to-volume ratio so that they can be better attacked by an enzyme. Therefore, the enzyme and its homologs may in fact play a heretofore unknown role in PET micro- and nanoparticle degradation. This hypothesis is supported by our observation that homologs of PET degrading enzymes can be found on a global level, covering a wide range of climate zones, in a large fraction of the genomes of *Amycolatopsis* and *Streptomyces*. Both these bacterial genera are ubiquitous soil and marine organisms.

In summary, our biochemical data significantly extend the knowledge of promiscuous esterases with

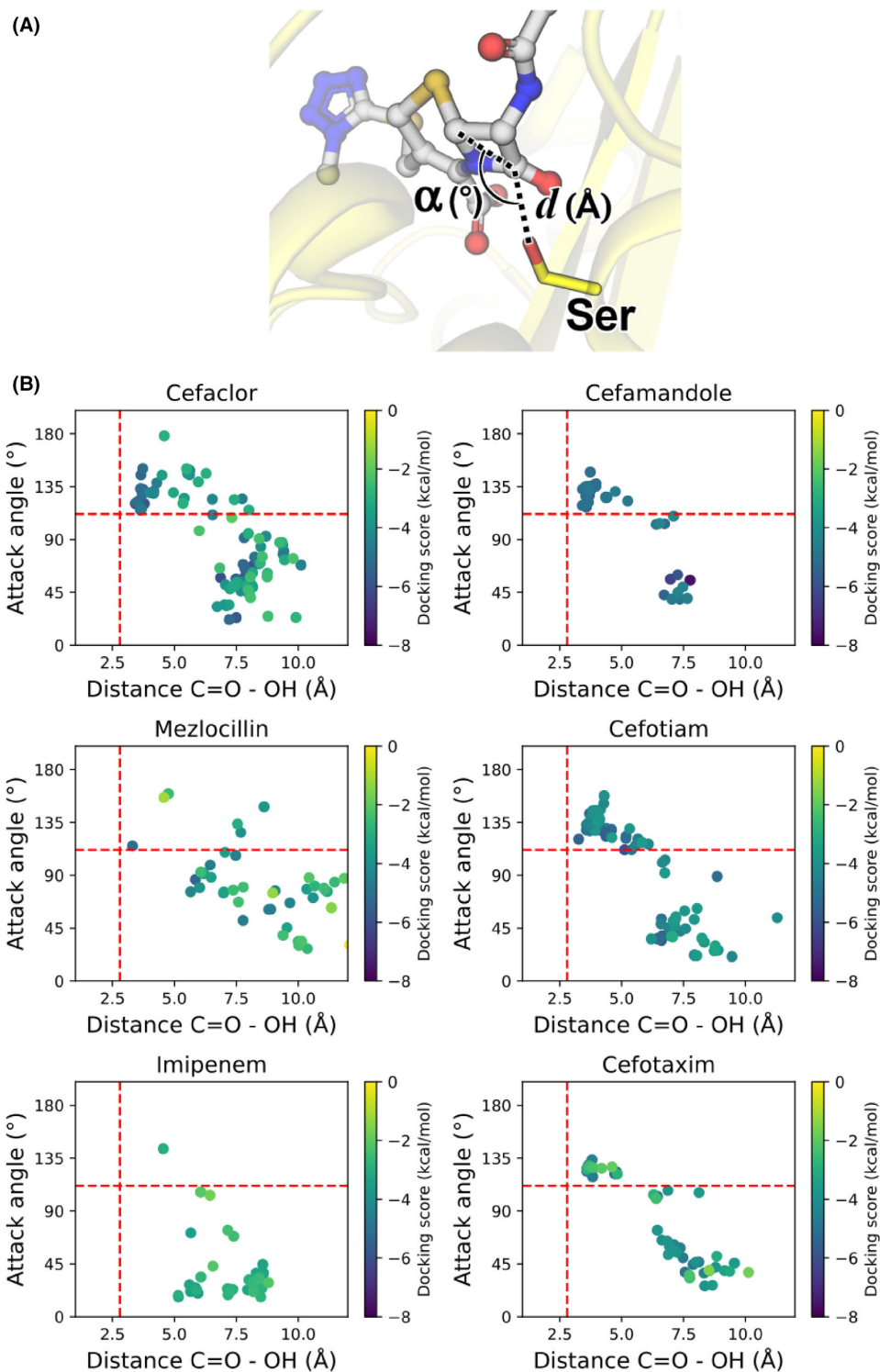


Fig. 8. Docking poses for β -lactam antibiotics in PET40 have a similar geometry as in a crystallographically determined serine β -lactamase/ β -lactam antibiotics complex. (A) Distance (d) and angle (α) between the protein and the substrate measured for the docking solutions. The structure shows the binding pose for the enzyme-substrate complex of a serine β -lactamase from *Mycobacterium tuberculosis* (PDB ID: 3NY4). Structures were generated using PYMOL [54]. (B) Dispersion plots showing the pairs of distance-angle values calculated for each docking solution of an antibiotic substrate in PET40. The color scale shows the docking score of the pose. The red dashed lines show the values observed in the crystal structure (PDB ID: 3NY4). Only imipenem yields no solution with similar geometry to the crystal complex.

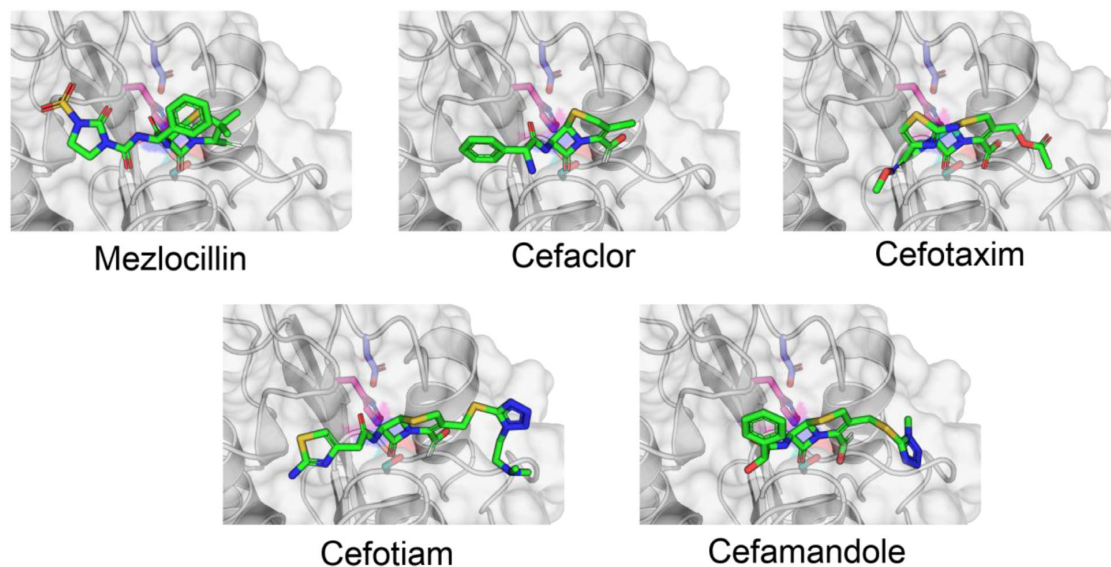


Fig. 9. Predicted binding poses for β -lactam antibiotics. The binding pose with the angle and distance that most closely resembles the crystal structure is shown for each antibiotic. The catalytic triad Ser-His-Asp is highlighted in cyan, purple, and violet, respectively. Structures were generated using PYMOL [54].

activity on PET derived from Gram-positive bacteria and provides PET40 as a novel promising and versatile candidate for further investigation and optimization. Within this framework, further possible substrates of the enzyme could be identified yielding more conceivable applications or present activities could be enhanced through alteration of the wildtype enzyme. Here, it could especially be of interest to elucidate the possible increase of the enzyme's activity on PET, for example through an amino acid exchange from Phe-Met-Trp to Tyr-Met-Trp in the substrate binding site. Furthermore, the data already presented here will help to advance our understanding on the evolution of genes encoding PET-active enzymes within the Gram-positive bacteria. Our research contributes to knowledge on the possible decomposition of marine and terrestrial PET litter and enables the development of an expanded phylogenetic framework for identifying the diversity of putative PETases in diverse microbial groups on a global scale.

Materials and methods

Bacterial strains, plasmids, and primers

Bacterial strains, plasmids, and primers employed in this study are listed in Table 5. *E. coli* clones were grown in LB medium (1% tryptone/peptone, 0.5% yeast extract, 1% NaCl) supplemented with appropriate antibiotics (25 $\mu\text{g}\cdot\text{mL}^{-1}$ kanamycin, or 100 $\mu\text{g}\cdot\text{mL}^{-1}$ ampicillin) at 37 °C for 18 h, if not indicated otherwise.

Databases used in this study and bioinformatic analysis

Nucleotide and amino acid sequences of the putative and confirmed PETases were acquired from databases integrated into the NCBI (<https://www.ncbi.nlm.nih.gov/>), UniProt (<http://www.uniprot.org/>) and IMG (JGI, <http://jgi.doe.gov/>) servers [63–65].

Sequence comparisons to other sequences deposited in the NCBI databases were conducted using the BLAST

Table 5. Bacterial strains and plasmids used in this work.

	Properties	Reference/source
Strain		
<i>Escherichia coli</i> DH5 α	<i>supE44</i> Δ <i>lacU169</i> (Φ 80 <i>lacZ</i> Δ M15) <i>hsdR17</i> <i>recA1</i> <i>endA1</i> <i>gyrA96</i> <i>thi-1</i> <i>relA1</i>	Invitrogen (Karlsruhe, Germany)
<i>E. coli</i> BL21 (DE3)	F ⁻ , <i>ompT</i> , <i>hsdS</i> B (<i>r_B</i> ⁻ <i>m_B</i> ⁻) <i>gal</i> , <i>dcm</i> , λ DE3	Novagen/Merck (Darmstadt, Germany)
<i>E. coli</i> SHuffle@ T7	<i>huA2</i> <i>lacZ</i> ::T7 <i>gene1</i> [<i>lon</i>] <i>ompT</i> <i>ahpC</i> <i>gal</i> λ att::pNEB3-r1-cDsbc (SpecR, <i>lacIq</i>) Δ <i>trxB</i> <i>sulA11</i> R(<i>mcr-73</i> ::miniTn10-TetS)2 [<i>dcm</i>] R(<i>zgb-210</i> ::Tn10 -TetS) <i>endA1</i> Δ <i>gor</i> Δ (<i>mcrC-mrr</i>)114::IS10	NEB (Frankfurt am Main, Germany)
Vector		
pET21a(+)	Expression vector, <i>lacI</i> , Amp ^R , T7- <i>lac</i> - promoter, C-terminal His ₆ -tag coding sequence	Novagen/Merck (Darmstadt, Germany)
pET21a(+):PET40	837 bp insert in pET21a(+) coding for PET40	This work
pET21a(+):PET40_S178A	837 bp insert in pET21a(+) coding for PET40_S178A	This work
pET21a(+):LCC	786 bp insert in pET21a(+) coding for LCC	This work, acc. to Sulaiman <i>et al.</i> [15]
pMAL-p4x::IsPETase	795 bp insert in pMAL-p4x coding for the wildtype IsPETase from <i>Ideonella sakaiensis</i> fused to a maltose binding protein for purification	Lab of Birte Hoecker, Univ. Bayreuth, acc. to Yoshida <i>et al.</i> [9]

alignment tools [66]. The profile HMM search [33] was carried out using the HMMER (<http://hmmmer.org>) webpage and a local version of the software (v3.1b2) [67] with downloaded datasets. Structural information on LCC (PDB 4EB0) and IsPETase (PDB 6EQE) was retrieved from the RCSB-PDB database [68].

The DNA sequence data were processed and analyzed using CHROMASPRO 2.1.8 (Technelysium, Brisbane, Qld, Australia) and SNAPGENE (GSL Biotech LLC, San Diego, CA, USA). The amino acid sequence alignment was constructed employing structural alignments with T-COFFEE [13]. Overall, the amino acid sequences of 23 enzymes were included in this alignment. The phylogenetic tree was constructed by Maximum Likelihood method using MEGAX [14] using 1000 bootstraps. GenBank entries of the sequences used are listed in Table 1 or were retrieved from the PAZY database (www.pazy.eu; [8]). UHPLC profiles were plotted and edited using software MATLAB version R2021a (The MathWorks, Inc., Natick, MA, USA).

Heterologous production of PET40 in *E. coli* BL21 (DE3)

The putative PET-active enzyme PET40 was found in a metagenomic dataset. For this, the gene sequences were optimized for expression in *E. coli* and synthesized into pET21a(+) vector at Biomatik (Wilmington, DE, USA). The resulting construct was sequenced at Eurofins (Ebersberg, Germany) and verified for correctness by comparing to the original sequences. Chemically competent *E. coli* BL21 (DE3) were used for heterologous expression of the predicted PETase gene. Cultures carrying the expression plasmid were grown aerobically in auto-induction medium (ZYM-5052) [69] containing 100 μ g·mL⁻¹ ampicillin for pET21a(+) at 37 °C until they reached an optical density

(OD₆₀₀) of 1.0. Proteins were produced afterwards at 22 °C for 16–20 h. Cells were harvested and lysed with pressure using a French press. From this lysate, recombinant PET40 was purified using nickel-ion affinity chromatography employing Ni-NTA agarose (Macherey-Nagel, Düren, Germany). The purified protein was analyzed by SDS/PAGE. Finally, the elution buffer was exchanged against 0.1 mM potassium phosphate buffer (pH 8.0) using a 10 kDa Amicon Tube (GE Health Care, Solingen, Germany).

PET degradation assay measured by UHPLC

To assay enzymatic PET hydrolysis, 5 mg of PET powder (Goodfellow GmbH, Bad Nauheim, Germany) were added to 1.5-mL Eppendorf tubes with 20 μ g of enzyme in 200 μ L of 100 mM potassium phosphate buffer at pH 8.0. Incubation was carried out under continuous shaking and at 400 r.p.m. in 1.5-mL microcentrifuge tubes. The incubation was made at PET40's optimal temperature of 40 °C if not stated otherwise.

The analysis of the degradation products was performed using an UltiMate™ 3000 UHPLC system (Thermo Scientific, Waltham, MA, USA) employing a Triart C18 column (YMC Europe GmbH, Dinslaken, Germany) and with a dimension of 100 \times 2.0 mm containing particles with 1.9 μ m diameter. Isocratic elution was made by using a mobile phase consisting of 20 : 80 (v/v) acetonitrile and water (acidified with 0.1% v/v trifluoroacetic acid) at a flowrate of 0.4 mL·min⁻¹. All UHPLC samples were prepared by mixing 50 μ L of incubation supernatant with 200 μ L acetonitrile (acidified with 1% vol trifluoroacetic acid), followed by a centrifugation at 10 000 *g* for 3 min. Following this, 200 μ L of the supernatant were transferred into 600 μ L of water and 15 μ L of sample were injected per measurement. The detection of breakdown products

was made at 254 nm with a VWD-3400 detector from Thermo Scientific. The quantification of peak areas was performed using the data analysis software supplied with the COMPASS HYSTAR software package from Bruker (Billerica, MA, USA).

Polyester polyurethane degradation assay with Impranil® DLN and phenol red

Impranil® DLN (Covestro AG, Leverkusen, Germany) was used as a model substrate for screening activity on an ester-based polyurethane. The assay was performed as previously described [30] with minor modifications. For sample preparation, 10 μL Impranil® DLN was added to a 96-well plate filled with 235 μL of *N*-(2-hydroxyethyl)piperazine-*N'*-3-propanesulfonic acid (EPPS) buffer containing phenol red (0.5 mM final concentration) as a pH indicator. After adding 5 μL of purified protein (1 $\text{mg}\cdot\text{mL}^{-1}$), the reaction was measured continuously at 550 nm during incubation at 40 °C in a microplate reader (BioTek Instruments Inc., Winooski, VT, USA) for 40 min. The reaction was assayed in triplicate per plate. Neither the actual structure of Impranil® DLN nor the degradation products are known. Therefore, in order to quantify the release of protons, a standard curve with acetic acid was employed.

Biochemical characterization of PET40 using pNP-esters

For activity tests, PET40 was assayed using purified recombinant protein. Unless otherwise indicated, a total amount of 0.25 μg of the enzyme was added to a substrate solution. The substrate solution contained 190 μL of 0.1 M potassium phosphate with a defined pH between 7 and 8 and 10 μL of 0.1 mM *p*NP-substrate dissolved in isopropanol. Samples were incubated for 10 min, and the assay was stopped by adding 200 mM of Na_2CO_3 . After this, the samples were centrifuged at 18 000 *g* for 3 min and at 4 °C. The *p*NP-esters with chain lengths of C4, C6, C8, C10, C12, C14, C16 and C18 were tested as substrates. For the identification of the optimal temperature, the samples were incubated at different temperatures ranging between 4 °C and 90 °C for a 10-min time period. Following the incubation at the defined temperatures, release of the yellow *p*NP-OH was measured at 405 nm in a plate reader (BioTek Instruments Inc.). All samples were measured at least in triplicate. The influence of pH on the activity of each enzyme was measured in either citrate phosphate (pH 3.0, 4.0 and 5.0), or potassium phosphate (pH 6.0, 7.0 and 8.0) and/or in carbonate bicarbonate buffer (pH 9.2 and 10.2). The influence of cofactors, solvents, detergents, and inhibitors on PET40 was assayed at different concentration levels. The possible cofactors Ca^{2+} , Co^{2+} , Cu^{2+} , Fe^{3+} , Mg^{2+} , Mn^{2+} , Ni^{2+} , and Zn^{2+} were assayed at a concentration of 1 and 10 mM. Detergent stability was

tested using a concentration of 1% and 5% of SDS (w/v), 1% and 5% of Triton X-100 and Tween 80 (v/v) in the test, respectively. Possible inhibitory effects of EDTA, DTT, and PMSF were assayed at 1 and 10 mM concentrations. The residual PET40 activity was determined after 10-min incubation at the optimal temperature of 40 °C with *p*NP-hexanoate (-C8) and at the optimal pH of pH8. Activity of PET40 after incubation with possible different cofactors detergents and solvents was assayed after 1 h of incubation in the presence of these substances.

Lactonase assay

The lactonase activity of PET 40 was investigated by performing a phenol red-assay according to Perez-Garcia *et al.* [49]. As substrates, δ -dodecalactone, γ -dodecalactone, γ -caprolactone and δ -octalactone (Sigma-Aldrich, Munich, Germany) were chosen, which release protons upon hydrolysis resulting in a pH shift. 100 $\text{mg}\cdot\text{mL}^{-1}$ stock solutions of the lactones were mixed with dimethyl sulfoxide and stored at -20 °C. 8 μL substrate was incubated with 5 μL protein (1 $\text{mg}\cdot\text{mL}^{-1}$) and 5 mM EPPS buffer including phenol red with a final concentration of 0.45 mM in a 250 μL reaction volume. At 40 °C, the enzymatic activity was measured at 550 nm every 15 min. The samples were measured in triplicates, including additional negative controls with enzyme-free buffer. The enzymatic activity, calculated in units ($\text{U}\cdot\text{mg}^{-1}$), was determined according to the Lambert–Beer law using the reported extinction coefficient of phenol red ($8450 \text{ m}^{-1}\cdot\text{cm}^{-1}$) [30] together with the highest determined initial reduction in extinction values throughout the first hour of measurement. One unit is defined as the amount of protein needed to transform 1 μmol of substrate in 1 min under the abovementioned assay conditions.

Disk-diffusion antibiotic sensitivity test

To test the lactamase activity of PET40, a disk diffusion test was conducted with antibiotic disks containing effective antibiotic concentrations. The disks containing mezlocillin 30 μg (MEZ 30), imipenem 10 μg (IPM 10), cefaclor 30 μg (CEC 30), cefamandole 30 μg (MA 30), cefotiam 30 μg (CFT 30), and cefotaxim 30 μg (CTX 30) were incubated with 20 μL of potassium buffer pH 8 containing 1 $\text{mg}\cdot\text{mL}^{-1}$ of the purified recombinant protein. The disks were incubated for over 17 h at 40 °C. As a negative control, disks were incubated with the same volume of enzyme-free buffer. Afterwards, the antibiotic disks were laid on LB-agar plates on which susceptible *E. coli* DH5 α cells had been spread. The agar plates were incubated overnight at 37 °C. The clear zone formation around the disks indicates the ZOI by various β -lactam antibiotics. The reduction of ZOI was calculated in comparison to the negative controls (Fig. 5).

Binding mode prediction via molecular docking

We applied the AlphaFold2-based workflow of ColabFold [70] to generate the 3D structural model of the PET40 wild-type. A single model was generated with 10 prediction cycles (--num_recycles) and structurally refined by running a relaxation with AMBER (--amber). The modeling was made before the crystal structure of PET40_S178A was solved. The structural model and the crystal structure have an RMSD of 1.26 overall and 0.44 in the binding site. All docked ligands were generated from their respective SMILES code [71] using OPENBABEL v.2.4.1 [72]. For the docking, we considered the following substrates: mono(2-hydroxyethyl) terephthalate (MHET), bis(2-hydroxyethyl) terephthalate (BHET), PET trimer (PET₃), methyl hexanoate (MH), polycaprolactone trimer (PCL₃), propane-1,2,3-triyl tributanoate (tributylin, TBT), 4-nitrophenyl decanoate (*p*NP-C10), and 4-nitrophenyl dodecanoate (*p*NP-C12).

The substrates were docked into the catalytic site of the PET40 wild-type utilizing a combination of AutoDock3 [46] as a docking engine and DrugScore²⁰¹⁸ [47,48] as an objective function [50]. Docking grids with a grid spacing of 0.5 Å were generated with DrugScore²⁰¹⁸ using converged pair potentials for all atom pairs. The position and dimension of the docking grid were automatically calculated by DrugScore²⁰¹⁸ using the largest substrate (PET₃) manually placed into the binding site as a reference. Accounting for a margin of 6 Å in every direction, the final docking grid has box dimensions of approximately 32 Å × 46 Å × 30 Å and is centered in the active site of PET40. We adapted an established procedure [47] to account for the high number of rotational degrees of freedom of the oligomeric substrates. The docking protocol considered 100 independent runs for each ligand using an initial population size of 100 individuals, a maximum number of 10⁵ generations, a maximum number of 5.0 × 10⁷ energy evaluations, a mutation rate of 0.02, a crossover rate of 0.8, and an elitism value of 1. All 100 docking solutions were clustered based on structural similarity (RMSD cut-off < 2 Å), yielding a few distinct binding modes. Of these, the best-scored pose was considered the final solution except for *p*NP-C10 and *p*NP-C12, for which the pose from the largest cluster was taken (Results section). The Lamarckian genetic algorithm was chosen for sampling in all approaches.

The distance between the reactive carbonyl carbon atom of the docked substrates and the hydroxy group oxygen of PET40_S178 was measured using PYTRAJ [73], a PYTHON package binding to the CPPTRAJ program [74].

The antibiotic compounds (mezlocillin, cefaclor, cefotaxim, cefotiam, cefamandole, and imipenem) were prepared for docking using LIGPREP [75]. Protonation states were assigned with EpiK at pH 7. Ligands were docked onto the same protein structure, using a grid of 35 Å in every direction, centered between the catalytic residues S178 and H256. Docking was carried out using GLIDE [76]

in standard precision mode, using OPLS_2005 as the force field and generating 50 poses per ligand. The distance between the serine hydroxyl and the carbonyl carbon as well as the angle between the serine hydroxyl, the carbonyl carbon, and the carbon opposite the carbonyl carbon in the lactam ring were calculated using PYMOL's PYTHON API. Reference values of distance and angle were calculated from the crystal structure of a serine β-lactamase from *Mycobacterium tuberculosis* bound to cefamandole (PDB ID 3NY4).

Site-directed mutagenesis to generate the inactive mutant PET40_S178A

Trying to obtain a cocrystal structure of PET40 with a substrate, an inactive mutant of PET40 was generated in which the active site Ser178 was replaced by Ala. Therefore, the primer pair PET40/S178ala_for (5'-GCTTAGGAGTTG TGGCCATGCGATGGGTGGTGG-3') and PET40/S178ala_rev (5'-GTGCCACCACCACCCATCGCATGG CCCACAAC-3') were used on PET40::pET21a(+) as a template in a three-step gradient-PCR ($T_{\text{ann}} = 55\text{--}61\text{ }^{\circ}\text{C}$, fragment size: 6138 bp), resulting in an amplification of the whole vector including the mutagenized insert. After PCR cleanup, the DNA mixture was digested with 1 μL *DpnI* overnight at 37 °C to cleave all methylated template DNA. The following day, the restriction enzyme was inactivated at 80 °C for 20 min and the reaction transformed into *E. coli* DH5α. Colonies were spread on LB agar plates containing 100 μg·mL⁻¹ ampicillin and incubated at 37 °C overnight. The isolated plasmids were sequenced using the primers pET_19_21_24_for (5'-ATATAGGCGCCAGCAA CC-3') and T7 Terminator: (5'-GCTAGTATTGCTCA CCGG-3') and the resulting sequence was checked for correctness.

Crystallization, data collection, data reduction, structure determination, refinement, and final model analysis

PET40_S178A was crystallized by sitting-drop vapor diffusion at 12 °C at a concentration of 11 mg·mL⁻¹ in 100 mM potassium phosphate buffer pH 7.0. 0.1 μL of this solution was mixed with 0.1 μL reservoir solution consisting of 0.2 M magnesium chloride hexahydrate, 10% (v/v) EG, 0.1 M 4-(2-hydroxyethyl)piperazine-1-ethanesulfonic acid (HEPES) pH 7.5, 15% (v/v) polyethylene glycol (PEG) Smear medium, 5% v/v 2-propanol. This drop was equilibrated against the reservoir solution and crystals formed after 4 weeks. Crystallization drops were overlaid with mineral oil, and the crystals were dragged through it for cryo-protection, and flash-frozen in liquid nitrogen.

Diffraction data were collected at 100 K at beamline ID23-1 (ESRF, Grenoble, France) using a 0.8856 Å wavelength.

Table 6. Data collection and refinement statistics for the PET40 mutant S178A. Values in parenthesis refer to the high-resolution shell.

PET40 S178A	
PDB ID	8A2C
Data collection	
Wavelength (Å)	0.8856
Space group	P2 ₁
Unit cell parameters	
<i>a</i> , <i>b</i> , <i>c</i> (Å)	46.0, 110.0, 47.9
α , β , γ (°)	90.00, 95.74, 90.00
Resolution (Å)	110.00–1.60 (1.63–1.60)
Number of unique reflections	61 003 (2989)
<i>R</i> _{merge}	0.075 (0.741)
<i>R</i> _{meas}	0.091 (0.895)
<i>R</i> _{pim}	0.051 (0.495)
$\langle I/\sigma(I) \rangle$	7.3 (1.5)
CC ^{1/2}	0.997 (0.613)
Completeness (%)	97.7 (97.4)
Multiplicity	3.0 (3.1)
Refinement	
Resolution (Å)	31.51–1.60
Number of reflections	60 973
<i>R</i> _{work} / <i>R</i> _{free} (%)	14.59/17.90
r.m.s. deviations	
Bond length (Å)	0.011
Bond angles (°)	1.140
Ramachandran plot	
Favored (%)	98.29
Allowed (%)	1.71
Outliers (%)	0

Data reduction was performed using the program package XDS [77] and AIMLESS [78] from the CCP4 suite [79]. The structure was solved via molecular replacement with PHASER [80] using an AlphaFold model as a search model. The initial model was refined through alternating cycles of manual model building in COOT [81,82] and automatic refinement using PHENIX [83] version 1.19.2_4158. Data collection and refinement statistics are reported in Table 6. The structure assembly was analyzed using PISA [44].

Acknowledgments

This work was in part supported by the BMBF within the programs MetagenLig (031B0571B), LipoBiocat (031B0837A, 031B0837B), and PlastiSea (031B867B) as well as by the EU commission's Horizon 2020 research and innovation program FuturEnzymes under grant agreement no. 101000327. The plasmid containing the IsPETase gene was kindly provided by Birte Höcker at the University of Bayreuth. We are grateful for computational support and infrastructure provided by the “Zentrum für Informations- und Medientechnologie” (ZIM) at the Heinrich Heine University Düsseldorf, and the computing time provided by the

John von Neumann Institute for Computing (NIC) to HG on the supercomputer JUWELS at Jülich Supercomputing Centre (JSC) (user ID: VSK33, lipases). The Center for Structural Studies is funded by the Deutsche Forschungsgemeinschaft (DFG Grant number 417919780 and INST 208/740-1 FUGG) to SHJS. We would like to thank Rebecka Molitor and Stephan Thies from the Institute of Molecular Enzyme Technology at the Heinrich Heine university Düsseldorf for NanoDSF measurements. Open Access funding enabled and organized by Projekt DEAL.

Conflict of interest

The authors declare no conflict of interest.

Author contributions

WRS, JC, and PP-G designed the study, coordinated manuscript writing and bioassays. HZ, and KP contributed to planning, assay conduction, writing, and data collection. RFD was involved in writing, protein expression, and UHPLC analysis. MG contributed to activity assays. HZ, JC, and PP-G were involved in enzyme structural work, bioinformatics, and initial phylogenetic analyses. EC, VA, and SHJS conducted crystallization and structure determination. JD, PAC, CP, and HG performed molecular docking analyses. CS was involved in planning and corrections. All authors contributed to manuscript writing and editing.

Peer review

The peer review history for this article is available at <https://www.webofscience.com/api/gateway/wos/peer-review/10.1111/febs.16924>.

Data availability statement

DNA sequences of the identified and in part functionally verified PET40 esterase is listed in (Table 2) and a new GenBank entry has been deposited with the codon optimized protein sequence of PET40 under the accession number ON332566. Coordinates and structure factors of the X-ray crystal structure of PET40 S178A were deposited to the Protein Data Bank with accession number 8A2C.

References

- Brandon JA, Jones W & Ohman MD (2019) Multidecadal increase in plastic particles in coastal ocean sediments. *Sci Adv* **5**, eaax0587.

- 2 Geyer R, Jambeck JR & Law KL (2017) Production, use, and fate of all plastics ever made. *Sci Adv* **3**, e1700782.
- 3 Danso D, Chow J & Streit WR (2019) Plastics: microbial degradation, environmental and biotechnological perspectives. *Appl Environ Microbiol* **85**, e01095-19.
- 4 Wei R & Zimmermann W (2017) Microbial enzymes for the recycling of recalcitrant petroleum-based plastics: how far are we? *J Microbiol Biotechnol* **10**, 1308–1322.
- 5 Kawai F, Kawabata T & Oda M (2019) Current knowledge on enzymatic PET degradation and its possible application to waste stream management and other fields. *Appl Microbiol Biotechnol* **103**, 4253–4268.
- 6 Chow J, Perez-Garcia P, Dierkes R & Streit WR (2022) Microbial enzymes will offer limited solutions to the global plastic pollution crisis. *J Microbiol Biotechnol* **16**, 195–217.
- 7 Tournier V, Duquesne S, Guillamot F, Cramail H, Taton D, Marty A & André I (2023) Enzymes' power for plastics degradation. *Chem Rev* **123**, 5612–5701.
- 8 Buchholz PCF, Feuerriegel G, Zhang H, Perez-Garcia P, Nover L-L, Chow J, Streit WR & Pleiss J (2022) Plastics degradation by hydrolytic enzymes: the plastics-active enzymes database—PAZy. *Proteins* **90**, 1443–1456.
- 9 Yoshida S, Hiraga K, Takehana T, Taniguchi I, Yamaji H, Maeda Y, Toyohara K, Miyamoto K, Kimura Y & Oda K (2016) A bacterium that degrades and assimilates poly(ethylene terephthalate). *Science* **351**, 1196–1199.
- 10 Wei R, von Haugwitz G, Pfaff L, Mican J, Badenhorst CPS, Liu W, Weber G, Austin HP, Bednar D, Damborsky J *et al.* (2022) Mechanism-based design of efficient PET hydrolases. *ACS Catal* **12**, 3382–3396.
- 11 Wang YZ, Zhou Y & Zylstra GJ (1995) Molecular analysis of isophthalate and terephthalate degradation by *Comamonas testosteroni* YZW-D. *Environ Health Perspect* **103** (Suppl 5), 9–12.
- 12 Choi KY, Kim D, Sul WJ, Chae J-C, Zylstra GJ, Kim YM & Kim E (2005) Molecular and biochemical analysis of phthalate and terephthalate degradation by *Rhodococcus* sp. strain DK17. *FEMS Microbiol Lett* **252**, 207–213.
- 13 Notredame C, Higgins DG & Heringa J (2000) T-coffee: a novel method for fast and accurate multiple sequence alignment. *J Mol Biol* **302**, 205–217.
- 14 Kumar S, Stecher G, Li M, Knyaz C & Tamura K (2018) MEGA X: molecular evolutionary genetics analysis across computing platforms. *Mol Biol Evol* **35**, 1547–1549.
- 15 Sulaiman S, Yamato S, Kanaya E, Kim J-J, Koga Y, Takano K & Kanaya S (2012) Isolation of a novel cutinase homolog with polyethylene terephthalate-degrading activity from leaf-branch compost by using a metagenomic approach. *Appl Environ Microbiol* **78**, 1556–1562.
- 16 Ribitsch D, Herrero Acero E, Greimel K, Dellacher A, Zitzenbacher S, Marold A, Rodriguez RD, Steinkellner G, Gruber K, Schwab H *et al.* (2012) A new esterase from *Thermobifida halotolerans* hydrolyses polyethylene terephthalate (PET) and polylactic acid (PLA). *Polymers* **4**, 617–629.
- 17 Roth C, Wei R, Oeser T, Then J, Follner C, Zimmermann W & Strater N (2014) Structural and functional studies on a thermostable polyethylene terephthalate degrading hydrolase from *Thermobifida fusca*. *Appl Microbiol Biotechnol* **98**, 7815–7823.
- 18 Wei R, Oeser T, Then J, Kuhn N, Barth M, Schmidt J & Zimmermann W (2014) Functional characterization and structural modeling of synthetic polyester-degrading hydrolases from *Thermomonospora curvata*. *AMB Express* **4**, 44.
- 19 Kawai F, Oda M, Tamashiro T, Waku T, Tanaka N, Yamamoto M, Mizushima H, Miyakawa T & Tanokura M (2014) A novel Ca(2+)-activated, thermostabilized polyesterase capable of hydrolyzing polyethylene terephthalate from *Saccharomonospora viridis* AHK190. *Appl Microbiol Biotechnol* **98**, 10053–10064.
- 20 Chertkov O, Sikorski J, Nolan M, Lapidus A, Lucas S, Del Rio TG, Tice H, Cheng J-F, Goodwin L & Pitluck S (2011) Complete genome sequence of *Thermomonospora curvata* type strain (B9 T). *Stand Genomic Sci* **4**, 13–22.
- 21 Müller R, Schrader H, Profe J, Dresler K & Deckwer W (2005) Enzymatic degradation of poly (ethylene terephthalate): rapid hydrolyse using a hydrolase from *T. fusca*. *Macromol Rapid Commun* **26**, 1400–1405.
- 22 Herrero Acero E, Ribitsch D, Steinkellner G, Gruber K, Greimel K, Eiteljoerg I, Trotscha E, Wei R, Zimmermann W, Zinn M *et al.* (2011) Enzymatic surface hydrolysis of PET: effect of structural diversity on kinetic properties of cutinases from *Thermobifida*. *Macromolecules* **44**, 4632–4640.
- 23 Bollinger A, Thies S, Katzke N & Jaeger KE (2020) The biotechnological potential of marine bacteria in the novel lineage of *Pseudomonas pertucinogena*. *Microb Biotechnol* **13**, 19–31.
- 24 Bollinger A, Thies S, Knieps-Grünhagen E, Gertzen C, Kobus S, Hoppner A, Ferrer M, Gohlke H, Smits SHJ & Jaeger KE (2020) A novel polyester hydrolase from the marine bacterium *Pseudomonas aestuvaria* – structural and functional insights. *Front Microbiol* **11**, 114.
- 25 Haernvall K, Zitzenbacher S, Yamamoto M, Schick MB, Ribitsch D & Guebitz GM (2017) A new arylesterase from *Pseudomonas pseudoalcaligenes* can hydrolyze ionic phthalic polyesters. *J Biotechnol* **257**, 70–77.

- 26 Zhang H, Perez-Garcia P, Dierkes RF, Applegate V, Schumacher J, Chibani CM, Sternagel S, Preuss L, Weigert S, Schmeisser C *et al.* (2022) The bacteroidetes *Aequorivita* sp. and *Kaistella jeonii* produce promiscuous esterases with PET-hydrolyzing activity. *Front Microbiol* **12**, 803896.
- 27 Joo S, Cho IJ, Seo H, Son HF, Sagong HY, Shin TJ, Choi SY, Lee SY & Kim KJ (2018) Structural insight into molecular mechanism of poly(ethylene terephthalate) degradation. *Nat Commun* **9**, 382.
- 28 Kawai F (2021) The current state of research on PET hydrolyzing enzymes available for biorecycling. *Catalysts* **11**, 206.
- 29 Carniel A, Valoni É, Nicomedes J, Gomes AC & Castro AM (2017) Lipase from *Candida antarctica* (CALB) and cutinase from *Humicola insolens* act synergistically for PET hydrolysis to terephthalic acid. *Process Biochem* **59**, 84–90.
- 30 Martinez-Martinez M, Coscolin C, Santiago G, Chow J, Stogios PJ, Bargiela R, Gertler C, Navarro-Fernandez J, Bollinger A, Thies S *et al.* (2018) Determinants and prediction of esterase substrate promiscuity patterns. *ACS Chem Biol* **13**, 225–234.
- 31 Nutschel C, Coscolin C, David B, Mulnaes D, Ferrer M, Jaeger K-E & Gohlke H (2021) Promiscuous esterases counterintuitively are less flexible than specific ones. *J Chem Inf Model* **61**, 2383–2395.
- 32 Danso D, Schmeisser C, Chow J, Zimmermann W, Wei R, Leggewie C, Li X, Hazen T & Streit WR (2018) New insights into the function and global distribution of polyethylene terephthalate (PET)-degrading bacteria and enzymes in marine and terrestrial metagenomes. *Appl Environ Microbiol* **84**, e02773-17.
- 33 Pérez-García P, Danso D, Zhang H, Chow J & Streit WR (2021) Exploring the global metagenome for plastic-degrading enzymes. *Methods Enzymol* **648**, 137–157.
- 34 Sonnendecker C, Oeser J, Richter PK, Hille P, Zhao Z, Fischer C, Lippold H, Blázquez-Sánchez P, Engelberger F & Ramírez-Sarmiento CA (2022) Low carbon footprint recycling of post-consumer PET plastic with a metagenomic polyester hydrolase. *ChemSusChem* **15**, e202101062.
- 35 Benson DA, Cavanaugh M, Clark K, Karsch-Mizrachi I, Lipman DJ, Ostell J & Sayers EW (2012) GenBank. *Nucleic Acids Res* **41**, D36–D42.
- 36 Chen I-MA, Chu K, Palaniappan K, Ratner A, Huang J, Huntemann M, Hajek P, Ritter S, Varghese N & Seshadri R (2021) The IMG/M data management and analysis system v. 6.0: new tools and advanced capabilities. *Nucleic Acids Res* **49**, D751–D763.
- 37 Ye J, Joseph SD, Ji M, Nielsen S, Mitchell DRG, Donne S, Horvat J, Wang J, Munroe P & Thomas T (2017) Chemolithotrophic processes in the bacterial communities on the surface of mineral-enriched biochars. *ISME J* **11**, 1087–1101.
- 38 Wei R, Oeser T & Zimmermann W (2014) Synthetic polyester-hydrolyzing enzymes from thermophilic actinomycetes. *Adv Appl Microbiol* **89**, 267–305.
- 39 Austin HP, Allen MD, Donohoe BS, Rorrer NA, Kearns FL, Silveira RL, Pollard BC, Dominick G, Duman R, El Omari K *et al.* (2018) Characterization and engineering of a plastic-degrading aromatic polyestherase. *Proc Natl Acad Sci USA* **115**, E4350–E4357.
- 40 Sulaiman S, You DJ, Kanaya E, Koga Y & Kanaya S (2014) Crystal structure and thermodynamic and kinetic stability of metagenome-derived LC-cutinase. *Biochemistry* **53**, 1858–1869.
- 41 Pettersen EF, Goddard TD, Huang CC, Couch GS, Greenblatt DM, Meng EC & Ferrin TE (2004) UCSF Chimera – a visualization system for exploratory research and analysis. *J Comput Chem* **25**, 1605–1612.
- 42 Teufel F, Armenteros JJA, Johansen AR, Gislason MH, Pihl SI, Tsirigos KD, Winther O, Brunak S, von Heijne G & Nielsen H (2021) SignalP 6.0 achieves signal peptide prediction across all types using protein language models. *bioRxiv*. doi: [10.1101/2021.06.09.447770](https://doi.org/10.1101/2021.06.09.447770)
- 43 Ollis DL, Cheah E, Cygler M, Dijkstra B, Frolov F, Franken SM, Harel M, Remington SJ, Silman I, Schrag J *et al.* (1992) The alpha/beta hydrolase fold. *Protein Eng* **5**, 197–211.
- 44 Krissinel E & Henrick K (2007) Inference of macromolecular assemblies from crystalline state. *J Mol Biol* **372**, 774–797.
- 45 Miyakawa T, Mizushima H, Ohtsuka J, Oda M, Kawai F & Tanokura M (2015) Structural basis for the Ca²⁺-enhanced thermostability and activity of PET-degrading cutinase-like enzyme from *Saccharomonospora viridis* AHK190. *Appl Microbiol Biotechnol* **99**, 4297–4307.
- 46 Morris GM, Goodsell DS, Halliday RS, Huey R, Hart WE, Belew RK & Olson AJ (1998) Automated docking using a Lamarckian genetic algorithm and an empirical binding free energy function. *J Comput Chem* **19**, 1639–1662.
- 47 Ditttrich J, Schmidt D, Pflieger C & Gohlke H (2018) Converging a knowledge-based scoring function: DrugScore2018. *J Chem Inf Model* **59**, 509–521.
- 48 Gohlke H, Hendlich M & Klebe G (2000) Knowledge-based scoring function to predict protein-ligand interactions. *J Mol Biol* **295**, 337–356.
- 49 Perez-Garcia P, Kobus S, Gertzen CG, Hoepfner A, Holzschek N, Strunk CH, Huber H, Jaeger K-E, Gohlke H & Kovacic F (2021) A promiscuous ancestral enzyme's structure unveils protein variable regions of the highly diverse metallo-β-lactamase family. *Commun Biol* **4**, 1–12.
- 50 Sotriffer CA, Gohlke H & Klebe G (2002) Docking into knowledge-based potential fields: a comparative evaluation of DrugScore. *J Med Chem* **45**, 1967–1970.

- 51 Mobley DL & Dill KA (2009) Binding of small-molecule ligands to proteins: “what you see” is not always “what you get”. *Structure* **17**, 489–498.
- 52 Schauperl M, Czodrowski P, Fuchs JE, Huber RG, Waldner BJ, Podewitz M, Kramer C & Liedl KR (2017) Binding pose flip explained via enthalpic and entropic contributions. *J Chem Inf Model* **57**, 345–354.
- 53 Wiene-Schmidt B, Oebbke M, Ngo K, Heine A & Klebe G (2021) Two methods, one goal: structural differences between cocrystallization and crystal soaking to discover ligand binding poses. *ChemMedChem* **16**, 292–300.
- 54 Schrödinger, LLC (2015) The PyMOL Molecular Graphics System, Version 2.0. Schrödinger, LLC, New York, NY.
- 55 Krüger DM, Jessen G & Gohlke H (2012) How good are state-of-the-art docking tools in predicting ligand binding modes in protein–protein interfaces? *J Chem Inf Model* **52**, 2807–2811.
- 56 Song Z, Xu T, Wang J, Hou Y, Liu C, Liu S & Wu S (2021) Secondary metabolites of the genus *Amycolatopsis*: structures, bioactivities and biosynthesis. *Molecules* **26**, 1884.
- 57 Nouioui I, Carro L, García-López M, Meier-Kolthoff JP, Woyke T, Kyrpides NC, Pukall R, Klenk H-P, Goodfellow M & Göker M (2018) Genome-based taxonomic classification of the phylum Actinobacteria. *Front Microbiol* **9**, 2007.
- 58 Xu L, Huang H, Wei W, Zhong Y, Tang B, Yuan H, Zhu L, Huang W, Ge M, Yang S *et al.* (2014) Complete genome sequence and comparative genomic analyses of the vancomycin-producing *Amycolatopsis orientalis*. *BMC Genomics* **15**, 363.
- 59 Adamek M, Alanjary M, Sales-Ortells H, Goodfellow M, Bull AT, Winkler A, Wibberg D, Kalinowski J & Ziemert N (2018) Comparative genomics reveals phylogenetic distribution patterns of secondary metabolites in *Amycolatopsis* species. *BMC Genomics* **19**, 426.
- 60 Chen S, Wu Q, Shen Q & Wang H (2016) Progress in understanding the genetic information and biosynthetic pathways behind *Amycolatopsis* antibiotics, with implications for the continued discovery of novel drugs. *Chembiochem* **17**, 119–128.
- 61 Hult K & Berglund P (2007) Enzyme promiscuity: mechanism and applications. *Trends Biotechnol* **25**, 231–238.
- 62 Leveson-Gower RB, Mayer C & Roelfes G (2019) The importance of catalytic promiscuity for enzyme design and evolution. *Nat Rev Chem* **3**, 687–705.
- 63 Coordinators NR (2017) Database resources of the National Center for Biotechnology Information. *Nucleic Acids Res* **45**, D12–D17.
- 64 The UniProt Consortium (2017) UniProt: the universal protein knowledgebase. *Nucleic Acids Res* **45**, D158–D169.
- 65 Markowitz VM, Chen IM, Palaniappan K, Chu K, Szeto E, Grechkin Y, Ratner A, Jacob B, Huang J, Williams P *et al.* (2012) IMG: the integrated microbial genomes database and comparative analysis system. *Nucleic Acids Res* **40**, D115–D122.
- 66 Agarwala R, Barrett T, Beck J, Benson DA, Bollin C, Bolton E, Bourexis D, Brister JR, Bryant SH, Lanese K *et al.* (2016) Database resources of the National Center for Biotechnology Information. *Nucleic Acids Res* **44**, D7–D19.
- 67 Mistry J, Finn RD, Eddy SR, Bateman A & Punta M (2013) Challenges in homology search: HMMER3 and convergent evolution of coiled-coil regions. *Nucleic Acids Res* **41**, e121.
- 68 Berman HM, Westbrook J, Feng Z, Gilliland G, Bhat TN, Weissig H, Shindyalov IN & Bourne PE (2000) The protein data bank. *Nucleic Acids Res* **28**, 235–242.
- 69 Studier FW (2005) Protein production by auto-induction in high density shaking cultures. *Protein Expr Purif* **41**, 207–234.
- 70 Mirdita M, Schütze K, Moriwaki Y, Heo L, Ovchinnikov S & Steinegger M (2022) ColabFold: making protein folding accessible to all. *Nat Methods* **19**, 679–682.
- 71 Weininger D (1988) SMILES, a chemical language and information system. 1. Introduction to methodology and encoding rules. *J Chem Inf Comput Sci* **28**, 31–36.
- 72 O’Boyle NM, Banck M, James CA, Morley C, Vandermeersch T & Hutchison GR (2011) Open babel: an open chemical toolbox. *J Chem* **3**, 1–14.
- 73 Nguyen H, Roe DR, Swails J & Case DA (2016) PYTRAJ: Interactive Data Analysis for Molecular Dynamics Simulations. Rutgers University, New Brunswick, NJ.
- 74 Roe DR & Cheatham TE III (2013) PTRAJ and CPPTRAJ: software for processing and analysis of molecular dynamics trajectory data. *J Chem Theor Comput* **9**, 3084–3095.
- 75 Schrödinger, LLC (2023) Schrödinger Release 2023-2: LigPrep. Schrödinger, LLC, New York, NY.
- 76 Schrödinger, LLC (2023) Schrödinger Release 2023-2: Glide. Schrödinger, LLC, New York, NY.
- 77 Kabsch W (2010) XDS. *Acta Crystallogr D* **66**, 125–132.
- 78 Evans PR & Murshudov GN (2013) How good are my data and what is the resolution? *Acta Crystallogr D* **69**, 1204–1214.
- 79 Winn MD, Ballard CC, Cowtan KD, Dodson EJ, Emsley P, Evans PR, Keegan RM, Krissinel EB, Leslie AG & McCoy A (2011) Overview of the CCP4 suite and current developments. *Acta Crystallogr D* **67**, 235–242.
- 80 McCoy AJ, Grosse-Kunstleve RW, Adams PD, Winn MD, Storoni LC & Read RJ (2007) Phaser crystallographic software. *J Appl Cryst* **40**, 658–674.

H. Zhang *et al.*

PET-degradation by PET40

- 81 Emsley P & Cowtan K (2004) Coot: model-building tools for molecular graphics. *Acta Crystallogr D* **60**, 2126–2132.
- 82 Emsley P, Lohkamp B, Scott WG & Cowtan K (2010) Features and development of Coot. *Acta Crystallogr D* **66**, 486–501.
- 83 Liebschner D, Afonine PV, Baker ML, Bunkoczi G, Chen VB, Croll TI, Hintze B, Hung LW, Jain S, McCoy AJ *et al.* (2019) Macromolecular structure determination using X-rays, neutrons and electrons: recent developments in Phenix. *Acta Crystallogr D* **75**, 861–877.

4 Discussion

Plastic and microplastic pollution poses a global threat to our ecosystem. Only a limited number of bacterial phyla are currently known to harbor PET-degrading enzymes. In this work, two novel PET-active enzymes affiliated with Bacteroidetes were described, providing the first experimental evidence that the bacterial PET degradation is not exclusively found within the phylum of Proteobacteria or Actinobacteria (Zhang et al., 2022a). In addition, PET40, as a diene lactone hydrolase (EC 3.1.1.45), represents one of the few enzymes in its class that can hydrolyze PET (Section 3).

4.1 Bacteroidetes as a rich resource for PET degradation

Bacteroidetes is a widely occurring phylum that predicted to be a resource with the highest potential for PET degradation in the marine environment (Danso et al., 2018). Its representatives can be found in various habitats, including sea water, soil, plants, fish and human gut (Wexler, 2007; Krieg et al., 2015; Hahnke et al., 2016; Munoz et al., 2016). However, PETases from this phylum have not been functionally identified (as of January 2022). In order to enrich the biodiversity of PET-active enzymes from Bacteroidetes, nine putative PETases were extracted from metagenomic sequences and partially investigated (Table 1, Section 2; Zhang et al. (2022a)). The functional screening revealed that PET27 from the genus *Aequorivita* and PET30 from the genus *Kaistella* are the most promising enzymes that are capable of partially breaking down the PET foil into its monomer TPA (Figure 2, Section 2). This provides the first evidence that Bacteroidetes has evolved enzymes that can degrade PET, thus verifying the prediction mentioned above (Danso et al., 2018). Furthermore, the obtained biochemical characteristics showed that both enzymes are typical esterases (EC 3.1), and they hydrolyze a spectrum of *p*NP substrates with a relatively shorter carbon chain length between C6 and C12 (Figure 3, Section 2). Similar observations have been described for PET-active enzymes, such as PET2 and PET40 (Danso et al., 2018; Zhang et al., 2023)).

Further structural analysis revealed that PET27 and PET30 are both typical α/β serine hydrolases and possess a Ser-His-Asp catalytic triad, which is consistent with other

reported PETases and cutinases (Yoshida et al., 2016; Han et al., 2017; Sulaiman et al., 2012). While the residues of substrates binding site are conserved or semi-conserved in PETase and homologous cutinases (Han et al., 2017), wherein the most active PETases (e.g. IsPETase, LCC) share a Tyr-Met-Trp motif, PET30 contains a Phe-Met-Tyr motif (Table 2; Figure 4, Section 2). After the successful mutation of the residues of PET30 by substituting them with the ones of IsPETase, no significant increase in its activity was observed. This implies that the enzymatic activity towards polymers depends on a combination of different factors, such as surface hydrophobicity, position and accessibility of critical residues, rather than only individual amino acids (Zhang et al., 2022a). The presented N-terminal signal peptide suggested that both enzymes are secreted proteins, as identified with all known active enzymes to date (Chow et al., 2022). The difference was observed for PET30 containing a PorC motif, which is involved in the transport of secreted proteins to the periplasm and has been identified as part of the type 9 secretion system of the Bacteroidetes phylum (Desvaux et al., 2009; Sato et al., 2010; de Diego et al., 2016).

Additionally, homologs of bacteroidetal enzymes are found across diverse climates (Figure 1, Section 2), likely due to the ability of Bacteroidetes to decompose a range of biopolymers, including cellulose, polysaccharide and algal cell walls (Thomas et al., 2011; Foley et al., 2016; Church, 2008). The origin of PET30, *Kaistella jeonii*, is able to colonize the PET surface, suggesting that it exists not only in aquatic habitats, but also can adhere to PET polymer under laboratory conditions (Supplementary Figure 5, Section 2). However, the mechanism of its attachment is not clear, due to the limitation of its cultivation in significant amounts, which corresponds to the previous studies that many marine bacteria have difficulties in growing in an artificial medium (Zengler et al., 2002; Alain und Querellou, 2009). Although the bacteroidetal enzymes PET27 and PET30 have a relatively low turnover rate towards PET, their abundance in the environment and significant activity at lower temperatures suggest that they may play a considerable role in the degradation of PET, particularly the PET microparticles in cold environments.

4.2 PET40 - A highly promiscuous esterase hydrolyzing PET

To date, the known PET-active enzymes have been mainly identified as cutinases (EC 3.1.1.74), lipases (EC 3.1.1.3) and carboxylesterases (EC 3.1.1.1). With PET40 hydrolyzing PET substrates, we have demonstrated one of the few PET-active enzymes affiliated with the diene lactone hydrolases (EC 3.1.1.45). PET40, a novel PET-active esterase originating from *Amycolatopsis* species of the Actinobacteria (Figure 1, Section 3), was found by a sequence-based search from GC-rich Gram-positive bacteria metagenomes. Biochemical characterization of PET40, which showed the catalytic activity against a broad range of substrates, has revealed its promiscuous nature. While known PETases like IsPETase or cutinase have been reported on their activity against PET as their initial substrate, PET40 has a relatively lower turnover rate. Conversely, PET40 showed the ability to hydrolyze a diverse expansive number of substrates, including Impranil® DLN, β -lactams and δ -lactones (Figure 2, 4 and 5, Section 3). This signifies that PET might not be the primary substrate for PET40, as this polymer started to exist in nature only in recent decades, the most wild-type enzymes have not yet evolved the capability of consuming PET as a preferable carbon source. The promiscuity of PET40 is likely due to the structural parameters such as the enzyme flexibility (Martinez-Martinez et al., 2018; Khersonsky und Tawfik, 2010; Nutschel et al., 2021; Nobeli et al., 2009) and the active site effective volume (Martinez-Martinez et al., 2018; Nutschel et al., 2021). The substrates that can be well accommodated in the active site are hydrolyzed more efficiently than partially recognized ones (Nutschel et al., 2021; Leveson-Gower et al., 2019; Hult und Berglund, 2007). This was echoed in our findings with respect to the activity analyses and binding mode prediction. The substrates shown to be hydrolyzed by PET40 fit well in the active site of PET40 in the docking experiments (e.g. PCL, BHET, *p*NP-C10/12), while interestingly, for the only non-degraded β -lactams, imipenem, no viable catalytical docking was predicted (Figure 6 and 9, Section 3). Thus, our results of the activity assay and the docking experiments can be mutually confirmed.

The amino acid sequence analysis revealed an N-terminal signal domain, indicating

that PET40 might be a secreted enzyme. As bulky polymers like PET are typically too large to be accessible for enzymes, bacteria tend to secrete PETases into their surrounding environment to be able to act on large substrates (Yoshida et al., 2016; Son et al., 2019; Taniguchi et al., 2019). The N-terminal signal peptide is present in all reported active PETases, and some of those even carry a PorC-like domain that is involved in the type 9 secretion system (Chow et al., 2022). For scrutinizing the mechanism underlying the hydrolytic activity of PET40, we successfully solved the crystal structure of PET40 at a resolution of 1.60 Å. PET40 shares characteristics with other bacterial PET-active enzymes, such as the α/β -fold, as well as the common Asp-His-Ser catalytic triad. The substrate binding site containing Phe-Met-Trp showed a divergent residue in the first position compared to IsPETase as well as to LCC with a Tyr-Met-Trp binding site (Figure 3, Section 3), but it is consistent with the bacteroidetal PET27 (Zhang et al., 2022a). The binding site is located at the protein surface, facilitating the access of small and large substrates, which might contribute to its promiscuous nature.

In summary, we identified and characterized the novel PET-active enzyme PET40 that belongs to the class of diene lactone hydrolases (EC 3.1.1.45), which is not commonly known to degrade PET, setting PET40 apart from other known PETases. The phylogenetic analysis demonstrated that PET40 was derived from *Amycolatopsis* genus of the Actinobacteria phylum. The genus *Amycolatopsis* currently contains more than 70 species and is closely related to the genus *Streptomyces*. PET40 homologs, found in a significant fraction within the two genera, suggest that the PET-degrading enzymes might occur more frequently than previously believed. Regarding the activity towards PET, PET40 is relatively less active than IsPETase and LCC (Table 3, Section 3). However, it showed significant hydrolytic activity against a wide range of other substrates, which revealed its promiscuity. Promiscuous enzymes like PET40 acting on PET as a side reaction confirmed the idea that numerous enzymes in the natural environment may not utilize PET as their primary carbon source, as bacteria most likely did not specifically evolve for this yet. With this respect, our results elucidated the promiscuity of PETases in detail and helped to understand the evolutionary trajectory of genes

encoding these enzymes. Finally, our research broadens the diversity of PET-degrading enzymes. It contributes to the knowledge of their potential implementation for plastics decomposition, by elucidating the multi-functionality of a novel PET-degrading enzyme.

4.3 Isolation of a novel polymer-degrader from crude oil-contaminated environmental samples

In combination with the search for PET-degrading microorganisms, enriching techniques were also implemented in this work. According to the previous study, the high potential of PET-degrading enzymes was observed in metagenomes of crude oil-contaminated samples (Danso et al., 2018). The mineral salt medium (M9 medium) was supplemented with PET foil or powder as the sole carbon source and inoculated with environmental samples, which were collected from crude oil-contaminated sites in Wietze, Germany. The enrichment cultures were incubated at 22 °C. For the functional screening, the M9 agar plate containing polycaprolactone (PCL) was used and inoculated with the liquid culture. Microorganisms enriched from the crude oil-contaminated soil sample showed growth on the selective PCL agar plate and formed a clear zone around colonies, indicating the hydrolytic activity towards PCL (Figure 2). The 16s rRNA analyses implied that they are closely related to *Pseudomonas fluorescens*, *Pseudomonas corrugata* and *Pseudomonas protegens*, with a similarity of over 99%.

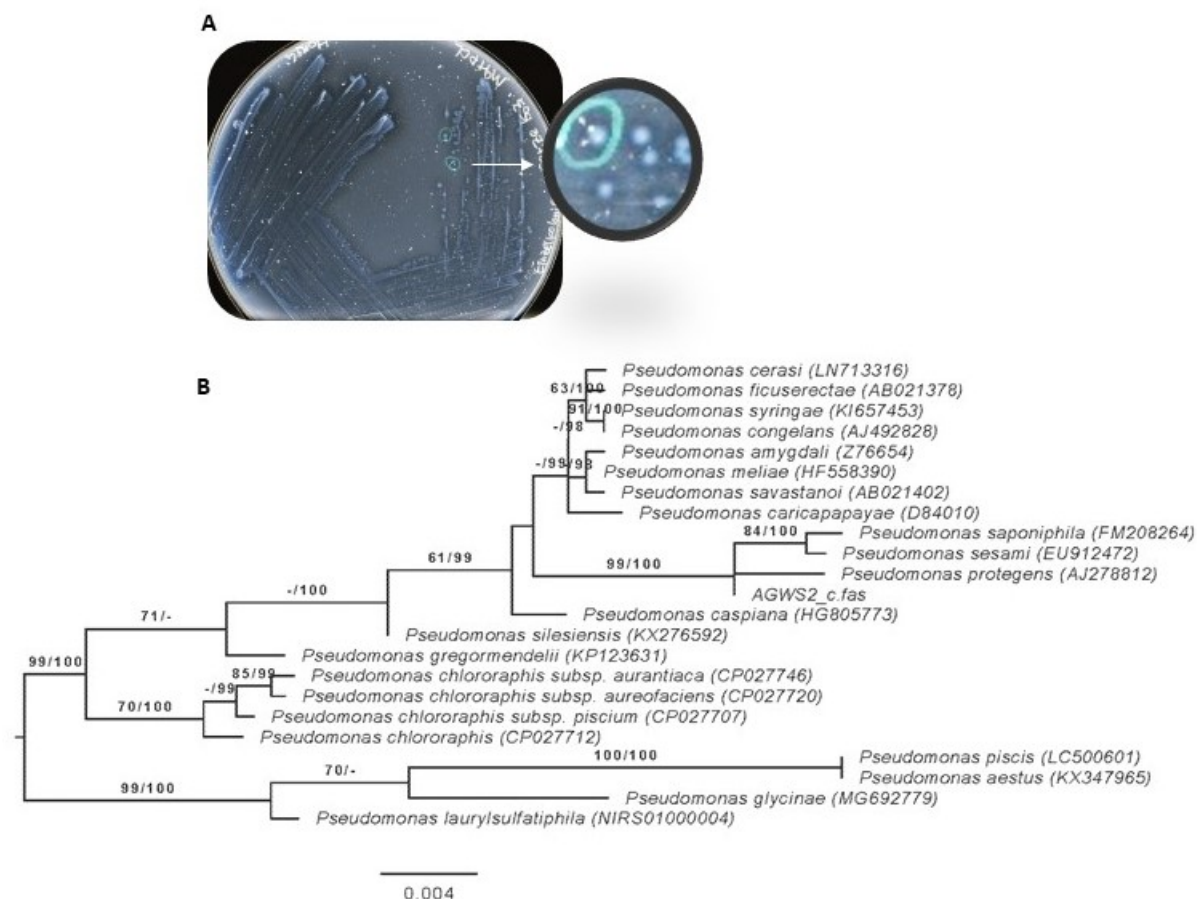


Figure 2: Phylogeny tree of a *Pseudomonas* species isolated from crude oil-contaminated environmental samples. (A) *Pseudomonas* species grow on the agar indicator plate containing PCL and form halos; (B) Maximum likelihood (ML) tree inferred under the GTR+GAMMA model and rooted by midpoint-rooting. The branches are scaled in terms of the expected number of substitutions per site. The numbers above the branches are support values when larger than 60% from ML (left) and maximum parsimony (MP, right) bootstrapping. Phylogenies were inferred by the GGDC web server (Meier-Kolthoff et al., 2013) available at <http://ggdc.dsmz.de/> using the DSMZ phylogenomics pipeline adapted to single genes. The multiple sequence alignment was created with MUSCLE (Edgar, 2004). ML and MP trees were inferred from the alignment with RAxML (Stamatakis, 2014) and TNT (Goloboff et al., 2008), respectively. For ML, rapid bootstrapping in conjunction with the autoMRE bootstopping criterion (Pattengale et al., 2010) and subsequent search for the best tree was used; for MP, 1000 bootstrapping replicates were used in conjunction with tree-bisection-and-reconnection branch swapping and ten random sequence addition replicates.

The genome DNA of one of these microorganisms was isolated for Illumina sequencing. The phylogeny tree constructed with GGDC (genome to genome distance calculator, <https://ggdc.dsmz.de/home.php>) indicated that the *Pseudomonas* species (Figure 2, marked as AGWS2 in the tree) isolated from Wietze environmental samples is closely related to *Pseudomonas protegens*. The obtained draft genome was compared

against a specific PET hydrolase HMM to investigate the potential PET-degrading candidate genes further. Unfortunately, no PET hydrolase was able to be identified. It is possible that the draft genome might not fully cover the related genes, or the gene responsible for hydrolytic activity shown on the PCL-agar plate might code a different hydrolase that has low similarity to the known PET hydrolyses. It is worth mentioning that the genus *Pseudomonas* has been reported on its activity on ester-based Polyurethane (Russell et al., 2011; Darby und Kaplan, 1968), in the production of which PCL is commonly used.

4.4 Identification of PET degradation activity

With consideration that the identification of PET-active enzymes is a major challenge due to the resistance of this synthetic polymer to microbial and enzymatic attacks, this work combined multiple techniques to evaluate PET degradation. As described above, in order to extract the PET-active microorganisms, crude oil-contaminated soil and water samples with the PET-degrading potential were collected and used for enrichment cultures. In addition to this enrichment approach, the database mining of promising enzymes was applied. After the analysis of obtained sequences coding these enzymes, the production of enzyme candidates was carried out using both *in-vitro* translation/transcription technologies and the heterogeneous expression with *E. coli* T7-SHuffle or BL21(DE3) strains. Since it is challenging to produce a sufficient amount of the purified enzymes for the functional screening step using the *in-vitro* technique, the focus was further placed on the enzyme production in *E. coli*. Afterwards, the functional screening was applied through various methods. The primary screening was conducted using agar plates containing specific substrates, including TBT, PCL and BHET. For biochemical characterization, *p*NP-esters were employed. Finally, PET substrates in powder and foil were implemented in the activity assay to assess the PET degradation by the purified enzyme candidates.

4.4.1 Production of recombinant PET-degrading enzymes

In order to assess the activity of the predicted PET-degrading enzymes, the expression vector containing these promising candidate genes was transformed in *E. coli* BL21 (DE3) for heterogeneous expression. The purified proteins were used for initial functional tests. The analysis of the expression and activity tests revealed that four of the nine candidate enzymes were not able to be produced in soluble and active form. Additionally, only a low yield of the purified protein was achieved (Table 1, Zhang et al. (2022a)). A possible reason for this is the toxicity of these enzymes to the host cell, which was already demonstrated in previous studies (Danso, 2019) and is a common obstacle faced in recombinant protein production (Rosano und Ceccarelli, 2014). The recombinant proteins are not able to be produced either in a sufficient amount for further biochemical characterizations or in the aggregated and inactive form (known as inclusion bodies). A high copy number of expression vectors and the lack of appropriate host and physical conditions (culture temperature, pH, etc.) can affect the protein homeostasis in *E. coli* and promote the misfolding of recombinant proteins, leading to the loss of their functionality (Gopal und Kumar, 2013; Bhatwa et al., 2021). Therefore, to avoid these issues and obtain desired proteins in a proper form, various factors must be considered regarding the optimization of the production conditions.

The main strategies to achieve a higher yield in recombinant protein production focus on reducing the formation of inclusion bodies. The approaches, including lowering the culture temperature and the inducer concentration, modifying culture medium and introducing co-factors to assist the protein conformation, are commonly implemented. In addition, using engineered strains suitable for toxic proteins and linking the protein to soluble peptide tags can improve production rate and solubility. In this work, the induction temperature was lowered and, in addition, a modified medium containing glucose was used, which has been shown to promote the yield of toxic proteins (Gopal und Kumar, 2013). Unfortunately, these applied strategies failed to overcome the difficulties in producing PET57-59 in a soluble and active form. Nevertheless, these strategies appear to have positively impacted the production of PET27 and PET30.

4.4.2 Methods for activity verification

After successfully producing the promising PET-degrading enzyme candidates, the substrates such as *p*NP-esters, TBT, PCL and BHET were used for the primary activity screening. In parallel, the purified enzymes were also tested for their hydrolytic activity against PET using an indicator agar plate containing PET nanoparticles (Pérez-García et al., 2021). For final verification of the PET-hydrolyzing activity, the purified enzymes were incubated with PET powder or foil under certain conditions, and the degradation products were analyzed using HPLC. Combining these approaches, we identified three novel enzymes, PET27, PET30 and PET40 that are capable of degrading PET and releasing the TPA monomer as the degradation product. However, we faced difficulties comparing their degradation efficiency with other known PETases, since different detection methods were employed for PET-degrading activity assessment. These methods are mostly based on the detection of the degradation products such as TPA, MHET and BHET. With respect to the substrates used, the commercially available PET foil and powder differ in the degree of crystallinity and the presence of additives, which can, directly and indirectly, interfere with the outcome of enzymatic degradation (Qi et al., 2017; Wright et al., 2021; Yang et al., 2020).

In order to partially overcome this issue, we needed to produce the IsPETase and conduct the degradation assay using the same conditions and substrates. Considering that the characteristics of these enzymes, e.g. optimum temperature and pH values (Qi et al., 2017), are important factors, which influence their activities, comparing their turnover rates is still a challenge due to the lack of a standardization of the comparative studies in this field. A suspension-based assay by measuring the absorbance of breakdown products might provide a possibility to compare the initial rates of these enzymes (Bååth et al., 2020), except for the technical complexities in the production of the MHET which is used as a standard for the assay. Developing and optimizing a standardized methodology would be beneficial for comparative biochemical analyses of the PET-active enzymes.

4.5 Conclusion and Outlook

The present study widens the knowledge of the biodiversity of PET-degrading enzymes by identifying and characterizing three novel PET-degrading enzymes, PET27, PET30 and PET40. Moreover, we demonstrated the first evidence that Bacteroidetes are involved in PET degradation. The data revealing the occurrence of homologs of PET-active enzymes through a variety of climate zones helps to understand the ecological role of the Bacteroidetes in the degradation of marine PET nanoparticles. The observation that the turnover rates of these enzymes against PET substrate are relatively low compared to the IsPETase implies that these PET-active enzymes might not have evolved the activity as their innate function yet but accidentally interact with this synthetic polymer as a side reaction. This was further exhibited by PET40, showing hydrolytic activity towards various substrates and revealing its promiscuous nature, which was also reinforced through molecular docking experiments. In summary, these research findings significantly extend the knowledge of microbial PET-degradation and provide promising candidates with the potential for utilization in diverse industrial contexts. This research demonstrated the activity of PET30 at low temperatures and the multi-functionality of PET40, showing that these enzymes may play an important role in the decomposition of PET waste in marine and domestic plastic contaminants.

Despite the difficulties in culturing many marine microorganisms under laboratory conditions, our microscopic analysis showed that *K. jeonii* can colonize surfaces of PET films after a few days of incubation. However, the mechanism of their interaction remains unclear and should be further investigated. Understanding their microbial attachment can help interpret their roles in the degradation processes, which will be beneficial for discovering microorganisms that are directly responsible for PET-degrading activity.

Overall, this study focused on the degradation activity of the novel PET-active enzymes under certain laboratory conditions, but their function in the natural environment needs to be assessed. In fact, the extent to which these microorganisms and enzymes can alleviate plastic pollution under natural conditions has not yet been proven. According to the calculations by Chow et al., 150 - 500 mg of the best-performing enzyme,

such as LCC or IsPETase, would be required to break down an average PET-bottle, assuming that these enzymes are stable and can exert their activity in nature as if they were under near-optimal conditions (Chow et al., 2022). Considering that the activity of these enzymes is significantly reduced in the natural environment, the importance of improving the enzyme activity and stability is further emphasized by the fact that there are trillion times more plastic contaminants than a singular PET bottle exists in our environment. As previously noted, PET nanoparticles being found in nearly all niches, including human organisms has raised concerns regarding their potential impact on human and animal health. Therefore, biotechnological methods in exploring and modifying PET-active enzymes will be still rewarding and meaningful to address these issues.

5 Other publication

5.1 Plastics degradation by hydrolytic enzymes: The plastics-active enzymes database—PAZy

Patrick C. F. Buchholz¹, Golo Feuerriegel², Hongli Zhang², Pablo Perez-Garcia², Lena-Luisa Nover², Jennifer Chow², Wolfgang R. Streit², Jürgen Pleiss¹

¹Institute of Biochemistry and Technical Biochemistry, University of Stuttgart, Stuttgart, Germany ²Department of Microbiology and Biotechnology, University of Hamburg, Hamburg, Germany

Published in:

Frontiers in Microbiology doi: 10.1002/prot.26325



Received: 30 November 2021 | Revised: 1 February 2022 | Accepted: 14 February 2022

DOI: 10.1002/prot.26325

RESEARCH ARTICLE



Plastics degradation by hydrolytic enzymes: The plastics-active enzymes database—PAZy

Patrick C. F. Buchholz¹ | Golo Feuerriegel² | Hongli Zhang² |
Pablo Perez-Garcia² | Lena-Luisa Nover² | Jennifer Chow² |
Wolfgang R. Streit² | Jürgen Pleiss¹

¹Institute of Biochemistry and Technical Biochemistry, University of Stuttgart, Stuttgart, Germany

²Department of Microbiology and Biotechnology, University of Hamburg, Hamburg, Germany

Correspondence

Jürgen Pleiss, Institute of Biochemistry and Technical Biochemistry, University of Stuttgart, Allmandring 31, D-70569 Stuttgart, Germany.
Email: juergen.pleiss@itb.uni-stuttgart.de

Wolfgang R. Streit, Department of Microbiology and Biotechnology, Universität Hamburg, Ohnhorststraße 18, D-22609 Hamburg, Germany.
Email: wolfgang.streit@uni-hamburg.de

Funding information

Bundesministerium für Bildung und Forschung, Grant/Award Numbers: 031B867B, 031B0837B, 031B0571B, 031B0571A, 031B0562A

Abstract

Petroleum-based plastics are durable and accumulate in all ecological niches. Knowledge on enzymatic degradation is sparse. Today, less than 50 verified plastics-active enzymes are known. First examples of enzymes acting on the polymers polyethylene terephthalate (PET) and polyurethane (PUR) have been reported together with a detailed biochemical and structural description. Furthermore, very few polyamide (PA) oligomer active enzymes are known. In this article, the current known enzymes acting on the synthetic polymers PET and PUR are briefly summarized, their published activity data were collected and integrated into a comprehensive open access database. The Plastics-Active Enzymes Database (PAZy) represents an inventory of known and experimentally verified enzymes that act on synthetic fossil fuel-based polymers. Almost 3000 homologs of PET-active enzymes were identified by profile hidden Markov models. Over 2000 homologs of PUR-active enzymes were identified by BLAST. Based on multiple sequence alignments, conservation analysis identified the most conserved amino acids, and sequence motifs for PET- and PUR-active enzymes were derived.

KEYWORDS

hidden Markov model, hydrolases, metagenome, polyethylene terephthalate degradation, polyurethane degradation, sequence motif

1 | INTRODUCTION

Today, we face the global challenge of plastics pollution in nearly all environments. The pollution has meanwhile reached levels that will ultimately have impact on our food chain and well-being within the next decades. A recent study implied that about 399 000 tons of plastics are present in the oceans alone, of which 69 000 tons are microplastics.¹ Thus, urgent actions need to be implemented for removal of plastics from the environment and by reducing the steady input into the environment.² Whereas it is perhaps more likely that large pieces

can be removed mechanically from ocean surfaces or terrestrial sites, smaller particles (microplastics) will remain there unless microbial or chemical degradation (i.e., weathering) will occur.^{3–5} Plastic waste is a valuable raw material, therefore recycling is a promising alternative to incineration, either as a basis of synthesis of polymers or as a carbon source for fermentation.⁶

Petroleum-based plastics are in general extremely stable and durable; hence, it is widely accepted that plastics do not degrade well in nature,⁷ nor can be directly used in fermentation. The degradation processes described so far are slow, and it was shown that a PET

This is an open access article under the terms of the Creative Commons Attribution License, which permits use, distribution and reproduction in any medium, provided the original work is properly cited.

© 2022 The Authors. *Proteins: Structure, Function, and Bioinformatics* published by Wiley Periodicals LLC.

bottle remains up to 48 years in the ocean until it is decomposed by microbial degradation.⁸ Within this setting, it is reasonable to speculate that prior to microbial and enzymatic degradation, mechanical treatment (waves, wind, friction) and photodegradation by UV light (especially for aromatic ring-containing polymers such as PET and PS) break down the debris into microplastics, thereby increasing the surface area, which mediates microbial degradation. For more details on microplastics-associated bacteria and fungi, we refer to excellent reviews of the field of plastics ecology.^{9–11} However, the colonization of microplastics does not necessarily indicate that the polymer is degraded, because additives are in general more bioavailable than the polymers. Therefore, measuring weight loss as an indicator for degradation might result in a false interpretation of the data,² and in the conclusion that we already have many plastics-active enzymes from different microbial sources. A detailed search in the PubMed database revealed that today roughly 2500 publications address the topic of plastics degradation. However, less than 60 described the isolation and biochemical characterization of plastics-active enzymes (Tables 1 and S1–S3). Nevertheless, while this obvious challenge can be met by better analytical techniques, the by far greater risk for misinterpretation of data comes from the unfiltered and noncritical use of the predicted plastic degrading microorganisms and consortia by not verified bioinformatic tools and pipelines.

For instance, one recent study developed *hidden Markov models* (HMMs) for some plastic degrading enzymes and predicted a global distribution even though no such enzymes have been biochemically characterized.⁴⁷ Others have developed phylogenetic trees and global distribution patterns by simply using automated literature searches without critical analyses of the data.⁴⁸ These very recent studies in high-ranking journals are perhaps only the tip of the iceberg, but clearly demonstrate that there is an urgent need for standardized and verified enzyme databases in this rapidly developing field. The non-critical and unfiltered use of many of the potential plastic degrading gene sequences ultimately leads to incorrect conclusions on the availability of plastic degrading enzymes and their role in nature. These studies do not only mislead research works, they furthermore suggest to environmentalists, policy and law makers, and even to the broader public audience that we would have solutions for the global plastics problem, which we however do not have. Within this framework, the proposed PAZy database will be a reliable and very useful tool giving an overview on truly functional enzymes.

Notably today, only for polyethylene terephthalate (PET), polyurethane ester-based (PUR), and polyamide (oligomers) (PA), a rather small number of degrading enzymes are known, but none for other major fossil-fuel based polymers such as PVC, PE, PP, and PS, and most of the ether-based PUR polymers. The known fossil-fuel based plastics-degrading enzymes are hydrolases, often annotated as lipases, esterases, cutinases, amidases, or proteases (E.C. 3.1.x). However, we have still a limited understanding of the mechanism of enzymatic degradation. It is not clear to which extent bacteria have evolved specific enzymes that bind to the polymers and cleave the bonds similar to the processes that occur when cellulose or other biopolymers are degraded. It is supposed that plastics-degrading enzymes are

exoenzymes, and it can be speculated that plastics-binding domains or proteins might contribute to degradation, similar to the role of cellulose binding domains or expansins in the degradation of cellulosic materials.

To advance the research field, we have collected information of the currently known and verified plastics-active enzymes in the Plastics-Active Enzymes Database (PAZy). Because we mainly focus on synthetic fossil fuel-based plastics, enzymes degrading bioplastics such polylactide (PLAs) or polyhydroxyalkanoate-based polymers (PHAs) were excluded in this manuscript. For the latter and their global distribution, we refer to two excellent review articles on PHA hydrolases.^{49,50}

Thus, we have included enzymes acting on low crystalline polymers PET and ester-based PUR. Since for none of the other fossil-based polymers (e.g., PE, PP, PVC, PS, ether-based PUR, larger PA polymers) truly functional enzymes are known, we have not yet included them. For nylon (PA), we have added the information on the few oligomer-active enzymes in the web-based version of the PAZy data base. Similarly, the web-based version contains information on enzymes acting on polylactic acid (PLA), polyhydroxyalkanoates (PHAs) and synthetic and natural rubber (NR, SR).

Despite the obvious lack of enzymes acting on many of the fossil fuel-based polymers, already the current version of the PAZy database will serve as a comprehensive resource for the identification of further novel plastics-active enzymes, pathways, or microorganisms for plastics removal in industry and the environment. It will further help to advance improved circular use of the different plastic types. This data base will serve as a first platform and will be developed further on over the next few years. PAZy will in general be a valuable repository and tool in this emerging field of plastics research.

2 | METHODS

2.1 | Data selection

Protein sequences with available UniProt identifiers and known activity against PET or PUR were downloaded from the Plastics Microbial Biodegradation Database⁵¹ (PMBD, <http://pmbd.genome-mining.cn/home/>) and NCBI GenBank. Based on available biochemical and/or structural data, in total 44 protein sequences were selected from the PMBD, with 34 and 10 UniProt identifiers for PET and PUR activity, respectively (as of November 2021).

2.2 | PETase homologs

We are aware that there are controversial discussions about the term PETase, but we prefer to define all PET-active enzymes as PETases. Sixteen protein sequences for enzymes with known activity against PET were clustered using CD-HIT (version 4.6.8-1) at a threshold of 90% sequence identity and a word length of 5 to derive a reduced set of 12 centroid sequences.^{52,53} These protein sequences were aligned

TABLE 1 Currently known and active PET hydrolases structural or molecular analyses

Microbial host, enzyme, gene	References	Genbank, UniProt ID ^a	PDB structure	WT enzymes and variants tested	Activity on PET foil, powder, bottle ^b
Proteobacteria-affiliated PET active enzymes					
<i>Ideonella sakaiensis</i> 201-F6, IsPETase, ISF6_4831	12	A0A0K8P6T7	5XFY	WT	
<i>Oleispira antarctica</i> RB-8, PET5, LipA	13	R4YKL9_OLEAN		WT	+
<i>Vibrio gazogenes</i> , PET6, Gene: BSQ33_03270	13	A0A1Z2SIQ1_VIBGA		WT	+
<i>Polyangium brachysporum</i> , PET12, Gene: AAW51_2473	13	A0A0G3BI90_9BURK		WT	+
<i>Pseudomonas pseudoalcaligenes</i> DSM 50188, PpCutA	14	KU695574			n.d.
<i>P. pelagia</i> DSM 25163 PpelaLip	14	KU695573			n.d.
<i>Pseudomonas aestusnigri</i> VGXO14, B7O88_11480, PE-H	15	A0A1H6AD45	6SBN 6SCD	WT, Y250S, S171A, D217A, H249A, G254S, S256N, I257S, Y258N, N259Q, ext.loop, Q294A, I219Y	6 mg MHET/L from PET film (WT and Y250S) in 24 h × 500 nM enzyme ⁻¹ ; and 0.1 mg/ MHET from PET bottle for Y250S in 24 h × 500 nM enzyme ⁻¹
<i>Pseudomonas mendocina</i> ATCC 53552, PmC	16	N20M5AZM016	2FX5		solubilized 250-μm thick films in 96 h
Actinobacterial enzymes					
LCC, leaf compost metagenome	17	G9BY57 AEV21261.1			12 mg TA _{eq.} × h ⁻¹ × mg enzyme ⁻¹ with WT enzyme
	18		4EBO		
	19			N197Q, N266Q, N239G, LCC-G	
	20		6THS 6THT	S165A, ICCG-S165A F243I/D238C/ S283C/ Y127G (ICCG), F243I/ D238C/ S283C/N246M (ICCM), F243W/D238C/ S283C/Y127G (WCCG) and F243W/D238C/ S283C/ N246M (WCCM), F243I/ D238C/ S283C/T96M, F243I/D238C/ S283C/ N246D, F243W/D238C/ S283C/T96M, F243W/ D238C/ S283C/N246D, F243I/D238C/ S283C, F243W/D238C/S283C, D238C/S283C, T96M, Y127G, F243I, F243W, N246D, N246M	105.6 ± 3.9 mg TA _{eq.} × h ⁻¹ × mg enzyme ⁻¹ , on commercial GF-PET with best variant
BhrPETase from HRB29 bacterium	21	GBD22443		WT	0.17 mM BHET, 3.66 mM MHET and 2.47 mM TA from nanoparticles in 20 h
<i>Thermobifida fusca</i> DSM43793, TfH, BTA-1	22–25	Q6A0I4_THEFU AJ810119		WT	+

(Continues)

TABLE 1 (Continued)

Microbial host, enzyme, gene	References	Genbank, UniProt ID ^a	PDB structure	WT enzymes and variants tested	Activity on PET foil, powder, bottle ^b
<i>T. fusca</i> DSM43793, TfH, BTA-2	22–25	AJ810119			+
<i>T. fusca</i> DSM 44342, TfH42_Cut1	26	E9LV10_THEFU ADV92528.1			41 mmol TA/mmol enzyme in 120 h
<i>T. fusca</i> , (strain xy) WSH03-11, Tfu_0882	27–29	Q47RJ7_THEFY			n.d.
<i>T. fusca</i> , (strain xy) WSH03-11, Tfu_0883	27	Q47RJ6_THEFY			n.d.
<i>T. fusca</i> , TfCut-2 (Cut2-kw3)	30	E5BBQ3_THEFU		G62A/F209A	31 ± 0.1 nmol min ⁻¹ cm ⁻² on films; 12-fold better than WT; lcPET film (200 μm) 97% ± 1.8% in 30 h
	31		4CG1 4CG2 4CG3		
	32		4CG1	G62A/I213S, G62A	42% weight loss after 50 h on film G62A/I213S, G62A 2.7-fold better than WT
<i>T. fusca</i> NTU22, TfAXE	33	ADM47605.1			n.d.
<i>T. fusca</i> NRRL B-8184, Cut1	34	JN129499.1			n.d.
<i>T. fusca</i> NRRL B-8184, Cut2	34	JN129500.1			n.d.
<i>Thermobifida cellulositytica</i> DSM44535, Thc_Cut1	26,35	ADV92526.1	5LUI		56 mmol TA/mmol enzyme in 120 h
<i>T. cellulositytica</i> DSM44535, Thc_Cut2	26,35	ADV92527.1	5LUJ 5LUL 5LUK	R29N/A30V, R19S/R29N/A30V	5 mmol TA/mmol enzyme in 120 h
<i>Thermobifida alba</i> AHL119, Est119, est2	36	F7IX06	6AID 3WYN 3VIS		n.d.
<i>Thermomonospora curvata</i> DSM43183, Tcur_1278	37	D1A9G5 ACY96861.1			n.d.
<i>T. curvata</i> DSM43183, Tcur0390	37	ACY95991.1			n.d.
<i>Thermobifida halotolerans</i> , Thh_Est	38	H6WX58			21.5 mmol TA × mol enzyme ⁻¹ in 2 h
<i>T. alba</i> , Est1 (Hydrolase 4)	39	BAI99230			n.d.
<i>Saccharomonospora viridis</i> AHK190, Cut190	40–42	W0TJ64 AB728484	4WFK 4WFI 4WFJ 7CTR 7CTS	S226P, S226P/R228S, S226P/R228S/ T262K, Q138A/D250C-E296C/ Q123H/ N202H, disulfide bonds at N250 and E296	30% increase in Q138A/D250C-E296C/Q123H/N202H variant, but no kinetic data
Firmicutes					
<i>Bacillus subtilis</i> 4P3-11, BsEstB	43	ADH43200.1			n.d.
Bacteroidetes					
<i>Aequorivita</i> sp. CIP111184, PET27	44	WP_111881932			Active on foil and powder
<i>Kaistella</i> (<i>Chryseobacteriu</i>) <i>jeonii</i> , PET30	44	WP_039353427	7PZJ		Active on foil and powder

TABLE 1 (Continued)

Microbial host, enzyme, gene	References	Genbank, UniProt ID ^a	PDB structure	WT enzymes and variants tested	Activity on PET foil, powder, bottle ^b
Metagenome, probably bacterial and phylogenetically unassigned					
PET2, from metagenome, affiliated no obvious affiliation, lipIAF5-2	13	C3RYLO ACC95208.1			+
	45		7ECB 7EC8	R47C/G89C/F105R/E110K/ S156P/G180A/T297P (PET2 7 M), F105R/E110K/ S156P/G180A/T297P, F105R/E110K/S156P/ T297P, R47C/G89C, F105R/E110K, Y262C/ L298C, L265C/A295C, D53P, F105R, E110K, Q134Y, S155D, S156P, W174H, G177A, G178A, G179A, G180A, Q183R, A192P, S202Q, T297P, L298R	6.8-fold increase over WT after 60 min in PET2 7 M variant
PET active enzymes from Eukaryotes					
<i>Candida antarctica</i> , lipase B, CalB	16	LIPB_PSEA2		WT	Solubilized 250- μ m thick films in 96 h
	46			WT	+
<i>Fusarium solani</i> , FsC	16	AAA33335.1	1OXM	WT	Solubilized 250- μ m thick films in 96 h
<i>Thermomyces (Humicola)</i> <i>insolens</i> , HiC	16	A0A075B5G4	4OYY, 4OYL	WT	Solubilized 250- μ m thick films in 96 h
	46			WT	+

Note: All WT enzymes listed were verified for their PET hydrolytic activities by either PET films, PET powder PET bottles, PET coupons, PET nanoparticles, or various synthesized model polyester polymers. Only isolates were included that are available in public strain repositories. Recently published variants of IsPETase and the LCC enzyme are summarized in Table S10.

Abbreviations: –, no activity observed; +, activity observed but not quantified; n.d., not determined.

^aActive link to NCBI Pubmed database.

^bCrystallinity of PET films, bottles, and samples and experimental conditions varied largely in the different studies and thus makes direct comparison difficult.

in a structure-guided multiple sequence alignment by T-COFFEE (version 11.00.8cbe486-1).⁵⁴ A profile HMM was derived from this multiple sequence alignment by HMMER (version 3.1b2, <http://hmmerr.org>). The profile HMM was trimmed by selecting alignment columns that corresponded to the region between amino acid positions 32 and 274 in the PETase from *Ideonella sakaiensis* (IsPETase, UniProt identifier A0A0K8P6T7) to avoid ambiguities at the N- and C-termini (Figure S1; Table S4). The profile HMM and the underlying multiple sequence alignment can be downloaded from <https://doi.org/10.18419/darus-2055>. This PETase-profile HMM was used to search both the NCBI nonredundant (nr) protein database and the Protein Data Bank (PDB) for an update of the Lipase Engineering Database (LED, <https://led.biotatnet.de>), which was previously established as a collection of protein sequences from α/β -hydrolases.^{55–57} Hits for the

PETase-profile HMM were selected from the HMMER results with a minimal score of 100, a minimal profile coverage of 95%, and a maximum ratio of bias/score of 10%.

HMMER was also used to identify the C-terminal region for the Type IX secretion system sorting domain, using the profile HMM TIGR04183, which was derived from a multiple sequence alignment of 889 protein sequences in the TIGRFAM database (<http://tigrfam.jcvi.org/cgi-bin/index.cgi>), with an E-value cut-off below 1.

2.3 | PURase homologs

Four protein sequences for enzymes with known activity against PUR served as queries for BLAST (blastp, version 2.10.0+) against the

NCBI nonredundant (nr) protein database and the PDB.⁵⁸ BLAST performance was improved by multithreading with GNU/Parallel (version 20170622-1).⁵⁹ The BLAST results were filtered by an *E*-value threshold of 10^{-10} and a minimal coverage of 50% to further update the LED.

2.4 | Conservation analyses

The PETase-profile HMM was applied for a standard numbering scheme, by aligning the 2930 sequences of PETase homologs from the LED against the respective profile HMM and subsequently assigning the position numbers from the *Is*PETase reference sequence as standard position numbers. For conservation analysis of PETase homologs, the frequency of amino acid residues or gaps was counted at each standard position.

For the conservation analysis of PURase homologs from LED superfamilies 11 and 13, two multiple sequence alignments were generated using Clustal Omega (version 1.2.4),⁶⁰ and the frequency of amino acid residues or gaps was counted at selected positions.

2.5 | Protein sequence networks

Sets of representative protein sequences were formed by clustering with CD-HIT to reduce the sample size and thus computational effort for pairwise sequence alignments. Values of pairwise sequence identity or similarity were calculated by the Needleman–Wunsch algorithm available in EMBOSS (version 6.6.0) with default gap opening and gap extension penalties of 10 and 0.5, respectively, and the substitution matrix BLOSUM62.^{61,62}

Collections of protein sequences were represented as protein sequence networks that depicted sequences as nodes connected by edges (lines). The edges in a protein sequence network were weighted by values of pairwise sequence identity or similarity. A threshold of the respective edge weights was chosen to select a subset of edges for the network. Protein sequence networks were visualized in Cytoscape (version 3.8.2) with the prefuse-force directed layout algorithm, taking the edge weights into account⁶³; edges of higher sequence identity or similarity were depicted preferably in closer vicinity to each other. The Python NetworkX package (version 1.11) was used to store the metadata of protein sequence networks in GraphML format, available for download at <https://doi.org/10.18419/darus-2054>.⁶⁴

3 | RESULTS

3.1 | Update of the LED

We focus only on validated enzymes acting on the synthetic and fossil fuel-based polymers PET and PUR. Detailed biochemical data of catalytically active enzymes (Tables 1 and S1–S3), analyzed sequences and structures of homologous proteins are comprised in the PAZy and

accessible at <https://www.pazy.eu>. Within the PAZy infrastructure, the LED (<https://led.biocatnet.de>) serves as the database for protein sequences and structures from different superfamilies of α/β -hydrolases and their sequence annotations, since all currently known enzyme activities toward PET or PUR were reported for α/β -hydrolases.

For the update of the LED, 4887 entries were downloaded from the NCBI nonredundant protein database, and 93 entries were downloaded from the PDB using the criteria mentioned in Section 2. The updated LED contains 283 672 sequence entries and 1590 PDB entries (an increase of 3034 and 33 entries compared to the previously published LED version from June 2019, respectively). For the update of the LED, sequences that shared at least 50% similarity were assigned to the same superfamily (Table S5). Sequences that shared at least 60% similarity were assigned to a homologous family; otherwise, they were assigned to a separate group containing all “singleton” sequences. A new superfamily was introduced for PURase homologs of Puda from *D. acidovorans*, as outlined in more detail below.

3.2 | PET active enzymes

3.2.1 | Biochemical properties

Our literature searches identified a total of over 35 wild-type enzymes that have been shown to catalyze the partial degradation of PET to oligomers or even to monomers, originating from four different bacterial phyla and one eukaryotic lineage (Table 1). No archaeal PETases have been functionally verified to date.

Many of the currently known PETases are thermostable enzymes, because the catalytic activity increases at temperatures close to the glass transition temperature (65°C) of PET due to the formation of flexible and thus enzyme-accessible amorphous domains.⁶⁵ Notably, few enzymes are active at lower temperatures implying they may play a role in cold-adapted PET degradation.⁶⁶ However, all known native PETases have rather low catalytic activity toward PET.

3.2.2 | Enzyme structures

All known PETases are α/β -hydrolases and are either cutinases, lipases, or esterases and grouped into EC 3.1.1.101; EC 3.1.1.1, EC 3.1.1.2; EC 3.1.1.3; and EC 3.1.1.74. Recently, the PETase from *I. sakainensis* was placed in a distinct class EC 3.1.1.101. In solution, PETases are supposed to be active as monomers.⁶⁷ A total of 12 structures affiliated with different organisms and the wild-type enzymes are available in the PDB. For the best characterized examples LCC and *Is*PETase, multiple entries of variants have been made. All PETases consist of a single domain, the α/β -hydrolase fold, which is formed by a central twisted β -sheet, flanked by two layers of α -helices,⁶⁸ and thus belong to a class of small α/β -hydrolases that consist only of the core domain without a mobile lid.⁵⁷ For a few PETase homologs from Bacteroidetes, an additional C-terminal sorting

domain for the Type IX secretion system has been annotated and was verified in the single structure published (Figure S5; Table 1). The Type IX secretion system comprises several protein components,⁶⁹ and the corresponding C-terminal domain was also found in other polymer-active enzymes such as cellulases and endo-1,4- β -glucanases.^{70–73} PETases share a conserved catalytic triad of serine, histidine, and aspartic acid, and a GX-type oxyanion hole, which stabilizes the reaction intermediate.⁷⁴ In the PETase homologs, the first oxyanion hole residue X is mostly a conserved aromatic residue such as tyrosine or phenylalanine. The second oxyanion-stabilizing residue is a conserved methionine following the serine of the catalytic triad. For the PETase from *I. sakaiensis*, several residues were suggested for substrate binding, such as an aromatic clamp formed by the first residue of the oxyanion hole and a second aromatic residue.⁷⁵ In addition to this subsite I, a second subsite II was proposed from the interaction observed in a modeled complex with a PET monomer.⁷⁶ Variants with increased catalytic activity were designed and tested. The most active enzymes are LCC variants, where the addition of disulfide bonds increased thermostability.²⁰ The two LCC quadruple variants F243 [W]-D238C-S283C-Y127G, which include the additional disulfide bond, are among the most active PETases described to date.

3.2.3 | Sequence network

For the comparison of PETase sequences, the profile HMM for PETases 13 was used to identify the PETase core domain, and the sequences of all core domains were aligned without considering

additional regions at the N- or C-termini (signal peptides or transport domains, respectively). In superfamily 1 of the LED, 31 560 sequences were annotated as GX-type, but only 2930 sequences were identified as PETase homologous by a profile HMM. At a threshold of 55% sequence similarity, the bacterial PETase core domains formed a large cluster, mainly originating from Actinobacteria or Proteobacteria (Figure 1). Most of the sequences from the PMBD were found in this cluster (Figure S3). In addition, a connected subgroup of PETase core domains from other bacterial phyla emerged, such as the PETase proteins from Bacteroidetes or Planctomycetes. Some homologs of PETase core domains occurred also in enzymes from extremophiles (Figure S4). The fungal PETase core domains such as the PETase homologs from *Fusarium* were separated from the bacterial PETase core domains. At a higher threshold of 60% sequence similarity, the sequences for PETase core domains from Bacteroidetes or Planctomycetes emerged as a separated cluster (Figure S5).

3.2.4 | Sequence motifs

The PETase-profile HMM 13 was applied to analyze the conservation of amino acid residues in the 2930 PETase core domains annotated in the LED (Table S6) in comparison to the equivalent positions in the PETase from *I. sakaiensis* (IsPETase, UniProt identifier A0A0K8P6T7) and LCC (UniProt identifier G9BY57). The catalytic triad, the previously suggested PET binding subsite I, which includes an aromatic clamp for possible substrate interaction, and PET binding subsite II from Joo et al.⁷⁶ were found to be highly conserved (Table 2). The

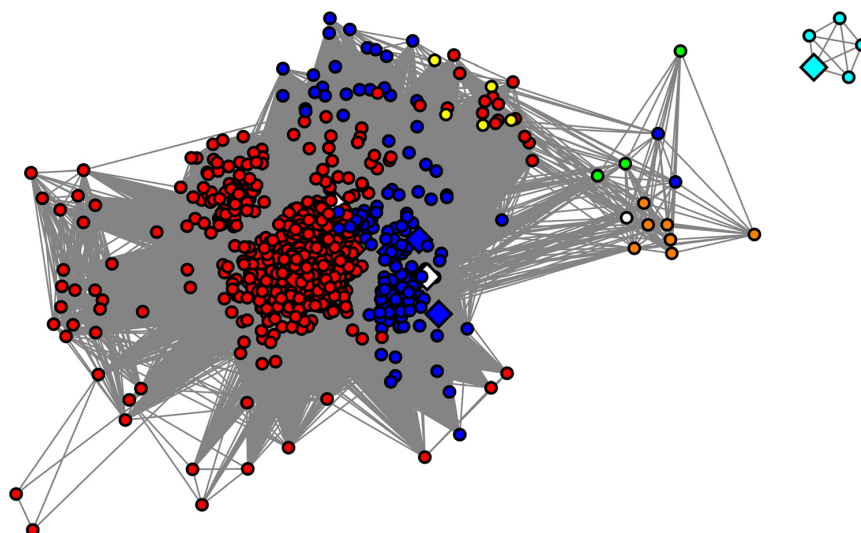


FIGURE 1 Network representation for 869 protein sequences of the “PETase core domain” linked by 318 773 edges. The protein sequences depicted here were selected by clustering at a threshold of 90% sequence identity. Edges (links) were selected at a threshold of 55% sequence similarity. Nodes are colored according to their annotated source organisms, with Actinobacteria in red ●, Proteobacteria in blue ●, Fungi in cyan ●, Bacteroidetes in orange ●, other bacteria from the FCB group in yellow ●, Planctomycetes in green ●, and unknown bacteria colored in white ○. See Section 2 for more details on the network layout. See Figures S2 and S3 for supplementary figures

TABLE 2 A selection of amino acid positions in the 2930 PETase homologs from the LED

Position in <i>IsPETase</i>	Amino acid or gap symbol	Annotations or substitutions	References
87	Y 51%, F 46%	Subsite I, aromatic clamp, oxyanion hole	75,76
88	T 76% (V 7%, L 5%, M 1%)	Subsite II	76
		Thermostability: T96 M in LCC	20
89	A 70% (G 12%, S 10%)	Subsite II	76
119	Q 69% (F8%, Y4%, W2%)	Subsite I	76
		Thermostability: Y127 G in LCC	20
139	Gap 91%	Extension in α -helix 2	75
140	Gap 80%	Extension in α -helix 2	75
141	Gap 90%	Extension in α -helix 2	75
159	H 87% (W9%)	Subsite II	75,76
160	S 100%	Catalytic triad	75
161	M 94%	Subsite I, oxyanion hole	76
185	W 77% (Y12%)	Subsite I, aromatic clamp, "wobbly tryptophane"	75,76
206	D 100%	Catalytic triad	75
208	V 54% (I 36%)	Substrate interaction	75
237	H 100%	Catalytic triad	75
238	F 64% (L 11%, S 8%, Y 3%)	Subsite II	75,76
		Binding & activity: F243 I in LCC	20
		Binding & activity: F243 W in LCC	20
241	N 56% (Q 12%)	Subsite II	76
		Thermostability: N246 D in LCC	20
		Thermostability: N246 M in LCC	20
242	(S 36%, T 32%, G 5%, I 4%)	Extended loop	75,76
243	(S 40%, G 11%, T 8%)	Extended loop	76
244	N 74% (G 3%, Y 3%)	Extended loop	76
245	-87%	Extended loop	76
246	-89%	Extended loop	76
247	-87%	Extended loop	76

Note: Amino acid residues that occurred in less than 50% of the sequences are listed in brackets for comparison with their previous mentions in literature. Amino acid substitutions "in LCC" refer to the position numbers used in Tournier et al.²⁰ Some positions only occurred in a small subset of all PETase homologs and are thus indicated as gap symbols (-). Percentages indicate values rounded to integers. Sixteen positions and their corresponding amino acid symbols marked in red indicate the suggested PETase sequence motif, whereas the ones marked in green indicate additional positions that were used to select the sequences mentioned in the main text.

extension of the second α -helix and the extended loop region, which were described previously as functionally relevant in *IsPETase*, were also found in several PETase homologs in the LED.

Using the position numbers from *IsPETase*, we suggest a typical PETase sequence motif written as follows (X stands for an arbitrary aa): [YF]87, Q119, X₃ 139–141, S160, M161, W185, D206, H237, X₆ 242–247, followed by one of the previously published aa substitutions from Tournier et al.²⁰ Interestingly, two sequences from an uncultured bacterium (NCBI: ACC95208.1) and *Alkalilimnicola ehrlichii* (NCBI: WP_116302080.1) were found to comprise the PETase sequence motif and W238, which was affiliated with improved activity and substrate binding. Further additional sequences (from *Caldimonas manganoxidans*, NCBI: WP_019560450.1, from *Caldimonas taiwanensis*, NCBI:WP_062195544.1, from *Rhizobacter*

gummiphilus, NCBI:WP_085749610.1, and from *Aquabacterium* sp., NCBI: MBI3384080.1) were found to comprise the PETase sequence motif and M241, which was mentioned as an aa substitution for improved thermostability. These six different and novel protein sequences, each selected by a sequence motif of 17 amino acid positions in total, are proposed for upcoming studies on PETase activity.

3.3 | Polyurethanes (PUR) active enzymes

3.3.1 | Biochemical properties

Polyurethanes comprise numerous possible polymers of diverse composition, such as combinations of different isocyanates with different

polyethers, polyesters, or polycarbonates.⁷⁷ The best studied PURases are α/β -hydrolases, as reviewed in more detail in Magnin et al.⁷⁷ Only 10 characterized PUR-degrading enzymes (PURases) have been reported, yet. Four recently identified enzymes (LCC, TfCut-2, Tcur_1278T, and Tcur0390) are cutinases from Actinomyces, which are also active on PET and have a broad substrate profile.⁷⁸ Further bacterial lipases from Betaproteobacteria have been identified and characterized, such as PueA and PueB from *Pseudomonas chlororaphis*. Whereas all the above-mentioned studies identified lipases or esterases, earlier studies reported that commercially available peptidases and proteases might also degrade thin PUR films.⁷⁹ Notably, none of the above-mentioned enzymes is able to act on ether bonds.

3.3.2 | Enzyme structure

The 10 known PURases belong to two groups (Table S1): four belong to the cutinases (LCC, TfCut-2, Tcur_1278T, and Tcur0390) and are similar to PETases. No crystal structures are available for the PURases PueA and PueB from *P. chlororaphis*, but structures of homologs indicate that they belong to superfamily 11 of the LED, which in addition to the core domain has a mobile N-terminal lid, which might mediate binding to the substrate interface and substrate access, and an additional C-terminal β -sandwich domain. The four PETases and PueA and PueB from *P. chlororaphis* are GX types.⁷⁴ Recently, a modeling study on the PURases from *P. chlororaphis* predicted putative substrate binding sites for PUR-like substrates.⁸⁰ However, a rearrangement of the substrate was observed upon the molecular simulation of the

complex, which is an additional challenge for the identification of the substrate binding site.⁸¹ Interestingly, most of the substrate binding residues predicted for PueA⁸⁰ are conserved (Table S7).

The PURase from *D. acidovorans* (UniProt identifier Q9WX47) does not belong to the GX type hydrolases, but has a sequence similarity to carboxylesterases of superfamily 13 and to the family PF00135 in Pfam, and thus belongs to the GGGX-type hydrolases.⁷⁴ Other carboxylesterases in the LED are members of superfamily 4, which have a mobile lid between β -strand -4 and -3 of the core domain. Because the PURase from *D. acidovorans* shared less than 50% sequence similarity to the sequences in the LED and due to the lack of experimental structure information, it was assigned to a new superfamily.

3.3.3 | Sequence network

A threshold of 60% similarity was used to construct protein sequence networks for LED superfamilies 11 and 13 whose members originated from Proteobacteria only (Figure 2). Two disconnected sequence networks emerged: a network of 127 representative sequences of superfamily 11, which contains the GX-type PURases PueA and PueB from *P. chlororaphis*, and a network of 15 representative sequences of superfamily 13, which contains the GGGX-type, the PURase PudA from *D. acidovorans*. In both superfamilies 11 and 13, the sequences originated mainly from Gammaproteobacteria, with the genus *Pseudomonas* being most frequently annotated in superfamily 11.

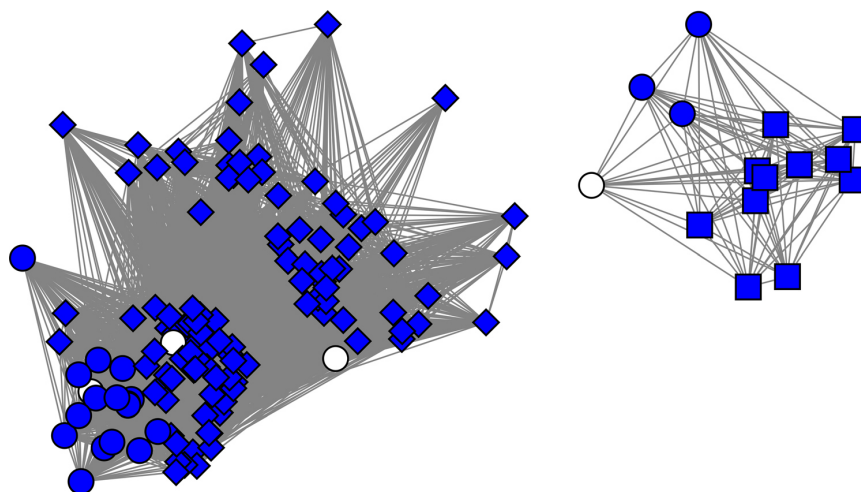


FIGURE 2 Network representation for 142 complete protein sequences similar to PURases linked by 6419 edges. The protein sequences depicted here were selected by clustering at a threshold of 90% sequence identity. Edges (links) were selected at a threshold of 60% global sequence similarity, without defining a core domain region. Nodes are colored according to their annotated source organisms, with Proteobacteria in blue and unknown bacteria in white. The network on the left represents sequences with an N-terminal lid and a C-terminal β -sandwich domain and contains 127 nodes connected by 6314 edges. Diamonds represent sequences originating from the genus *Pseudomonas* (from the class Gammaproteobacteria). The network on the right represents sequences similar to carboxylesterases and contains 15 nodes connected by 105 edges. Squares represent sequences originating from the class of Betaproteobacteria. See Section 2 for more details on the network layout

3.3.4 | Sequence motifs

Two sequence motifs were reported previously in Howard et al.⁸² for the PURase from *P. chlororaphis*, PueA (Table 3). The occurrence of the serine hydrolase motif (GX SXG) and the secretion signal sequence motif (GGXGXDXXX) were confirmed for the vast majority of all 2054 sequence entries in a multiple sequence alignment for superfamily 11 of the LED. Most PURase homologs from superfamily 11 have a GHSLG motif flanking the catalytic serine and secretion motif GGKGN DYLE. For sequences from superfamily 11 in the LED, the catalytic triad is formed by serine, aspartate, and histidine. In addition, most sequences in superfamily 11 (2039 out of 2054) matched the profile HMM for an RTX calcium-binding nonapeptide repeat (PFAM PF00353), which supports the previous suggestion of a Type I secretion system for protein translocation.⁸³

Prominent amino acid positions in superfamily 13, which comprises homologs of the PURase Puda from *D. acidovorans*, include the GX SXG serine hydrolase motif, a catalytic triad of serine, aspartate, and histidine, and a putative PUR binding region at Puda positions 347–395.⁸⁴ Many of these positions were found to be conserved within the sequences of superfamily 13 (Table 4). Most PURase homologs from superfamily 13 have the motif GESAG flanking the catalytic serine, the motif VPX₃G[ST]X₂DE at the catalytic glutamate, and the motif AXHX₃[L]XY flanking the catalytic histidine. In addition,

TABLE 3 Amino acid positions mentioned in Howard et al.⁸² and their occurrence in 2054 PURase homologs from the LED (superfamily 11)

Position in PueA	Amino acid	Annotation
204	G 100%	Serine hydrolase motif GX SXG
205	H 99%	Serine hydrolase motif GX SXG
206	S 100%	Serine hydrolase motif GX SXG, catalytic triad
207	L 99%	Serine hydrolase motif GX SXG
208	G 100%	Serine hydrolase motif GX SXG
254	D 100%	Catalytic triad
312	H 100%	Catalytic triad
381	G 99%	Secretion motif GGXGXDXXX
382	G 98%	Secretion motif GGXGXDXXX
383	K 39%, R 18%, A 16%, S 13%	Secretion motif GGXGXDXXX
384	G 98%	Secretion motif GGXGXDXXX
385	N 78%, A 16%	Secretion motif GGXGXDXXX
386	D 99%	Secretion motif GGXGXDXXX
387	Y 57%, F 42%	Secretion motif GGXGXDXXX
388	L 72%, I 27%	Secretion motif GGXGXDXXX
389	E 91%	Secretion motif GGXGXDXXX

Note: Position numbers refer to PueA from *Pseudomonas chlororaphis*, that is, UniProt identifier A1Z374. Percentages indicate values rounded to integers. Position in the motif is marked in bold.

several positions in the putative PUR binding region were found to be conserved, including mostly hydrophobic amino acids (Table S8).

4 | DISCUSSION

4.1 | Sequence annotations of plastics-active enzymes

Enzymes of different EC classes have been proposed to contribute to degradation of PET or PUR. α/β -hydrolases annotated as cutinases, esterases, or lipases were described to catalyze the hydrolysis of ester bonds and were collected in the PMBD,⁵¹ and peroxidases and laccases have been reported to enhance degradation of PUR.⁸⁵ For most types of plastics, however, knowledge on enzymatic degradation is missing, although materials such as polypropylene (PP) are produced

TABLE 4 Amino acid positions mentioned in Nomura et al.⁸⁴ and adjacent amino acid positions that occur in at least 50% of the 44 PURase homologs from the LED (superfamily 13)

Position in Puda	Amino acid	Annotation
223	G 100%	Serine hydrolase motif GX SXG
224	E 90%	Serine hydrolase motif GX SXG
225	S 100%	Serine hydrolase motif GX SXG, catalytic triad
226	A 97%	Serine hydrolase motif GX SXG
227	G 100%	Serine hydrolase motif GX SXG
340	V 100%	
341	P 97%	
342	V 64%	
343	(I 33%, V 30%, M 26%)	
345	G 100%	
346	S 50% (T 42%)	
347	N 71%	
349	D 92%	
350	E 100%	Catalytic triad
457	A 95%	
458	A 66%	
459	H 100%	Catalytic triad
462	E 78%	
463	L 69% (I 30%)	
464	Q 83%	
465	Y 92%	
466	L 83%	

Note: Position numbers refer to Puda from *Delftia acidovorans*, that is, UniProt identifier Q9WX47. Similar amino acid residues occurring in less than 50% of the sequences are indicated in brackets for comparison. Positions of a putative substrate binding region are listed in Table S5 for comparison. Position in the motif is marked in bold.

in large scales and contribute extensively to global plastics pollution. In this article, we focus on PET- and PUR-degrading α/β -hydrolases due to the availability of sequence information and detailed experimental data from literature and public databases.⁵¹

Many PETase homologs were found in the NCBI nonredundant protein database, due to the sequencing efforts of the cutinase-expressing bacterial phyla such as Actinobacteria and Proteobacteria. In contrast, sequences from fungal origin are unrepresented. The usage of metagenomics is expected to further broaden the scope of currently known PETases.¹³ The PETase sequence motif suggested herein (Table 2) is based on current knowledge from literature, such as the occurrence of an additional flexible loop region and amino acids that seem relevant for interaction with PET. The seven suggested PETase candidates can be used as starting points for wet-lab experiments, such as protein design experiments for improved PETase activity or thermostability.

Although PETases and PURases share the α/β -hydrolase fold as catalytic domain, their structure and their oxyanion hole types differ. All the 2930 PETase homologs belong to a large family (36 936 sequences) of GX-types,⁷⁴ which consist of the core domain only (superfamily 1 in the Lipase Engineering Database⁵⁷), whereas PURases belong to either of three superfamilies: superfamily 1, superfamily 11, which consists of GX-types with two additional domains, an N-terminal mobile lid and a C-terminal β -sandwich domain (2054 sequences), or to superfamily 13, which are carboxylesterases of the GGGX-type (44 sequences). Ample structural information is available for PET-degrading α/β -hydrolases, especially for LCC and *Is*PETase, whereas the structures of PUR-degrading α/β -hydrolases have not been resolved, yet. The former has also inspired the design of improved PETase variants, as recently demonstrated for variants based on LCC.²⁰ Previously, conserved subsite I, subsite II, and an extended loop region were identified in *Is*PETase and used for a systematic comparison with its homologs,⁷⁶ which was confirmed by our conservation analysis of 2930 protein sequences. The profile HMM for PETases and the derived standard numbering scheme is available at the PAZy. It will help in the identification and comparison of amino acid positions reported in literature and will facilitate the design of new PETase variants. The design and construction of variants has already led to a number of highly active enzymes. The most active variants and their functional properties are summarized in Table S9. Notably, the engineered DuraPETase had an almost 300-fold increased activity as compared to the wild-type enzyme.

Likewise for PURases, homology models predict substrate binding regions.^{80,81} Recently, a putative PURases was identified in the Proteobacterium *Serratia liquefaciens*.⁸⁶ Similarly, most putative PURases in the PAZy are from Proteobacteria (mainly from *P. chlororaphis* and *D. acidovorans*).

4.2 | Major challenges in searches for plastics-active enzymes

Today, identifying truly plastic-active genes and enzymes is a very challenging task. This is especially true for enzymes acting on fossil-

based polymers. Thus one of the major challenges will be the identification of novel enzymes for polymers for which none are currently known.^{2,87} Thus, we urgently need enzymes acting on PE, PP, PVC, but also on polymeric PA and PU ether bonds. Within this framework, the identification of plastic-specific binding domains, expansins, or loosensins will be of high relevance. Once these are identified they can be used to further improve enzymes acting PET and PUR. Thereby, a combination of modern synthetic biology approaches together with enzyme engineering approaches will be the appropriate tools to generate the best performing enzymes.

Further we realized the lack of a common PET or PUR model substrate, which would allow the direct comparison of the kinetic parameters of different plastics-active enzymes. In contrast, kinetic analysis is generally performed for typical esterase substrates such as pNP-caproate. This data, however, does not allow a reliable prediction of the actual plastics activity. The few enzymes that have been characterized using polymers were tested on different polymer types, and pretreatment was used to enable better degradation (see Table 1 for references). In addition, all kinetic data were recorded using single point measurements, thus the hydrolysis of the polymer could not be separated from the attachment of the enzyme to the polymer surface or from the hydrolysis of the resulting oligomers. Within this framework, a characterization of surface area and a control of surface properties such as crystallinity would be favorable to obtain better and more reliable kinetic data on the actual polymer.

The accumulation of verified plastics-active enzymes in databases with a reliable structure–function analysis will allow more predictive searches to rapidly and reliably identify novel and more active enzymes. Thereby, it will allow to foster the search and development of novel pathways to create designer bugs using to solve the plastics problem.

4.3 | How can databases contribute to a solution of the plastics waste problem?

For an efficient enzymatic degradation of plastics, we see four challenges. First, enzyme families other than α/β -hydrolases should be considered. For instance, laccases or peroxidases can also act on PUR.⁷⁷ First reports have been published but fell short in the identification of proteins and genes. Enzymatic or nonenzymatic degradation of other plastics components such as dyes or additives from commercial sources might need further investigations, too. Second, there is an increasing need for comparable data on plastics degradation. The comparability and reproducibility of data on enzymatic plastics degradation is impeded by the variety of possible substrates, for example, in case of plastics built from several types of monomers. Furthermore, physical properties of plastic materials can differ remarkably among different commercial suppliers, for example, thickness of plastic foils, number of additives, or crystallinity.

Finally, incorrect annotation of genome and metagenome datasets has resulted in the accumulation of many false positive plastic degrading enzymes in various publications but also in PMBD. Removing these from the databases is a major task. By manual

curation, the PAZy lists only enzymes that degrade synthetic polymers as verified by biochemical or genetical complementation analyses. Thus, all genes and enzymes listed in PAZy are truly functional. In contrast, PMDB also contains putative enzymes, microbes, or microbial consortia, which are active on short oligomers and additives.

Within this setting, the PAZy database provides information on several well studied enzymes supplemented by the protein sequences and structures of homologous sequences, which enables the search for novel candidates and the design of enzyme variants. Most protein sequences and functional data are available for PETases, for which several positions were already assessed experimentally for substrate binding or thermostability in earlier studies from literature (Table 2). The standard numbering scheme of PETase homologs facilitates the comparison of different amino acid positions from literature and the identification of sequence motifs for PETases, as shown for the comparison between *IsPETase*, LCC, and other PETase homologs. In upcoming studies, the PAZy database will be updated to cover sequences from other protein family databases than the LED, depending on the availability of structures and biochemical data. Further, the underlying web platform of the PAZy database makes it easier to share knowledge on various plastics degrading enzymes in a more comparable way. Thus, it can be expected that the suggested sequence motifs for PETases or PURases will be refurbished, as more experimental data on residues for substrate binding or thermostability are made available in the future.

ACKNOWLEDGMENTS

This work was supported in part by the Bundesministerium für Bildung und Forschung within the programs MarBiotech (O31B0562A), MetagenLig (FKZ O31B0571A and O31B0571B), LipoBiocat (O31B0837B), and PlastiSea (O31B867B). GF was in part funded through the University of Hamburg and the Excellence strategy of the BMBF. Open access funding enabled and organized by Projekt DEAL.

DATA AVAILABILITY STATEMENT

The data that support the findings of this study are openly available in PAZy—The Plastics-Active Enzymes Database at <https://pazy.eu>.

ORCID

Patrick C. F. Buchholz  <https://orcid.org/0000-0001-5967-3777>

Pablo Perez-Garcia  <https://orcid.org/0000-0003-2248-3544>

Jennifer Chow  <https://orcid.org/0000-0002-7499-5325>

Wolfgang R. Streit  <https://orcid.org/0000-0001-7617-7396>

Jürgen Pleiss  <https://orcid.org/0000-0003-1045-8202>

REFERENCES

- Hohn S, Acevedo-Trejos E, Abrams JF, Fulgencio de Moura J, Spranz R, Merico A. The long-term legacy of plastic mass production. *Sci Total Environ*. 2020;746:141115. doi:10.1016/j.scitotenv.2020.141115
- Danso D, Chow J, Streit WR. Plastics: environmental and biotechnological perspectives on microbial degradation. *Appl Environ Microbiol*. 2019;85(19):e01095-19. doi:10.1128/AEM.01095-19
- Shaw DG, Day RH. Colour- and form-dependent loss of plastic microdebris from the North Pacific Ocean. *Mar Pollut Bull*. 1994;28(1):39-43. doi:10.1016/0025-326X(94)90184-8
- Mohammadian M, Allen NS, Edge M, Jones K. Environmental degradation of poly (ethylene terephthalate). *Text Res J*. 1991;61(11):690-696. doi:10.1177/004051759106101109
- Day M, Wiles DM. Photochemical degradation of poly(ethylene terephthalate). II. Effect of wavelength and environment on the decomposition process. *J Appl Polym Sci*. 1972;16(1):191-202. doi:10.1002/app.1972.070160117
- Sadler JC, Wallace S. Microbial synthesis of vanillin from waste poly(ethylene terephthalate). *Green Chem*. 2021;23(13):4665-4672. doi:10.1039/d1gc00931a
- Webb HK, Arnott J, Crawford RJ, Ivanova EP. Plastic degradation and its environmental implications with special reference to poly(ethylene terephthalate). *Polymers*. 2013;5(1):1-18. doi:10.3390/polym5010001
- Müller RJ, Kleeberg I, Deckwer WD. Biodegradation of polyesters containing aromatic constituents. *J Biotechnol*. 2001;86(2):87-95. doi:10.1016/S0168-1656(00)00407-7
- Kirstein IV, Wichels A, Gullans E, Krohne G, Gerdt G. The plastisphere – uncovering tightly attached plastic “specific” microorganisms. *PLoS One*. 2019;14(4):e0215859. doi:10.1371/journal.pone.0215859
- Yang Y, Liu W, Zhang Z, Grossart HP, Gadd GM. Microplastics provide new microbial niches in aquatic environments. *Appl Microbiol Biotechnol*. 2020;104(15):6501-6511. doi:10.1007/s00253-020-10704-x
- Amaral-Zettler LA, Zettler ER, Mincer TJ. Ecology of the plastisphere. *Nat Rev Microbiol*. 2020;18(3):139-151. doi:10.1038/s41579-019-0308-0
- Yoshida S, Hiraga K, Takehana T, et al. A bacterium that degrades and assimilates poly(ethylene terephthalate). *Science*. 2016;351(6278):1196-1199. doi:10.1126/science.aad6359
- Danso D, Schmeisser C, Chow J, et al. New insights into the function and global distribution of polyethylene terephthalate (PET)-degrading bacteria and enzymes in marine and terrestrial metagenomes. *Appl Environ Microbiol*. 2018;84(8):e02773-17. doi:10.1128/AEM.02773-17
- Haernvall K, Zitzenbacher S, Wallig K, et al. Hydrolysis of ionic phthalic acid based polyesters by wastewater microorganisms and their enzymes. *Environ Sci Technol*. 2017;51(8):4596-4605. doi:10.1021/ACS.EST.7B00062/SUPPL_FILE/E57B00062_SI_001.PDF
- Bollinger A, Thies S, Knieps-Grünhagen E, et al. A novel polyester hydrolase from the marine bacterium *Pseudomonas aestusnigri*: structural and functional insights. *Front Microbiol*. 2020;11:114. doi:10.3389/fmicb.2020.00114
- Ronkvist ÅM, Xie W, Lu W, Gross RA. Cutinase-catalyzed hydrolysis of poly(ethylene terephthalate). *Macromolecules*. 2009;42(14):5128-5138. doi:10.1021/MA9005318
- Sulaiman S, Yamato S, Kanaya E, et al. Isolation of a novel cutinase homolog with polyethylene terephthalate-degrading activity from leaf-branch compost by using a metagenomic approach. *Appl Environ Microbiol*. 2012;78(5):1556-1562. doi:10.1128/AEM.06725-11
- Sulaiman S, You DJ, Kanaya E, Koga Y, Kanaya S. Crystal structure and thermodynamic and kinetic stability of metagenome-derived LC-cutinase. *Biochemistry*. 2014;53(11):1858-1869. doi:10.1021/bi401561p
- Shirke AN, White C, Englaender JA, et al. Stabilizing leaf and branch compost Cutinase (LCC) with glycosylation: mechanism and effect on PET hydrolysis. *Biochemistry*. 2018;57(7):1190-1200. doi:10.1021/acs.biochem.7b01189
- Tournier V, Topham CM, Gilles A, et al. An engineered PET depolymerase to break down and recycle plastic bottles. *Nature*. 2020;580(7802):216-219. doi:10.1038/s41586-020-2149-4
- Xi X, Ni K, Hao H, Shang Y, Zhao B, Qian Z. Secretory expression in *Bacillus subtilis* and biochemical characterization of a highly thermostable polyethylene terephthalate hydrolase from bacterium HR29. *Enzyme Microb Technol*. 2021;143:109715. doi:10.1016/J.ENZMICTEC.2020.109715
- Dresler K, Van Den Heuvel J, Müller RJ, Deckwer WD. Production of a recombinant polyester-cleaving hydrolase from *Thermobifida fusca* in *Escherichia coli*. *Bioprocess Biosyst Eng*. 2006;29(3):169-183. doi:10.1007/s00449-006-0069-9

23. Müller R-J, Schrader H, Profe J, Dresler K, Deckwer W-D. Enzymatic degradation of poly(ethylene terephthalate): rapid hydrolyse using a hydrolase from *T. fusca*. *Macromol Rapid Commun*. 2005;26(17):1400-1405. doi:10.1002/MARC.200500410
24. Kleeberg I, Hetz C, Kroppenstedt RM, Müller RJ, Deckwer WD. Biodegradation of aliphatic-aromatic copolyesters by *Thermomonospora fusca* and other thermophilic compost isolates. *Appl Environ Microbiol*. 1998;64(5):1731-1735. doi:10.1128/aem.64.5.1731-1735.1998
25. Kleeberg I, Welzel K, VandenHeuvel J, Müller RJ, Deckwer WD. Characterization of a new extracellular hydrolase from *Thermobifida fusca* degrading aliphatic-aromatic copolyesters. *Biomacromolecules*. 2005; 6(1):262-270. doi:10.1021/bm049582t
26. Acero EH, Ribitsch D, Steinkellner G, et al. Enzymatic surface hydrolysis of PET: effect of structural diversity on kinetic properties of Cutinases from *Thermobifida*. *Macromolecules*. 2011;44(12):4632-4640. doi:10.1021/MA200949P
27. Chen S, Tong X, Woodard RW, Du G, Wu J, Chen J. Identification and characterization of bacterial cutinase. *J Biol Chem*. 2008;283(38): 25854-25862. doi:10.1074/jbc.M800848200
28. Su L, Woodard RW, Chen J, Wu J. Extracellular location of *Thermobifida fusca* cutinase expressed in *Escherichia coli* BL21(DE3) without mediation of a signal peptide. *Appl Environ Microbiol*. 2013; 79(14):4192-4198. doi:10.1128/AEM.00239-13
29. Lykidis A, Mavromatis K, Ivanova N, et al. Genome sequence and analysis of the soil cellulolytic actinomycete *Thermobifida fusca* YX. *J Bacteriol*. 2007;189(6):2477-2486. doi:10.1128/JB.01899-06
30. Furukawa M, Kawakami N, Tomizawa A, Miyamoto K. Efficient degradation of poly(ethylene terephthalate) with *Thermobifida fusca* Cutinase exhibiting improved catalytic activity generated using mutagenesis and additive-based approaches. *Sci Rep*. 2019;9(1):16038. doi:10.1038/s41598-019-52379-z
31. Roth C, Wei R, Oeser T, et al. Structural and functional studies on a thermostable polyethylene terephthalate degrading hydrolase from *Thermobifida fusca*. *Appl Microbiol Biotechnol*. 2014;98(18):7815-7823. doi:10.1007/s00253-014-5672-0
32. Wei R, Oeser T, Schmidt J, et al. Engineered bacterial polyester hydrolases efficiently degrade polyethylene terephthalate due to relieved product inhibition. *Biotechnol Bioeng*. 2016;113(8):1658-1665. doi:10.1002/bit.25941
33. Huang YC, Chen GH, Chen YF, Chen WL, Yang CH. Heterologous expression of thermostable acetylxllyan esterase gene from *Thermobifida fusca* and its synergistic action with xylanase for the production of xylooligosaccharides. *Biochem Biophys Res Commun*. 2010; 400(4):718-723. doi:10.1016/j.bbrc.2010.08.136
34. Hegde K, Veeranki VD. Production optimization and characterization of recombinant cutinases from *Thermobifida fusca* sp. NRRL B-8184. *Appl Biochem Biotechnol*. 2013;170(3):654-675. doi: 10.1007/s12010-013-0219-x
35. Ribitsch D, Hromic A, Zitzenbacher S, et al. Small cause, large effect: structural characterization of cutinases from *Thermobifida cellulolytica*. *Biotechnol Bioeng*. 2017;114(11):2481-2488. doi: 10.1002/bit.26372
36. Kitadokoro K, Kakara M, Matsui S, et al. Structural insights into the unique polylactate-degrading mechanism of *Thermobifida alba* cutinase. *FEBS J*. 2019;286(11):2087-2098. doi:10.1111/febs.14781
37. Wei R, Oeser T, Then J, et al. Functional characterization and structural modeling of synthetic polyester-degrading hydrolases from *Thermomonospora curvata*. *AMB Express*. 2014;4(1):1-10. doi: 10.1186/s13568-014-0044-9
38. Ribitsch D, Acero EH, Greimel K, et al. A New Esterase from *Thermobifida halotolerans* hydrolyses polyethylene terephthalate (PET) and polylactic acid (PLA). *Polymers*. 2012;4:617-629. doi: 10.3390/POLYM4010617
39. Hu X, Thumarat U, Zhang X, Tang M, Kawai F. Diversity of polyester-degrading bacteria in compost and molecular analysis of a thermoactive esterase from *Thermobifida alba* AHK119. *Appl Microbiol Biotechnol*. 2010;87(2):771-779. doi:10.1007/s00253-010-2555-x
40. Kawai F, Oda M, Tamashiro T, et al. A novel Ca²⁺-activated, thermostabilized polyesterase capable of hydrolyzing polyethylene terephthalate from *Saccharomonospora viridis* AHK190. *Appl Microbiol Biotechnol*. 2014;98(24):10053-10064. doi:10.1007/s00253-014-5860-y
41. Oda M, Yamagami Y, Inaba S, et al. Enzymatic hydrolysis of PET: functional roles of three Ca²⁺ ions bound to a cutinase-like enzyme, Cut190*, and its engineering for improved activity. *Appl Microbiol Biotechnol*. 2018;102(23):10067-10077. doi: 10.1007/s00253-018-9374-x
42. Emori M, Numoto N, Senga A, et al. Structural basis of mutants of PET-degrading enzyme from *Saccharomonospora viridis* AHK190 with high activity and thermal stability. *Proteins Struct Funct Bioinforma*. 2021;89(5):502-511. doi:10.1002/PROT.26034
43. Ribitsch D, Heumann S, Trotscha E, et al. Hydrolysis of polyethyleneterephthalate by p-nitrobenzylesterase from *Bacillus subtilis*. *Biotechnol Prog*. 2011;27(4):951-960. doi:10.1002/BTPR.610
44. Zhang H, Dierkes R, Pérez-García P, et al. The abundance of mRNA transcripts of bacteroidetal polyethylene terephthalate (PET) esterase genes may indicate a role in marine plastic degradation. 2021. doi: 10.21203/RS.3.RS-567691/V2
45. Nakamura A, Kobayashi N, Koga N, Iino R. Positive charge introduction on the surface of thermostabilized PET hydrolase facilitates PET binding and degradation. *ACS Catal*. 2021;11:8550-8564. doi: 10.1021/ACSCATAL.1C01204/SUPPL_FILE/CS1C01204_SI_003.AVI
46. Carniel A, Valoni É, Nicomedes J, da Conceição Gomes A, Machado de Castro A. Lipase from *Candida antarctica* (CALB) and cutinase from *Humicola insolens* act synergistically for PET hydrolysis to terephthalic acid. *Process Biochem*. 2017;59:84-90. doi:10.1016/J.PROCBIO.2016.07.023
47. Zrimec J, Kokina M, Jonasson S, Zorrilla F, Zeleznik A. Plastic-degrading potential across the global microbiome correlates with recent pollution trends. *MBio*. 2021;12(5):e02155-21. doi: 10.1128/MBIO.02155-21
48. Gambarini V, Pantos O, Kingsbury JM, Weaver L, Handley KM, Lear G. Phylogenetic distribution of plastic-degrading microorganisms. *mSystems*. 2021;6:1. e01112-20. doi: 10.1128/MSYSTEMS.01112-20
49. Viljakainen VR, Hug LA. The phylogenetic and global distribution of bacterial polyhydroxyalkanoate bioplastic-degrading genes. *Environ Microbiol*. 2021;23(3):1717-1731. doi:10.1111/1462-2920.15409
50. Hajighasemi M, Nocek BP, Tchigvintsev A, et al. Biochemical and structural insights into enzymatic depolymerization of polylactic acid and other polyesters by microbial carboxylesterases. *Biomacromolecules*. 2016;17(6):2027-2039. doi:10.1021/ACS.BIOMAC.6B00223/SUPPL_FILE/BM6B00223_SI_001.PDF
51. Gan Z, Zhang H. PMBD: a comprehensive plastics microbial biodegradation database. *Database (Oxford)*. 2019;2019:baz119. doi: 10.1093/database/baz119
52. Li W, Godzik A. Cd-hit: a fast program for clustering and comparing large sets of protein or nucleotide sequences. *Bioinformatics*. 2006; 22:1658-1659. doi:10.1093/bioinformatics/btl158
53. Fu L, Niu B, Zhu Z, Wu S, Li W. CD-hit: accelerated for clustering the next-generation sequencing data. *Bioinformatics*. 2012;28(23):3150-3152. doi:10.1093/bioinformatics/bts565
54. Notredame C, Higgins DG, Heringa J. T-coffee: a novel method for fast and accurate multiple sequence alignment. *J Mol Biol*. 2000; 302(1):205-217. doi:10.1006/jmbi.2000.4042
55. Agarwala R, Barrett T, Beck J, et al. Database resources of the National Center for Biotechnology Information. *Nucleic Acids Res*. 2018;46(D1):D8-D13. doi:10.1093/nar/gkx1095
56. Berman HM, Westbrook J, Feng Z, et al. The Protein Data Bank. *Nucleic Acids Res*. 2000;28(1):235-242. doi:10.1093/nar/28.1.235

57. Bauer TL, Buchholz PCF, Pleiss J. The modular structure of α - β -hydrolases. *FEBS J*. 2019;287(5):1035-1053. doi:10.1111/febs.15071
58. Altschul SF, Gish W, Miller W, Myers EW, Lipman DJ. Basic local alignment search tool. *J Mol Biol*. 1990;215(3):403-410. doi:10.1016/S0022-2836(05)80360-2
59. Tange O. GNU parallel: the command-line power tool. *login. USENIX Mag*. 2011;36(1):42-47.
60. Sievers F, Wilm A, Dineen D, et al. Fast, scalable generation of high-quality protein multiple sequence alignments using Clustal Omega. *Mol Syst Biol*. 2011;7(1):539. doi:10.1038/msb.2011.75
61. Needleman SB, Wunsch CD. A general method applicable to the search for similarities in the amino acid sequence of two proteins. *J Mol Biol*. 1970;48(3):443-453.
62. Rice P, Longden I, Bleasby A. EMBOSS: the European molecular biology open software suite. *Trends Genet*. 2000;16(1):276-277. doi:10.1016/j.cocis.2008.07.002
63. Shannon P, Markiel A, Ozier O, et al. Cytoscape: a software environment for integrated models of biomolecular interaction networks. *Genome Res*. 2003;13(11):2498-2504. doi:10.1101/gr.1239303
64. Hagberg AA, Schult DA, Swart PJ. Exploring network structure, dynamics, and function using NetworkX. In: Varoquaux G, Vaught T, Millman J, eds. Proceedings of the 7th Python in Science Conference; 2008:11-15.
65. Alves NM, Mano JF, Balaguer E, Meseguer Dueñas JM, Gómez Ribelles JL. Glass transition and structural relaxation in semi-crystalline poly(ethylene terephthalate): a DSC study. *Polymer*. 2002;43(15):4111-4122. doi:10.1016/S0032-3861(02)00236-7
66. Zhang H, Perez-García P, Dierkes RF, et al. The *Bacteroidetes Aequorivita* sp. and *Kaistella jeonii* produce promiscuous Esterases with PET-hydrolyzing activity. *Front Microbiol*. 2022;12:3874. doi:10.3389/fmicb.2021.803896
67. Kitadokoro K, Thumarat U, Nakamura R, et al. Crystal structure of cutinase Est119 from *Thermobifida alba* AHK119 that can degrade modified polyethylene terephthalate at 1.76 Å resolution. *Polym Degrad Stab*. 2012;97(5):771-775. doi:10.1016/j.polydegradstab.2012.02.003
68. David L, Cheah E, Cygler M, et al. The α / β hydrolase fold. *Protein Eng Des Sel*. 1992;5(3):197-211. doi:10.1093/protein/5.3.197
69. Lasica AM, Ksiazek M, Madej M, Potempa J. The type IX secretion system (T9SS): highlights and recent insights into its structure and function. *Front Cell Infect Microbiol*. 2017;7:215. doi:10.3389/fcimb.2017.00215
70. Raut MP, Couto N, Karunakaran E, Biggs CA, Wright PC. Deciphering the unique cellulose degradation mechanism of the ruminal bacterium *Fibrobacter succinogenes* S85. *Sci Rep*. 2019;9(1):16542. doi:10.1038/s41598-019-52675-8
71. Suen G, Weimer PJ, Stevenson DM, et al. The complete genome sequence of fibrobacter succinogenes s85 reveals a cellulolytic and metabolic specialist. *PLoS One*. 2011;6(4):e18814. doi:10.1371/journal.pone.0018814
72. Arntzen M, Várnai A, Mackie RI, Eijsink VGH, Pope PB. Outer membrane vesicles from *Fibrobacter succinogenes* S85 contain an array of carbohydrate-active enzymes with versatile polysaccharide-degrading capacity. *Environ Microbiol*. 2017;19(7):2701-2714. doi:10.1111/1462-2920.13770
73. Brumm P, Mead D, Boyum J, et al. Functional annotation of *Fibrobacter succinogenes* S85 carbohydrate active enzymes. *Appl Biochem Biotechnol*. 2011;163(5):649-657. doi:10.1007/s12010-010-9070-5
74. Pleiss J, Fischer M, Peiker M, Thiele C, Schmid RD. Lipase engineering database: understanding and exploiting sequence-structure-function relationships. *J Mol Catal - B Enzym*. 2000;10(5):491-508. doi:10.1016/S1381-1177(00)00092-8
75. Fecker T, Galaz-Davison P, Engelberger F, et al. Active site flexibility as a hallmark for efficient PET degradation by *I. sakaiensis* PETase. *Biophys J*. 2018;114(6):1302-1312. doi:10.1016/j.bpj.2018.02.005
76. Joo S, Cho J, Seo H, et al. Structural insight into molecular mechanism of poly(ethylene terephthalate) degradation. *Nat Commun*. 2018;9(1):382. doi:10.1038/s41467-018-02881-1
77. Magnin A, Pollet E, Phalip V, Avérous L. Evaluation of biological degradation of polyurethanes. *Biotechnol Adv*. 2020;39:107457. doi:10.1016/j.biotechadv.2019.107457
78. Schmidt J, Wei R, Oeser T, et al. Degradation of polyester polyurethane by bacterial polyester hydrolases. *Polymers*. 2017;9(2):65. doi:10.3390/POLYM9020065
79. Phua SK, Castillo E, Anderson JM, Hiltner A. Biodegradation of a polyurethane in vitro. *J Biomed Mater Res*. 1987;21(2):231-246. doi:10.1002/jbm.820210207
80. do Canto VP, Thompson CE, Netz PA. Polyurethanases: three-dimensional structures and molecular dynamics simulations of enzymes that degrade polyurethane. *J Mol Graph Model*. 2019;89:82-95. doi:10.1016/j.jmgm.2019.03.001
81. do Canto VP, Thompson CE, Netz PA. Computational studies of polyurethanases from pseudomonas. *J Mol Model*. 2021;27(2):46. doi:10.1007/s00894-021-04671-x
82. Howard GT, Crother B, Vicknair J. Cloning, nucleotide sequencing and characterization of a polyurethanase gene (pueB) from *Pseudomonas chlororaphis*. *Int Biodeterior Biodegrad*. 2001;47(3):141-149. doi:10.1016/S0964-8305(01)00042-7
83. Bumba L, Masin J, Macek P, et al. Calcium-driven folding of RTX domain β -rolls ratchets translocation of RTX proteins through type I secretion ducts. *Mol Cell*. 2016;62(1):47-62. doi:10.1016/j.molcel.2016.03.018
84. Nomura N, Shigeno-Akutsu Y, Nakajima-Kambe T, Nakahara T. Cloning and sequence analysis of a polyurethane esterase of *Comamonas acidovorans* TB-35. *J Ferment Bioeng*. 1998;86(4):339-345. doi:10.1016/S0922-338X(99)89001-1
85. Ignat L, Ignat M, Ciobanu C, Doroftei F, Popa VI. Effects of flax lignin addition on enzymatic oxidation of poly(ethylene adipate) urethanes. *Ind Crops Prod*. 2011;34(1):1017-1028. doi:10.1016/j.indcrop.2011.03.010
86. Salgado CA, de Almeida FA, Barros E, Baracat-Pereira MC, Bagliniere F, Vanetti MCD. Identification and characterization of a polyurethanase with lipase activity from *Serratia liquefaciens* isolated from cold raw cow's milk. *Food Chem*. 2021;337:127954. doi:10.1016/j.foodchem.2020.127954
87. Wei R, Zimmermann W. Microbial enzymes for the recycling of recalcitrant petroleum-based plastics: how far are we? *J Microbial Biotechnol*. 2017;10(6):1308-1322. doi:10.1111/1751-7915.12710

SUPPORTING INFORMATION

Additional supporting information may be found in the online version of the article at the publisher's website.

How to cite this article: Buchholz PCF, Feuerriegel G, Zhang H, et al. Plastics degradation by hydrolytic enzymes: The plastics-active enzymes database—PAZY. *Proteins*. 2022; 1-14. doi:10.1002/prot.26325

Supporting information

Plastics degradation by hydrolytic enzymes: the Plastics-Active Enzymes Database

Patrick C. F. Buchholz¹, Golo Feuerriegel², Hong Li Zhang², Pablo Perez-Garcia², Lena-Luisa
Nover², Jennifer Chow², Wolfgang R. Streit², Jürgen Pleiss^{1*}

¹Institute of Biochemistry and Technical Biochemistry, University of Stuttgart, Stuttgart,
Germany

²Department of Microbiology and Biotechnology, University of Hamburg, Hamburg, Germany

***Corresponding author:**

Jürgen Pleiss
Institute of Biochemistry and Technical Biochemistry,
University of Stuttgart, Allmandring 31,
D-70569 Stuttgart, Germany
Tel. +49 -711-685-63191
E-Mail: Juergen.Pleiss@itb.uni-stuttgart.de
ORCID: 0000-0003-1045-8202

Tables

TABLE S1: Currently known and active PUR hydrolases together acting on the polymer and on oligomers. Only purified or recombinant enzymes are listed. Some entries derived from genome or metagenome sequencing have been included. The enzymes are known as esterases (EC.3.) and are only active on polyester-based PU, but not on polyether-based PU.

Microbial host/enzyme/gene	Reference	Genbank /UniProt ID	PDB Structure	WT Enzymes and variants tested	Activity on
Bacterial PU-active enzymes					
LCC, leaf compost metagenome (uncultured bacterium; 97 % identical with ammonia oxidizing bacterium HR29 gene locus GBD22443). <i>T. fusca</i> , TfCut-2 (Cut2-kw3)	1	G9BY57 AEV21261.1	4EB0	WT enzyme	Impranil, Elastollan B85A-10 and C85A-10, 200 h 4-5 % weight loss
<i>T. curvata</i> , DSM43183 <i>Tcur_1278T</i>		E5BBQ3 THEFU D1A9G5 ACY96861.1	-		
<i>T. curvata</i> , DSM43183 Tcur0390		ACY95991.1	-		
<i>Comamonas (Deftia) acidovorans</i> TB-35 PUR Esterase, PudA	2-6	BAA76305.1	-	WT enzyme	On solid PUR
<i>Alicyclophilus</i> BQ1 and BQ8 Specific enzymes not identified	7	-	-	WT enzyme	PU films
<i>Bacillus subtilis</i> , strain not specified	8	-	-	WT enzyme	Impranil DLN
Lipase, enzyme purified <i>Corynebacterium</i> sp. (strain not defined)	9	-	-	WT enzyme	PU films
<i>Esterase activity assayed, but not purified</i> <i>Pseudomonas</i> sp.	10	-	-	WT enzyme	Impranil DLN, NMR and IR analyses
Lipase <i>Pseudomonas</i> sp. TD41 Genes/enzymes/pathway <u>not</u> identified	11	Whole genome WOVH01000000	-	WT enzyme	Uses PU-diol solution = polyurethane oligomers, as N and C source Impranil DLN
<i>Pseudomonas chlororaphis</i> <i>Esterase, lipase</i> <i>PueA, PueB</i>	12-16	AAD22743.1 AAF01331.1	-	WT enzyme	Impranil DLN
<i>Pseudomonas fluorescens</i> <i>Esterase, PulA</i>	17,18	AAF66684.1	-	WT enzyme	Impranil, 3g/l in 4-5 days
<i>Acinetobacter gernerii</i> P7 <i>Esterase purified</i>	19	-	-	WT enzyme	Impranil
Metagenome, probably bacterial and phylogenetically unassigned					
Mixed microbial community Growth on oligomers	20	-	-	WT enzyme	PolyLack modifications

Predicted genes/enzymes from patent	<i>Patent</i> <i>WO201924</i> <i>3293A1</i>	-	-	WT enzyme	Impranil DLN
PU-active enzymes from Eukaryotes					
<i>Curvularia senegalensis</i> Esterase, purified	21	-	-	WT enzyme	PU agar
Papain (Peptidase frpm Papaya)	22	-	-	WT enzyme	Thin medical PU films, Biomera, Avcothane, Tecoflexa
Urease (Hydrolase, Mung beans)					
Trypsin (Human Peptidase)	23	-	-	WT enzyme	Films of Pellethane 2363-80AE

TABLE S2: Recently identified PU-active eukaryotes without specific enzymes identified.

PU active culture supernatants from Eukaryotes but no specific enzymes identified	Reference
<i>Alternaria</i> sp. NSIP2, NSINR1 and NSIPV1 <i>N. ramulariae</i> , <i>P. viridicatum</i> <i>Phoma</i> . strain NSIA1	24
<i>Aspergillus flavus</i> (ITCC 6051)	25,26
<i>Aspergillus</i> sp. strain S45 <i>Penicillium brasilianum</i> <i>Alternaria</i> sp. <i>Aspergillus flavus</i>	27
<i>Alternaria tenuissima</i>	28
<i>Cladosporium cladosporioides</i> complex: <i>C. pseudocladosporioides</i> , <i>C. tenuissimum</i> , <i>C. asperulatum</i> , <i>C. montecillanum</i> <i>Aspergillus fumigatus</i> <i>Penicillium chrysogenum</i>	29

TABLE S3: Currently known and active PA hydrolases together with recent publications of variants. Wild-type (WT) enzymes listed were verified using cyclic and/or linear 6-aminohexanoate oligomers.

Microbial host/enzyme/gene	Reference	WT Enzymes and variants tested	Activity on
PA oligomer active enzymes from Bacteria			
NylA, NylB, NylC	30–36	WT enzyme	cyclic and linear 6-aminohexanoate oligomers
<i>Arthrobacter</i> sp. K172, <i>Pseudomonas aeruginosa</i>	37–39	WT enzyme	
PA oligomer active enzymes from Eukaryotes			
White rot fungus, no gene identified, protein purified	40	WT enzymes	

TABLE S4: Nine different PDB structures were used for the structure-guided multiple sequence alignment of twelve protein sequences by T-COFFEE ⁴¹ (**Figure S1**).

UniProt identifier	PDB identifier	Chain
A0A0G3BI90	6QGC	D
A0A0K8P6T7	6QGC	D
C3RYL0	6SBN	A
D1A9G5	1JFR	B
E9LVH7	5LUI	A
F7IX06	3WYN	B
G9BY57	4EB0	A
H6WX58	6AID	A
R4YKL9	6SBN	A
UPI0003945E1F	6SBN	A
W0TJ64	7CEF	B
X0BTD8	5AJH	C

TABLE S5: Comparison between the previous and the updated release of the Lipase Engineering Database (LED, <https://led.biocatnet.de>). Individual sequence entries are summarized in protein entries by a threshold of 98% global sequence identity. PDB entries refer to structure entries from the Protein Data Bank. Homologous families and superfamilies were formed to further categorize the sequence and protein entries (see main text for details). Two superfamilies named Sfam 1 (“core domain”) and Sfam 11, (“N-terminal lid and C-terminal domain”) were updated, and a new superfamily was formed (Sfam 13, “carboxylesterase-like”).

Number of ...	From	Previous release	Updated release	Increase
Sequence entries		280,638	283,672	3034
Protein entries		198,844	200,578	1734
PDB entries	LED	1557	1590	33
Homologous families		2772	2780	8
Superfamilies		12	13	1
Sequence entries		35,088	36,936	1848
Protein entries	Sfam 1	25,869	27,305	1436
PDB entries		266	299	33
Homologous families		389	394	4
Sequence entries		912	2054	1142
Protein entries	Sfam 11	405	665	260
PDB entries		9	9	0
Homologous families		2	4	2
Sequence entries			44	44
Protein entries	Sfam 13		38	38
PDB entries			0	0
Homologous families			2	2

TABLE S6: Amino acids occurring in at least 70% of all 2930 PETase core domains.

Position in IsPETase	Amino acid	Frequency [%]	Position in IsPETase	Amino acid	Frequency [%]	Position in IsPETase	Amino acid	Frequency [%]
32	Y	74	107	V	96	179	A	78
34	R	84	108	V	94	181	P	80
35	G	91	111	I	84	182	L	79
36	P	92	113	T	96	184	P	76
38	P	95	118	D	98	185	W	77
39	T	87	120	P	87	197	P	97
42	S	73	122	S	71	198	T	93
45	A	87	123	R	99	202	G	75
48	G	97	124	G	73	206	D	100
49	P	71	126	Q	92	209	A	87
57	V	91	127	L	83	211	V	70
62	G	93	128	L	78	214	H	77
63	F	93	129	A	88	217	P	79
64	G	83	130	A	96	218	F	74
65	G	86	131	L	88	219	Y	96
66	G	93	132	D	82	221	S	70
67	T	76	133	Y	77	222.1	P	72
68	I	79	134	L	85	228	A	77
69	Y	84	138	S	83	229	Y	83
70	Y	91	145	V	82	231	E	91
71	P	98	146	R	71	232	L	76
72	T	85	148	R	81	235	A	76
74	T	81	150	D	94	237	H	100
76	G	90	153	R	94	240	P	74
77	T	84	154	L	85	244	N	74
78	F	74	156	V	89	257	W	90
79	G	90	158	G	100	258	L	80
80	A	77	159	H	87	259	K	94
85	P	99	160	S	100	260	R	78
86	G	100	161	M	94	261	F	79
88	T	76	162	G	100	263	D	94
92	S	70	163	G	99	265	D	97
96	W	93	164	G	96	266	T	76
98	G	89	165	G	97	267	R	96
99	P	82	167	L	88	268	Y	92
100	R	81	169	A	89	270	Q	77
101	L	81	170	A	82	271	F	96
102	A	97	173	R	76	272	L	86
103	S	96	174	P	76	273	C	95
105	G	99	176	L	84	274	P	82
106	F	97	178	A	95			

TABLE S7: The occurrence of amino acids at selected possible substrate-interacting positions previously published in ⁴² for PU substrates made of polybutylene adipate and five different isocyanate moieties: 4,4'-methylene diphenyl diisocyanate; 2,4-toluene diisocyanate; 2,6-toluene diisocyanate; 4,4'-methylenebis(cyclohexyl isocyanate; and 1,6-hexamethylene diisocyanate. Position numbers refer to PueA from *Pseudomonas chlororaphis*, i.e., UniProt identifier A1Z374. Amino acids occurring in at least 50% of all 2054 PURase homologues from the LED (superfamily 11) are marked in grey color. Amino acids occurring in less than 50% of the sequences are listed for comparison with previously mentioned amino acid residues from ⁴² written in bold font.

Position in PueA	Amino acid	Frequency [%]
37	A	54
40	Y	73
41	Q	58
287	S	59
	N	40
289	N	92
311	I	36
	L	23
314	L	70
316	T	49
317	G	61
320	D	87
324	R	98
329	K	30
332	D	55
344	N	91
367	G	99
369	T	99
386	N	78
466	I	28
	M	24
548	S	65
576	G	29
	D	6
577	Y	26
	Q	2
615	V	69

TABLE S8: Amino acid positions of the putative PUR binding region mentioned in ¹⁴ that occur in at least 50% of the 44 PURase homologues from the LED (superfamily 13). Position numbers refer to Puda from *Delftia acidovorans*, i.e., UniProt identifier Q9WX47. Similar amino acid residues occurring in less than 50% of the sequences are indicated in brackets for comparison. Position numbers in decimal notation indicate insertions with respect to Puda.

Position in Puda	Amino acid	Frequency [%]
347	N	71
349	D	93
350	E	100
351	Y	(48)
	W	(31)
353	L	83
354	F	74
	Y	(24)
356	A	81
359	E	86
360	L	52
364.1	A	50
364.2	A	52
365	L	83
366	T	57
367	A	64
368	A	50
370	Y	79
377	G	79
388	Y	100
389	P	86
390	L	69

TABLE S9: Recently published variants for *IsPETase*

Reference	PDB entry	Amino acid positions exchanged	Catalytic traits
43	<u>5XFZ</u> <u>5XFY</u> <u>5XG0</u> <u>5XH2</u> <u>5XH3</u>	R103G/S131A, S185H, C174S, C210S, W156A, S131A, I179A, W130A, M132A, Y58A, T59A R132G/S160A	
44	<u>6EQE</u> <u>6EQD</u> <u>6EQG</u> <u>6EQF</u> <u>6EQH</u>	W185A, S238F/W159H	+, crystallinity changes observed
45, 46	<u>5XJH</u> <u>5YNS</u>	R280A, S160A, D206A, H237A, Y87A, M161A, W185A, I208A, W159A, S238A, N241A, R280A, W159H, S238F, C203A/C239A	+, only relative data using 200 nM of enzyme
47	<u>6IJ4</u> <u>6IJ3</u> <u>6IJ6</u> <u>6IJ5</u>	P181A, S121D, S121E, D186H, D186F, D186I, D186L, D186V, P181A, P181G, P181S, S121D/D186H, S121E/D186H, S121D/D186H/R280A, S121E/D186H/R280A, S121D/P181A/D186H, S121E/P181A/D186H	14-fold increased activity of S121E/D186H/R280A over WT; 83 μ M TA and 37 μ M MHET released after 1-10 days
48	<u>6ILW</u>	N241F, W159F, S93M	n.d.
49	<u>6ANE</u>	C176A, C212A, C176A-C212A	n.d.
50	<u>6KY5</u>	L117F/Q119Y/T140D/W159H/G165A/I168R/A180I/S188Q/S214H/R280A (DuraPETase)	Over 300-fold enhanced degradation of semi-crystalline (30 %) PET films over WT at 37 °C
51		R280A/S121E/D186H/N233C/S282C	Increased activity of 6.8-fold after 72 hours; 4.9-fold after 6 days over WT
52		K95N/S121E/D186H/F201I/R280A K95N/S121E/D186H/F201I/N233C/R280A/ S282C, L117F/Q119Y/T140D/W159H/G165A/I168R/A180I/S188Q/S214H/N233C/R280A/S282C, K95N/L117F/Q119Y/S121E/T140D/W159H/G165A/I168R/A180I/S188Q/F201I/S214H/R280A, K95N/L117F/Q119Y/S121E/T140D/W159H/G165A/I168R/A180I/S188Q/F201I/S214H/N233C/R280A/S282C	
53		W159H/S238A/S121E/D186H, W159H/S238A	10.6 mM reaction products (TA, MHET, BHET) from 9 mg/mL PET microparticles in 48 h x 0.1 mg/mL enzyme
54		S121E/D186H/R280A/S207R/P181V/S214Y/N233C/S282C/S213E/Q119K/R90T/N212K/R224L/Q182M/S61V/K95N/N241C/K252M/S58A/M154G/T270Q (HotPETase)	Increased activity over S121E/D186H/R280A ⁴⁷ at 40-70 °C
55		W159H/F229Y, W159H, F229Y	W159H/F229Y degradation rate of 23.4 mg PET x h ⁻¹ x mg enzyme ⁻¹ on PET bottle preform
56		S136E	3.3-fold increase on commercial Gf-PET over WT

TABLE S10: Recently published variants for LCC

Reference	PDB entry	Amino acid positions exchanged	Catalytic traits
57		N197Q, N266Q, N239G, LCC-G	
58	6THS 6THT	S165A, ICCG-S165A F243I/D238C/S283C/Y127G (ICCG), F243I/D238C/S283C/N246M (ICCM), F243W/D238C/ S283C/Y127G (WCCG) and F243W/D238C/S283C/N246M (WCCM), F243I/D238C/S283C/T96M, F243I/D238C/S283C/N246D, F243W/D238C/S283C/T96M, F243W/D238C/S283C/N246D, F243I/D238C/S283C, F243W/D238C/S283C, D238C/S283C, T96M, Y127G, F243I, F243W, N246D, N246M	105.6 ± 3.9 mg TA _{eq.} X h ⁻¹ x mg enzyme ⁻¹ , on commercial GF-PET with best variant

Figures

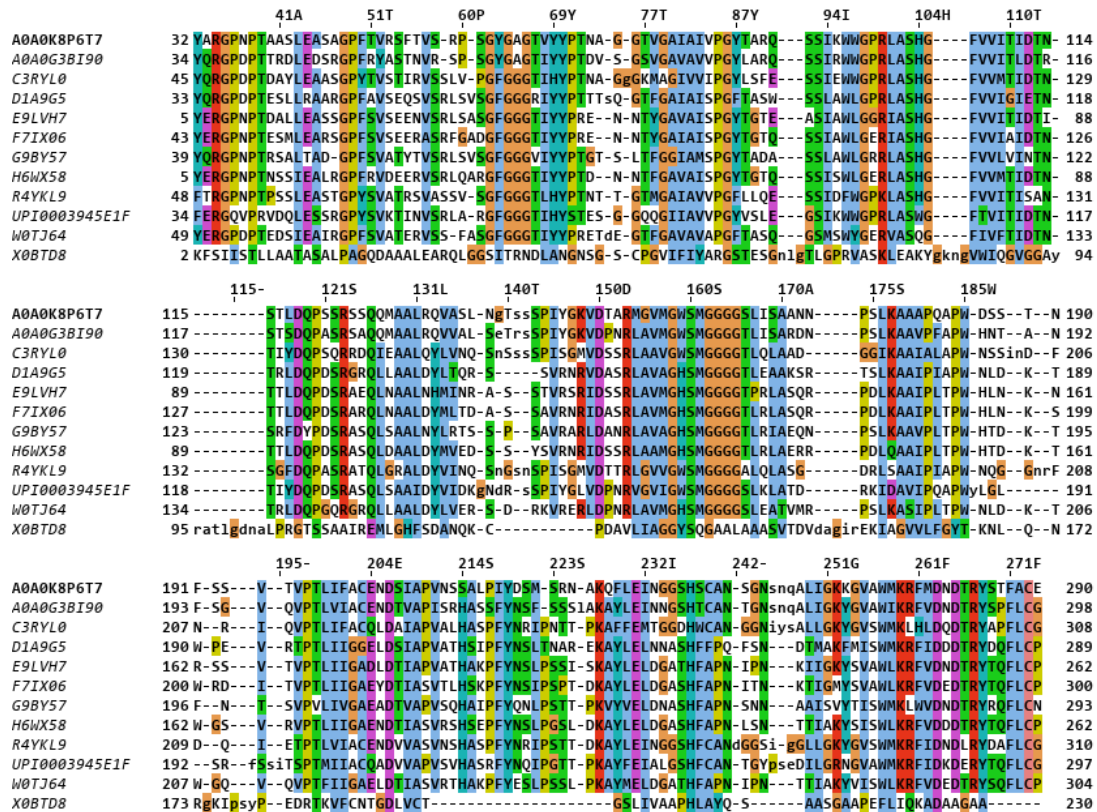


FIGURE S1: The protein sequences of twelve PETase homologues from the PMBD⁵⁹ were aligned by T-COFFEE⁴¹ (Table S2) to generate a profile hidden Markov model (HMM), which was used for the identification of PETase homologues in the LED and the standard numbering scheme. The image was created with Jalview⁶⁰ using Clustalx coloring scheme (version 2.11.1.4). Column numbers in the header indicate positions within the sequence from *Ideonella sakaiensis* (UniProt identifier A0A0K8P6T7, first row). Capital letters indicate alignment columns that were used to derive the profile HMM.

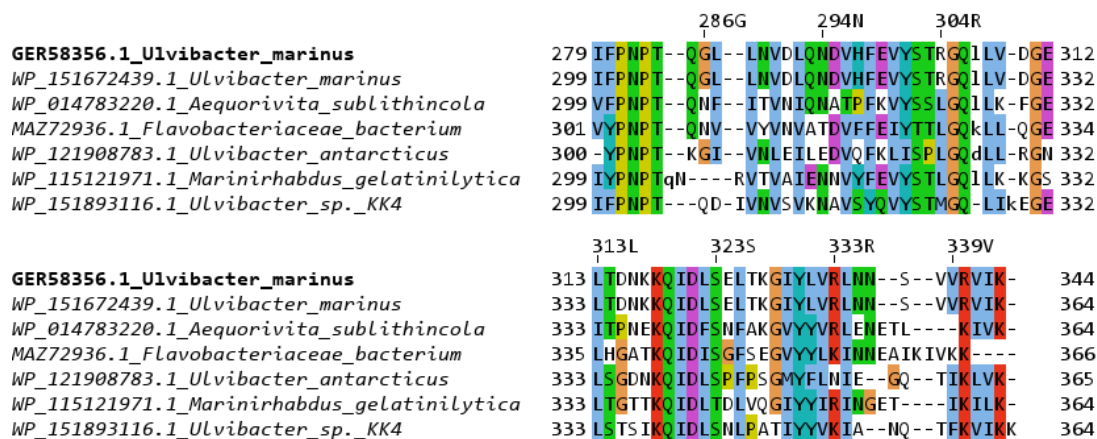


FIGURE S2: Seven exemplary, putative PETase homologues originating from the phylum Bacteroidetes, listed with NCBI accession and taxonomic source names, comprise a C-terminal domain for recognition of the type IX secretion system. The image was created according to the methods described for **Figure S1**.

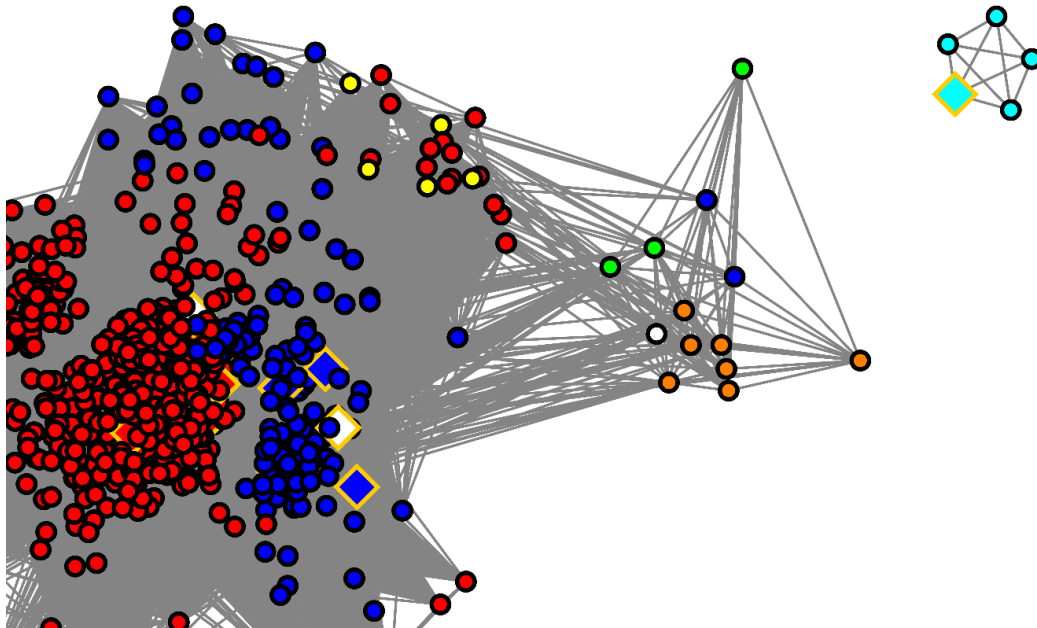


FIGURE S3: Zoom onto the protein sequence networks from **Figure 1**. Representative sequences that correspond to the query sequences from the PMBD⁵⁹ are indicated as diamonds with yellow border.

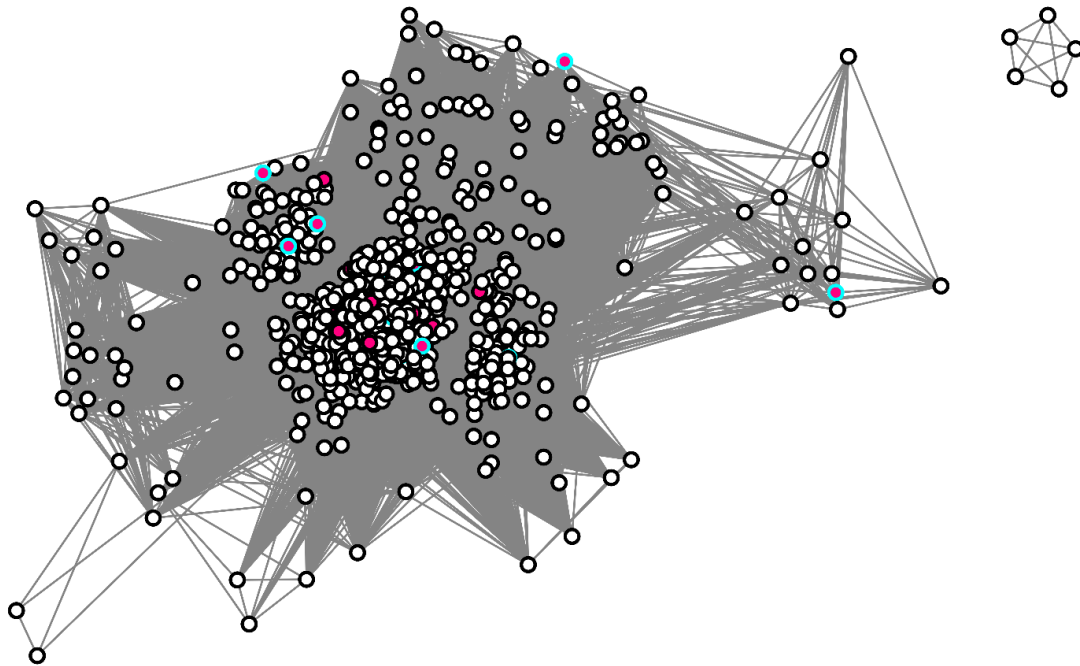


FIGURE S4: Protein sequence networks from **Figure 1** with annotations from the BacDive database ⁶¹. Sequences that originate from thermophilic hosts are shown in magenta. Additionally, sequences that originate from psychrophilic hosts are shown with cyan borders.

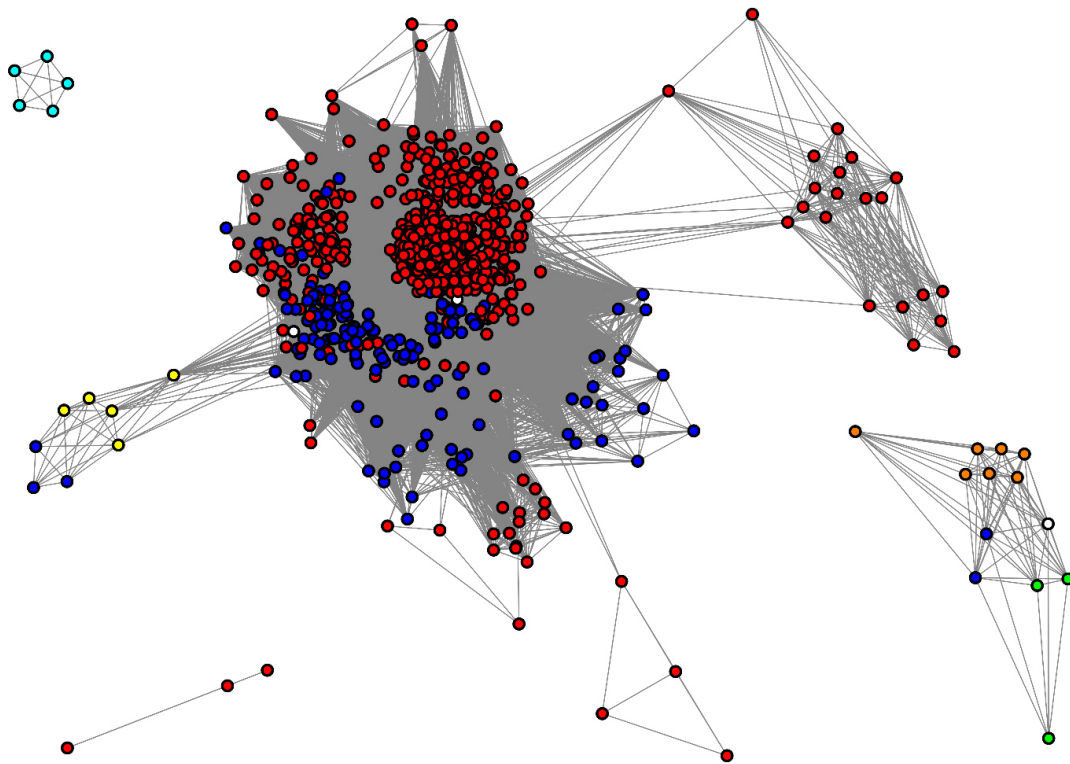


FIGURE S5: Network representation for 869 protein sequences of the “PETase core domain” linked by 270,165 edges. The protein sequences depicted here were selected by clustering at a threshold of 90% sequence identity. Edges (links) were selected at a threshold of 60% sequence similarity. Nodes are coloured according to their annotated source organisms, with Fungi in cyan ●, Actinobacteria in red ●, Proteobacteria in blue ●, Bacteroidetes in orange ●, other bacteria from the FCB group in yellow ●, Planctomycetes in green ●, and unknown bacteria coloured in white ○.

References

1. Schmidt J, Wei R, Oeser T, et al. Degradation of Polyester Polyurethane by Bacterial Polyester Hydrolases. *Polymers (Basel)*. 2017;9(2):65. doi:10.3390/POLYM9020065
2. Nomura N, Shigeno-Akutsu Y, Nakajima-Kambe T, Nakahara T. Cloning and sequence analysis of a polyurethane esterase of *Comamonas acidovorans* TB-35. *J Ferment Bioeng*. 1998;86(4):339-345. doi:10.1016/S0922-338X(99)89001-1
3. Nakajima-Kambe T, Onuma F, Akutsu Y, Nakahara T. Determination of the polyester polyurethane breakdown products and distribution of the polyurethane degrading enzyme of *Comamonas acidovorans* strain TB-35. *J Ferment Bioeng*. 1997;83(5):456-460. doi:10.1016/S0922-338X(97)83000-0
4. Shigeno-Akutsu Y, Nakajima-Kambe T, Nomura N, Nakahara T. Purification and properties of culture-broth-secreted esterase from the polyurethane degrader *Comamonas acidovorans* TB-35. *J Biosci Bioeng*. 1999;88(5):484-487. doi:10.1016/S1389-1723(00)87663-X
5. Akutsu Y, Nakajima-Kambe T, Nomura N, Nakahara T. Purification and properties of a polyester polyurethane-degrading enzyme from *Comamonas acidovorans* TB-35. *Appl Environ Microbiol*. 1998;64(1):62-67. doi:10.1128/aem.64.1.62-67.1998
6. Nakajima-Kambe T, Onuma F, Kimpara N, Nakahara T. Isolation and characterization of a bacterium which utilizes polyester polyurethane as a sole carbon and nitrogen source. *FEMS Microbiol Lett*. 1995;129(1):39-42. doi:10.1016/0378-1097(95)00131-N
7. Ocegüera-Cervantes A, Carrillo-García A, López N, et al. Characterization of the Polyurethanolytic Activity of Two Alicyclophilus sp. Strains Able To Degrade Polyurethane and N-Methylpyrrolidone. *Appl Environ Microbiol*. 2007;73(19):6214-6223. doi:10.1128/AEM.01230-07
8. Rowe L, Howard GT. Growth of *Bacillus subtilis* on polyurethane and the purification and characterization of a polyurethanase-lipase enzyme. *Int Biodeterior Biodegradation*. 2002;50(1):33-40. doi:10.1016/S0964-8305(02)00047-1
9. Kay MJ, Morton LHG, Prince EL. Bacterial degradation of polyester polyurethane. *Int Biodeterior*. 1991;27(2):205-222. doi:10.1016/0265-3036(91)90012-G
10. Biffinger JC, Barlow DE, Cockrell AL, et al. The applicability of Impranil®DLN for gauging the biodegradation of polyurethanes. *Polym Degrad Stab*. 2015;120:178-185. doi:10.1016/J.POLYMDEGRADSTAB.2015.06.020
11. Espinosa MJC, Blanco AC, Schmidgall T, et al. Toward Biorecycling: Isolation of a Soil Bacterium That Grows on a Polyurethane Oligomer and Monomer. *Front Microbiol*. 2020;0:404. doi:10.3389/FMICB.2020.00404
12. Howard GT, Ruiz C, Hilliard NP. Growth of *Pseudomonas chlororaphis* on apolyester–polyurethane and the purification and characterization of a polyurethanase–esterase enzyme. *Int Biodeterior Biodegradation*. 1999;43(1-2):7-12. doi:10.1016/S0964-8305(98)00057-2
13. Ruiz C, Main T, Hilliard NP, Howard GT. Purification and characterization of two polyurethanase enzymes from *Pseudomonas chlororaphis*. *Int Biodeterior Biodegradation*. 1999;43(1-2):43-47. doi:10.1016/S0964-8305(98)00067-5
14. Howard GT, Crother B, Vicknair J. Cloning, nucleotide sequencing and characterization of a polyurethanase gene (*pueB*) from *Pseudomonas chlororaphis*. *Int Biodeterior Biodegrad*. 2001;47(3):141-149. doi:10.1016/S0964-8305(01)00042-7
15. Howard GT, Mackie RI, Cann IKO, et al. Effect of insertional mutations in the *pueA*

- and pueB genes encoding two polyurethanases in *Pseudomonas chlororaphis* contained within a gene cluster. *J Appl Microbiol.* 2007;103(6):2074-2083. doi:10.1111/J.1365-2672.2007.03447.X
16. Stern R V, Howard GT. The polyester polyurethanase gene (pueA) from *Pseudomonas chlororaphis* encodes a lipase. *FEMS Microbiol Lett.* 2000;185(2):163-168. doi:10.1111/j.1574-6968.2000.tb09056.x
 17. Howard GT, Blake RC. Growth of *Pseudomonas fluorescens* on a polyester–polyurethane and the purification and characterization of a polyurethanase–protease enzyme. *Int Biodeterior Biodegradation.* 1998;42(4):213-220. doi:10.1016/S0964-8305(98)00051-1
 18. Vega RE, Main T, Howard GT. Cloning and expression in *Escherichia coli* of apolyurethane-degrading enzyme from *Pseudomonas fluorescens*. *Int Biodeterior Biodegradation.* 1999;43(1-2):49-55. doi:10.1016/S0964-8305(98)00068-7
 19. Howard GT, Norton WN, Burks T. Growth of *Acinetobacter gernerii* P7 on polyurethane and the purification and characterization of a polyurethanase enzyme. *Biodegrad 2012* 234. 2012;23(4):561-573. doi:10.1007/S10532-011-9533-6
 20. Gaytán I, Sánchez-Reyes A, Burelo M, et al. Degradation of Recalcitrant Polyurethane and Xenobiotic Additives by a Selected Landfill Microbial Community and Its Biodegradative Potential Revealed by Proximity Ligation-Based Metagenomic Analysis. *Front Microbiol.* 2020;0:2986. doi:10.3389/FMICB.2019.02986
 21. Crabbe JR, Campbell JR, Thompson L, Walz SL, Schultz WW. Biodegradation of a colloidal ester-based polyurethane by soil fungi. *Int Biodeterior Biodegrad.* 1994;33(2):103-113. doi:10.1016/0964-8305(94)90030-2
 22. Phua SK, Castillo E, Anderson JM, Hiltner A. Biodegradation of a polyurethane in vitro. *J Biomed Mater Res.* 1987;21(2):231-246. doi:10.1002/jbm.820210207
 23. Bouvier M, Chawla AS, Hinberg I. In vitro degradation of a poly(ether urethane) by trypsin. *J Biomed Mater Res.* 1991;25(6):773-789. doi:10.1002/jbm.820250607
 24. Cosgrove L, McGeechan PL, Robson GD, Handley PS. Fungal communities associated with degradation of polyester polyurethane in soil. *Appl Environ Microbiol.* 2007;73(18):5817-5824. doi:10.1128/AEM.01083-07
 25. Mathur G, Prasad R. Degradation of polyurethane by *Aspergillus flavus* (ITCC 6051) isolated from soil. *Appl Biochem Biotechnol.* 2012;167(6):1595-1602. doi:10.1007/s12010-012-9572-4
 26. Magnin A, Pollet E, Phalip V, Avérous L. Evaluation of biological degradation of polyurethanes. *Biotechnol Adv.* 2020;39. doi:10.1016/j.biotechadv.2019.107457
 27. Osman M, Satti SM, Luqman A, Hasan F, Shah Z, Shah AA. Degradation of Polyester Polyurethane by *Aspergillus* sp. Strain S45 Isolated from Soil. *J Polym Environ* 2017 261. 2018;26(1):301-310. doi:10.1007/S10924-017-0954-0
 28. Oprea S, Potolinca VO, Gradinariu P, Oprea V. Biodegradation of pyridine-based polyether polyurethanes by the *Alternaria tenuissima* fungus. *J Appl Polym Sci.* 2018;135(14):46096. doi:10.1002/APP.46096
 29. Álvarez-Barragán J, Domínguez-Malfavón L, Vargas-Suárez M, González-Hernández R, Aguilar-Osorio G, Loza-Tavera H. Biodegradative Activities of Selected Environmental Fungi on a Polyester Polyurethane Varnish and Polyether Polyurethane Foams. *Appl Environ Microbiol.* 2016;82(17):5225-5235. doi:10.1128/AEM.01344-16
 30. Negoro S, Ohki T, Shibata N, et al. Nylon-oligomer Degrading Enzyme/Substrate

- Complex: Catalytic Mechanism of 6-Aminohexanoate-dimer Hydrolase. *J Mol Biol.* 2007;370(1):142-156. doi:10.1016/j.jmb.2007.04.043
31. Yasuhira K, Uedo Y, Shibata N, Negoro S, Takeo M, Higuchi Y. Crystallization and X-ray diffraction analysis of 6-aminohexanoate-cyclic-dimer hydrolase from *Arthrobacter* sp. KI72. *Acta Crystallogr Sect F Struct Biol Cryst Commun.* 2006;62(12):1209-1211. doi:10.1107/S1744309106045076
 32. Negoro S, Ohki T, Shibata N, et al. X-ray crystallographic analysis of 6-aminohexanoate-dimer hydrolase: Molecular basis for the birth of a nylon oligomer-degrading enzyme. *J Biol Chem.* 2005;280(47):39644-39652. doi:10.1074/jbc.M505946200
 33. Nagai K, Yasuhira K, Tanaka Y, et al. Crystallization and X-ray diffraction analysis of nylon hydrolase (NylC) from *Arthrobacter* sp. KI72. *Acta Crystallogr Sect F Struct Biol Cryst Commun.* 2013;69(10):1151-1154. doi:10.1107/S1744309113024263
 34. KINOSHITA S, TERADA T, TANIGUCHI T, et al. Purification and Characterization of 6-Aminohexanoic-Acid-Oligomer Hydrolase of *Flavobacterium* sp. KI72. *Eur J Biochem.* 1981;116(3):547-551. doi:10.1111/j.1432-1033.1981.tb05371.x
 35. Yasuhira K, Tanaka Y, Shibata H, et al. 6-Aminohexanoate oligomer hydrolases from the alkalophilic bacteria *Agromyces* sp. strain KY5R and *Kocuria* sp. strain KY2. *Appl Environ Microbiol.* 2007;73(21):7099-7102. doi:10.1128/AEM.00777-07
 36. KINOSHITA S, NEGORO S, MURAMATSU M, BISARIA VS, SAWADA S, OKADA H. 6-Aminohexanoic Acid Cyclic Dimer Hydrolase. A New Cyclic Amide Hydrolase Produced by *Acromobacter guttatus* KI72. *Eur J Biochem.* 1977;80(2):489-495. doi:10.1111/j.1432-1033.1977.tb11904.x
 37. Tosa T, Chibata I. Utilization of Cyclic Amides and Formation of ω -Amino Acids by Microorganisms. *J Bacteriol.* 1965;89(3):919-920. doi:10.1128/jb.89.3.919-920.1965
 38. Prijambada ID, Negoro S, Yomo T, Urabe I. Emergence of nylon oligomer degradation enzymes in *Pseudomonas aeruginosa* PAO through experimental evolution. *Appl Environ Microbiol.* 1995;61(5):2020-2022. doi:10.1128/aem.61.5.2020-2022.1995
 39. Kanagawa K, Oishi M, Negoro S, Urabe I, Okada H. Characterization of the 6-aminohexanoate-dimer hydrolase from *pseudomonas* sp. NK87. *J Gen Microbiol.* 1993;139(4):787-795. doi:10.1099/00221287-139-4-787
 40. Deguchi T, Kitaoka Y, Kakezawa M, Nishida T. Purification and characterization of a nylon-degrading enzyme. *Appl Environ Microbiol.* 1998;64(4):1366-1371. doi:10.1128/aem.64.4.1366-1371.1998
 41. Notredame C, Higgins DG, Heringa J. T-coffee: A novel method for fast and accurate multiple sequence alignment. *J Mol Biol.* 2000;302(1):205-217. doi:10.1006/jmbi.2000.4042
 42. do Canto VP, Thompson CE, Netz PA. Polyurethanases: Three-dimensional structures and molecular dynamics simulations of enzymes that degrade polyurethane. *J Mol Graph Model.* 2019;89:82-95. doi:10.1016/j.jmgm.2019.03.001
 43. Han X, Liu W, Huang JW, et al. Structural insight into catalytic mechanism of PET hydrolase. *Nat Commun.* 2017;8(1). doi:10.1038/s41467-017-02255-z
 44. Austin HP, Allen MD, Donohoe BS, et al. Characterization and engineering of a plastic-degrading aromatic polyesterase. *Proc Natl Acad Sci U S A.* 2018;115(19):E4350-E4357. doi:10.1073/pnas.1718804115
 45. Joo S, Cho IJ, Seo H, et al. Structural insight into molecular mechanism of

- poly(ethylene terephthalate) degradation. *Nat Commun.* 2018;9(1). doi:10.1038/s41467-018-02881-1
46. Wei R, Song C, Gräsing D, et al. Conformational fitting of a flexible oligomeric substrate does not explain the enzymatic PET degradation. *Nat Commun* 2019 101. 2019;10(1):1-4. doi:10.1038/s41467-019-13492-9
 47. Son HF, Cho IJ, Joo S, et al. Rational Protein Engineering of Thermo-Stable PETase from *Ideonella sakaiensis* for Highly Efficient PET Degradation. *ACS Catal.* 2019;9(4):3519-3526. doi:10.1021/ACSCATAL.9B00568
 48. Liu C, Shi C, Zhu S, Wei R, Yin CC. Structural and functional characterization of polyethylene terephthalate hydrolase from *Ideonella sakaiensis*. *Biochem Biophys Res Commun.* 2019;508(1):289-294. doi:10.1016/j.bbrc.2018.11.148
 49. Fecker T, Galaz-Davison P, Engelberger F, et al. Active Site Flexibility as a Hallmark for Efficient PET Degradation by *I. sakaiensis* PETase. *Biophys J.* 2018;114(6):1302-1312. doi:10.1016/j.bpj.2018.02.005
 50. Cui Y, Chen Y, Liu X, et al. Computational Redesign of a PETase for Plastic Biodegradation under Ambient Condition by the GRAPE Strategy. *ACS Catal.* 2021;11(3):1340-1350. doi:10.1021/ACSCATAL.0C05126/SUPPL_FILE/CS0C05126_SI_001.PDF
 51. Zhong-Johnson EZL, Voigt CA, Sinskey AJ. An absorbance method for analysis of enzymatic degradation kinetics of poly(ethylene terephthalate) films. *Sci Reports* 2021 111. 2021;11(1):1-9. doi:10.1038/s41598-020-79031-5
 52. Brott S, Pfaff L, Schuricht J, et al. Engineering and evaluation of thermostable IsPETase variants for PET degradation. *Eng Life Sci.* Published online 2021. doi:10.1002/ELSC.202100105
 53. Pirillo V, Orlando M, Tessaro D, Pollegioni L, Molla G. An Efficient Protein Evolution Workflow for the Improvement of Bacterial PET Hydrolyzing Enzymes. *Int J Mol Sci* 2022, Vol 23, Page 264. 2021;23(1):264. doi:10.3390/IJMS23010264
 54. Bell E, Smithson R, Kilbride S, et al. Directed Evolution of an Efficient and Thermostable PET Depolymerase. Published online December 29, 2021. doi:10.26434/CHEMRXIV-2021-MCJH6
 55. Meng X, Yang L, Liu H, et al. Protein engineering of stable IsPETase for PET plastic degradation by Premuse. *Int J Biol Macromol.* 2021;180:667-676. doi:10.1016/J.IJBIOMAC.2021.03.058
 56. Rennison A, Winther JR, Varrone C. Rational Protein Engineering to Increase the Activity and Stability of IsPETase Using the PROSS Algorithm. *Polym* 2021, Vol 13, Page 3884. 2021;13(22):3884. doi:10.3390/POLYM13223884
 57. Shirke AN, White C, Englaender JA, et al. Stabilizing Leaf and Branch Compost Cutinase (LCC) with Glycosylation: Mechanism and Effect on PET Hydrolysis. *Biochemistry.* 2018;57(7):1190-1200. doi:10.1021/acs.biochem.7b01189
 58. Tournier V, Topham CM, Gilles A, et al. An engineered PET depolymerase to break down and recycle plastic bottles. *Nature.* 2020;580(7802):216-219. doi:10.1038/s41586-020-2149-4
 59. Gan Z, Zhang H. PMBD: a Comprehensive Plastics Microbial Biodegradation Database. *Database (Oxford).* 2019;2019. doi:10.1093/database/baz119
 60. Waterhouse AM, Procter JB, Martin DMA, Clamp M, Barton GJ. Jalview Version 2-A multiple sequence alignment editor and analysis workbench. *Bioinformatics.*

2009;25(9):1189-1191. doi:10.1093/bioinformatics/btp033

61. Reimer LC, Vetschinova A, Carbasse JS, et al. BacDive in 2019: Bacterial phenotypic data for High-throughput biodiversity analysis. *Nucleic Acids Res.* 2019;47(D1):D631-D636. doi:10.1093/nar/gky879

References

- Alain, K., und Querellou, J. (2009): Cultivating the uncultured: limits, advances and future challenges. *Extremophiles*, **13**, S. 583–594.
- Alves, N. M., Mano, J. F., Balaguer, E., Duenas, J. M. M., und Ribelles, J. L. G. (2002): Glass transition and structural relaxation in semi-crystalline poly(ethylene terephthalate): a DSC study. *Polymer*, **43** (15), S. 4111–4122. 560yf Times Cited:86 Cited References Count:55.
- Amaral-Zettler, L. A., Zettler, E. R., und Mincer, T. J. (2020): Ecology of the plastisphere. *Nature Reviews Microbiology*, **18** (3), S. 139–151.
- Andrady, A. L. (2011): Microplastics in the marine environment. *Marine pollution bulletin*, **62** (8), S. 1596–1605.
- Araújo, R., Silva, C., O’Neill, A., Micaelo, N., Guebitz, G., Soares, C. M., Casal, M., und Cavaco-Paulo, A. (2007): Tailoring cutinase activity towards polyethylene terephthalate and polyamide 6, 6 fibers. *Journal of Biotechnology*, **128** (4), S. 849–857.
- Awaja, F., und Pavel, D. (2005): Recycling of PET. *European Polymer Journal*, **41** (7), S. 1453–1477. 939kh Times Cited:289 Cited References Count:174.
- Barnes, D. K. A., Galgani, F., Thompson, R. C., und Barlaz, M. (2009): Accumulation and fragmentation of plastic debris in global environments. *Philosophical Transactions of the Royal Society B: Biological Sciences*, **364** (1526), S. 1985–1998.
- Barth, M., Oeser, T., Wei, R., Then, J., Schmidt, J., und Zimmermann, W. (2015): Effect of hydrolysis products on the enzymatic degradation of polyethylene terephthalate nanoparticles by a polyester hydrolase from *Thermobifida fusca*. *Biochemical Engineering Journal*, **93**, S. 222–228. Ay1ol Times Cited:10 Cited References Count:49.
- Bayer, T., Pfaff, L., Branson, Y., Becker, A., Wu, S., Bornscheuer, U. T., und Wei, R. (2022): Biosensor and chemo-enzymatic one-pot cascade applications to detect and transform PET-derived terephthalic acid in living cells. *Isience*, **25** (5), S. 104326.

- Bhatwa, A., Wang, W., Hassan, Y. I., Abraham, N., Li, X.-Z., und Zhou, T. (2021): Challenges associated with the formation of recombinant protein inclusion bodies in *Escherichia coli* and strategies to address them for industrial applications. *Frontiers in Bioengineering and Biotechnology*, **9**, S. 630551.
- Bollinger, A., Thies, S., Knieps-Grunhagen, E., Gertzen, C., Kobus, S., Hoppner, A., Ferrer, M., Gohlke, H., Smits, S. H. J., und Jaeger, K. E. (2020): A Novel Polyester Hydrolase From the Marine Bacterium *Pseudomonas aestusnigri* - Structural and Functional Insights. *Front Microbiol*, **11**, S. 114. Bollinger, Alexander Thies, Stephan Knieps-Grunhagen, Esther Gertzen, Christoph Kobus, Stefanie Hoppner, Astrid Ferrer, Manuel Gohlke, Holger Smits, Sander H J Jaeger, Karl-Erich eng Switzerland Front Microbiol. 2020 Feb 13;11:114. doi: 10.3389/fmicb.2020.00114. eCollection 2020.
- Bombelli, P., Howe, C. J., und Bertocchini, F. (2017): Polyethylene bio-degradation by caterpillars of the wax moth *Galleria mellonella*. *Current Biology*, **27** (8), S. R292–R293.
- Brandon, A. M., Gao, S.-H., Tian, R., Ning, D., Yang, S.-S., Zhou, J., Wu, W.-M., und Criddle, C. S. (2018): Biodegradation of Polyethylene and Plastic Mixtures in Mealworms (Larvae of *Tenebrio molitor*) and Effects on the Gut Microbiome. *Environmental Science and Technology*, **52** (11), S. 6526–6533.
- Browne, M. A., Crump, P., Niven, S. J., Teuten, E., Tonkin, A., Galloway, T., und Thompson, R. (2011): Accumulation of microplastic on shorelines worldwide: sources and sinks. *Environmental science and technology*, **45** (21), S. 9175–9179.
- Buchholz, P. C. F., Feuerriegel, G., Zhang, H., Perez-Garcia, P., Nover, L.-L., Chow, J., Streit, W. R., und Pleiss, J. (2022): Plastics degradation by hydrolytic enzymes: The plastics-active enzymes database—PAZy. *Proteins: Structure, Function, and Bioinformatics*, **90** (7), S. 1443–1456.
- Bååth, J. A., Borch, K., und Westh, P. (2020): A suspension-based assay and

- comparative detection methods for characterization of polyethylene terephthalate hydrolases. *Analytical biochemistry*, **607**, S. 113873.
- Carniel, A., Valoni, E., Nicomedes, J., Gomes, A. D., und de Castro, A. M. (2017): Lipase from *Candida antarctica* (CALB) and cutinase from *Humicola insolens* act synergistically for PET hydrolysis to terephthalic acid. *Process Biochemistry*, **59**, S. 84–90. Fe1na Times Cited:3 Cited References Count:24.
- Carr, S. A., Liu, J., und Tesoro, A. G. (2016): Transport and fate of microplastic particles in wastewater treatment plants. *Water research*, **91**, S. 174–182.
- Cassone, B. J., Grove, H. C., Elebute, O., Villanueva, S. M. P., und LeMoine, C. M. R. (2020): Role of the intestinal microbiome in low-density polyethylene degradation by caterpillar larvae of the greater wax moth, *Galleria mellonella*. *Proceedings of the Royal Society B: Biological Sciences*, **287** (1922), S. 20200112.
- Chamas, A., Moon, H., Zheng, J., Qiu, Y., Tabassum, T., Jang, J. H., Abu-Omar, M., Scott, S. L., und Suh, S. (2020): Degradation Rates of Plastics in the Environment. *ACS Sustainable Chemistry and Engineering*, **8** (9), S. 3494–3511. doi: 10.1021/acssuschemeng.9b06635.
- Charles, T. C., Liles, M. R., und Sessitsch, A. (2017): *Functional metagenomics: tools and applications*. Springer.
- Chaves, M. R., Lima, M. L., Malafatti-Picca, L., De Angelis, D. A., Castro, A. M. d., Valoni, E., und Marsaioli, A. J. (2018): A practical fluorescence-based screening protocol for polyethylene terephthalate degrading microorganisms. *Journal of the Brazilian Chemical Society*, **29**, S. 1278–1285.
- Chow, J., Perez-Garcia, P., Dierkes, R., und Streit, W. R. (2022): Microbial enzymes will offer limited solutions to the global plastic pollution crisis. *Microbial Biotechnology*.
- Church, M. J. (2008): Resource control of bacterial dynamics in the sea. *Microbial ecology of the oceans*, S. 335–382.

- Cooper, D. A., und Corcoran, P. L. (2010): Effects of mechanical and chemical processes on the degradation of plastic beach debris on the island of Kauai, Hawaii. *Marine Pollution Bulletin*, **60** (5), S. 650–654.
- Cragg, G. M., und Newman, D. J. (2013): Natural products: a continuing source of novel drug leads. *Biochimica et Biophysica Acta (BBA)-General Subjects*, **1830** (6), S. 3670–3695.
- Danso, D. (2019): *Function and global distribution of polyethylene terephthalate (PET)-degrading bacteria and enzymes in marine and terrestrial metagenomes*. Thesis.
- Danso, D., Schmeisser, C., Chow, J., Zimmermann, W., Wei, R., Leggewie, C., Li, X., Hazen, T., und Streit, W. R. (2018): New Insights into the Function and Global Distribution of Polyethylene Terephthalate (PET)-Degrading Bacteria and Enzymes in Marine and Terrestrial Metagenomes. *Appl Environ Microbiol*, **84** (8). Danso, Dominik Schmeisser, Christel Chow, Jennifer Zimmermann, Wolfgang Wei, Ren Leggewie, Christian Li, Xiangzhen Hazen, Terry Streit, Wolfgang R eng Research Support, Non-U.S. Gov't Appl Environ Microbiol. 2018 Apr 2;84(8). pii: AEM.02773-17. doi: 10.1128/AEM.02773-17. Print 2018 Apr 15.
- Danso, D., Chow, J., und Streit, W. R. (2019): Plastics: Microbial Degradation, Environmental and Biotechnological Perspectives. *Appl Environ Microbiol*. Danso, Dominik Chow, Jennifer Streit, Wolfgang R Appl Environ Microbiol. 2019 Jul 19. pii: AEM.01095-19. doi: 10.1128/AEM.01095-19.
- Darby, R. T., und Kaplan, A. M. (1968): Fungal susceptibility of polyurethanes. *Applied microbiology*, **16** (6), S. 900–905. 16349806[pmid] PMC547551[pmcid] Appl Microbiol.
- Day, M., und Wiles, D. M. (1972): Photochemical degradation of poly(ethylene terephthalate). II. Effect of wavelength and environment on the decomposition process. *Journal of Applied Polymer Science*, **16** (1), S. 191–202.
- de Diego, I., Ksiazek, M., Mizgalska, D., Koneru, L., Golik, P., Szmigielski, B., Nowak, M., Nowakowska, Z., Potempa, B., Houston, J. A., Enghild, J. J., Thøgersen, I. B., Gao,

- J., Kwan, A. H., Trehwella, J., Dubin, G., Gomis-Rüth, F. X., Nguyen, K.-A., and Potempa, J. (2016): The outer-membrane export signal of *Porphyromonas gingivalis* type IX secretion system (T9SS) is a conserved C-terminal -sandwich domain. *Scientific reports*, **6**, S. 23123–23123. 27005013[pmid] PMC4804311[pmcid] srep23123[PII].
- Derraik, J. G. B. (2002): The pollution of the marine environment by plastic debris: a review. *Marine pollution bulletin*, **44** (9), S. 842–852.
- Desvaux, M., Hébraud, M., Talon, R., und Henderson, I. R. (2009): Outer membrane translocation: numerical protein secretion nomenclature in question in mycobacteria. *Trends in microbiology*, **17** (8), S. 338–340.
- Dierkes, R. F., Wypych, A., Pérez-García, P., Danso, D., Chow, J., und Streit, W. R. (2023): An Ultra-Sensitive *Comamonas thiooxidans* Biosensor for the Rapid Detection of Enzymatic Polyethylene Terephthalate (PET) Degradation. *Applied and Environmental Microbiology*, **89** (1), S. e01603–22.
- Duan, J., Bolan, N., Li, Y., Ding, S., Atugoda, T., Vithanage, M., Sarkar, B., Tsang, D. C. W., und Kirkham, M. B. (2021): Weathering of microplastics and interaction with other coexisting constituents in terrestrial and aquatic environments. *Water Research*, **196**, S. 117011.
- Edgar, R. C. (2004): MUSCLE: multiple sequence alignment with high accuracy and high throughput. *Nucleic acids research*, **32** (5), S. 1792–1797.
- Eriksen, M., Lebreton, L. C. M., Carson, H. S., Thiel, M., Moore, C. J., Borerro, J. C., Galgani, F., Ryan, P. G., und Reisser, J. (2014): Plastic Pollution in the World’s Oceans: More than 5 Trillion Plastic Pieces Weighing over 250,000 Tons Afloat at Sea. *Plos One*, **9** (12). Aw9yp Times Cited:183 Cited References Count:42.
- Fagerburg, D. R., und Clauberg, H. (2004): *Photodegradation of Poly(Ethylene Terephthalate) and Poly(Ethylene/1,4-Cyclohexylenedimethylene Terephthalate)*, S. 609–641. John Wiley and Sons, Ltd.

- Falkenstein, P., Gräsing, D., Bielytskyi, P., Zimmermann, W., Matysik, J., Wei, R., and Song, C. (2020): UV Pretreatment Impairs the Enzymatic Degradation of Polyethylene Terephthalate. *Frontiers in Microbiology*, **11** (689).
- Ferrer, M., Martínez-Martínez, M., Bargiela, R., Streit, W. R., Golyshina, O. V., and Golyshin, P. N. (2016): Estimating the success of enzyme bioprospecting through metagenomics: current status and future trends. *Microbial biotechnology*, **9** (1), S. 22–34.
- Flemming, H.-C., Wingender, J., Szewzyk, U., Steinberg, P., Rice, S. A., and Kjelleberg, S. (2016): Biofilms: an emergent form of bacterial life. *Nature Reviews Microbiology*, **14** (9), S. 563–575.
- Foley, M. H., Cockburn, D. W., and Koropatkin, N. M. (2016): The Sus operon: a model system for starch uptake by the human gut Bacteroidetes. *Cellular and Molecular Life Sciences*, **73** (14), S. 2603–2617.
- Gewert, B., Plassmann, M. M., und MacLeod, M. (2015): Pathways for degradation of plastic polymers floating in the marine environment. *Environmental Science: Processes and Impacts*, **17** (9), S. 1513–1521.
- Geyer, R., Jambeck, J. R., und Law, K. L. (2017): Production, use, and fate of all plastics ever made. *Science Advances*, **3** (7), S. e1700782.
- Gigault, J., Halle, A. t., Baudrimont, M., Pascal, P.-Y., Gauffre, F., Phi, T.-L., El Hadri, H., Grassl, B., und Reynaud, S. (2018): Current opinion: What is a nanoplastic? *Environmental Pollution*, **235**, S. 1030–1034.
- Goloboff, P. A., Farris, J. S., und Nixon, K. C. (2008): TNT, a free program for phylogenetic analysis. *Cladistics*, **24** (5), S. 774–786.
- Gopal, G. J., und Kumar, A. (2013): Strategies for the production of recombinant protein in *Escherichia coli*. *The protein journal*, **32**, S. 419–425.

- Gotoh, K., Yasukawa, A., und Kobayashi, Y. (2011): Wettability characteristics of poly(ethylene terephthalate) films treated by atmospheric pressure plasma and ultraviolet excimer light. *Polymer Journal*, **43** (6), S. 545–551.
- Gregory, M. R. (2009): Environmental implications of plastic debris in marine settings—entanglement, ingestion, smothering, hangers-on, hitch-hiking and alien invasions. *Philosophical Transactions of the Royal Society B-Biological Sciences*, **364** (1526), S. 2013–2025.
- Hahnke, R. L., Meier-Kolthoff, J. P., García-López, M., Mukherjee, S., Huntemann, M., Ivanova, N. N., Woyke, T., Kyrpides, N. C., Klenk, H. P., und Göker, M. (2016): Genome-Based Taxonomic Classification of Bacteroidetes. *Front Microbiol*, **7**, S. 2003. 1664-302x Hahnke, Richard L Meier-Kolthoff, Jan P García-López, Marina Mukherjee, Supratim Huntemann, Marcel Ivanova, Natalia N Woyke, Tanja Kyrpides, Nikos C Klenk, Hans-Peter Göker, Markus Journal Article Front Microbiol. 2016 Dec 20;7:2003. doi: 10.3389/fmicb.2016.02003. eCollection 2016.
- Han, X., Liu, W., Huang, J. W., Ma, J., Zheng, Y., Ko, T. P., Xu, L., Cheng, Y. S., Chen, C. C., und Guo, R. T. (2017): Structural insight into catalytic mechanism of PET hydrolase. *Nat Commun*, **8** (1), S. 2106. Han, Xu Liu, Weidong Huang, Jian-Wen Ma, Jiantao Zheng, Yingying Ko, Tzu-Ping Xu, Limin Cheng, Ya-Shan Chen, Chun-Chi Guo, Rey-Ting eng Research Support, Non-U.S. Gov't England Nat Commun. 2017 Dec 13;8(1):2106. doi: 10.1038/s41467-017-02255-z.
- Hegde, K., und Veeranki, V. D. (2013): Production optimization and characterization of recombinant cutinases from *Thermobifida fusca* sp. NRRL B-8184. *Appl Biochem Biotechnol*, **170** (3), S. 654–75. Hegde, Krishnamoorthy Veeranki, Venkata Dasu eng Research Support, Non-U.S. Gov't Appl Biochem Biotechnol. 2013 Jun;170(3):654-75. doi: 10.1007/s12010-013-0219-x. Epub 2013 Apr 19.
- Herrero Acero, E., Ribitsch, D., Steinkellner, G., Gruber, K., Greimel, K., Eiteljoerg, I., Trotscha, E., Wei, R., Zimmermann, W., und Zinn, M. (2011): Enzymatic surface

- hydrolysis of PET: effect of structural diversity on kinetic properties of cutinases from *Thermobifida*. *Macromolecules*, **44** (12), S. 4632–4640.
- Hohn, S., Acevedo-Trejos, E., Abrams, J. F., Fulgencio de Moura, J., Spranz, R., und Merico, A. (2020): The long-term legacy of plastic mass production. *Science of The Total Environment*, **746**, S. 141115.
- Howard, G. T. (2002): Biodegradation of polyurethane: a review. *International Biodeterioration and Biodegradation*, **49** (4), S. 245–252.
- Hult, K., und Berglund, P. (2007): Enzyme promiscuity: mechanism and applications. *Trends in Biotechnology*, **25** (5), S. 231–238.
- Jenner, L. C., Rotchell, J. M., Bennett, R. T., Cowen, M., Tentzeris, V., und Sadofsky, L. R. (2022): Detection of microplastics in human lung tissue using FTIR spectroscopy. *Science of the Total Environment*, **831**, S. 154907.
- Kale, S. K., Deshmukh, A. G., Dudhare, M. S., und Patil, V. B. (2015): Microbial degradation of plastic: a review. *Journal of Biochemical Technology*, **6** (2), S. 952–961.
Dv5ih Times Cited:1 Cited References Count:84.
- Kawai, F., Oda, M., Tamashiro, T., Waku, T., Tanaka, N., Yamamoto, M., Mizushima, H., Miyakawa, T., und Tanokura, M. (2014): A novel Ca(2)(+)-activated, thermostabilized polyesterase capable of hydrolyzing polyethylene terephthalate from *Saccharomonospora viridis* AHK190. *Appl Microbiol Biotechnol*, **98** (24), S. 10053–64. Kawai, Fusako Oda, Masayuki Tamashiro, Tomonari Waku, Tomonori Tanaka, Naoki Yamamoto, Masaki Mizushima, Hiroki Miyakawa, Takuya Tanokura, Masaru eng Research Support, Non-U.S. Gov't Germany Appl Microbiol Biotechnol. 2014 Dec;98(24):10053-64. doi: 10.1007/s00253-014-5860-y. Epub 2014 Jun 15.
- Khersonsky, O., und Tawfik, D. S. (2010): Enzyme promiscuity: a mechanistic and evolutionary perspective. *Annu Rev Biochem*, **79**, S. 471–505. 1545-4509 Khersonsky, Olga Tawfik, Dan S Journal Article Research Support, Non-U.S. Gov't Review United

- States Annu Rev Biochem. 2010;79:471-505. doi: 10.1146/annurev-biochem-030409-143718.
- Kirstein, I. V., Kirmizi, S., Wichels, A., Garin-Fernandez, A., Erler, R., Löder, M., und Gerdts, G. (2016): Dangerous hitchhikers? Evidence for potentially pathogenic *Vibrio* spp. on microplastic particles. *Marine environmental research*, **120**, S. 1–8.
- Kirstein, I. V., Wichels, A., Gullans, E., Krohne, G., und Gerdts, G. (2019): The Plastisphere – Uncovering tightly attached plastic “specific” microorganisms. *PLOS ONE*, **14** (4), S. e0215859.
- Kleeberg, I., Welzel, K., Vandenheuvel, J., Muller, R. J., und Deckwer, W. D. (2005): Characterization of a new extracellular hydrolase from *Thermobifida fusca* degrading aliphatic-aromatic copolyesters. *Biomacromolecules*, **6** (1), S. 262–70. Kleeberg, I Welzel, K Vandenheuvel, J Muller, R-J Deckwer, W-D eng Biomacromolecules. 2005 Jan-Feb;6(1):262-70. doi: 10.1021/bm049582t.
- Krieg, N., Ludwig, W., Euzéby, J., und Whitman, W. (2015): *Bacteroidetes phyl. nov.*, S. 1–2.
- Laist, D. W. (1987): Overview of the biological effects of lost and discarded plastic debris in the marine environment. *Marine pollution bulletin*, **18** (6), S. 319–326.
- Laurila-Pant, M., Lehtikoinen, A., Uusitalo, L., und Venesjärvi, R. (2015): How to value biodiversity in environmental management? *Ecological indicators*, **55**, S. 1–11.
- Leslie, H. A., Van Velzen, M. J., Brandsma, S. H., Vethaak, A. D., Garcia-Vallejo, J. J., und Lamoree, M. H. (2022): Discovery and quantification of plastic particle pollution in human blood. *Environment international*, **163**, S. 107199.
- Leveson-Gower, R. B., Mayer, C., und Roelfes, G. (2019): The importance of catalytic promiscuity for enzyme design and evolution. *Nature Reviews Chemistry*, **3** (12), S. 687–705.

- Li, S., Yang, X., Yang, S., Zhu, M., und Wang, X. (2012): Technology prospecting on enzymes: application, marketing and engineering. *Computational and structural biotechnology journal*, **2** (3), S. e201209017.
- Lim, H. C. (2017): *Thermoplastic polyesters*, S. 527–543. Elsevier.
- Markel, U., Essani, K. D., Besirlioglu, V., Schiffels, J., Streit, W. R., und Schwaneberg, U. (2020): Advances in ultrahigh-throughput screening for directed enzyme evolution. *Chemical Society Reviews*, **49** (1), S. 233–262.
- Martinez-Martinez, M., Coscolin, C., Santiago, G., Chow, J., Stogios, P. J., Bargiela, R., Gertler, C., Navarro-Fernandez, J., Bollinger, A., Thies, S., Mendez-Garcia, C., Popovic, A., Brown, G., Chernikova, T. N., Garcia-Moyano, A., Bjerga, G. E. K., Perez-Garcia, P., Hai, T., Del Pozo, M. V., Stokke, R., Steen, I. H., Cui, H., Xu, X., Nocek, B. P., Alcaide, M., Distaso, M., Mesa, V., Pelaez, A. I., Sanchez, J., Buchholz, P. C. F., Pleiss, J., Fernandez-Guerra, A., Glockner, F. O., Golyshina, O. V., Yakimov, M. M., Savchenko, A., Jaeger, K. E., Yakunin, A. F., Streit, W. R., Golyshin, P. N., Guallar, V., Ferrer, M., und The Inmare, C. (2018): Determinants and Prediction of Esterase Substrate Promiscuity Patterns. *ACS Chem Biol*, **13** (1), S. 225–234. 1554-8937 Martinez-Martinez, Monica Coscolin, Cristina Santiago, Gerard Orcid: 0000-0002-0506-3049 Chow, Jennifer Stogios, Peter J Bargiela, Rafael Gertler, Christoph Navarro-Fernandez, Jose Bollinger, Alexander Thies, Stephan Mendez-Garcia, Celia Popovic, Ana Brown, Greg Chernikova, Tatyana N Garcia-Moyano, Antonio Bjerga, Gro E K Perez-Garcia, Pablo Hai, Tran Del Pozo, Mercedes V Stokke, Runar Steen, Ida H Cui, Hong Xu, Xiaohui Nocek, Boguslaw P Alcaide, Maria Distaso, Marco Mesa, Victoria Pelaez, Ana I Sanchez, Jesus Buchholz, Patrick C F Pleiss, Jurgen Orcid: 0000-0003-1045-8202 Fernandez-Guerra, Antonio Glockner, Frank O Golyshina, Olga V Yakimov, Michail M Savchenko, Alexei Jaeger, Karl-Erich Yakunin, Alexander F Orcid: 0000-0003-0813-6490 Streit, Wolfgang R Golyshin, Peter N Guallar, Victor Orcid: 0000-0002-4580-1114 Ferrer, Manuel Orcid: 0000-0003-4962-4714 The Inmare Consortium BB/M029085/1/Biotechnology and Biological Sciences Research

- Council/United Kingdom Journal Article Research Support, Non-U.S. Gov't United States ACS Chem Biol. 2018 Jan 19;13(1):225-234. doi: 10.1021/acscchembio.7b00996. Epub 2017 Dec 20.
- Masaki, K., Kamini, N. R., Ikeda, H., und Iefuji, H. (2005): Cutinase-like enzyme from the yeast *Cryptococcus* sp strain S-2 hydrolyzes polylactic acid and other biodegradable plastics. *Applied and Environmental Microbiology*, **71** (11), S. 7548–7550. 983IN Times Cited:41 Cited References Count:19.
- Meier-Kolthoff, J. P., Auch, A. F., Klenk, H.-P., und Göker, M. (2013): Genome sequence-based species delimitation with confidence intervals and improved distance functions. *BMC bioinformatics*, **14**, S. 1–14.
- Miranda, M. N., Silva, A. M., und Pereira, M. F. R. (2020): Microplastics in the environment: A DPSIR analysis with focus on the responses. *Science of the Total Environment*, **718**, S. 134968.
- Mitrano, D. M., Wick, P., und Nowack, B. (2021): Placing nanoplastics in the context of global plastic pollution. *Nature Nanotechnology*, **16** (5), S. 491–500.
- Mohammadian, M., Allen, N., Edge, M., und Jones, K. (1991): Environmental Degradation of Poly (ethylene Terephthalate). *Textile Research Journal*, **61** (11), S. 690–696.
- Moore, C. J. (2008): Synthetic polymers in the marine environment: a rapidly increasing, long-term threat. *Environmental research*, **108** (2), S. 131–139.
- Mora, C., Tittensor, D. P., Adl, S., Simpson, A. G., und Worm, B. (2011): How many species are there on Earth and in the ocean? *PLoS biology*, **9** (8), S. e1001127.
- Mueller, R.-J. (2006): Biological degradation of synthetic polyesters—Enzymes as potential catalysts for polyester recycling. *Process Biochemistry*, **41** (10), S. 2124–2128.

- Munoz, R., Rosselló-Móra, R., und Amann, R. (2016): Revised phylogeny of Bacteroidetes and proposal of sixteen new taxa and two new combinations including Rhodothermaeota phyl. nov. *Syst Appl Microbiol*, **39** (5), S. 281–96. 1618-0984 Munoz, Raul Rosselló-Móra, Ramon Amann, Rudolf Journal Article Germany Syst Appl Microbiol. 2016 Jul;39(5):281-96. doi: 10.1016/j.syapm.2016.04.004. Epub 2016 May 12.
- Müller, R., Schrader, H., Profe, J., Dresler, K., und Deckwer, W. (2005): Enzymatic degradation of poly (ethylene terephthalate): rapid hydrolyse using a hydrolase from *T. fusca*. *Macromolecular rapid communications*, **26** (17), S. 1400–1405.
- Nobeli, I., Favia, A. D., und Thornton, J. M. (2009): Protein promiscuity and its implications for biotechnology. *Nature biotechnology*, **27** (2), S. 157–167.
- Nutschel, C., Coscolín, C., David, B., Mulnaes, D., Ferrer, M., Jaeger, K.-E., und Gohlke, H. (2021): Promiscuous esterases counterintuitively are less flexible than specific ones. *Journal of chemical information and modeling*, **61** (5), S. 2383–2395.
- Pattengale, N. D., Alipour, M., Bininda-Emonds, O. R., Moret, B. M., und Stamatakis, A. (2010): How many bootstrap replicates are necessary? *Journal of computational biology*, **17** (3), S. 337–354.
- Plasticseurope (2022): Plastics - The facts 2022.
- Prata, J. C., da Costa, J. P., Lopes, I., Duarte, A. C., und Rocha-Santos, T. (2020): Environmental exposure to microplastics: An overview on possible human health effects. *Science of the total environment*, **702**, S. 134455.
- Pérez-García, P., Danso, D., Zhang, H., Chow, J., und Streit, W. R. (2021): Exploring the global metagenome for plastic-degrading enzymes. *Methods Enzymol*, **648**, S. 137–157. 1557-7988 Pérez-García, Pablo Danso, Dominik Zhang, Hongli Chow, Jennifer Streit, Wolfgang R Journal Article United States Methods Enzymol. 2021;648:137-157. doi: 10.1016/bs.mie.2020.12.022. Epub 2021 Jan 20.
- Qi, X., Ren, Y., und Wang, X. (2017): New advances in the biodegradation of Poly (lactic) acid. *International Biodeterioration Biodegradation*, **117**, S. 215–223.

- Ragusa, A., Svelato, A., Santacroce, C., Catalano, P., Notarstefano, V., Carnevali, O., Papa, F., Rongioletti, M. C. A., Baiocco, F., und Draghi, S. (2021): Plasticenta: First evidence of microplastics in human placenta. *Environment international*, **146**, S. 106274.
- Rahman, A., Sarkar, A., Yadav, O. P., Achari, G., und Slobodnik, J. (2021): Potential human health risks due to environmental exposure to nano-and microplastics and knowledge gaps: A scoping review. *Science of the Total Environment*, **757**, S. 143872.
- Rex, W., und Tennant, D. (1949): Polymeric linear terephthalic esters.
- Ribitsch, D., Heumann, S., Trotscha, E., Acero, E. H., Greimel, K., Leber, R., Birner-Gruenberger, R., Deller, S., Eiteljoerg, I., Remler, P., Weber, T., Siegert, P., Maurer, K. H., Donelli, I., Freddi, G., Schwab, H., und Guebitz, G. M. (2011): Hydrolysis of Polyethyleneterephthalate by p-Nitrobenzylesterase from *Bacillus subtilis*. *Biotechnology Progress*, **27** (4), S. 951–960. 810EG Times Cited:13 Cited References Count:66.
- Ribitsch, D., Acero, E. H., Przylucka, A., Zitzenbacher, S., Marold, A., Gamerith, C., Tscheliessnig, R., Jungbauer, A., Rennhofer, H., Lichtenegger, H., Amenitsch, H., Bonazza, K., Kubicek, C. P., Druzhinina, I. S., und Guebitz, G. M. (2015): Enhanced Cutinase-Catalyzed Hydrolysis of Polyethylene Terephthalate by Covalent Fusion to Hydrophobins. *Applied and Environmental Microbiology*, **81** (11), S. 3586–3592. Ch3fa Times Cited:11 Cited References Count:30.
- Ribitsch, D., Hromic, A., Zitzenbacher, S., Zartl, B., Gamerith, C., Pellis, A., Jungbauer, A., Lyskowski, A., Steinkellner, G., Gruber, K., Tscheliessnig, R., Herrero Acero, E., und Guebitz, G. M. (2017): Small cause, large effect: Structural characterization of cutinases from *Thermobifida cellulositica*. *Biotechnol Bioeng*, **114** (11), S. 2481–2488. Ribitsch, Doris Hromic, Altijana Zitzenbacher, Sabine Zartl, Barbara Gamerith, Caroline Pellis, Alessandro Jungbauer, Alois Lyskowski, Andrzej Steinkellner, Georg Gruber, Karl Tscheliessnig, Rupert Herrero Acero, Enrique Guebitz, Georg M eng

- Research Support, Non-U.S. Gov't Biotechnol Bioeng. 2017 Nov;114(11):2481-2488. doi: 10.1002/bit.26372. Epub 2017 Aug 15.
- Ronkvist, A. M., Xie, W., Lu, W., und Gross, R. A. (2009): Cutinase-Catalyzed Hydrolysis of Poly(ethylene terephthalate). *Macromolecules*, **42** (14), S. 5128–5138.
- Rosano, G. L., und Ceccarelli, E. A. (2014): Recombinant protein expression in *Escherichia coli*: advances and challenges. *Frontiers in microbiology*, **5**, S. 172.
- Roth, C., Wei, R., Oeser, T., Then, J., Follner, C., Zimmermann, W., und Strater, N. (2014): Structural and functional studies on a thermostable polyethylene terephthalate degrading hydrolase from *Thermobifida fusca*. *Appl Microbiol Biotechnol*, **98** (18), S. 7815–23. Roth, Christian Wei, Ren Oeser, Thorsten Then, Johannes Follner, Christina Zimmermann, Wolfgang Strater, Norbert eng Germany Appl Microbiol Biotechnol. 2014 Sep;98(18):7815-23. doi: 10.1007/s00253-014-5672-0. Epub 2014 Apr 13.
- Russell, J. R., Huang, J., Anand, P., Kucera, K., Sandoval, A. G., Dantzler, K. W., Hickman, D., Jee, J., Kimovec, F. M., Koppstein, D., Marks, D. H., Mittermiller, P. A., Núñez, S. J., Santiago, M., Townes, M. A., Vishnevetsky, M., Williams, N. E., Vargas, M. P. N., Boulanger, L.-A., Bascom-Slack, C., und Strobel, S. A. (2011): Biodegradation of polyester polyurethane by endophytic fungi. *Applied and environmental microbiology*, **77** (17), S. 6076–6084. 21764951[pmid] PMC3165411[pmcid] AEM.00521-11[PII] Appl Environ Microbiol.
- Sanluis-Verdes, A., Colomer-Vidal, P., Rodriguez-Ventura, F., Bello-Villarino, M., Spinola-Amilibia, M., Ruiz-Lopez, E., Illanes-Vicioso, R., Castroviejo, P., Aiese Cigliano, R., und Montoya, M. (2022): Wax worm saliva and the enzymes therein are the key to polyethylene degradation by *Galleria mellonella*. *Nature Communications*, **13** (1), S. 1–11.
- Sato, K., Naito, M., Yukitake, H., Hirakawa, H., Shoji, M., McBride, M. J., Rhodes, R. G., und Nakayama, K. (2010): A protein secretion system linked to bacteroidete

- gliding motility and pathogenesis. *Proceedings of the National Academy of Sciences*, **107** (1), S. 276–281.
- Sax, L. (2010): Polyethylene terephthalate may yield endocrine disruptors. *Environmental Health Perspectives*, **118** (4), S. 445–448.
- Schmidt, J., Wei, R., Oeser, T., Dedavid, E. S. L. A., Breite, D., Schulze, A., und Zimmermann, W. (2017): Degradation of Polyester Polyurethane by Bacterial Polyester Hydrolases. *Polymers (Basel)*, **9** (2), S. 65. Schmidt, Juliane Wei, Ren Oeser, Thorsten Dedavid E Silva, Lukas Andre Breite, Daniel Schulze, Agnes Zimmermann, Wolfgang eng Switzerland Polymers (Basel). 2017 Feb 16;9(2). pii: polym9020065. doi: 10.3390/polym9020065.
- Shaw, D. G., und Day, R. H. (1994): Colour- and form-dependent loss of plastic micro-debris from the North Pacific Ocean. *Marine Pollution Bulletin*, **28** (1), S. 39–43.
- Simon, E. (1839): Ueber den flüssigen Storax (*Styrax liquidus*). *Ann. Pharm*, **31** (3), S. 265–277.
- Son, H. F., Cho, I. J., Joo, S., Seo, H., Sagong, H.-Y., Choi, S. Y., Lee, S. Y., und Kim, K.-J. (2019): Rational Protein Engineering of Thermo-Stable PETase from *Ideonella sakaiensis* for Highly Efficient PET Degradation. *ACS Catalysis*, **9** (4), S. 3519–3526.
- Stamatakis, A. (2014): RAxML version 8: a tool for phylogenetic analysis and post-analysis of large phylogenies. *Bioinformatics*, **30** (9), S. 1312–1313.
- statista.com (2022):.
- Steele, H. L., Jaeger, K.-E., Daniel, R., und Streit, W. R. (2009): Advances in recovery of novel biocatalysts from metagenomes. *Microbial Physiology*, **16** (1-2), S. 25–37.
- Streit, W. R., und Schmitz, R. A. (2004): Metagenomics—the key to the uncultured microbes. *Curr Opin Microbiol*, **7** (5), S. 492–8. Streit, Wolfgang R Schmitz, Ruth A eng Review England Curr Opin Microbiol. 2004 Oct;7(5):492-8. doi: 10.1016/j.mib.2004.08.002.

- Sulaiman, S., Yamato, S., Kanaya, E., Kim, J. J., Koga, Y., Takano, K., und Kanaya, S. (2012): Isolation of a novel cutinase homolog with polyethylene terephthalate-degrading activity from leaf-branch compost by using a metagenomic approach. *Appl Environ Microbiol*, **78** (5), S. 1556–62. Sulaiman, Sintawee Yamato, Saya Kanaya, Eiko Kim, Joong-Jae Koga, Yuichi Takano, Kazufumi Kanaya, Shigenori eng Research Support, Non-U.S. Gov't Appl Environ Microbiol. 2012 Mar;78(5):1556-62. doi: 10.1128/AEM.06725-11. Epub 2011 Dec 22.
- Tamoor, M., Samak, N. A., Jia, Y., Mushtaq, M. U., Sher, H., Bibi, M., und Xing, J. (2021): Potential use of microbial enzymes for the conversion of plastic waste into value-added products: A viable solution. *Frontiers in Microbiology*, S. 3632.
- Taniguchi, I., Yoshida, S., Hiraga, K., Miyamoto, K., Kimura, Y., und Oda, K. (2019): Biodegradation of Pet: Current Status and Application Aspects. *ACS Catal.*, **9**, S. 4089.
- Thomas, F., Hehemann, J. H., Rebuffet, E., Czjzek, M., und Michel, G. (2011): Environmental and gut Bacteroidetes: the food connection. *Frontiers in Microbiology*, **2**, S. 16.
- Tournier, V., Topham, C. M., Gilles, A., David, B., Folgoas, C., Moya-Leclair, E., Kamionka, E., Desrousseaux, M. L., Texier, H., Gavalda, S., Cot, M., Guemard, E., Dalibey, M., Nomme, J., Cioci, G., Barbe, S., Chateau, M., Andre, I., Duquesne, S., und Marty, A. (2020): An engineered PET depolymerase to break down and recycle plastic bottles. *Nature*, **580** (7802), S. 216–219. Tournier, V Topham, C M Gilles, A David, B Folgoas, C Moya-Leclair, E Kamionka, E Desrousseaux, M-L Texier, H Gavalda, S Cot, M Guemard, E Dalibey, M Nomme, J Cioci, G Barbe, S Chateau, M Andre, I Duquesne, S Marty, A eng Research Support, Non-U.S. Gov't England Nature. 2020 Apr;580(7802):216-219. doi: 10.1038/s41586-020-2149-4. Epub 2020 Apr 8.
- Wang, F., Wong, C. S., Chen, D., Lu, X., Wang, F., und Zeng, E. Y. (2018): Interaction of toxic chemicals with microplastics: a critical review. *Water research*, **139**, S. 208–219.
- Webb, H. K., Arnott, J., Crawford, R. J., und Ivanova, E. P. (2013): Plastic Degradation

- and Its Environmental Implications with Special Reference to Poly(ethylene terephthalate). *Polymers*, **5** (1), S. 1–18. 185DO Times Cited:2 Cited References Count:96.
- Wei, R., und Zimmermann, W. (2017): Microbial enzymes for the recycling of recalcitrant petroleum-based plastics: how far are we? *Microbial biotechnology*, **10** (6), S. 1308–1322. 28371373[pmid] PMC5658625[pmcid].
- Wei, R., Oeser, T., Billig, S., und Zimmermann, W. (2012): A high-throughput assay for enzymatic polyester hydrolysis activity by fluorimetric detection. Report 1860-6768, Wiley Online Library.
- Wei, R., Oeser, T., Barth, M., Weigl, N., Luebs, A., Schulz-Siegmund, M., Hacker, M. C., und Zimmermann, W. (2014): Turbidimetric analysis of the enzymatic hydrolysis of polyethylene terephthalate nanoparticles. *Journal of Molecular Catalysis B-Enzymatic*, **103**, S. 72–78.
- Welzel, K., Müller, R. J., und Deckwer, W. D. (2002): Enzymatischer Abbau von Polyester-Nanopartikeln. *Chemie Ingenieur Technik*, **74** (10), S. 1496–1500.
- Wexler, H. M. (2007): Bacteroides: the good, the bad, and the nitty-gritty. *Clin Microbiol Rev*, **20** (4), S. 593–621. 1098-6618 Wexler, Hannah M Journal Article Research Support, U.S. Gov't, Non-P.H.S. Review Clin Microbiol Rev. 2007 Oct;20(4):593-621. doi: 10.1128/CMR.00008-07.
- Wright, R. J., Langille, M. G. I., und Walker, T. R. (2021): Food or just a free ride? A meta-analysis reveals the global diversity of the Plastisphere. *The ISME Journal*, **15** (3), S. 789–806.
- Yang, J., Yang, Y., Wu, W.-M., Zhao, J., und Jiang, L. (2014): Evidence of Polyethylene Biodegradation by Bacterial Strains from the Guts of Plastic-Eating Waxworms. *Environmental Science and Technology*, **48** (23), S. 13776–13784.
- Yang, Y., Liu, W., Zhang, Z., Grossart, H.-P., und Gadd, G. M. (2020): Microplastics

- provide new microbial niches in aquatic environments. *Applied Microbiology and Biotechnology*, **104** (15), S. 6501–6511.
- Yoshida, S., Hiraga, K., Takehana, T., Taniguchi, I., Yamaji, H., Maeda, Y., Toyohara, K., Miyamoto, K., Kimura, Y., und Oda, K. (2016): A bacterium that degrades and assimilates poly(ethylene terephthalate). *Science*, **351** (6278), S. 1196–9. Yoshida, Shosuke Hiraga, Kazumi Takehana, Toshihiko Taniguchi, Ikuo Yamaji, Hironao Maeda, Yasuhito Toyohara, Kiyotsuna Miyamoto, Kenji Kimura, Yoshiharu Oda, Kohei eng Research Support, Non-U.S. Gov't Science. 2016 Mar 11;351(6278):1196-9. doi: 10.1126/science.aad6359.
- Zengler, K., Toledo, G., Rappé, M., Elkins, J., Mathur, E. J., Short, J. M., und Keller, M. (2002): Cultivating the uncultured. *Proceedings of the National Academy of Sciences*, **99** (24), S. 15681–15686.
- Zhang, H., Perez-Garcia, P., Dierkes, R. F., Applegate, V., Schumacher, J., Chibani, C. M., Sternagel, S., Preuss, L., Weigert, S., Schmeisser, C., Danso, D., Pleiss, J., Almeida, A., Hocker, B., Hallam, S. J., Schmitz, R. A., Smits, S. H. J., Chow, J., und Streit, W. R. (2022a): The Bacteroidetes *Aequorivita* sp. and *Kaistella jeonii* Produce Promiscuous Esterases With PET-Hydrolyzing Activity. *Front Microbiol*, **12**, S. 803896. Zhang, Hongli Perez-Garcia, Pablo Dierkes, Robert F Applegate, Violetta Schumacher, Julia Chibani, Cynthia Maria Sternagel, Stefanie Preuss, Lena Weigert, Sebastian Schmeisser, Christel Danso, Dominik Pleiss, Juergen Almeida, Alexandre Hocker, Birte Hallam, Steven J Schmitz, Ruth A Smits, Sander H J Chow, Jennifer Streit, Wolfgang R eng Switzerland Front Microbiol. 2022 Jan 5;12:803896. doi: 10.3389/fmicb.2021.803896. eCollection 2021.
- Zhang, H., Dierkes, R. F., und Streit, W. R. (2022b): *Microbial Degradation of Plastics*, Band 11B. ASM International, ASM Handbooks online.
- Zhang, H., Dierkes, R. F., Perez-Garcia, P., Costanzi, E., Dittrich, J., Cea, P. A., Gurschke, M., Applegate, V., Partus, K., und Schmeisser, C. (2023): The

metagenome-derived esterase PET40 is highly promiscuous and hydrolyses polyethylene terephthalate (PET). *The FEBS Journal*.

Zheng, Y., Yanful, E. K., und Bassi, A. S. (2005): A review of plastic waste biodegradation. *Critical reviews in biotechnology*, **25** (4), S. 243–250.

Acknowledgments

I would like to express my deepest gratitude to my advisor Prof. Dr. Wolfgang R. Streit for his invaluable mentorship and unwavering belief in my potential. His insightful feedback and positivity steered me through every stage of this research. I am truly indebted to his guidance and consistent encouragement that gave me strength to accomplish this dissertation successfully. Thank you for rigorously editing and structuring this work.

I would also like to thank Prof. Dr. Sigrun Reumann and all other members of my examination committee for taking the time to evaluate my work.

I am also thankful to Dr. Pablo Perez-Garcia and Dr. Jennifer Chow for their unreserved support from day one until our publication. Thank you for extending your support whenever I needed and all the thoughtful discussions. I am also grateful to Dr. Christel Schmeisser, Dr. Dominik Danso and Angela Jordan for all their support, thank you for endless patience especially at the start of my PhD journey. I am also indebted to Robert Dierkes for his brilliant support in the HPLC work and the great work together on the publication of PET40 paper.

Furthermore, I would like to thank all my colleagues of the microbiology and biotechnology department for the nicest working atmosphere, and all the good times we had in and outside of the lab. Thank you for the many scientific discussions and craziest non-scientific brainstorming sessions in the coffee breaks.

I owe special thanks to my friends, who graciously offered moral support and understanding. Their belief in me kept me grounded and focused.

I thank my family for their endless love. Words cannot describe my gratitude to my parents, my brother, my niece, and my nephew. Your unconditional love and faith in me have shaped who I am and fueled my determination to pursue this goal. Without you, It would not have been possible to achieve this goal. 谢谢你们无私的爱。

15.01.2025, 小丽